THE UNIVERSITY *of* EDINBURGH

Characterisation of carbonaceous particulate matter in Edinburgh

Mark Hammonds

A thesis submitted in fulfilment of the requirements
for the degree of Doctor of Philosophy
to the
University of Edinburgh

2011

Abstract

Airborne particulate matter (PM) has important harmful effects on human health, as well as a number of other important atmospheric effects. Although progress has been made in understanding the sources and effects of PM, there remains considerable uncertainty on a number of issues, including the nature of a lot of the carbonaceous material, which comprises 30–50% on average of PM mass. This project aims to compare different methods of PM measurement, and contribute understanding to the nature and origin of the carbonaceous fraction of PM.

Daily samples of PM_{10} were collected from three sites in the Edinburgh area using Partisol-Plus 2025 Sequential Air Samplers: 1) Urban Background (20 August 2008 until 21 April 2010); 2) Rural (25 February 2009 until 21 April 2009); and 3) Roadside (10 September 2009 until 21 April 2010). These localities provided PM that was, respectively, representative of: 1) city-wide background air; 2) air at a location distanced from population centres, roads and industrial areas; and 3) air influenced by the emissions associated with traffic.

Gravimetric PM_{10} concentration ($\mu g\, m^{-3}$) was determined for each daily filter sample, after a blank correction to compensate for the relative humidity (RH)-influenced change in filter mass over time. The correction was successful, with good agreement attained between the Partisol and a PM_{10} Tapered Element Oscillating Microbalance Filter Dynamics Measurement System (TEOM-FDMS) co-located at the Urban Background site. The general levels of PM_{10} measured in this monitoring campaign indicate that the air in Edinburgh was relatively clean. The main factor causing exceedance of the daily European Union (EU) limit value was shown to be transport of PM_{10} from areas of mainland Europe. High PM_{10} concentrations were also strongly associated with calm weather conditions in Edinburgh, which allowed the build-up of particulate pollution over time.

Aethalometer-equivalent daily concentrations of black carbon (BC) were determined by measuring the optical reflectance of the PM_{10} filters from the Partisol samplers. The conversion of reflectance values to BC concentrations relied on a number of correction factors, which may have impacted on the accuracy of the results with time and location. The concentration of BC in Edinburgh was shown to be relatively low, with the daily variation being controlled by local emissions and meteorology. BC as a proportion of PM_{10} increased with sampling location in the order: Rural < Urban Background < Roadside. Predominantly traffic-related BC concentrations increased during periods of low wind speed and were not greatly influenced by long-range transport of aerosol.

Daily water-soluble organic matter (WSOM) concentrations were obtained by aqueous extraction of the filter samples and measurement of the dissolved organic carbon (DOC). About 11% on average of the Edinburgh PM_{10} was WSOM. The majority of this WSOM seemed to have originated from air masses outside of the city, although there was a minor contribution from urban traffic sources. A solid phase extraction (SPE) procedure was used to isolate about one-third of the WSOM as hydrophobic compounds and this revealed a relative increase in the amount of less oxygenated material from traffic sources. Higher than average WSOM concentrations were strongly associated with calm weather conditions that allowed the transient build-up of particle concentrations. Some of the peaks in WSOM concentration were related to the transport of air masses from areas of mainland Europe where biogenic secondary organic aerosol (SOA) and biomass burning were likely sources. Analysis of the WSOM samples by UV-Vis absorption spectroscopy showed clear seasonal trends in the composition of hydrophobic water-soluble organic matter (HWSOM), interpreted as predominance of lower molecular weight aliphatic compounds in summer but predominance of larger aromatic and polyconjugated compounds in winter.

Raman spectra were obtained for different carbonaceous reference materials. The results of curve fitting for these spectra gave D1 band full width at half maximum (FWHM) values that distinguished between diesel exhaust particles from a local bus and a humic acid sample. Analysis of Edinburgh PM_{10} samples using Raman microspectroscopy (RM) showed a variation in the structural order of the carbon compounds present between that of soot and HUmic-LIke Substances (HULIS), with a tendency towards more soot-like material being present. There was no strong relationship between carbonaceous order and BC concentration, showing that coloured organic compounds have the potential to influence reflectance measurements.

The combination of these measurement approaches has yielded insights into the nature and variation in carbonaceous PM material with time and sampling location.

Declaration

I hereby declare that this thesis was composed by myself and that the work described within is my own, except where explicitly stated otherwise.

Mark Hammonds

April 2012

Acknowledgements

It is a great pleasure to be able to thank all of the people who have supported me throughout the course of my PhD. Firstly, thanks go to my supervisor Mat Heal for employing me to work on this project, providing all of the help I could hope for, and hosting a number of enjoyable group meals. I acknowledge the financial support from NERC, and the superb working and learning environment afforded by the School of Chemistry at the University of Edinburgh. Although some of my research has been fairly solitary, I have had the pleasure of the company of a number of good colleagues: Catherine Hardacre (I will remember the climbs); Emanuel Blei (I will not forget the day out collecting collars); Eilidh Morrison (I will not forget the day out collecting collars); Nichola Copeland; and Pawel Misztal.

I would like to thank various people and organisations who have helped this project to run. Archie Forrest at the City of Edinburgh Council for support at the Urban Background monitoring site. Neil Cape and Gavin Phillips at the Centre for Ecology & Hydrology for support at the Rural monitoring site. Robert Calder at the University of Edinburgh for helping to set up the Roadside monitoring site. Iain Beverland at the University of Strathclyde for assistance in obtaining the Partisol samplers, and for providing a location to condition and weigh the filter samples. Paul Quincey at the National Physical Laboratory for providing BC data. Andrei Gromov and the rest of Eleanor Campbell's research group for training and the use of the Raman microscope. John Parker at the Scottish Agricultural College for TOC analyser training and support. Ann Mennin at the School of Geosciences for assistance with the freeze drier and 7-figure MC 5 micro-balance. Donald Robertson at the School of Chemistry for showing me how to operate the UV-Vis spectrometer. Logan Mackay at SIRCAMS for analysing samples on the FT-ICR mass spectrometer.

Further invaluable support was provided in the School of Chemistry and I express my gratitude to everyone involved: Stuart Johnstone for Glass blowing (producing

Quickfit® test-tubes); Stuart Mains at the Mechanical Workshop (chamfering the corners of Partisol filter cassettes); and Donald Palin at the Electronics Workshop (fixing the furnace). Thanks to the project students who helped along the way: Ryan; Iain; Rasha; Carol; and Bing Qin.

Other assistance was provided by a Lothian Buses driver who allowed me to scrape some PM from the exhaust of the bus he was driving; and Karl Ropkins with many useful emails concerning the use of R software and the 'openair' tool.

A big thanks to all of my friend friends who have made my time in Edinburgh such an enjoyable one and the Edinburgh University Hillwalking Club for all the great times in the mountains. Special mention must go to Claire for her support during the final stages of my PhD.

Finally and importantly thanks to my Mum and Dad for all of their help, and for providing a wonderful space in which to write. I dedicate this thesis to them.

Contents

List of Figures

List of Tables

Chapter 1

Introduction

Airborne particulate matter (PM) consists of solid and/or liquid particles that are suspended in air and can originate from anthropogenic and/or natural sources. These particles vary in size (from around a few nm to $\sim 100\,\mu m$ in diameter) and shape, and have complex chemical compositions [AQEG, 2005]. They also have extremely diverse impacts on the atmosphere, climate, and public health [Pöschl, 2005]. Aerosol is a suspension of PM in gas but the term aerosol is often used when the intention is to refer to just the particles. From this use follows the common but technically incorrect interpretation that aerosol $\equiv$ particles $\equiv$ PM.

PM is commonly classified according to size fraction. PM_x describes particles with aerodynamic diameters $\leqslant$ x µm. As PM has various shapes, aerodynamic diameter is used to describe the aerodynamic behaviour of a particle if it was a perfect sphere with a density of $1\,g\,cm^{-3}$. The following size fractions are often referred to:

PM_{10} aerodynamic diameter $\leqslant 10\,\mu m$; contains coarse particles that can reach the upper part of airways and lungs

$PM_{2.5}$ aerodynamic diameter $\leqslant 2.5\,\mu m$; contains fine particles that can penetrate more deeply into the lungs and which are therefore potentially more dangerous

$PM_{10\text{-}2.5}$ aerodynamic diameter $10 - 2.5\,\mu m$; the coarse fraction of PM_{10}

In practice PM sampling devices use precisely designed and calibrated sampling heads to select for the required size fraction. Air is drawn through the size-selective head at the specified flow rate and the smaller particles are able to follow the streamlines and enter the device. Larger particles tend to cross the streamlines and impact on the inside of the head and therefore do not enter the sampling device. It is not possible

to design a sampling head with complete step-change cut-off for particle size selection (i.e., where 100% of particles of diameter $\leqslant$ the specified size pass through the head and 0% of particles of diameter $>$ the specified size pass through) so sampling heads are designed with 50% penetration at the specified aerodynamic diameter (i.e., where 50% of particles of diameter = to the specified size pass through the head, $>$ 50% of particles of diameter $<$ the specified size pass through, and $<$ 50% of particles of diameter $>$ the specified size pass through) as shown in Figure 1.1. PM_x is therefore operationally defined as the fraction of particles that pass through an inlet with a 50% efficiency cut-off, with a specified sampling efficiency curvature, for particles with an aerodynamic diameter of x µm. This allows PM_x to be precisely defined for air quality legislation. PM_{10} legislation and sampling are discussed further in Chapter 2.

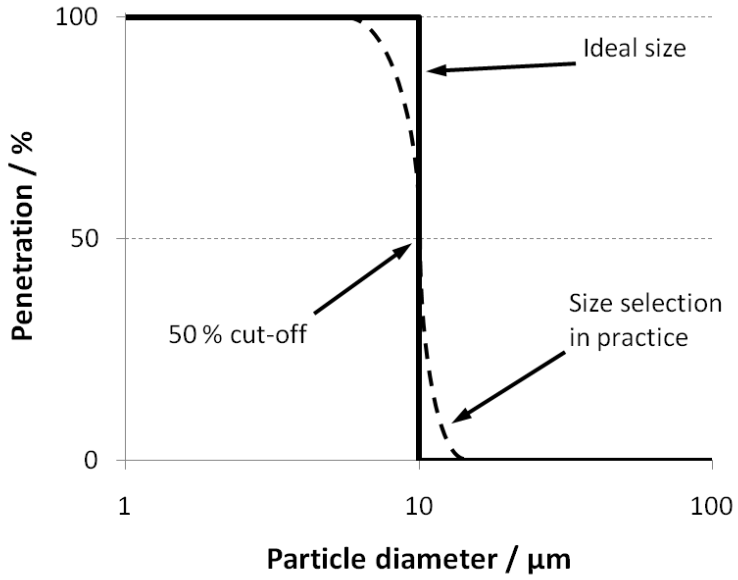

Figure 1.1: Graph to represent cut-off efficiency for a PM_{10} sampling head.

1.1 Effects of PM

1.1.1 Human health

More than 10 years ago Pope [2000] reported that there were more than 150 published epidemiologic studies on the health effects of PM, with the general conclusion that the epidemiologic evidence suggests PM is an important risk factor in cardiopulmonary morbidity and mortality. A seminal example of one of these publications is a study in six US cities by Dockery et al. [1993], which concluded "Although the effects of other,

unmeasured risk factors cannot be excluded with certainty, these results suggest that fine particulate air pollution, or a more complex pollution mixture associated with fine particulate matter, contributes to excess mortality in certain U.S. cities". Similar results continue to be published with, for example, the Nurses' Health Study by Puett et al. [2008] reporting that exposure to $10\,\mu g\,m^{-3}$ greater annual average PM_{10} concentration was associated with a 16% increase in all-cause mortality and a 43% increase in coronary heart disease (taking into account other factors that may have affected coronary heart disease such as body mass index, exercise levels and smoking).

Of potentially more relevance to the PM_{10} collected in the Edinburgh area for this work is the study conducted in Edinburgh by Prescott et al. [1998], which showed that between 1992 and 1995 there was a positive association between the number of hospital cardiovascular admissions each day and the mean PM_{10} level of the previous three days. A study in London [Atkinson et al., 2010] investigated the association of different PM metrics (e.g., size, number and composition) with daily deaths and hospital admissions. Atkinson et al. [2010] found that particle number concentration was associated with daily mortality and admissions for cardiovascular diseases, and that secondary pollutants (the secondary portion $PM_{2.5}$, nitrate and sulphate) were more important for respiratory outcomes.

In summary, the negative health effects arise through exposure to PM by inhalation, on both short and long time-scales. PM aggravates asthma and causes other respiratory symptoms such as coughs and bronchitis in children, and seriously affects health in adults, increasing deaths from cardiovascular and respiratory diseases and lung cancer [WHO, 2005]. There is still uncertainty in explaining exactly what aspect of PM (i.e. the chemical composition of the particles and/or the size and shape of the particles themselves) causes negative health impacts so further information on the nature of PM is likely to be beneficial.

1.1.2 Climate

PM also has important direct and indirect impacts on climate. The direct effects are cooling through the scattering and reflection of solar radiation, and warming through absorption of terrestrial radiation [Pöschl, 2005]. The indirect effects are from PM acting as cloud condensation nuclei (CCN), leading to the formation of cloud droplets. The clouds thus formed play a key role in the Earth's radiation budget by absorbing terrestrial radiation and reflecting solar radiation [Sun and Ariya, 2006]. A major reason for the continued study of the properties of PM is the importance of its climatic effects

and the need to improve the current level of scientific understanding (LOSU), as shown in Figure 1.2. Not only is there a relatively low LOSU in the warming effect of black carbon (BC) on snow but there is also a low LOSU in the cooling due to the direct and indirect effects of PM. More information about the exact nature and sources of PM should help improve understanding of its role in the earth's climate.

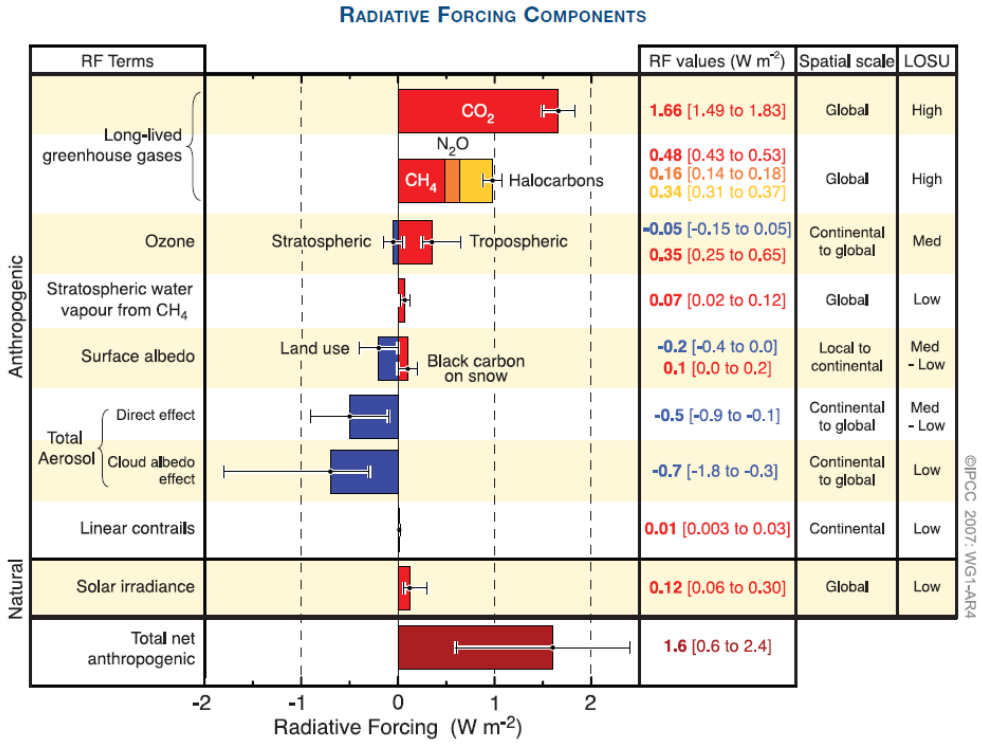

Figure 1.2: "Global average radiative forcing (RF) estimates and ranges in 2005 for anthropogenic carbon dioxide (CO_2), methane (CH_4), nitrous oxide (N_2O) and other important agents and mechanisms, together with the typical geographical extent (spatial scale) of the forcing and the assessed level of scientific understanding (LOSU). The net anthropogenic radiative forcing and its range are also shown. These require summing asymmetric uncertainty estimates from the component terms, and cannot be obtained by simple addition. Additional forcing factors not included here are considered to have a very low LOSU. Volcanic aerosols contribute an additional natural forcing but are not included in this figure due to their episodic nature. The range for linear contrails does not include other possible effects of aviation on cloudiness." Taken from Solomon et al. [2007].

Due to the health effects and climatic influence of PM, legislation is in place that requires the monitoring of PM_{10} concentrations, and this is discussed further in Chapter 2.

1.2 Composition of PM

Unlike other pollutants, PM is not a simple, single molecular entity but consists of a huge range of chemical species from different sources. Physical and chemical processes that occur during the atmospheric life cycle of aerosols are briefly summarised in Figure 1.3. Primary particles are emitted directly into the atmosphere through man-made processes (e.g., engine emissions from transport; erosion of the road by traffic; abrasion of brakes and tyres; industrial, commercial and domestic fuel burning; and construction activities) and natural processes (e.g., pollen; wind-blown dust; and sea spray). Secondary particles are formed in the atmosphere by chemical reactions of gaseous pollutants from anthropogenic sources (e.g., nitrogen oxides emitted by traffic and industrial combustion processes; ammonia, primarily from agriculture; and sulphur dioxide from the combustion of sulphur-containing fuels) and biogenic sources (e.g., volatile organic compounds from vegetation) [AQEG, 2005]. The reaction of organic compounds in the air leads to the formation of secondary organic aerosol (SOA) but detail of the pathways involved remains to be clarified.

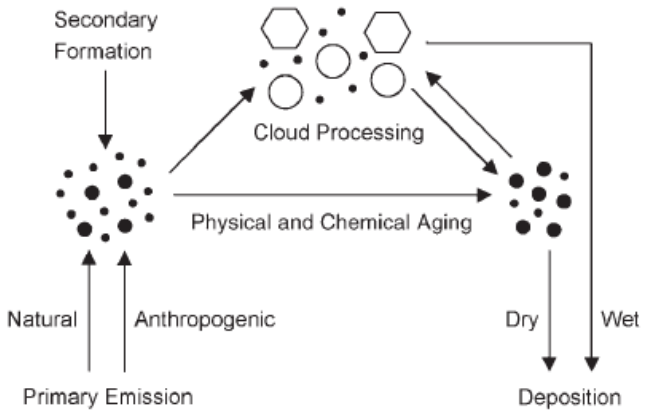

Figure 1.3: "Atmospheric cycling of aerosols." Taken from Pöschl [2005].

Carbonaceous components (organic matter (OM) and BC/elemental carbon (EC)) contribute a significant fraction to PM composition (30–50% on average in the UK), not just at roadside sites (between 1 m of the kerbside and the back of the pavement of a busy road) but also urban background sites (a location distanced from sources and therefore broadly representative of city-wide background conditions) [AQEG, 2005]. BC and EC are both measures of carbonaceous soot in PM but due to the different techniques used in their measurement they are not necessarily representative of the same quantity. BC is determined optically and EC is determined thermochemically, and this is discussed further in Chapter 3 and Chapter 6.

Our present understanding of the composition, physical and chemical properties, sources and transformation characteristics of the total carbon (TC) fraction of PM is limited, and its environmental and health effects remain highly uncertain [Fuzzi et al., 2006]. Since carbonaceous components are abundant in urban PM, and they have potential negative impacts upon human health, it will be this fraction that is studied in this project, in order to contribute understanding both to its exact nature and origin, and to those aspects that are the most harmful. A large proportion of OM in PM is water soluble (i.e., water-soluble organic matter (WSOM)), and may be released once the particles settle on the lung surface, making the study of these compounds an area of particular interest. The analysis of WSOM is presented in Chapter 4 and Chapter 5.

1.3 Characterisation of PM

The overwhelming complexity of the carbonaceous material in PM means there is great difficulty in characterising this fraction. A range of sophisticated and sensitive chemical analytical techniques are now available that can help identify chemical characteristics of the carbon-containing part of PM. Use of these techniques on PM samples of varying spatial and temporal characteristics should help to reduce the current levels of uncertainty about their chemical composition. Prominent organic substance classes and their main sources are summarised in Table 1.1. Attempts to characterise individual compounds in carbonaceous PM do not account for all of the species present, with even the most comprehensive investigations only identifying 10–40% of organic PM on a molecular level [Pöschl, 2005]. Therefore, analysis of the bulk properties of this fraction should give a better understanding of the overall chemical characteristics. The following section is a brief overview of some techniques that have been used to study the carbonaceous fraction of PM collected on filters.

1.3.1 Bulk properties

1.3.1.1 OC-EC determination

The amount of organic carbon (OC) and EC in PM can be determined by thermochemical oxidation and evolved gas analysis (CO_2 detection) of a filter sample by controlling the temperature and atmosphere in the instrument used, and by an optical feature that corrects for pyrolytically generated carbon, which can be formed during the analysis of some materials [Birch and Cary, 1996]. When analysing using this technique it is

Table 1.1: Prominent organic PM components. Adapted from Pöschl [2005].

Substance Classes	Sources
aliphatic hydrocarbons	biomass, fossil-fuel combustion
aliphatic alcohols and carbonyls	biomass, SOA/aging
levoglucosan	biomass burning
fatty acids and other alkanoic acids	biomass, SOA/aging
aliphatic dicarboxylic acids	SOA/aging
aromatic (poly-)carboxylic acids	SOA/aging, soil/dust
multifunctional aliphatic and aromatic compounds (OH, CO, COOH)	SOA/aging, soil/dust
polycyclic aromatic hydrocarbons (PAHs)	fossil-fuel combustion, biomass burning
nitro- and oxy-PAHs	fossil-fuel combustion, biomass burning, SOA/aging
proteins and other amino compounds	biomass
cellulose and other carbohydrates	biomass
secondary organic oligomers/polymers and humic-like substances	SOA/aging, soil/dust

assumed that the sample is homogenously distributed since the instrument calculates the amount of OC, EC and TC (= OC + EC) from a small area of the filter.

A punch of the filter is placed in the sample oven of the instrument and the OC is volatilised from the filter whilst the temperature is stepped up to above 800 °C. A carrier gas (helium) drives the evolved OC through granular MnO_2 (maintained at 870 °C), which oxidises it to CO_2. A hydrogen flow is then introduced and a nickel-firebrick methanator (held at 500 °C) reduces the CO_2 to CH_4. A flame ionisation detector (FID) is used to quantify the CH_4. The concentration of CH_4 measured is assumed to be the OC concentration, once a pyrolisis correction is applied. A typical thermogram produced by this instrument is shown in Figure 1.4, which includes the profiles of the laser transmittance, temperature and FID. In the next stage of the analysis the oven temperature is lowered and the carrier gas changed to O_2/He. The temperature is stepped up to above 800 °C again, and the volatilised and oxidised EC is measured in the same way as with the OC.

The transmittance is continuously measured throughout the analysis by a helium-neon laser and a photodetector. When pyrolisis occurs there is an increase in light absorption, resulting in a decrease in transmittance. When the sample comes into contact with O_2 the pyrolytically generated char ("EC") is oxidised and increases the transmittance. The amount of char produced is the quantity required to return to the level of transmittance

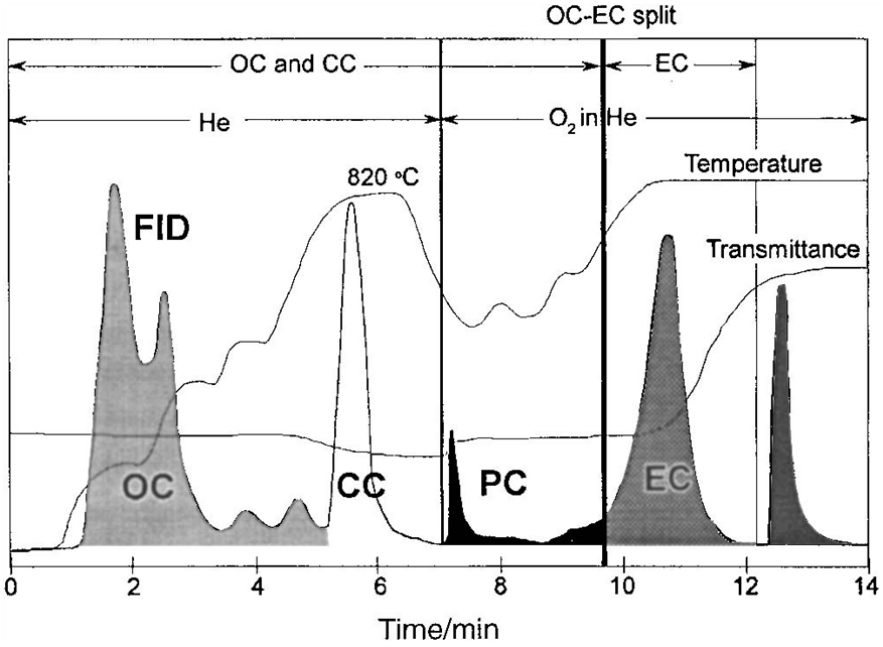

Figure 1.4: A typical thermogram from thermal-optical instrumentation. Taken from Birch and Cary [1996]. The three traces correspond to oven temperature, filter transmittance and FID response. Peaks correspond to organic (OC); carbonate (CC); pyrolytic (PC); and elemental (EC) carbon. The final peak is a methane calibration peak.

at the start of the analysis. By retrospectively assigning a portion of the elemental carbon peak to the organic fraction the pyrolised OC can be corrected for. A vertical line is drawn in the thermogram (Figure 1.4) to represent the "split" time, defined to separate the OC from the EC.

The above is a description of one instrument and protocol used for the determination of EC and OC but others are used. Apportionment into fractions labelled EC and OC depends on the nature of the samples analysed, the analysis protocols, and the instrumentation applied [Chow et al., 2004]. This carbonaceous PM is therefore hard to characterise since the different analytical techniques used by different researchers are likely to give different results.

1.3.1.2 ^{14}C accelerator mass spectrometry

Radiocarbon (^{14}C) measurements of airborne PM are used to distinguish between OC and EC of fossil and contemporary carbon origin [Szidat et al., 2004]. In this method OC and EC are transformed into CO_2 in a stream of O_2 at 340 and 650 °C, respectively, and reduced to filamentous C to produce a target for subsequent ^{14}C accelerator mass spectrometry measurements. ^{14}C has a half-life of 5730 years so none is present in fossil

carbon, whereas contemporary carbon contains ~ 1 in 1012 atoms of ^{14}C, and this can be detected by the accelerator mass spectrometer. By measuring the amount of fossil and contemporary carbon present in the OC and EC fractions of filter samples a simple 'top down' source apportionment can be made, as shown in Figure 1.5.

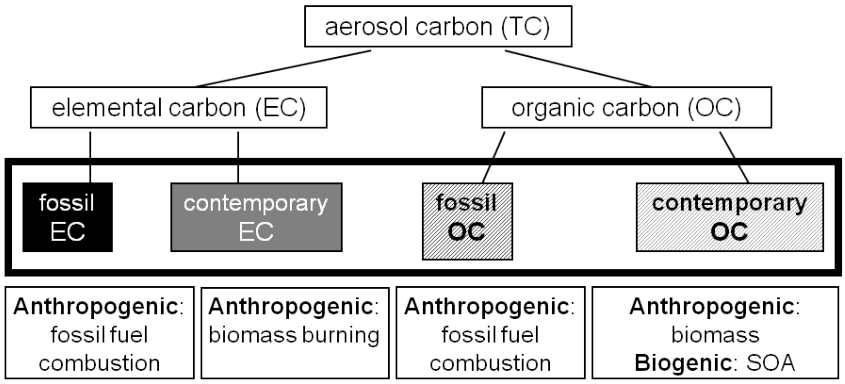

Figure 1.5: Top down source apportionment for fossil and contemporary carbon in OC and EC.

A challenge with the measurement of fossil and contemporary carbon in OC and EC is in determining an accurate split between the OC and EC fractions, as described in Section 1.3.1.1. In spite of this difficulty, such data have been determined for three European cities: Zürich [Szidat et al., 2006]; Göteborg [Szidat et al., 2009]; and Birmingham [Heal et al., 2011]. Szidat et al. [2006] found that EC mainly originated from fossil fuel usage during summer in Zürich but had a substantial biomass-burning emission source in winter. OC mainly originated from biogenic SOA during summer but had a substantial wood combustion source in winter, with $\sim 30\%$ from fossil fuels throughout the year. For winter in Göteborg, Szidat et al. [2009] found that an urban site was substantially more influenced by fossil EC emissions than a rural site. For summer they found that biogenic SOA emissions dominated OC concentrations. A more pronounced fossil signal throughout the year was observed for Göteborg [Szidat et al., 2009] than was previously reported for Zürich [Szidat et al., 2006]. It was suggested that the fossil impact was larger when local sources dominated and long-range transport caused an enhanced non-fossil signal. Heal et al. [2011] found no seasonality in their data from Birmingham and reported the following average contributions to TC in $PM_{2.5}$: 27% fossil EC; 20% fossil OC; 2% biomass EC; 10% biomass OC; and 41% biogenic OC. Up to 29% of the total $PM_{2.5}$ was estimated to derive from biogenic SOA. The conclusion of "a significant and ubiquitous contribution from non-fossil biogenic sources to the carbon in terrestrial aerosol" [Heal et al., 2011] was consistent with findings from elsewhere in Europe.

1.3.1.3 Fluorescence spectroscopy

Three-dimensional excitation-emission matrix (EEM) fluorescence spectra of WSOM extracted from aerosol samples were measured by Duarte et al. [2004]. The EEM profiles of the WSOM showed two well-defined excitation/emission ($\lambda_{Exc}/\lambda_{Em}$) peaks at $\lambda_{Exc}/\lambda_{Em} \approx 240/405$ nm and $\lambda_{Exc}/\lambda_{Em} \approx 310/405$ nm. These were located at shorter wavelengths than reported in the literature for natural WSOM (i.e., humic substances), indicating a smaller content of both aromatic structures and condensed unsaturated bond systems in the WSOM fraction of PM [Duarte et al., 2004].

1.3.1.4 Fourier transform infrared spectroscopy

Fourier transform infrared (FT-IR) spectroscopy can be used to determine the chemical characteristics and functional groups present in bulk WSOM extracted from PM samples. An example of the functional groups assigned by Duarte et al. [2005] is shown in Figure 1.6. Duarte et al. [2005] showed that autumn samples exhibited spectroscopic signals typical of lignin breakdown products (e.g., aromatics, phenols, ketones and methoxyl groups), highlighting the major contribution of wood burning processes in the chemical properties of the WSOM fraction of PM at this time of the year.

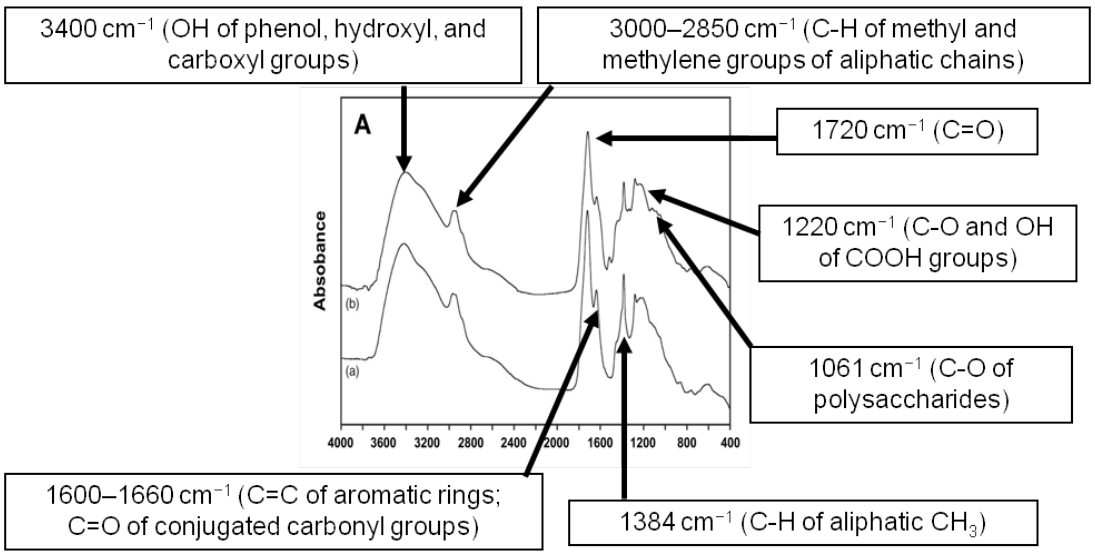

Figure 1.6: "FT-IR spectra of the WSOC isolated from the aqueous extracts of the aerosol samples collected in the summer (a) and autumn (b) seasons." Adapted from Duarte et al. [2005].

1.3.1.5 Nuclear magnetic resonance spectroscopy

The most common nuclear magnetic resonance (NMR) method for the characterisation of natural organic matter (NOM), which can also be used for the analysis of PM, is solid-state NMR, mainly via cross polarization and magic angle spinning (CPMAS)-^{13}C NMR. Solid-state NMR has a number of benefits compared to liquid-state NMR, including: no concentration limit; no solvent effects; minimal sample handling; the ability to analyse highly insoluble fractions (e.g., BC); the stability of samples in the solid state; and the ability to analyse whole PM samples [Cook, 2004].

It was reported by Duarte et al. [2005] that solid state CPMAS-^{13}C NMR of WSOM from PM can reveal differences between the chemical structure of summer and autumn samples from a rural part of Portugal. The autumn samples were richer in aromatic carbons (as shown in Figure 1.7), which are typical for lignin breakdown products, highlighting a possible major contribution from wood burning processes to PM [Duarte et al., 2005]. Another study using solid-state ^{13}C NMR [Sannigrahi et al., 2006] indicated that water-soluble (WS) OC in urban Atlanta aerosol particles was mostly aliphatic in nature ($\sim$ 95% by C mass). Of this C mass $\sim$ 80% came from alkyl and oxygenated alkyls, $\sim$ 10% from carboxylic acids, and $\sim$ 4% from aromatic functional groups.

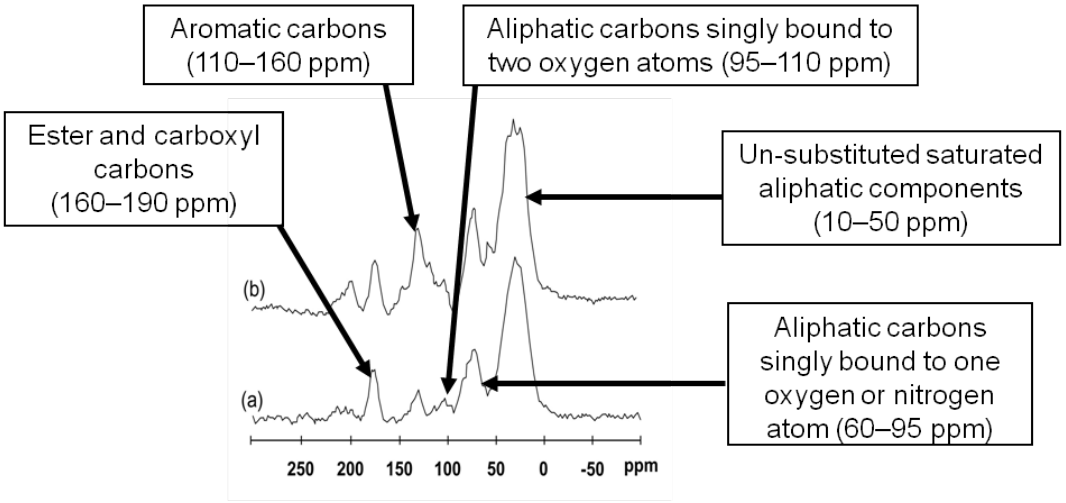

Figure 1.7: "CP-MAS ^{13}C NMR spectra of the water-soluble organic matter isolated from the aerosol samples collected in the summer (a) and autumn (b) seasons." Adapted from Duarte et al. [2005].

Proton NMR (^{1}H-NMR) is commonly used in chemistry for the investigation of small molecules, due to the high natural abundance and receptivity of protons. However, it may not be as useful for the study of WSOM in PM due to the very strong water signal in the ^{1}H-NMR spectrum and the lack of resolution compared to ^{13}C-NMR [Cook, 2004].

^{1}H-NMR spectroscopy has other drawbacks for the analysis of organic compounds: although details on the chemical environment of protons can be obtained, alternative interpretations of the spectra are possible due to the lack of information on the carbon structures present; and acidic hydrogens (like those of –OH and –COOH groups) can undergo chemical exchange with the D_2O solvent and elude detection [Graber and Rudich, 2006].

Even though ^{1}H-NMR spectroscopy of WSOM has drawbacks, it can be used to determine the presence of certain functional groups and their quantities. This can help highlight seasonal differences and give an indication of PM sources, for example, emission of aromatic compounds by wood burning or slower degradation reactions of aromatics in winter [Samburova et al., 2007]. Characteristic ^{1}H-NMR fingerprints can be derived for three major aerosol sources: biomass burning; secondary formation from anthropogenic and biogenic volatile organic compounds; and emission from the ocean. These source fingerprints can be related to the chemical properties of the organic mixtures, which determine their reactivity and their physicochemical properties, and ultimately the fate of the organic particles in the atmosphere [Decesari et al., 2007].

Due to the complexity of PM NMR spectroscopy, peak overlap can be a major problem hindering analysis. Therefore, being able to disperse the data into a second dimension could be highly beneficial. Most 2D NMR experiments used in the study of NOM are based on through-bond interactions (homonuclear and heteronuclear) and through-space interactions [Cook, 2004]. Having control over how the data is dispersed is one of the reasons why 2D NMR could be a powerful and useful technique for the study of PM.

1.3.1.6 Elemental analysis

Elemental analysis is used to determine the percent of C, H, N and O in a sample. Information about the chemical characteristics (e.g., the level of oxygenated functional groups and saturated systems) can be inferred from these values and the calculated O/C, H/C and OM/OC ratios. Results of WSOM from PM samples collected in Hungary indicated the predominance of oxygenated functional groups and a low H/C ratio, implying the presence of unsaturated or polyconjugated structures [Kiss et al., 2002]. The results of Kiss et al. [2002] also allowed an OM/OC ratio of 1.9 to be calculated, which did not change with the seasons, and this value is used in Chapter 4.

1.3.1.7 Liquid chromatography mass spectrometry

Kiss et al. [2003] used liquid chromatography mass spectrometry (LC-MS) to gain average molecular weight values in the 200–300 Da range for the OM isolated from rural fine aerosol samples collected in Hungary, but no seasonal variation was observed. Possible sources of error when using electrospray ionization (ESI) with LC-MS, which would lead to the results of Kiss et al. [2003] being inaccurate, are: fragmentation in the ESI source; formation of multiply-charged ions; and the differing ionization and detection efficiencies of different components [Graber and Rudich, 2006]. However, high resolution mass spectrometry (MS) techniques (e.g., Fourier transform ion cyclotron resonance mass spectrometry (FT-ICR-MS)) could still be useful for identifying a number of chemical species present in PM and only require a relatively small quantity of material to generate enough signal to produce a useful spectrum.

1.3.1.8 Laser desorption/ionisation mass spectrometry

Samburova et al. [2005b] used laser desorption/ionisation mass spectrometry (LDI-MS) to investigate the molecular weight of WSOM from PM and found the most intense signals in the mass spectra to be between m/z 150 and 500. Test experiments suggested that fragmentation was not significant and did not lead to an underestimation of the molecular weight distribution. LDI-MS data are dominated by singly charged ions, compared to ESI-MS, reducing the likelihood of multiply charged ions causing measurement artefacts when using this technique [Samburova et al., 2005b].

1.3.1.9 Aerosol mass spectrometer

The Aerodyne aerosol mass spectrometer (AMS) can be used to obtain quantitative measurements of the chemical composition of non-refractory sub-micron particles with high time and size resolution [Zhang et al., 2007]. Analysis of the individual particles provides information on the bulk PM sample. A summary of AMS data from different global locations is shown in Figure 1.8 and clearly highlights the ubiquity of organic material (green portion of pie charts) in PM. Zhang et al. [2007] deconvoluted organic aerosol (OA) data from 37 field campaigns into hydrocarbon-like organic aerosol (HOA) and several types of oxygenated organic aerosol (OOA) components. OOA was reported to be ubiquitous in the OA fraction of different atmospheric environments, on average accounting for: 64% at urban sites; 83% at urban downwind sites; and 95% at

rural/remote sites. Increases in OOA were mainly due to SOA and not the oxidation of HOA (which originates from primary combustion sources).

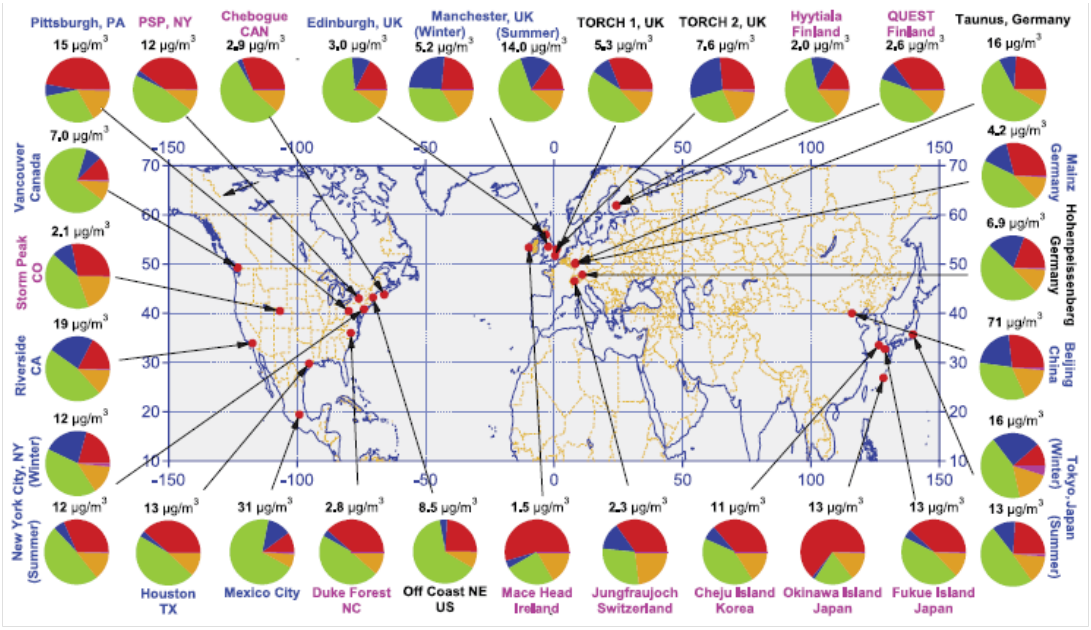

Figure 1.8: "Colors for the study labels indicate the type of sampling location: urban areas (blue), <100 miles downwind of major cites (black), and rural/remote areas >100 miles downwind (pink). Pie charts show the average mass concentration and chemical composition: organics (green), sulfate (red), nitrate (blue), ammonium (orange), and chloride (purple)". Taken from Zhang et al. [2007].

1.3.2 Mass closure

A simple model of aerosol chemistry was constructed by Harrison et al. [2003] for airborne PM_{10} at roadside and urban background locations in London and Birmingham. Numerical factors reported by Harrison et al. [2003] were used to convert seven measured species into seven major PM components:

Iron to iron rich dust

Calcium to calcium salts ($CaSO_4 \cdot 2\,H_2O$)

Chloride to sea salt (NaCl)

EC to EC

OC to OM

Sulphate to ammonium sulphate ($(NH_4)_2SO_4$)

Nitrate to ammonium nitrate (in fine PM) / sodium nitrate (in coarse PM) (NH_4NO_3 / $NaNO_3$)

The small proportion of mass that was unaccounted for was attributed to strongly bound water and the model was able to account for a very large proportion of the variance in mass concentrations at all of the sites. Data generated by Harrison et al. [2003] was analysed by Harrison et al. [2004] in the context of the magnitude of concentrations and the composition of the roadside increment (difference between roadside and urban background PM concentration). Average roadside mass increments were 11.5 $\mu g\,m^{-3}$ of PM_{10} and 8.5 $\mu g\,m^{-3}$ of $PM_{2.5}$, and the roadside particle increment was mainly composed of EC, OM and iron-rich dusts. More recently, Yin and Harrison [2008] used the pragmatic mass closure model of Harrison et al. [2003] and found that the coefficients determined in the earlier mass closure study still provided a good mass closure, even with the inclusion of a rural site.

Although the mass closure model described by Harrison et al. [2003] is a useful tool to apportion major components of airborne particles, it is limited in the speciation of organic material in PM. Yin et al. [2010] therefore incorporated the results of chemical analyses of organic marker species (including n-alkanes, hopanes, polycyclic aromatic hydrocarbons (PAHs), organic acids and sterols) from West Midlands $PM_{2.5}$ into the US environmental protection agency (EPA) chemical mass balance (CMB) model. Key tracers for diesel engines and wood smoke/biomass burning were EC and levoglucosan, repsectively. The CMB model was used to show that urban background and rural carbonaceous particles mainly came from road traffic sources, with smaller contributions from vegetative detritus, wood smoke, natural gas, coal, and dust/soil [Yin et al., 2010]. A SOA source of OM was also identified by the CMB model.

1.4 Line fitting of bivariate data

The techniques used to measure the properties of PM inevitably generate data. Analysing these data to gain understanding is therefore a key stage in the study of PM. This section moves away from the properties and measurement of PM, and briefly summarises the surprisingly complex step of fitting a straight line to bivariate data.

Investigating the linear relationship of bivariate data is a routine practice in many areas of science and is an important part of this project. When comparing two different

instruments measuring the same quantity the linear relationship can be used to test the level of agreement. A line fitted to a bivariate dataset can also be used to predict the outcome of a measurement (e.g., the result of an analytical test from a particular concentration of a solution) or describe an average relationship between two measured quantities (e.g., how much of PM_{10}, on average, is composed of BC.)

A straight line fitted to bivariate data as y and x values on a scatter plot has the following form:

$$y = a + b \cdot x \tag{1.4.1}$$

where

a = intercept

b = slope

The intercept and slope are commonly calculated by linear regression, which is a method of fitting lines for predicting y from known values of x. The term regression originally came from Galton [1886] due to the property of 'regression towards mediocrity' (i.e. regression towards the mean). In ordinary least squares (OLS) regression, the line is estimated by minimising the sum of squares of residuals from the line in the y direction, as shown by (A) in Figure 1.9. Although useful as a method of prediction, OLS is not the best method of fitting a line when the value of b between two sets of results is of primary interest [Warton et al., 2006]. This is because of bias in the OLS method from only minimising the residuals in the y direction, when the intention is to summarise the two-dimensional relationship between y and x in one dimension. If there is no reason for choosing a variable y to be dependant on x, the OLS method of fitting a line is not the most appropriate. When applying OLS to data with random variability in y and x the likely outcome is that the slope (b) will be underestimated and the intercept (a) overestimated [Davis, 1986]. Despite this, OLS is often used in situations where it is not the most appropriate technique [Ayers, 2001]. This is most likely due to it being the most well known method of line-fitting and the only method available in ubiquitous software like Microsoft Excel. In contrast, on occasions when the OLS method is not used the reason often stated is that x is not a fixed variable, or x has been measured with error so OLS is not appropriate. This is a misconception, and OLS regression can be used when x is measured with error, as long as the results are interpreted in the context of predicting y from values of x measured with error [Warton et al., 2006].

If the aim is to find how strongly y and x are related a suitable statistic is r^2 (the square of the correlation coefficient). The value of r^2 shows the proportion of variation in y

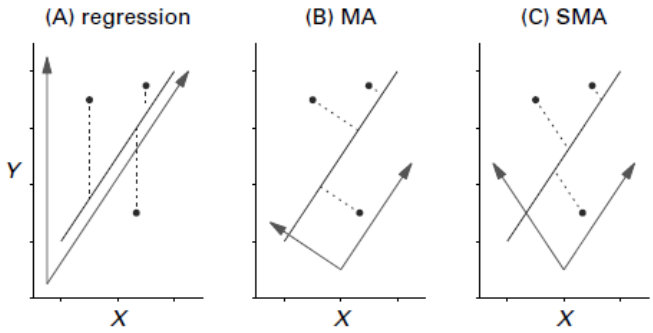

Figure 1.9: "The direction in which residuals are measured is (A) vertical for linear regression (B) perpendicular to the line for major axis estimation (C) the fitted line reflected about the y axis for standardised major axis estimation. Axes are plotted on the same scale. The broken lines indicate residuals, and the arrows represent the fitted and residual axes, which are useful for understanding methods of estimation and inference about these lines." Taken from Warton et al. [2006].

that can be explained by linear regression on x [Warton et al., 2006] and can have values between 0 and 1. In this case it does not matter which values are chosen as y, and which as x, as the r^2 value will be the same in both possible situations. Assuming positive y and x values, an r value of $+1$ represents a perfect positive linear correlation in the y and x directions, and an r value of -1 represents a perfect inverse linear correlation of y in the x direction. The value of r^2 reduces as the linear relationship breaks down towards $r^2 = 0$, and this value indicates no linear relationship. Although r^2 is a useful measure of the strength of the relationship between two variables, it does not measure the agreement between them [Bland and Altman, 1986]. Perfect agreement only occurs when all of the points lie on the $y = x$ line but perfect correlation can occur for a straight line of any gradient. Bland and Altman [1986] give reasons for being cautious when using the square of the correlation coefficient, for example:

1. If the range of values used in a comparison is wide, the correlation will be greater than if it was narrow. As the range of values increases, the likelihood of a high correlation also increases.

2. Quite high correlations can be obtained for data which seem to be in poor agreement. Although the correlation is high, the magnitude of the difference between values may be larger than is reasonable for being able to state that they agree.

A more appropriate line-fitting method for summarising bivariate data is the major axis (MA). This line is estimated by minimising the sum of squares of residuals perpendicular to the line, as shown by (B) in Figure 1.9. Another term for the MA

line-of-best-fit is 'orthogonal regression', and this technique treats both the y and x variables equally. The MA method assumes that the ratio of variances of residuals in both the y and x directions is 1 [Warton et al., 2006]. This equal treatment of y and x is both a benefit and drawback of the MA line. When the two variables are measured on similar scales, it seems reasonable to give the y and x directions equal weight when minimising residual distances from the fitted line. However, when the scales of the variables are considerably different, giving the y and x directions equal weight is likely to bias the result of the fit.

A better linear model for bivariate data with scales that are not comparable is the standardised major axis (SMA) (also known as the 'reduced major axis'). It is this method that was recommended by Ayers [2001] when comparing different methods of PM_{10} sampling. This recommendation may appear flawed since both PM_{10} sampling methods in such a comparison should be measuring on the same scale, and therefore suited to MA line described in the previous paragraph. However, there is currently no consensus in the literature about which is the most suitable line-fitting method to use. The SMA calculates the MA on standardised data, then rescales the MA to the original axis [Warton et al., 2006]. Estimation of the line is by minimising the sum of squares of residuals reflected about the y axis of the line, as shown by (C) in Figure 1.9.

Consideration of the appropriate method of line-fitting was made for the scatter plots of y and x data presented in this thesis. The r^2 value was used to show the strength of the linear relationship in bivariate datasets. Each of the three methods of fitting a line discussed here were used, depending on the situation. For example:

OLS An aqueous solution of PM was made in the laboratory and the WSOM concentration of this solution was determined by dissolved organic carbon (DOC) analysis (Chapter 4). The OLS line was used to determine the WSOM concentration according to the amount of PM dissolved in water.

MA All instances comparing the same quantity measured at different sites use the MA estimate of the best-fit line. The MA was also used when fitting a line between concentrations (all in $\mu g\,m^{-3}$) of different PM metrics (i.e., BC versus PM_{10}). It could be argued that the differences in the magnitudes of the variables analysed suggest the SMA as a more appropriate line-fitting method. However, it was decided to follow the recommendation by Legendre and Legendre [1998], based on the results of simulation studies, to use the MA if both variables are expressed in the same physical units.

SMA When changes in UV-Vis absorbance were plotted against WSOM concentrations the SMA was used to fit the data because of the different units in the y and x axes (Chapter 5).

If r^2 values are high the three line-fitting methods will give similar results. All line-fitting calculations were carried out using the 'lmodel2' package in R statistical software [R Development Core Team, 2011]. The results of these calculations were checked against the results from the 'scatterPlot' function using the 'openair' package [Carslaw and Ropkins, 2011] in R. This was done to ensure that the correct y and x assignments were made.

1.5 Project aims and thesis layout

This aims of this project were to compare different methods of PM measurement, and contribute understanding to the nature and origin of the carbonaceous fraction of PM. Chapter 2 describes the sampling of PM_{10} and the gravimetric determination of mass concentrations. Comparisons are made between three different sites in the Edinburgh area and potential PM_{10} sources are discussed. A comparison between two different PM_{10} sampling devices is also described. Chapter 3 discusses the determination of BC concentrations from optical reflectance measurements on PM_{10} filters and the results of this analysis. Chapter 4 describes the aqueous extraction of PM_{10} filters to obtain WSOM samples, the solid phase extraction (SPE) procedure carried out to obtain hydrophobic water-soluble organic matter (HWSOM) from these samples, and the measurement of their DOC concentration. Variations in H/WSOM concentration and potential sources are discussed. Chapter 5 describes the analysis of the HWSOM samples by ultraviolet-visible (UV-Vis) absorption spectroscopy and discusses a seasonal trend in the results. Chapter 6 examines the Raman microspectroscopy (RM) of carbonaceous reference materials and PM_{10} from the Edinburgh area. A summary of conclusions from the thesis and potential future work are presented in Chapter 7.

Chapter 2

Sampling of PM_{10} and analysis of concentrations

2.1 Introduction

Due to the health effects and climatic influence of airborne pollution, the United Kingdom (UK) is required to report air quality data, on an annual basis, under the following European Directives: The Council Directive on ambient air quality and cleaner air for Europe (2008/50/EC) [European Union, 2008]; and The Fourth Daughter Directive 2004/107/EC under the Air Quality Framework Directive (1996/62/EC) [European Union, 2004]. As part of this legislation, the levels of particulate matter (PM) with an aerodynamic diameter less than 10 µm (PM_{10}) should be monitored, in all relevant exposure locations, for comparison against Air Quality Standards (AQS). The Automatic Urban and Rural Network (AURN) is currently the largest automatic monitoring network in the UK and is the main network used for compliance reporting against the Directives. Data from the AURN are available on the Air Quality Archive website (`http://uk-air.defra.gov.uk`).

The measurements carried out in the AURN should be carried out using the reference method, as defined in the European Committee on Standardisation (CEN) standard EN12341 [CEN, 1999], or equivalent. PM_{10} monitoring in the UK was mainly based on the Tapered Element Oscillating Microbalance (TEOM) monitor, until it was shown that this is not equivalent to the reference method [Harrison et al., 2006]. The TEOM works by drawing air through a type-approved aerodynamic PM_{10} sampling inlet (which has a 50 % efficiency cut-off at 10 µm aerodynamic diameter) and measuring the mass of particles deposited on an oscillating microbalance (Figure 2.1). Benefits of the TEOM include: the generation of automated, real-time data; high time resolution (1 h or better); a response that is directly linked to mass; and greater precision than reference weighing

methods. Negative aspects of the TEOM are: the heated inlet and filter (50 °C), which can cause the loss of semi-volatile components compared with the reference method, leading to inaccurate results; high capital costs; and relative immobility.

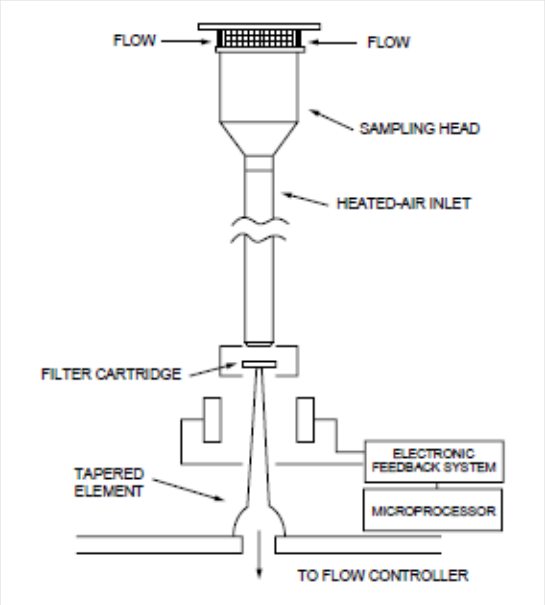

Figure 2.1: Schematic of a TEOM monitor developed by Rupprecht and Patashnick (taken from QUARG [1996]).

The measurement devices that are equivalent to the reference method (for example, the Partisol-Plus 2025 Sequential Air Sampler and a TEOM retrofitted with a Filter Dynamics Measurement System (FDMS)) also tend to be expensive and not portable. The Tapered Element Oscillating Microbalance Filter Dynamics Measurement System (TEOM-FDMS) is designed to reduce the inaccuracies of the standard TEOM system caused by the loss of semi-volatile components. The Partisol 2025 is a filter-based gravimetric technique that draws air through a type-approved aerodynamic sampling inlet (see image in Figure 2.2). Benefits of the Partisol are: the principle of absolute mass measurement; the filter storage and exchange system permits the operation of the device for up to 16 days of daily sampling between site visits; and the availability of the filter for analysis once the mass concentration has been measured. Negative aspects include: poor time resolution (24 h); data not being available until days or weeks after sampling; labour intensiveness; high operating costs; immobility; and problems with precision and accuracy caused by handling, humidity effects, etc.

Rigorous procedures of validation and ratification of the sampling and analysis undertaken in this project were important to ensure that the data obtained are of a sufficient quality. The established monitoring networks in the UK that operate to meet

Figure 2.2: A Partisol-Plus 2025 Sequential Air Sampler fitted with a PM_{10} aerodynamic sampling inlet (taken from the Partisol Operating Manual [Rupprecht & Patashnick Co., Inc., 1998]).

the European Directives each have a robust and documented quality assurance (QA) and quality control (QC) programme. This is to ensure that the data obtained are [Griffin et al., 2010]:

- Representative of ambient concentrations existing in the various areas under investigation.
- Sufficiently accurate and precise to meet specified monitoring objectives.
- Comparable and reproducible. Results must be internally consistent and comparable with international or other accepted standards, if these exist.
- Consistent with time. This is particularly important if long-term trend analysis of the data is to be undertaken.

- Representative over the period of measurement; for most purposes, a yearly data capture rate of not less than 90 % is usually required for determining compliance with EC Limit Values where applicable.

- Consistent with Data Quality Objectives. The uncertainty requirements of the European Union (EU) Directives are specified as data quality objectives. In the UK, all air quality data meet the data quality requirements of the EU Directives.

- Consistent with methodology guidance defined in EC Directives for relevant pollutants and measurement techniques. The use of tested and approved analysers that conform to Standard Method (or equivalent) requirements and harmonised on-going QA/QC procedures allows a reliable and consistent quantification of the uncertainties associated with measurements of air pollution.

2.2 Particulate matter sampling

Cleanliness and preventing the samples from being contaminated were key parts of the project. Specific procedures are mentioned in the relevant sections but some general points are made here. Gloves (purple nitrile or powder-free latex) were worn at all times in the laboratory or when handling filters in the field. All laboratory surfaces and equipment were wiped before use to remove dust. Plastic items used for the handling, storage and transport of filters were cleaned with deionised water (18 MΩ) and methanol (LC-MS), and dried overnight, before use. The names '10 MΩ' and '18 MΩ'' are used throughout this thesis to describe deionised water with resistivities of 10 MΩ cm and 18 MΩ cm, respectively.

2.2.1 Monitoring locations

Daily (midnight to midnight) samples of PM_{10} were collected from an Urban Background site (St Leonards; Elevation: 75 m; Ordnance Survey (OS) Grid Reference: NT263731; Figure 2.3) in central Edinburgh, using a Partisol-Plus 2025 Sequential Air Sampler (Rupprecht & Pataschnick Co., Inc., Albany, USA, now part of Thermo Fisher Scientific), from 20 August 2008 until 21 April 2010. A picture of the site, and the Partisol in operation at the site, are seen in Figure 2.4. Edinburgh is a city near the east coast of Scotland, with a population of $\sim 500,000$ and a relatively low level of heavy industry.

The site, which is part of the UK AURN, is located within a small park area, adjacent to a medical centre car park, with the nearest main road being ~ 35 m away (Figure 2.5). The air sampled here should be removed enough from most point sources to be broadly representative of city-wide background concentrations.

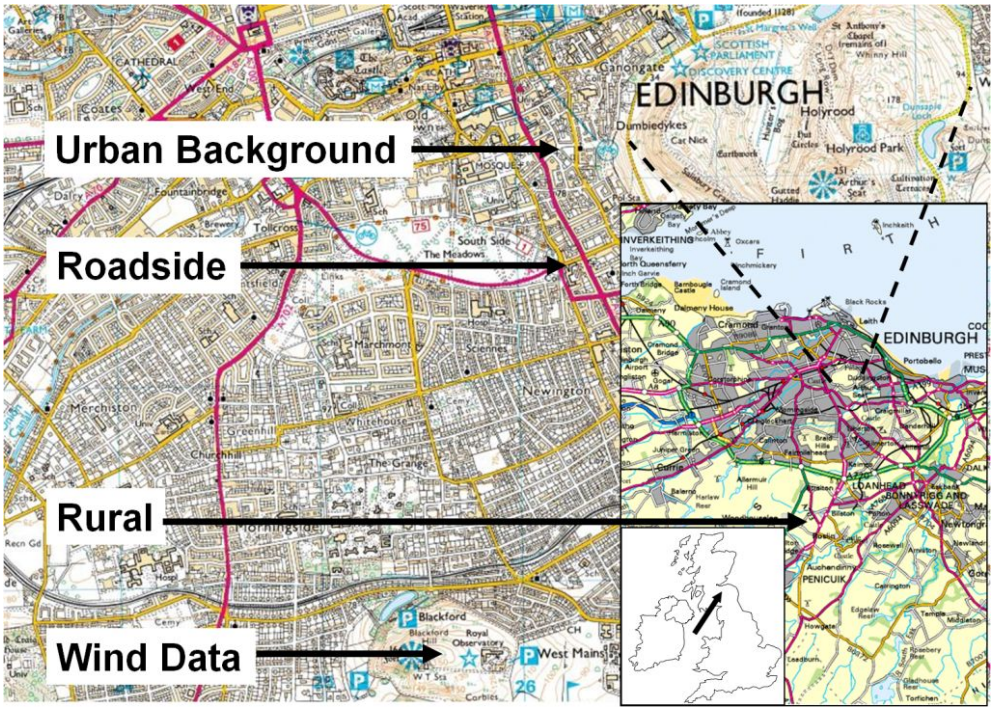

Figure 2.3: A map of Edinburgh and surrounding area showing the location of the monitoring sites used in this project.

A Rural site (Bush Estate; Elevation: 180 m; OS Grid Reference: NT246639; Figure 2.3), ~ 10 km south of the centre of Edinburgh, was used to test the air at a location distanced from population centres, roads and industrial areas (to coincide with a European Monitoring and Evaluation Programme (EMEP) aerosol monitoring campaign). EMEP is a European programme set up by Member States under the Convention on Long-range Transboundary Air Pollution to provide governments with qualified scientific information on air pollutants. This site, also part of the UK AURN, is located within the grounds of the Centre for Ecology and Hydrology (CEH). The surrounding area is generally open, with the nearest road being ~ 500 m away. Daily (midnight to midnight) samples of PM_{10} were collected from 25 February 2009 until 21 April 2009.

From 10 September 2009 until 21 April 2010, daily (midnight to midnight) samples of PM_{10} were also collected with a second Partisol 2025 gravimetric sampler from a Roadside site (Summerhall Place; Elevation: 75 m; OS Grid Reference: NT263726; Figure 2.3). This site, located next to the the Summerhall buildings of the Royal

(a) Urban Background location. **(b)** Partisol in operation.

Figure 2.4: Pictures of the Urban Background site.

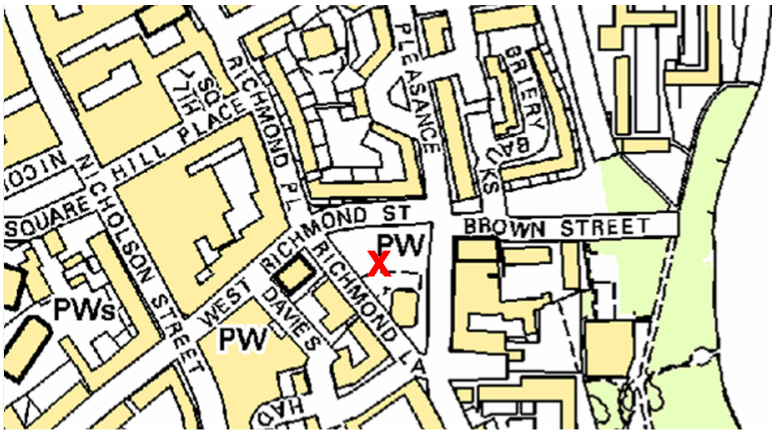

Figure 2.5: A map of the Urban Background site. The approximate location of the monitor is indicated by a red cross. Buildings are shown in yellow.

(Dick) School of Veterinary Studies, was within 7 m of a busy road junction, where two main roads intersect (Figure 2.6). The air sampled here should be influenced by the emissions associated with nearby traffic. A picture of the Partisol at this site is shown in Figure 2.7.

2.2.2 Operation of the Partisol-Plus 2025 Sequential Air Samplers

Two different Partisol samplers were used for this project. They were differentiated by their serial numbers: Partisol 9902 was used at the Urban Background site; Partisol

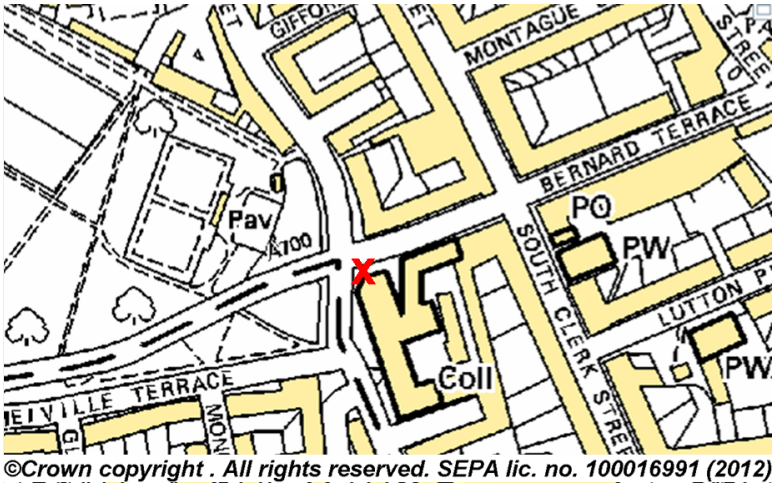

Figure 2.6: A map of the Roadside site. The approximate location of the monitor is indicated by a red cross. Buildings are shown in yellow.

Figure 2.7: A picture of the Partisol at the Roadside location.

9811 was used at the Rural and Roadside sites. These instruments were purchased for a previous project that analysed the metal content of PM samples from Edinburgh [Hibbs, 2002]. To ensure that the monitors were in full working order prior to sampling, a service was carried out by Air Monitors Ltd (a UK company specialising in air quality monitoring and management). Pre-calibrated instruments were used to validate the Partisols' operation. Test results were entered and the sampler automatically adjusted the corresponding offsets based upon these inputs. These instruments were then used to check that the Partisol flow-rates, and readings of temperature and pressure, were correct

(or within the allowed tolerance range, specified in the Operating Manual [Rupprecht & Patashnick Co., Inc., 1998]).

2.2.2.1 Partisol 9902 service

The unit was serviced, audited, calibrated and checked for leaks. The filter-exchange-unit top and bottom v-seals were replaced. Training was provided in the operation and routine maintenance of the monitor. Initially, a faulty flow sensor prevented the calibration of flow so this was replaced. The results of the checks, after any necessary repairs or adjustments, are shown in Table 2.1.

Table 2.1: Results of the Partisol 9902 service.

	Instrument	Measured	Error	Permitted Tolerance
Ambient Temperature (°C)	19.4	19.4	0.0	± 2
Filter Temperature (°C)	21.4	21.4	0.0	± 2
Ambient Pressure (mmHg)	740	740	0	± 10
Flow ($1\,min^{-1}$)	16.67	16.67	0.00 %	± 4 %

2.2.2.2 Partisol 9811 service

The unit was serviced, audited, calibrated and checked for leaks. The filter-exchange-unit top and bottom v-seals were replaced, and the PM_{10} head was cleaned. Initially, the automatic-filter-exchange mechanism was not working, due to poor pump pressure (< 20 psi), so the pump was rebuilt. This increased the pump pressure to 40 psi and fixed the filter-exchange mechanism. The results of the checks, after any necessary repairs or adjustments, are shown in Table 2.2.

2.2.2.3 Routine servicing and maintenance

Once the Partisol samplers were running it was important to carry out regular service procedures to maintain consistent performance. The procedures were carried out according to the instructions in the Partisol Service Manual [Rupprecht & Patashnick Co., Inc., 1998]. During a previous PM monitoring campaign it was determined by Hibbs

Table 2.2: Results of the Partisol 9811 service.

	Instrument	Measured	Error	Permitted Tolerance
Ambient Temperature (°C)	20.0	20.2	0.2	± 2
Filter Temperature (°C)	21.7	21.8	0.1	± 2
Ambient Pressure (mmHg)	740	740	0	± 10
Flow ($l\,min^{-1}$)	16.69	16.71	0.12 %	± 4 %

[2002] that the following verification procedures should be performed on a monthly basis:

1. Ambient Air Temperature
2. Filter Temperature
3. Ambient Pressure
4. External Leak Check
5. Flow Verification

This time-scale was chosen to ensure that adequate performance was maintained without being too labour intensive. The temperature probe used for the checks was validated against the instrument used by Air Monitors Ltd during the initial service. The temperature values were within 0.5 °C of the calibrated temperature probe. Sea-level pressure values (hPa) for Edinburgh were obtained from the History Data section of the Weather Underground website (`www.wunderground.com`). To compare these values with those of the Partisol the following conversion was used: 1 hPa = 0.750061 mmHg.

To ensure tightness during the external leak check, a filter cassette containing a new 47 mm filter (Figure 2.8a) was installed in the sampling position. The flow audit adapter was installed on the end of the sample tube and the valve was closed (Figure 2.8b). The check was controlled through the Partisol control screen, and a vacuum was automatically pulled once it was started. A fail message was displayed at the end of the leak check cycle if a pressure drop of more than 25 mmHg was detected. However, Air Monitors Ltd advised that a pressure drop of < 100 mmHg was acceptable as it did not cause a problem with the running of the instrument.

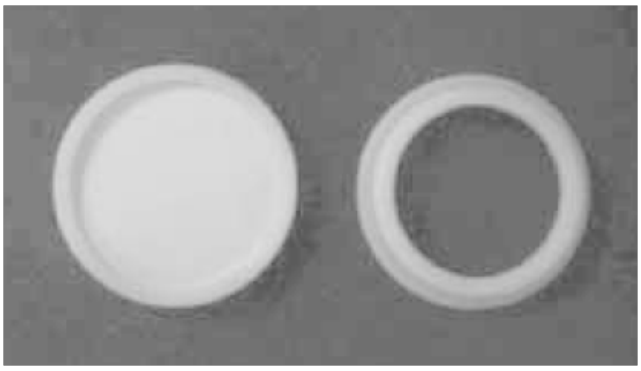

(a) 47 mm filter placed in the bottom section of a cassette (left). The top part of the cassette is shown on the right.

(b) Flow audit adapter, placed on the inlet tube, with the valve in a closed position.

Figure 2.8: Pictures of a filter cassette and flow audit adapter, take from the Partisol Operating manual [Rupprecht & Patashnick Co., Inc., 1998].

Flow was verified using a Streamline Flow Transfer Standard (FTS) flowmeter (Chinook Engineering, Wyoming, USA). The Streamline FTS is an orifice-type type flow-meter that determines flow rate from the pressure drop across the device. The FTS was installed on the external sample tube (Figure 2.9) and flow initiated from the Partisol's audit menu. Using the measured pressure drop, and local temperature and pressure values, the flow-rate was computed using the (National Institute of Standards and Technology (NIST)-traceable) calibration constants provided with the FTS.

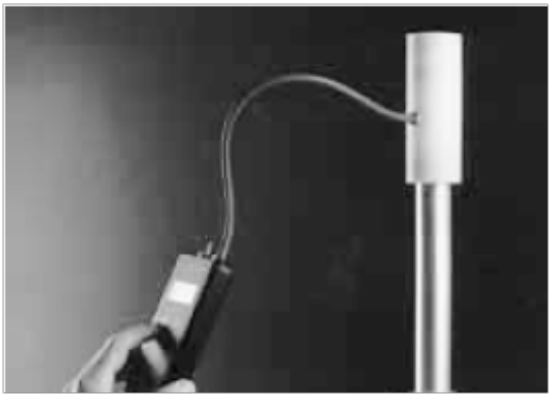

Figure 2.9: Streamline FTS installed on the external sample tube of the Partisol (image taken from the Partisol Operating Manual [Rupprecht & Patashnick Co., Inc., 1998]).

A summary of results of these verifications at the Urban Background site from 20 August 2008 until 21 April 2010 is shown in Table 2.3. All temperature, pressure and flow measurements were within the allowed tolerance limits. The majority of leak checks gave pressure drops less than 50 mmHg. On two occasions (17 June 2009 and 21 October 2009) the leak check failed (values of 227 and 155 mmHg, respectively). Both of these leaks were repaired by replacing perished v-rings.

Table 2.3: Summary of results of the Urban Background verification procedures from 20 August 2008 until 21 April 2010.

	Mean of Difference ($n = 17$) ($Instrument - Measured$)	SD of Difference ($n = 17$) ($Instrument - Measured$)	Permitted Tolerance
Ambient Air Temperature	$-0.9\,^{\circ}\mathrm{C}$	$0.4\,^{\circ}\mathrm{C}$	$\pm 2\,^{\circ}\mathrm{C}$
Filter Temperature	$0.7\,^{\circ}\mathrm{C}$	$0.4\,^{\circ}\mathrm{C}$	$\pm 2\,^{\circ}\mathrm{C}$
Ambient Pressure	-6 mmHg	2 mmHg	± 10 mmHg
Flow ($\mathrm{l\,min^{-1}}$)	1.27 %	0.62 %	± 4 %
External Leak	53 mmHg (Mean of Results)	55 mmHg (SD of Results)	< 100 mmHg

A summary of the results of the verification procedures at the Rural and Roadside sites, from 25 February 2009 until 21 April 2009 and 10 September 2009 until 21 April 2010, is shown in Table 2.4. All temperature, pressure and flow measurements were within the allowed tolerance limits. The majority of leak checks gave pressure drops less than 70 mmHg. On one occasion (1 October 2009) the leak check failed (value of 117 mmHg). This leak was repaired by replacing a perished v-ring.

The PM_{10} inlets were maintained by cleaning on a monthly basis. The inlet was taken apart; cleaned with deionised water (10 MΩ), cotton swabs, a small soft-bristle brush and paper towels; left to air dry; and reassembled; all according to the instructions in the Service Manual [Rupprecht & Patashnick Co., Inc., 1998]. The inlet was inspected for wear, and a thin film of silicone grease was applied to any O-rings and screw-threads to ensure a leak-free fit. 23 h of sampling must occur for a valid daily sample. It was therefore necessary for the validation and maintenance procedures to take less than an hour. To assist with this, a clean PM_{10} inlet was taken along on the monthly site visits and exchanged with the dirty one.

Table 2.4: Summary of results of the Rural and Roadside verification procedures.

	Mean of Difference ($n = 9$) ($Instrument - Measured$)	SD of Difference ($n = 9$) ($Instrument - Measured$)	Permitted Tolerance
Ambient Air Temperature	0.3 °C	0.6 °C	± 2 °C
Filter Temperature	1.0 °C	0.2 °C	± 2 °C
Ambient Pressure	−7 mmHg	2 mmHg	± 10 mmHg
Flow ($l\,min^{-1}$)	1.59 %	0.79 %	± 4 %
External Leak	51 mmHg (Mean of Results)	37 mmHg (SD of Results)	< 100 mmHg

The Partisol-Plus samplers contain two air intake filters, which clean the air-flow drawn into the instrument enclosures by fans. They were cleaned with a brush, after a six month period, to prevent blockages due to a build-up of dust.

The filter cassettes that hold the filters inside the Partisol were inspected for damage and cleaned (with deionised water (18 MΩ) and MeOH (LC-MS)) after each use. Any damaged filter cassettes were discarded. After cleaning, the cassettes were covered and left to dry overnight. They were added to a filter cassette magazine, which was then capped, placed in a metal transport container (Figure 2.10), and stored in a dark cupboard until use.

2.2.2.4 Particulate matter collection

Samples of PM_{10} were collected using the Partisol-Plus 2025 Sequential Air Samplers onto pre-baked (at 500 °C for 10 h) high-purity quartz (SiO_2) microfibre filters (47 mm diameter; QM-A; Whatman plc, Kent, UK). Typical filter thickness was 475 µm; typical mass is 87 $g\,m^{-2}$ (as specified). The filters were pre-baked to remove any organic contaminants that would interfere with future analysis. To prevent further contamination, the filters were wrapped in pre-baked (at 500 °C for 10 h) aluminium foil (Figure 2.11) and stored frozen (−30 °C) until they were required. Any filters that showed visible signs of damage were discarded. Quartz filters were used because of their thermal stability (which allowed them to be pre-baked without being damaged), high particle collection efficiency, and relatively low cost.

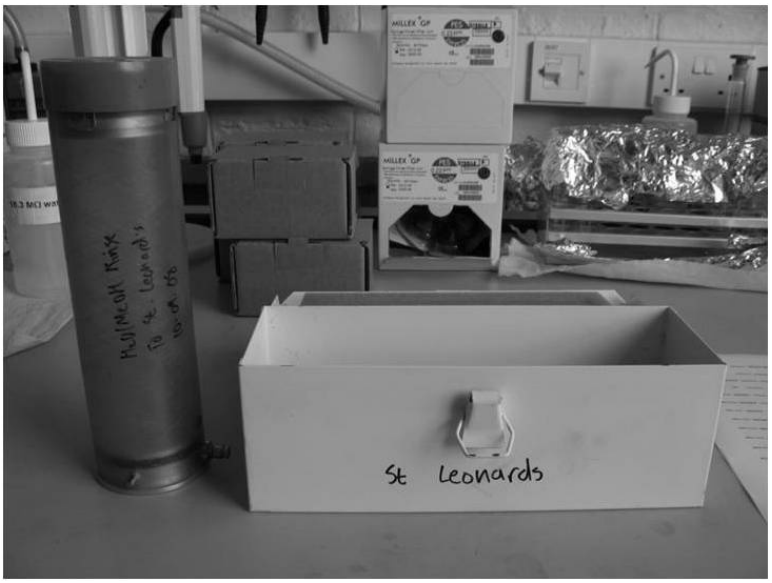

Figure 2.10: Filter cassette magazine (front left) and metal transport container (front right).

Figure 2.11: Pre-baked Whatman QM-A filters inside pre-baked aluminium foil, prior to storage in the freezer.

Prior to sampling, the filters were weighed (the weighing procedure is described in more detail in Section 2.3.1). For this they were removed from the freezer and transferred into polystyrene PetriSlides™ (Millipore, Billerica, USA), or Petri dishes, using plastic tweezers. The PetriSlides™, Petri dishes and plastic tweezers where cleaned the day before use with deionised water (18 MΩ) and MeOH (LC-MS), covered, and left to dry overnight. An image of the Petri dishes in the drying tray is shown in Figure 2.12a.

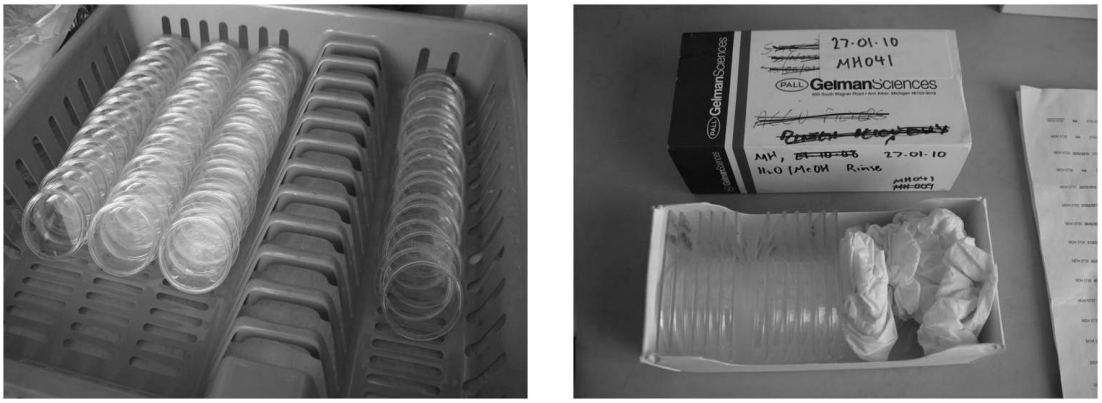

(a) Petri dishes on the drying tray, in the laboratory, prior to being covered and left overnight.

(b) Petrislides™ stored in a cardboard box, prior to tansport to the weighing location.

Figure 2.12: Pictures of PetriSlides™ and Petri dishes in use.

The filters were then stored in a cardboard box (Figure 2.12b) for transport to, and from, the weighing location (laboratory in the Department of Civil Engineering at the University of Strathclyde, Glasgow, Scotland). Once the filters had been weighed, and returned to Edinburgh, they were stored in a freezer (−30 °C) until required for sampling. The filters were then transferred into individual filter cassettes, and the cassettes transferred into the magazine. Each magazine could hold 16 filter cassettes. For each two-week sampling period, 14 daily PM_{10} samples could be collected along with 2 Machine Blanks. The Machine Blank filters were handled in exactly the same way as the sample filters, apart from the fact that no air was drawn through them during the sampling period. The Machine Blanks enabled the detection, and correction, of any physical, or chemical, changes that occurred to the filters during the processing period. One was placed near the top of the filter cassette magazine, the other near the bottom.

Once the cassettes were added to the magazine, it was placed in the metal transport container and transported to the monitoring location. The enclosure of the Partisol was opened and the magazine (with unexposed filters) was added to the left-hand mounting position (the 'supply tube', see Figure 2.13). It was important to ensure that

the air-pressure tube was attached to the supply tube, as this allowed the automatic filter-exchange mechanism to work. An empty magazine was added to the right-hand mounting position as the 'storage tube' (Figure 2.13). Each filter cassette had a unique identification-number which was entered into the Partisol's memory (in the order that the filters would be sampled). This allowed cross-referencing with the filter-code, date of sampling and volume of air sampled. It was also necessary to enter the identification-numbers of the Machine Blanks to prevent these from being sampled.

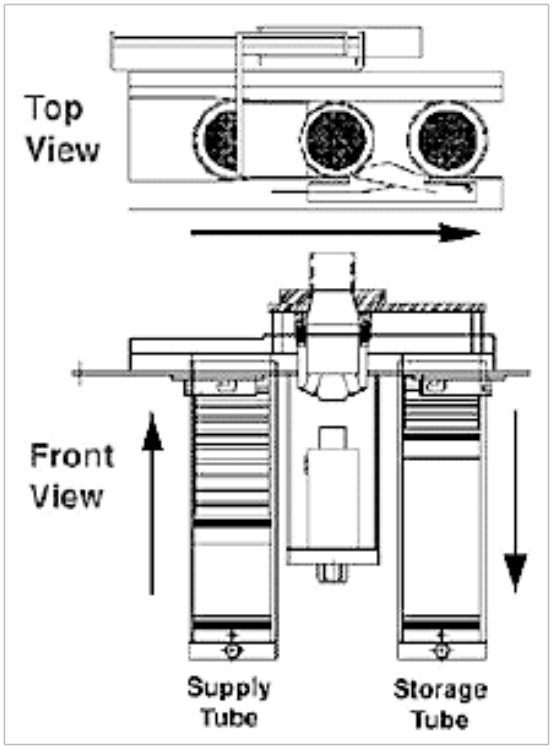

Figure 2.13: The Partisol-Plus Sampler's filter exchange mechanism (image taken from the Partisol Operating Manual [Rupprecht & Patashnick Co., Inc., 1998]).

The Partisol was set up to start sampling on the following midnight, and automatically exchange filters at every midnight thereafter. On the first midnight a filter would be automatically moved from the sample tube to the sampling position (Figure 2.13). On each subsequent midnight the next filter from the storage tube was moved into the sampling position, whilst the recently-sampled filter was moved into the storage tube. The Partisol flow-rate of $\sim 16.7\,\mathrm{l\,min^{-1}}$ meant that $\sim 1\,\mathrm{m^3\,h^{-1}}$ of air was sampled, which is equivalent to $\sim 24\,\mathrm{m^3\,d^{-1}}$.

After a two week period the supply tube would be empty and the storage tube full. A fresh supply of weighed, unexposed filters was taken to the monitoring location. The full storage tube was removed from the Partisol, placed in the metal transport container

and returned to the laboratory. The empty supply tube was moved to the storage position. The magazine containing the unexposed filters now became the supply tube. The magazines could be exchanged, and the relevant data entered, without stopping the Partisol. Data stored in the Partisol was downloaded onto a laptop.

Once back in the laboratory the exposed filters were removed from the magazine using a bulb pump (Figure 2.14a), and the filters removed from the cassette using a Cassette Separator Tool (Figure 2.14b). The filters were then transferred to the PetriSlide™, or Petri dish, that they came from and transported, in a cardboard box (Figure 2.12b), to the weighing location. After weighing, the filter boxes were returned to the laboratory and stored in a freezer (−30 °C) until further analysis was carried out.

(a) Use of a bulb pump and Cassette Removal Sleeve to remove filter cartridges from the magazine.

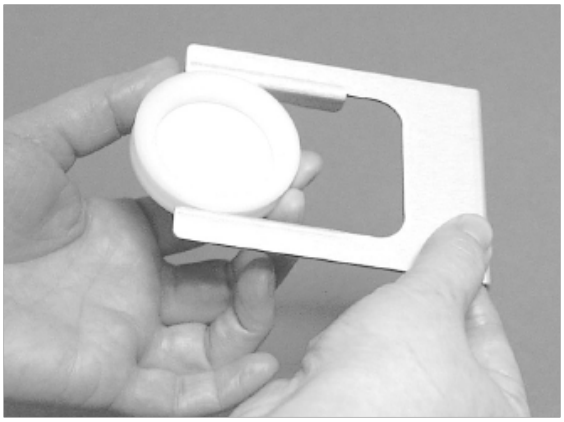

(b) Use of a Cassette Separator Tool to remove a filter from a cassette.

Figure 2.14: Pictures to show the removal of filters from a magazine (taken from the Partisol Operating Manual [Rupprecht & Patashnick Co., Inc., 1998]).

2.2.2.5 Sample errors

If there was an error with the Partisol (for example, failure of the automatic filter exchange mechanism) a small red light on the top of the unit would flash and an error code was displayed on the screen. Site visits usually only occurred every other week so it was possible that an error would not be noticed immediately and, therefore, a number of days worth of samples could be lost. Fortunately, site operators (SOs) from the City of Edinburgh Council were present at the Urban Background location on most days and could therefore report any errors with the Partisol. This allowed a relatively quick

response to any obvious problems. A summary of the errors that led to sample losses is shown in Table 2.5 and Figure 2.15.

Table 2.5: Summary of sampling days lost due to errors.

Partisol Number	Number of Days Sampling	Number of Days Lost	% of Days Lost
9902	610	34	6
9811	257	23	9

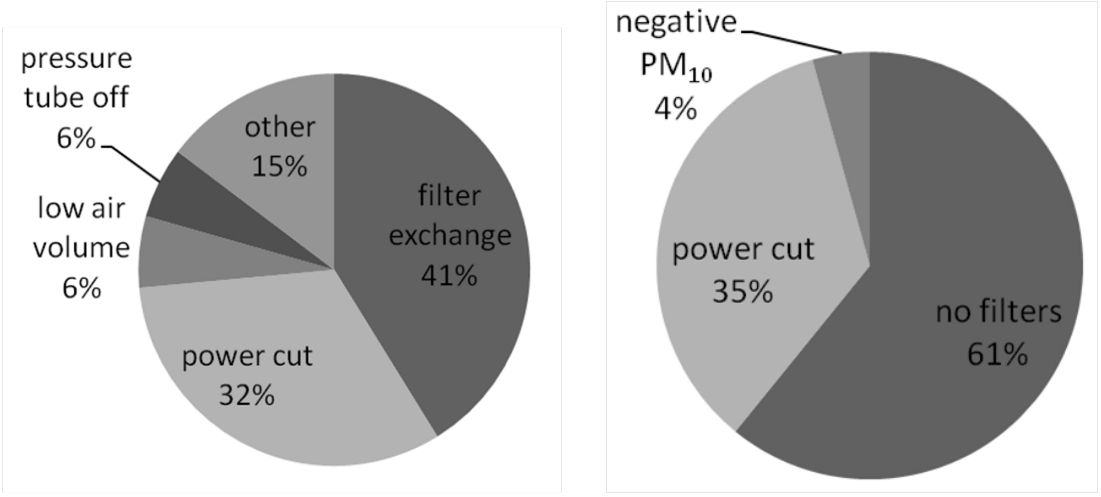

(a) Partisol 9902 (Urban Background). **(b)** Partisol 9811 (Rural and Roadside).

Figure 2.15: Summary of errors that led to sample losses.

At both sites fewer than 10 % of the sampling days were lost. At the Urban Background site the majority of the lost days were due to problems with the automatic filter exchange mechanism. This was a persistent problem at the beginning of the sampling campaign that was caused by the shape of the filter cassettes, and 14 sampling days were lost. After investigation into this problem, and advice from Air Monitors Ltd, it was discovered that the perpendicular corners (Figure 2.16) on the majority of the filter cassettes were catching in the mechanism and preventing the automatic change from taking place. To solve this, the corners of the cassettes were chamfered, as shown in Figure 2.16, to allow a smooth transition to occur.

The other major problem that happened at the Urban Background site was a power-cut on 3 May 2009. This was not noticed until 6 May 2009 and, although a site visit was made, it was not possible to get the Partisol running because the installed circuit-breaker

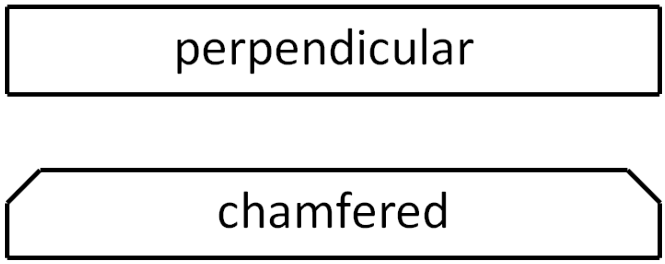

Figure 2.16: Representation of a cross-section of the filter cassettes to show the perpendicular and chamfered corner designs.

was not working. This was returned to the laboratory for repair and the Partisol was back in full operation on 14 May 2009. The power-cut caused 11 sampling days to be lost.

There was a power-cut at the Rural site on 4 March 2009 which caused a loss of 8 sampling days. Although power returned immediately to the site after the cut the Partisol did not automatically resume operation. It was not until the scheduled site visit, on 11 March 2009, that the instrument was switched back on to allow sampling to restart the following midnight.

A full two-week sampling period was lost at the Roadside site during the period from 24 September until 7 October 2009. A batch of pre-weighed filters was not available for this period, due to human error, and this could not be resolved until the next visit to the weighing facility.

2.3 Determination of PM_{10} concentration

Section 2.2 describes the use of Partisol-Plus 2025 Sequential Air Samplers to collect PM_{10} samples. In order to determine the PM_{10} concentration ($\mu g\,m^{-3}$) the mass of particles collected, and volume of air sampled, needs to be known.

2.3.1 Mass determination

Filter weighing was carried out in a laboratory in the Department of Civil Engineering at the University of Strathclyde. The balance and associated equipment were allocated bench space away from other laboratory instrumentation. The site was level, away from direct exposure to sunlight or heat, and removed from any drafts. An MC 5 micro-

balance (Sartorius AG, Goettingen, Germany), which had the following specifications, was used for filter weighing:

Weighing capacity = 5.1 g

Readability = 1 µg

Linearity $\leq \pm$ 4 µg

The Sartorius MC 5 had a separate weighing cell, with draft shield, and electronic computing device. The computing device was used to operate the balance and was attached to another computer to enable the automatic input of measured masses into an Excel spreadsheet. This automatic input of masses saved time and prevented errors that could arise from manually typing in the data.

The weighing protocol was adapted from the Satorius Micro Operating Instructions, and the protocols used by Hibbs [2002], and Butterfield and Quincey [2007]. The bench and weighing equipment were wiped clean with paper towels before use. The balance was levelled, switched on and left to warm up for 30 min before the weighing session started. To equilibrate the balance to laboratory conditions, the draft shield was opened and closed 3 times. A 20 mg calibration mass was then placed under the flow of an ionising blower (Stat-Attack, Static Solutions, Barnsley, United Kingdom) for 10 s to remove any static charges that could affect the balance's performance. Calibration masses were always handled with clean tweezers to prevent any contamination that would alter their mass. When not being used they were stored in a wooden container. The calibration mass was weighed 3 times, without recording the result, to exercise the balance.

Now the balance was ready to be calibrated. This was done in two stages:

Internal Linearisation The balance was unloaded and tared (with the draft shield closed). The linearisation was started, the built-in weights were internally applied (one after the other) by servomotor, and the balance was automatically linearised.

Internal Calibration The balance automatically self-calibrated after the internal linearisation procedure. The built-in calibration weights were internally applied by servomotor and removed at the end of calibration.

The Operating Instructions do not fully explain the difference between Linearisation and Calibration but give the following recommendation: "Relinearize your balance each time you set it up in a different area or recalibrate (re-adjust) it when the ambient conditions change (for example, temperature or barometric pressure). Even if these conditions are constant, the balance should be calibrated once a day. To meet the highest requirements for accurate weighing, we recommend that you calibrate the balance before each weighing series or set the isoCAL self-calibrating function to ON." As the balance was only being used once every two weeks it was decided to relinearise it before use. The "isoCal" function was used and the balance would self-calibrate under the following conditions:

- Two hours passed since the balance was turned on ("cold start")
- The difference between the current temperature and the temperature during the last calibration procedure was greater than ± 1 K
- (Up to) four hours passed since the last automatic calibration

2.3.1.1 Balance testing

In order to test the precision of the balance, a 20 mg (0.020000 g) F1 calibration mass was weighed, three times, at the beginning and end of each weighing session (the accuracy was confirmed by testing the mass on another balance). A calibration was performed before each three weighings. The means and standard deviations of these weighings over time are shown in Figure 2.17.

The highest standard deviation for one of the weighing sessions (i.e., worst-case scenario) occurred on 13 August 2009:

Mean	0.020004 g
Standard Deviation	1.63 µg
Number of Measurements	6

Assuming a normal distribution, the 95 % confidence intervals of this measurement were ± 1.30 µg, which is ± 0.01 % of the mean value. This highlights a high level of precision of the balance during each weighing session.

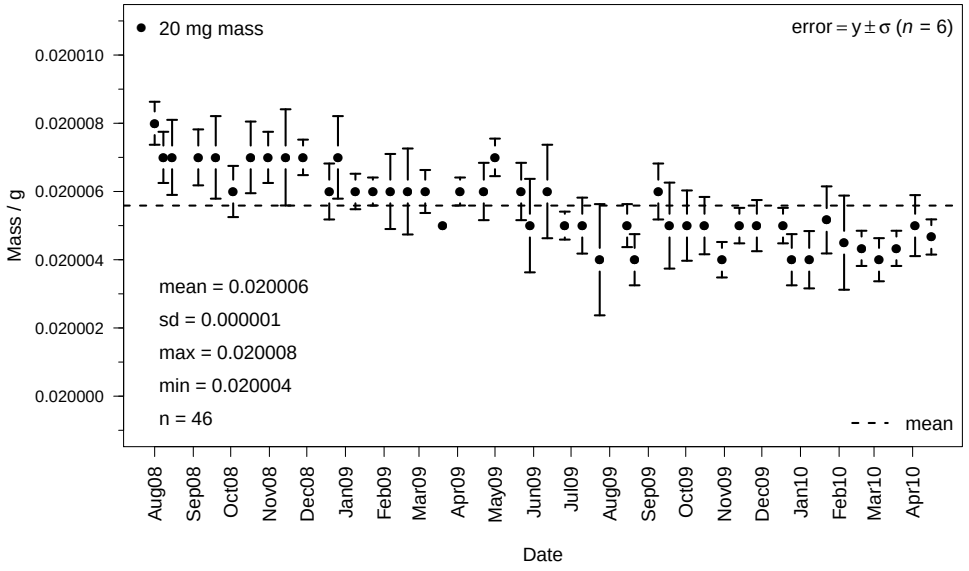

Figure 2.17: Results of weighing the 20 mg calibration mass. The black circles and error bars show the means and standard deviations of 6 measurements, respectively. Other values shown are the summary statistics for the means of the 46 weighing sessions.

For the 20 mg mass, the 46 measurement means are within 4 µg of each other (this range is 0.02 % of the mean), and the standard deviation of the 46 means is 1 µg. Although these values are relatively low, and are well within the tolerance of the F1 mass of 0.020000 ± 0.000030 g, the mean tended to decrease over time (Figure 2.17). This decrease suggests a potential systematic error in these measurements. Hibbs [2002] speculated that this mass may have been contaminated at some point in the past, with a fingerprint, for example. Repeated handling of the mass could slowly lead to the contamination being worn away, causing a steady decrease in the measured mass as seen in Figure 2.17.

A 200 mg (0.200000 g) F1 mass was also tested in the same way, i.e., weighed three times at the beginning and end of each weighing session, and the results are shown in Figure 2.18.

The majority of standard deviations ($n = 6$) are small, especially compared to the tolerance of the F1 calibration mass: 0.200000 ± 0.000060 g. However, there was a relatively large step-change in the mean mass of the 200 mg control. On 10 September 2009 the mass was cleaned due to some dust being present. This caused a decrease in mean mass of 5 µg compared to the previous measurement. On 29 September 2009 the mass was accidentally dropped before the final three weighings. This required further cleaning, which caused a further drop in mean mass of 3 µg, and a relatively large standard deviation of 4 µg (the mean of the 46 individual standard deviations is only

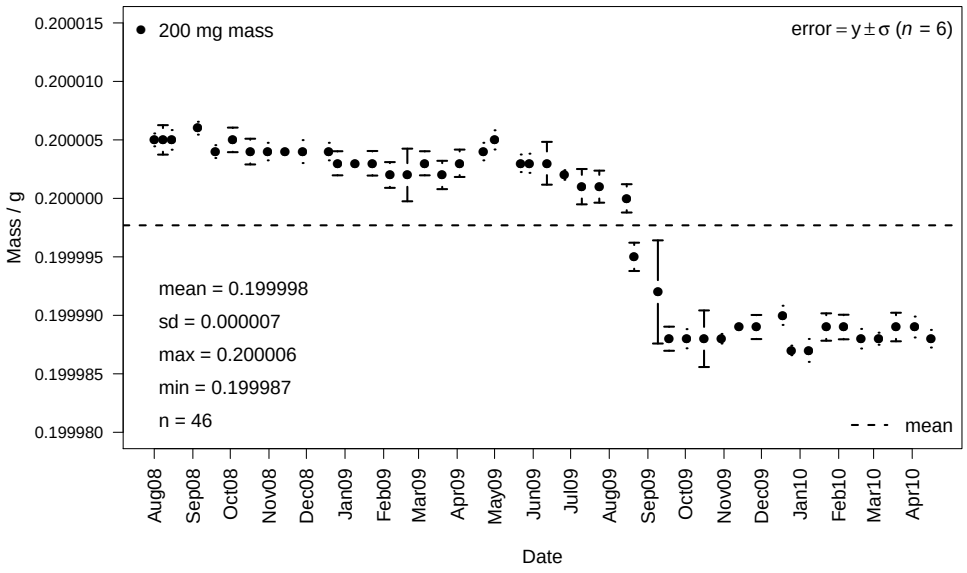

Figure 2.18: Results of weighing the 200 mg calibration mass. The black circles and error bars show the means and standard deviations of 6 measurements, respectively. Other values shown are the summary statistics for the means of the 46 weighing sessions.

1 µg). After these incidents the values for the 200 mg mass remained relatively stable (Figure 2.18), giving confidence in the precision of the balance. This observation could go some way to explaining the hypothesis for the mass loss of the 20 mg standard. The cleaning of the 200 mg mass after being dropped removed the potential for further mass loss from slow wearing away of some contamination. Routine cleaning of the masses was not carried out, in an attempt to prevent problems due to mass change. As some mass change over time was observed, in hindsight, routine cleaning may have been a better approach.

Some testing was done in Edinburgh to assess the accuracy of the balance used for filter weighing in Glasgow. The masses were weighed on a 6-figure balance in Glasgow and a 7-figure MC 5 micro-balance (Sartorius AG, Goettingen, Germany) in Edinburgh. The Edinburgh MC 5 balance had the following specifications:

Weighing capacity $= 2.1$ g

Readability $= 0.1$ µg

Linearity $\leq \pm\ 0.9$ µg

The Edinburgh balance was similar in design and operation to the balance routinely used in Glasgow, but with an improved specification. Results of weighing the 200 mg

and 20 mg test masses are shown in Table 2.6. For the 20 mg control, only the test in September showed a difference, which was only 1 µg. For the 200 mg control, the tests in April and September gave differences between the two balances of 2 µg, and 3 µg, respectively. Although a higher level of agreement between the two balances for the 200 mg mass would be ideal, there is no indication the the balance being used in Glasgow was inaccurate. Also, the low standard deviations of repeated measurements ($\leqslant 1$ µg) show that there was a high level of precision.

Table 2.6: Results of weighing the control masses in Edinburgh and Glasgow.

		200 mg		20 mg	
Date	Location	Mean ($n = 6$)	Standard Deviation	Mean ($n = 6$)	Standard Deviation
23/04/2009	Glasgow	0.200003	0.000001	0.020006	0.000000
29/04/2009	Edinburgh	0.200005	0.000000	0.020006	0.000000
10/09/2009	Glasgow	0.199995	0.000001	0.020004	0.000001
22/09/2009	Edinburgh	0.199998	0.000001	0.020005	0.000000

The decrease in mass of the 200 mg control between April and September, for the reasons already discussed, was also picked up by the balance in Edinburgh. This is further evidence that this was a problem intrinsic to the mass piece and not an indication of inaccuracy of the balance used for the routine weighing.

2.3.1.2 Filter checking

Successful implementation of mitigation measures, over a number of decades, has led to a decrease in PM concentrations in the UK [AQEG, 2005; Griffin et al., 2010]. Because of this, the mass of PM available to be measured is reduced, so factors affecting the accuracy of filter weighing (for example, dependence on humidity, or balance drift) have become more significant [Brown et al., 2006]. Quartz filters were selected for this project due to their compliance with the requirements of EN12341 [CEN, 1999] and suitability for the chemical analysis that would take place after weighing, although Maggs et al. [2009] subsequently concluded that quartz filters were less well suited to high accuracy determinations of PM mass than other materials.

It is well-known that humidity during weighing can affect the measured mass of PM. To deal with this issue, filters are often conditioned and weighed under controlled

conditions of humidity and temperature: $50 \pm 5\%$ relative humidity (RH) and $20 \pm 1\,°C$, for example. Temperature and humidity control was not possible in the laboratory used in this project so filters were stored and weighed in ambient conditions. The minimum and maximum temperature and humidity both between the 'conditioning' period and during each weighing session were recorded. Time series of these data are shown in Figure 2.19.

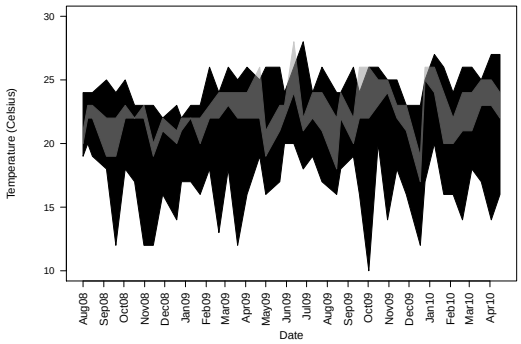

(a) Temperature range during the conditioning (black) and weighing (grey) periods.

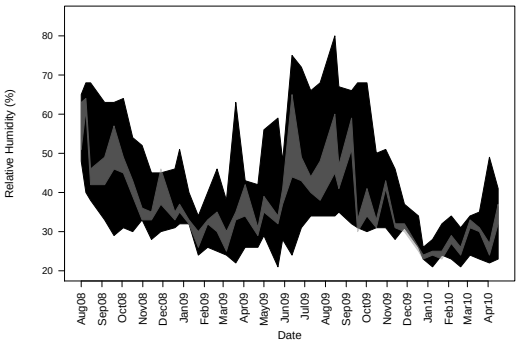

(b) RH range during the conditioning (black) and weighing (grey) periods.

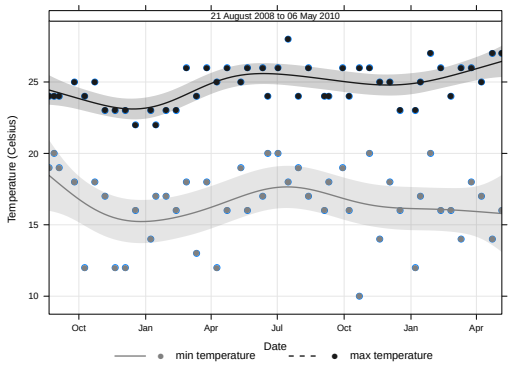

(c) Minimum and maximum conditioning temperatures, with a 'smoothed' line.

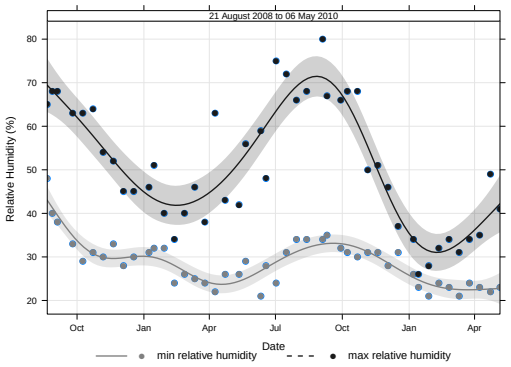

(d) Minimum and maximum conditioning RHs, with a 'smoothed' line.

Figure 2.19: Time series of temperature and RH changes in the weighing laboratory. 'Smoothed' lines are splines calculated using a general additive model by the openair package [Carslaw and Ropkins, 2011] in R [R Development Core Team, 2011].

It is clear from Figure 2.19a and Figure 2.19b that a wide range of temperatures and humidities were experienced in the laboratory between each weighing session (usually 2 weeks), but that the range was (unsurprisingly) lower during the actual weighing sessions (~ 6 h). A seasonal trend in temperature (highest in the summer; lowest in the winter) is observed in the laboratory, although not nearly as pronounced as the outdoor trend, due to central-heating, insulation, shading, etc. The variation in maximum

humidity is pronounced, which would be expected to have a noticeable effect on the masses of the quartz filters [Brown et al., 2006; Maggs et al., 2009].

To quantify this effect, the same six control quartz filters (Whatman, QM-A) were weighed in the middle of every weighing session. The balance was internally calibrated before these weighings began. A piece of pre-baked (500 °C; 10 h) aluminium foil was placed on the balance pan and the balance tared. The aluminium foil protected the filters from contamination and was useful for rapidly stabilising the effect of static charges [Brown et al., 2006]. Each filter was held under the anti-static blower for 10 s, then repeatedly weighed until the three values were within 5 µg of each other. The mean mass of these three weighings was calculated. The change in mass (current mass − original mass), from session to session, is plotted in Figure 2.20.

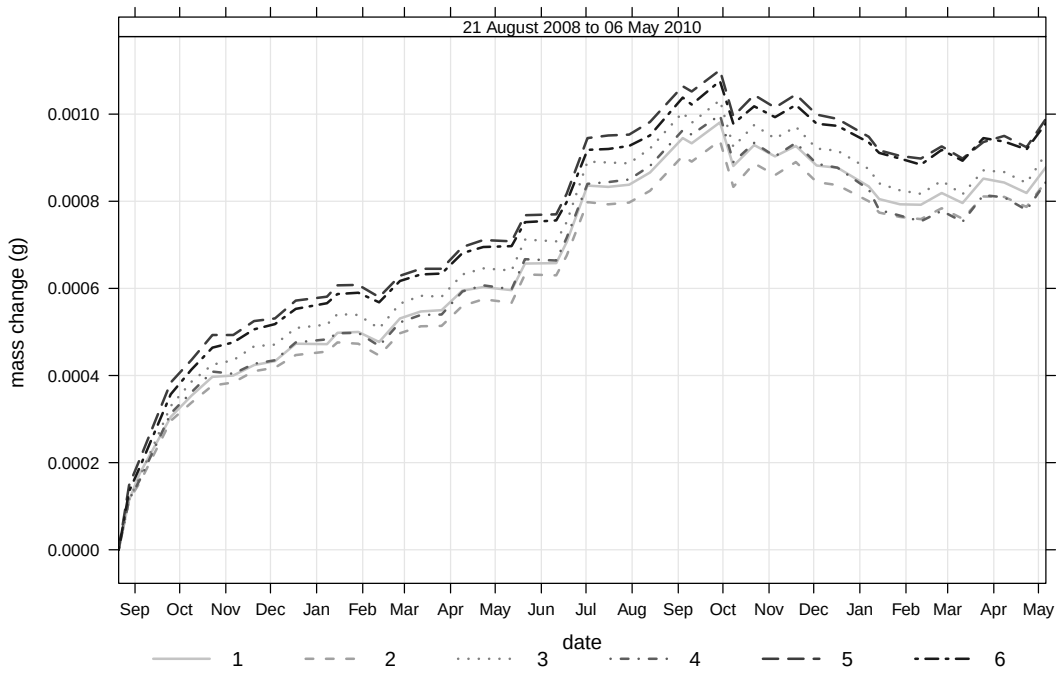

Figure 2.20: Time series of change in mean mass (current mass − original mass) of the 6 control filters. Standard deviations of each mean were so small that they are not plotted.

In general, the mass of each control filter increased over time. The initial mass increase was relatively rapid, by up to 0.4 mg in the first couple of months to October 2008. The mass increase was then slower, and the mass reached a maximum of ∼1.1 mg by October 2009. There was then a steady decrease and increase, giving a maximum mass change of ∼1.0 mg by May 2010. This shows that the filters took many weeks to equilibrate in the Glasgow laboratory. Although overall mass change varied slightly

with filter, Figure 2.20 shows that all of the filters had the same trend in mass change over time. This is confirmed by the scatter plots in Figure 2.21 of mass changes between individual filters. Although there are some differences, most of the mass changes were the same, regardless of which filter was weighed.

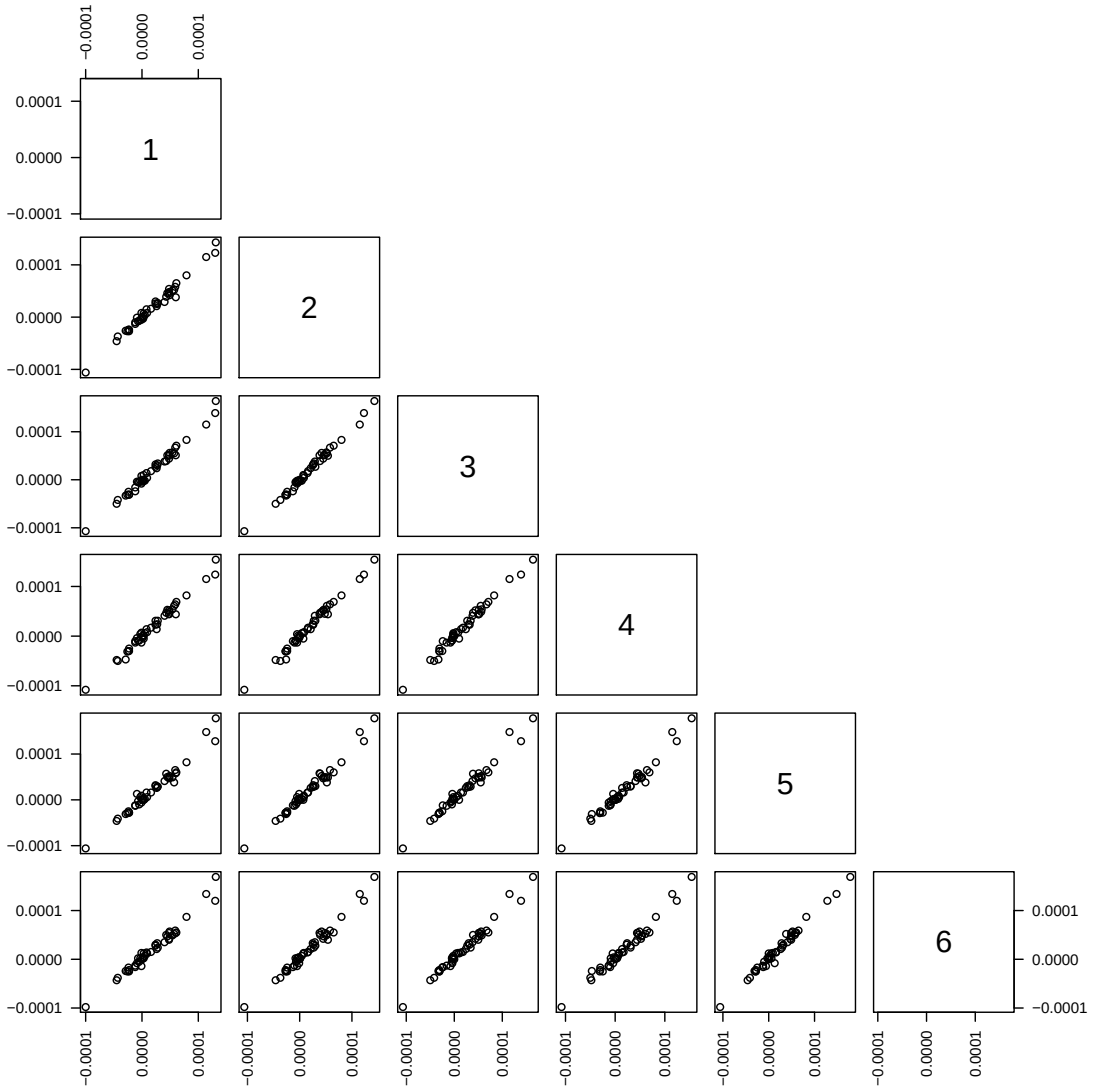

Figure 2.21: Scatter plots of change in mean mass (current mass − previous mass; g) of the 6 control filters.

Is this increase in mass, over time, caused by changes in humidity? This can be investigated by comparing the between weighing change in mass (current mass − previous mass) with the RH at the time of weighing (maximum RH value during weighing is taken). Figure 2.22a shows that high RHs tend to cause a mass increase (with higher RHs giving the highest increases), and lower RHs tend to cause a mass decrease. There is some scatter in this relationship but the $r^2 = 0.47$ suggests that

the humidity was having a causative effect. The explanation for this is that moisture was absorbed by, or released from, the filters depending on the RH. The ordinary least squares (OLS) relationship (Figure 2.22a) gives, on average, a 31 µg increase in filter mass for every 10 % increase in RH. This is higher than the value of 20 µg per 10 % increase in RH reported by Brown et al. [2006] for Whatman QM-A filters. The mean mass of PM_{10} collected at the Urban Background site was 351 µg. A 31 µg increase in filter mass from a 10 % increase in RH is, therefore, $\sim 9\%$ of the mass of PM_{10} on a typical filter sampled in this project.

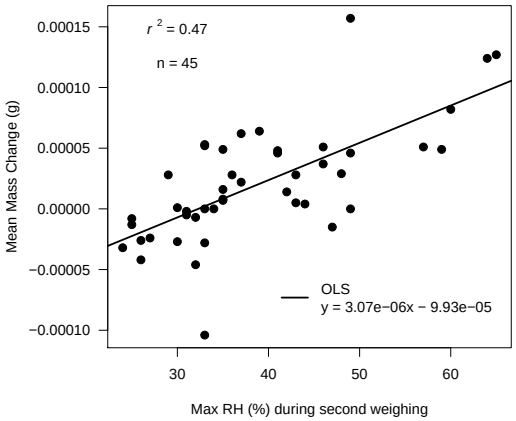

(a) Change in mean mass (current mass − previous mass) versus the maximum RH (%) at the time of weighing.

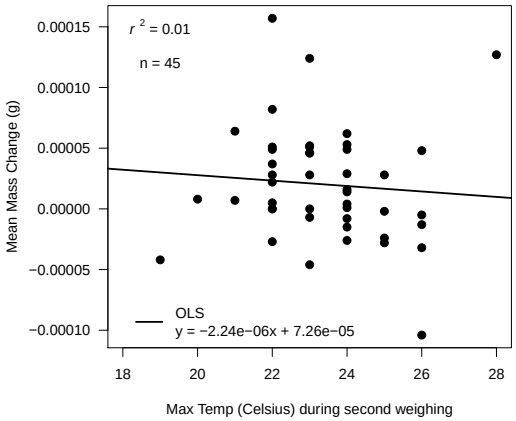

(b) Change in mean mass (current mass − previous mass) versus the maximum temperature (°C) at the time of weighing.

Figure 2.22: Scatter plots of control filter mass changes with RH and temperature. Points are the mean mass change of the 6 control filters.

The OLS relationship also shows that, on average, these filter mass should remain stable at $\sim 32\,\%$ RH. If it were possible, this would have been the ideal RH at which to store and weigh these filters. The conditioning parameters of 45–55% RH set out in the European standards [Brown et al., 2006] would have most likely caused an increase in filter mass over time. Of course, this is purely considering the behaviour of the filters themselves, not the additional effects of RH on the PM content of loaded filters. There was no apparent relationship between filter mass and temperature (Figure 2.22b). The outcome of this testing is that control filters should be included in each batch of sample filters to correct for any mass changes that occur with humidity. The control filters also permit compensation for any drift in the balance. This use of control filters is likely to be at least as important to accurate weighing than controlling the temperature and humidity of the weighing laboratory.

2.3.1.3 Sample filter weighing

The next stage in determining PM_{10} concentration was weighing the filters before and after sampling. Due to the size of a filter cassette magazine, and the need to have blank filters to adjust for mass changes in the filters themselves, a 'batch' would consist of 16 filters. This included 14 filters for the daily samples, which conveniently allowed two-week sampling period (i.e., a routine could be established where the Partisol was visited on the same day every other week) and 2 blank filters. The blank filters were designated 'Machine Blanks'. The Machine Blanks were handled, stored and tested in exactly the same way as the samples. To recap (from Section 2.2.2.4), after baking (at 500 °C for 10 h) in aluminium foil, the filters were wrapped in the aluminium foil and frozen (−30 °C) until they were required. They were then placed in clean PetriSlides™ (or Petri dishes) using clean plastic tweezers, the 16 PetriSlides™ were placed in a cardboard box, and the box transported the next day to the weighing laboratory in Glasgow. To coincide with the established sampling period, the box was left in the weighing laboratory, next to the balance, for 2 weeks of 'conditioning'. This was an attempt to let the filters equilibrate but, as illustrated in Section 2.3.1.2, this would actually take much longer than 2 weeks. The minimum and maximum temperatures and RHs were measured during this conditioning period (see results in Figure 2.19).

After the two week conditioning period, the 14 unexposed filters and 2 Machine Blanks were weighed. The weighing of the filters started after the calibration masses were weighed (see Section 2.3.1.1). Before filter weighing, an internal Calibration Test was carried out. Once this was started, the built-in calibration weights (5 g) were internally applied by servomotor. Afterwards, the deviation of the momentary weight readout from the target weight was indicated. If this value was $> \pm 2$ µg the balance was recalibrated.

Each filter was held under the anti-static blower for 10 s, then repeatedly weighed until three values were within 5 µg of each other. The values were automatically entered into a spreadsheet and the mean mass of these three weighings was calculated. After every six filters, the balance was checked with an internal Calibration Test. If the drift was $> \pm 2$ µg the balance was recalibrated. Also, to ensure the accuracy of the balance throughout the weighing process, the "isoCal" function was left on.

The day after weighing the filters were returned to the freezer (−30 °C) until they were required (in just under two weeks time) for PM sampling. After sampling, the exposed filters were transported to the weighing laboratory and the box was again left next to the balance for another 2 weeks of 'conditioning'. The filters were then weighed in

exactly the same way as described above for the unexposed filters. In principle the mass of PM_{10} (g) collected could now be calculated from the difference between the mean masses of the exposed and unexposed filters. However, as the mass of the quartz filters was likely to have changed over time, the mass change of the 2 Machine Blanks was subtracted from the measured PM_{10} mass (g; all sample filter masses are the means of 3 weighings; the Machine Blank masses are the means of 6 weighings):

$$\begin{aligned}\text{Corrected PM}_{10}\text{ Mass} &= (\text{Post-Sampling Filter Mass} - \text{Pre-Sampling Filter Mass}) \\ &- (\text{Post-Sampling Machine Blank Mass} - \text{Pre-Sampling Machine Blank Mass})\end{aligned} \tag{2.3.1}$$

Figure 2.23 shows that the mean mass change of the Machine Blanks tended to increase with an increase in RH. This matches the trend seen with the control filters but the correlation is not as good ($r^2 = 0.29$ versus $r^2 = 0.47$) and, on average, the magnitude of the change is greater (slope of 7.18×10^{-6} versus 3.07×10^{-6}). It is likely that the greater scatter in the mass change of the Machine Blanks was due to:

1. The greater range of conditions (of temperature and RH) that these filters experienced. Only the temperature and humidity in the weighing laboratory were being measured and used for this comparison, but the filters were also being moved between laboratories, and stored in a freezer and Partisol monitor.

2. The longer period of time between weighings and the possible changes in ambient conditions during this period of time. The control filters were generally weighed every two weeks. After the first weighing of the Machine Blank filters, they were frozen for two weeks, left in a Partisol for two weeks, and 'conditioned' in the weighing laboratory for two weeks, before being weighed again (i.e., there was a six week period between weighings).

The length of time between weighings could also explain the greater magnitude of mass change in the Machine Blanks. In general, the mass of filters increases due to the intake of moisture, and as more time passes the mass tends to increase (Figure 2.20). Also, the rate of mass increase tends to be greatest during the beginning of the 'conditioning' period (Figure 2.20). All of the weighings of Machine Blank filters were at the beginning of this period, compared with the control filters that were measured continuously.

A summary of the between weighing mass changes of the Machine Blank filters, at all of the sites, is shown in Table 2.7. The average mass increase at the Urban Background site was 253 µg. There was a lot of variation in the mass change of the Machine Blanks, however, as reflected by the standard deviation, and minimum and maximum values.

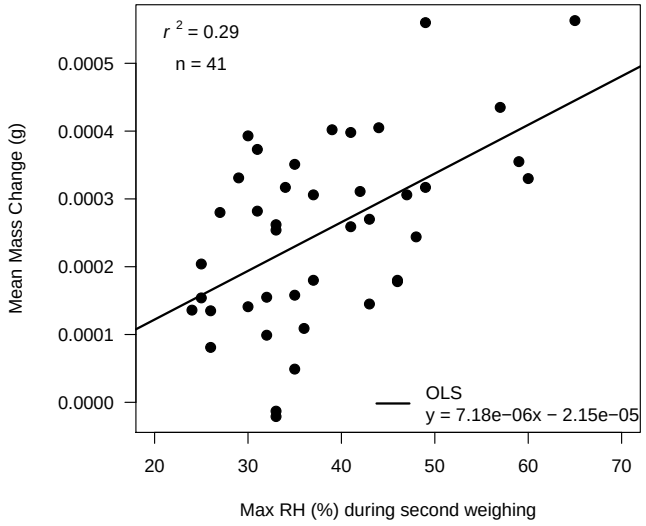

Figure 2.23: Scatter plot of the between-weighing change in mean mass (current mass − previous mass; g) of the two Machine Blank filters from the Urban Background location versus maximum RH in the weighing laboratory at the time of weighing. Rural and Roadside Machine Blanks have not been plotted as fewer measurements were made.

Also, the masses determined for the Rural and Roadside sites had their own variability (which was mainly due to the number of samples and when they were measured). This shows that having Machine Blank filters in each batch of measurements is necessary to make accurate corrections.

Table 2.7: Summary of Machine Blank filter mass changes between weighing.

Mass	Urban Background	Rural	Roadside
Mean / g	0.000253	0.000376	0.000204
SD / g	0.000136	0.000034	0.000091
Min/ g	-0.000021	0.000335	0.000023
Max/ g	0.000563	0.000413	0.000400
n	41	4	15

2.3.2 Flow rate

The final stage in the determination of PM_{10} concentration ($\mu g\,m^{-3}$) was the measurement of daily air flow in the Partisol. The flow rate of the Partisol monitors was checked on a monthly basis to ensure that the flow-rate measurements were accurate.

This was set at $16.7\,\mathrm{l\,min^{-1}}$ to collect $24\,\mathrm{m^3}$ of air per day. If during the monthly check the measured flow-rate was $> \pm 4\%$ from the measured value, then the monitor would be re-calibrated. However, this never happened. A daily sample would not be counted if $< 23\,\mathrm{m^3}$ of air was sampled. Table 2.8 shows a summary of the daily volumes of air sampled by the Partisols at the different monitoring sites.

Table 2.8: Summary of daily Partisol volumes of air sampled.

Flow	Urban Background	Rural	Roadside
Mean / $\mathrm{m^3}$	23.94	23.99	24.00
SD / $\mathrm{m^3}$	0.10	0.04	0.04
n	555	49	195

The mean daily volume of air sampled by the Partisol at the Urban Background site was 0.25 % away from the ideal of $24\,\mathrm{m^3}$. At a 95 % confidence level the daily volume of air sampled by this monitor was 23.93–23.95 $\mathrm{m^3}$. The monitor used at the Rural and Roadsite sites had even more accurate and precise volumes.

2.4 Results and discussion

The daily PM_{10} concentration ($\mathrm{\mu g\,m^{-3}}$) was calculated by using the volume of air sampled ($\mathrm{m^3}$), as derived from the measured flow rate ($\mathrm{l\,min^{-1}}$), to convert the PM_{10} mass (Equation (2.3.1); in g), as shown in the following equation:

$$PM_{10}\ \text{Concentration} = \frac{PM_{10}\ \text{Mass} \times 1,000,000}{\text{Sampled Volume}} \tag{2.4.1}$$

2.4.1 Data capture

PM_{10} concentration was calculated for as many days as possible, at all the sites. Unfortunately, complete data capture did not occur for the following reasons: filter exchange error; power-cut; no filters; leaving the pressure hose off the filter magazine; low air volume; filter damage; negative PM_{10} concentration; and stopping the Partisol monitor to adjust the time. The data capture for the project is summarised in Table 2.9.

Table 2.9: Record of PM_{10} concentration data capture at the three monitoring locations.

	Urban Background	Rural	Roadside
Days Sampling	610	56	224
Number of Samples	576	48	209
Data Capture %	94	86	93

AEA (a global sustainability consultancy) carry out the QA and QC activities for the AURN on behalf of the UK Department for Environment, Food and Rural Affairs (Defra), Scottish Government, Welsh Assembly Government and Department of the Environment (DOE) in Northern Ireland. In a recent report by AEA [Eaton, 2011], the ratified data-capture (%) by quarter in 2010, for PM_{10}, was: Q1 = 85.1; Q2 = 81.0; and Q3 = 77.5. This was an average for all sites in the AURN. Data capture rates were calculated using the actual data capture as daily averages against the total number of days in the relevant period; service and maintenance were counted as lost data [Eaton, 2011]. All of these values were below the required 90 % target. In this project, data capture at the Urban Background and Roadside sites were > 90 %, which can be viewed as being good. The poorer data capture at the Rural site was mainly due to a power-cut at the beginning of the measuring campaign. This was not spotted quickly and had a large impact on the relatively short measuring period. If the campaign were longer, more days of successful sampling would have improved the data capture. Overall, the performance of the Partsiol samplers used in this project was satisfactory.

2.4.2 Mass concentration

A summary of the PM_{10} mass concentration ($\mu g\,m^{-3}$) from all of the sites is shown in Table 2.10.

PM_{10} concentrations are reported to the nearest integer, as this is the level of precision used in reports from the AURN. Although higher precision and accuracy was demonstrated in the balance used for weighing, and in the flow-rate measurements, the variation in filter mass over time (plus the potential for the loss/gain of semi-volatile material from/to the PM) means that an integer value is an appropriate level of reporting precision.

Table 2.10: Overview of PM_{10} mass concentrations at all of the monitoring sites.

PM_{10} Concentration	Urban Background	Rural	Roadside
Mean / $\mu g\,m^{-3}$	15	14	18
SD / $\mu g\,m^{-3}$	8	10	9
Minimum / $\mu g\,m^{-3}$	1	2	3
Maximum / $\mu g\,m^{-3}$	58	42	53
n	576	48	209

Griffin et al. [2010] reported that, for the UK network overall, the annual mean PM_{10} concentration for 2009 was $19\,\mu g\,m^{-3}$ at urban background sites, and $22\,\mu g\,m^{-3}$ at roadside sites. The mean PM_{10} concentration measured in this work for 2009 in Edinburgh was $15\,\mu g\,m^{-3}$ at the Urban Background site (the annual mean for 2009 is the same as the mean for the whole sampling period shown in Table 2.10). PM_{10} concentrations in Edinburgh were lower than the national average. Measurements for the whole of 2009 were not made at the Roadside site so a comparison with the UK average cannot be made. The mean PM_{10} concentration for the whole of the sampling period at the Roadside site in Edinburgh ($18\,\mu g\,m^{-3}$) was also lower than the UK average for 2009.

For a more meaningful comparison of the PM_{10} results it would be necessary to provide some quantitative indication of their quality. A generally accepted procedure for characterising the quality of the result of a measurement is presented in the Guide to the Expression of Uncertainty in Measurement (GUM) [Joint Committee for Guides in Metrology, 2008]. This is done by expressing the result of a measurement as an estimate of the measurand along with an associated measurement uncertainty. The GUM describes uncertainty as consisting of several components that can be grouped into two categories, depending on how their numerical value was estimated:

1. statistical methods

2. other means

Each input into the value of the measurand will have an estimated value and an uncertainty associated with it. These uncertainties can be evaluated as described in the GUM and used to determine a combined uncertainty. Reporting the measurement result along with the combined uncertainty should provide a range of values that could

be reasonably attributed to the measurand, but it may be necessary to multiply the combined uncertainty by a coverage factor to increase confidence in this range.

2.4.3 Site inter-comparison

The daily PM_{10} concentration is variable but with the same trend being followed at the different monitoring locations (Figure 2.24). This suggests some commonality in sources of PM and of meteorology across the sites. It would be expected, due to a direct influence from traffic-related emissions, that noticeably higher values would be seen at the Roadside site and lower values in a Rural location.

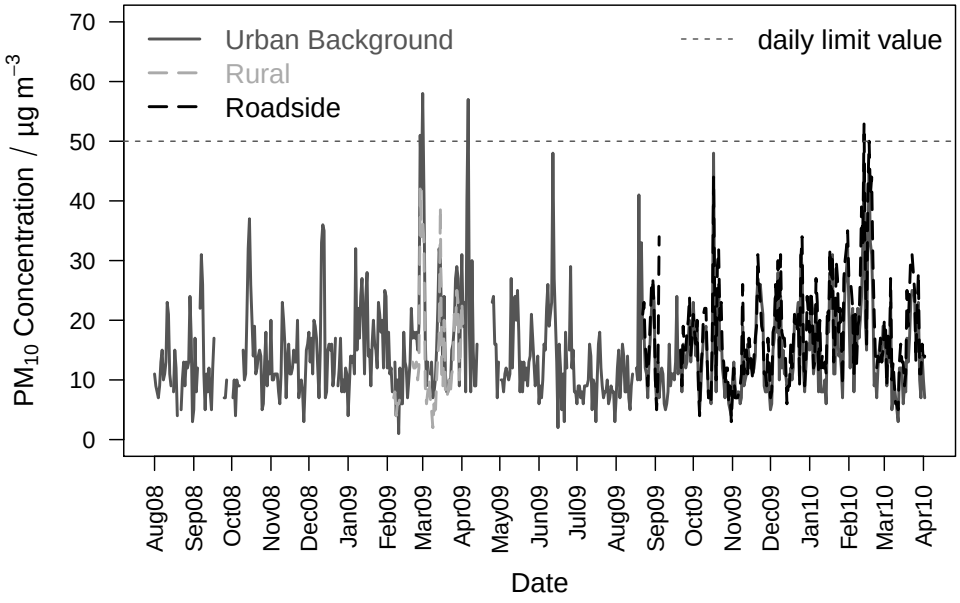

Figure 2.24: Time series of daily PM_{10} measurements from the three monitoring sites.

A clearer picture of the relationships between PM_{10} concentrations at the different sites is shown in Figure 2.25. The linear correlation between PM_{10} mass concentration at Rural and Urban Background sites is good ($r^2 = 0.85$; Figure 2.25a), which suggests similar sources of PM or meteorological factors affecting the sites. On the majority of occasions when the level of Rural PM_{10} was high so was Urban Background PM_{10} (and vice versa). This indicates that most of the PM_{10} in Edinburgh was due to the general background concentration, rather than sources within the city. There were still some PM_{10} sources (e.g., traffic and industry) within the city at the time of this comparison: most of the points in the plot are below the $y = x$ line and the gradient of the major axis relationship is < 1 (Figure 2.25a). The average of the Urban Background PM_{10}

concentration increments (Urban Background – Rural) of 4 µg m^{-3} is an indication of the amount of PM_{10}, on average, that came from urban sources in Edinburgh, which is $\sim 30\%$ of the mean Urban Background PM_{10} concentration.

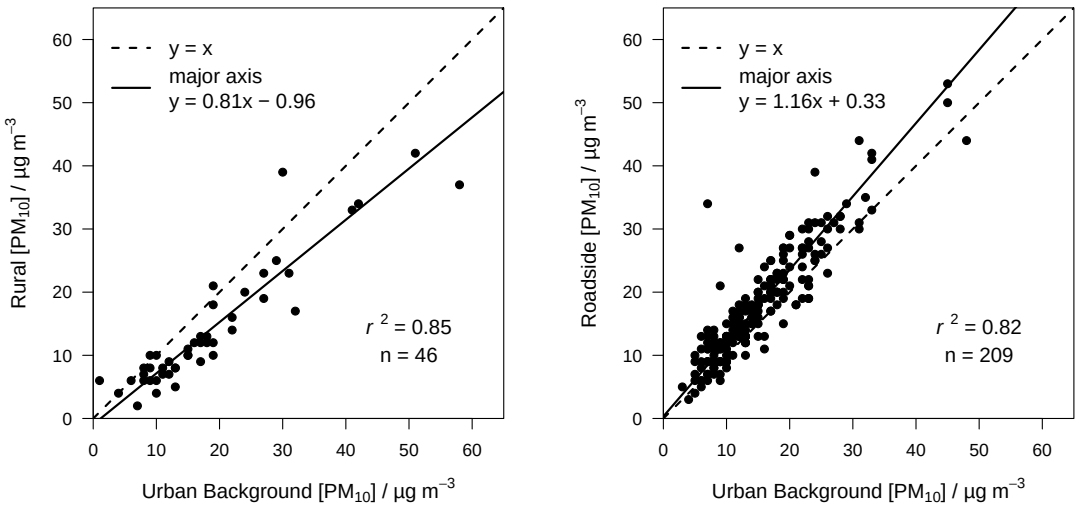

(a) Rural versus Urban Background **(b)** Roadside versus Urban Background

Figure 2.25: Scatter plots of daily PM_{10} measurements from the three monitoring sites.

The particulate pollution levels at the Roadside site would be expected to be higher than at the Urban Background site due to emissions from vehicle exhausts and re-suspension of road dust. PM_{10} concentrations at both sites are more similar than perhaps expected and there is a good linear agreement at both sites ($r^2 = 0.82$; Figure 2.25b). This shows that when PM_{10} was high at one site it was high at the other (and vice versa), and most of the PM mass was from the same location and controlled by common meteorology. Direct traffic emissions do not appear to have a large impact on the PM_{10} concentration, although the levels at the Roadside site are higher by 16% on average (as shown by the major axis slope of in Figure 2.25b). The average of the Roadside PM_{10} concentration increments (Roadside – Urban Background) of 3 µg m^{-3} is an indication of the amount of PM_{10}, on average, that came from traffic sources. This is considerably lower than the roadside mass increment of 11.5 µg m^{-3} for PM_{10} reported by Harrison et al. [2004].

The lower average roadside increment in this work could be due to lower traffic volumes in Edinburgh compared with London/Birmingham [Harrison et al., 2004]. The PM_{10} sampler in Edinburgh was also further from the kerbside (within 7 m) than those used in the analysis by Harrison et al. [2004] (within 1 m), which could lead to some of the vehicle-related PM not being sampled. Traffic sources of PM_{10} would also be missed if the wind was not coming from the road so it is possible that wind direction, possibly

influenced by the close proximity of buildings (see the map in Figure 2.6), is the reason for a lower roadside increment in Edinburgh. Harrison et al. [2004] found traffic-related elemental carbon (EC) to contribute an average of 6.5 µg m^{-3} to the roadside PM_{10} increment so there was a clear influence from exhaust emissions. Improvements in vehicle emission abatement since 2000–2002, when the samples from London/Birmingham were collected [Harrison et al., 2004], could explain the lower roadside increment found during this project in Edinburgh (as samples were collected from 2008–2010).

In summary, although the same time periods are not being compared, the expected trend of mean PM_{10} concentrations (Rural < Urban Background < Roadside; Table 2.10) is apparent for the Edinburgh monitoring sites, even if the differences in magnitude are not large. As the Rural site was distanced from population centres, roads and industrial areas (i.e., major sources of PM_{10}) the PM_{10} concentration here should be the lowest. Although the Urban Background location should be distanced from sources of PM_{10}, city-wide background concentrations were higher than at the Rural site due to the fact that the monitor was closer to these sources (i.e., roads and industrial areas). The Roadside site was next to a busy road junction, so the higher PM_{10} concentrations were due to direct traffic sources.

2.4.4 Limit values

The Griffin et al. [2010] report showed that ambient levels of PM_{10} were below the long-term limit values for the protection of human health (annual mean of 40 µg m^{-3}) throughout the UK in 2009. The Urban Background mean PM_{10} concentration in Edinburgh for 2009 was well below this level, and below the stricter AQS Provisional Objective of 18 µg m^{-3} in Scotland (which was to be achieved by 31 December 2010). Although annual means are not available for the Edinburgh Rural and Roadside sites, the results in Table 2.10 suggest the the limit value would not be exceeded.

According the the European Directives, the 24 h mean limit value for PM_{10} concentration is 50 µg m^{-3} and this should not be exceeded on more than 35 days per year (with the stricter AQS Provisional Objectives only allowing up to 7 exceedances per year). A time series of the PM_{10} concentrations from the three monitoring sites (Figure 2.24) shows the 24 h mean limit value for PM_{10} concentration being exceeded on 4 occasions (Urban Background on 18 March 2009, 20 March 2009, and 25 April 2009; Roadside on 4 March 2010). On 8 March 2010 at the Roadside site the PM_{10} concentration was 50 µg m^{-3}. There were no exceedances at the Rural site, but the monitoring period here was relatively short.

The first two of the Urban Background PM_{10} exceedances occurred during an episode (concentration $\geqslant 40\,\mu g\,m^{-3}$) extending from 18 March 2009 to 21 March 2009. This episode was also picked up at the Rural site but the concentrations were lower. Air mass back-trajectory plots of this period (Figure 2.26a) show that the air arriving at the Urban Background site had passed over the north of France and Benelux (Belgium, Netherlands and Luxembourg) regions, and tended to re-circulate over the UK. Griffin et al. [2010] showed a build-up of PM over northern France and Benelux on 16 and 17 March. It is likely that this PM was picked up and transported to the UK, with the re-circulation of air over the UK prolonging the elevated levels of PM_{10}. The air arriving at the Urban Background site before (17 March 2009) and after (22 March 2009) this pollution episode, when the air was cleaner, had followed a trajectory over the Atlantic ocean (Figure 2.26b). This is further evidence that the 18–21 March pollution episode was caused by transport from mainland Europe.

The next exceedance at the Urban Background site happened during another PM_{10} episode (concentration $\geqslant 40\,\mu g\,m^{-3}$), from 24–25 April 2009. Similar to the episode in March 2009, air arriving before and after the event had travelled over the Atlantic ocean (Figure 2.27). For the two days of the pollution episode, there is evidence of recirculation of air over the UK and conditions that would allow the long-range transport of pollution from Europe (Figure 2.27). For an episode earlier in April 2009, detected elsewhere in the UK, European PM forecasting models suggested that the elevated levels were due to long-range transport of a combination of secondary pollution from Europe, smoke from agricultural fires in western Russia, and dust from sandstorms over northern Africa [Griffin et al., 2010]. Due to the direction of travel of the air masses, similar sources are likely for the event seen at the Urban Background site later in April 2009. Also, stable weather conditions would help the build-up of PM pollution due to poor dispersion of local emissions.

The final exceedance ($53\,\mu g\,m^{-3}$) observed in this monitoring campaign was at the Roadside site on 4 March 2010. There were also PM_{10} concentrations above $40\,\mu g\,m^{-3}$ at the Urban Background site on 4 March and at the Roadside Site on 7–10 March 2010. This time, the air-mass back trajectories provide no evidence of long-range transport of PM from Europe (Figure 2.28). The air arriving over Scotland during this period was generally from the north Atlantic and should be relatively clean. However, stagnant and dry conditions, present at the time, would prevent the dispersion of local PM emissions and lead to an increase in concentrations, especially close to sources (i.e., busy roadsides) as seen here.

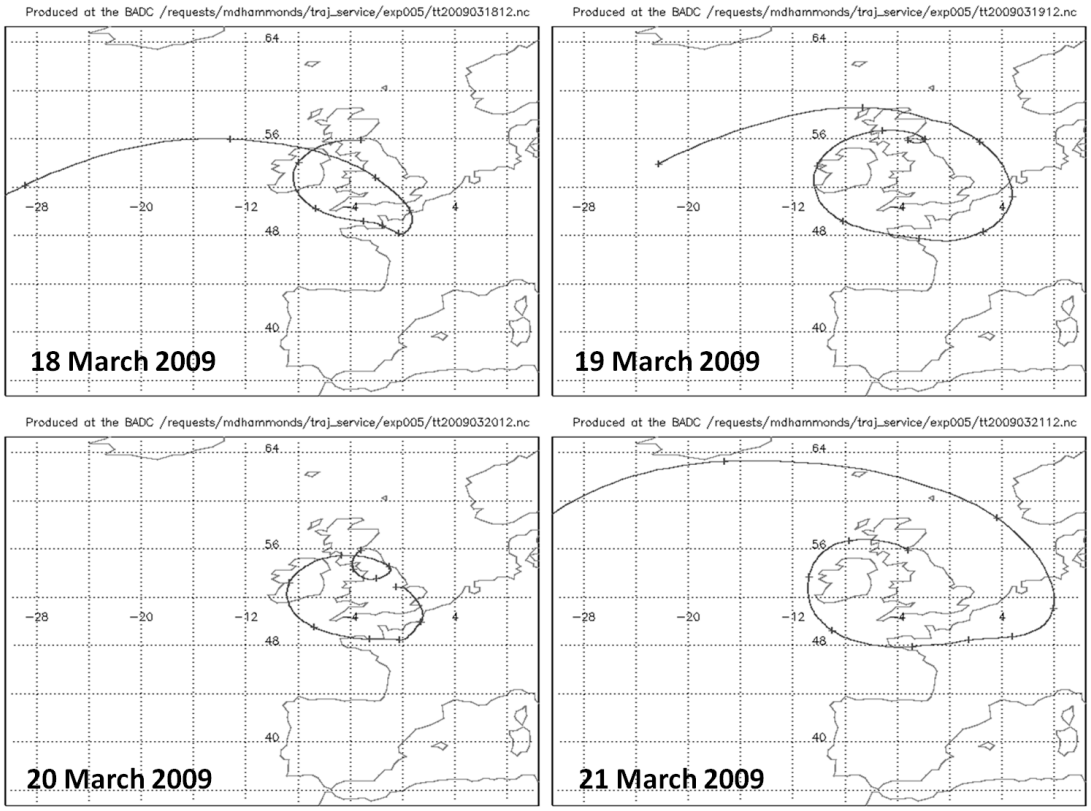

(a) Days during the PM_{10} episode: 18–21 March 2009.

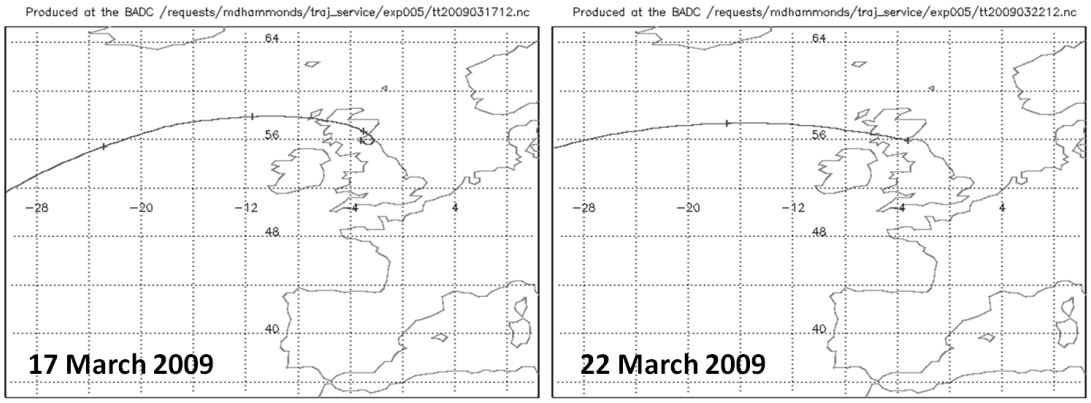

(b) Days before (17 March 2009) and after (22 March 2009) the PM_{10} episode.

Figure 2.26: 5-day air-mass back trajectories for midday arrival at the Urban Background sampling site at the 900 hPa level. Markers are at 12 h intervals. Data from the BADC Trajectory Service (`http://badc.nerc.ac.uk/community/trajectory/`)

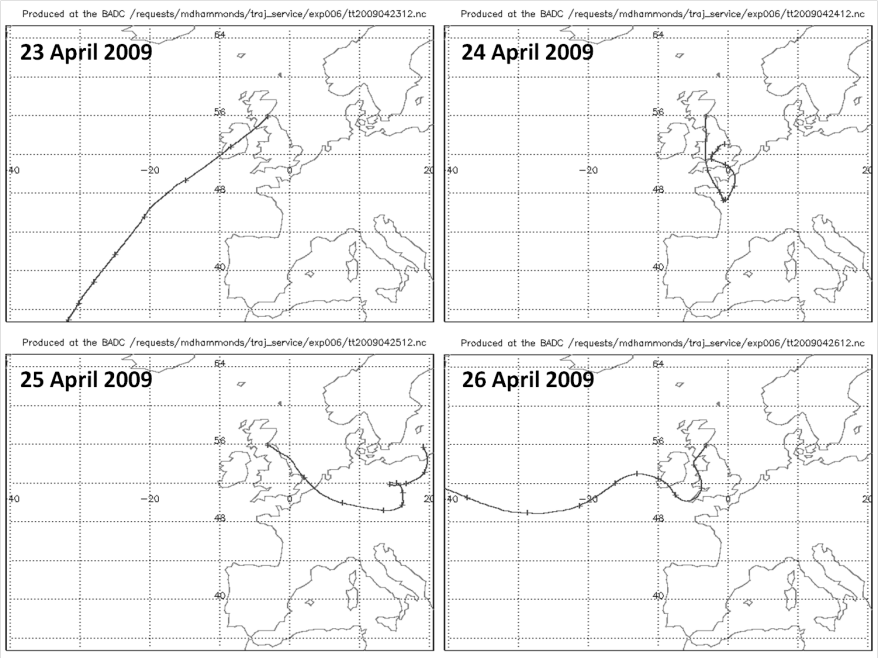

Figure 2.27: 5-day air-mass back trajectories for midday arrival at the Urban Background sampling site at the 900 hPa level, from 23–26 April 2009. Markers are at 12 h intervals. Data from the BADC Trajectory Service (`http://badc.nerc.ac.uk/community/trajectory/`)

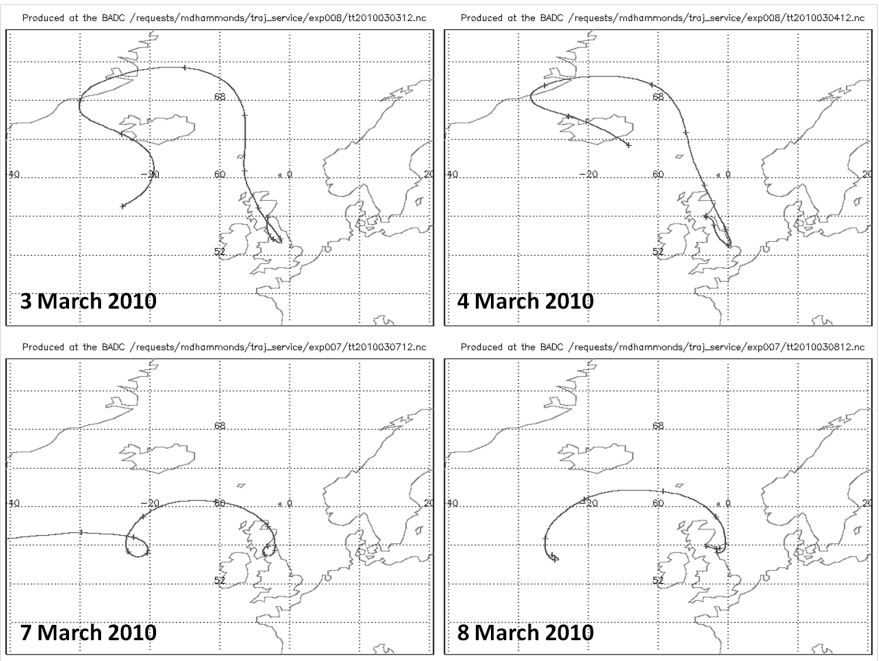

Figure 2.28: 5-day air-mass back trajectories for midday arrival in Edinburgh at the 900 hPa level, on 3, 4, 7 and 8 March 2010. Markers are at 12 h intervals. Data from the BADC Trajectory Service (`http://badc.nerc.ac.uk/community/trajectory/`)

2.4.5 Comparison with wind data

Mean hourly wind direction and wind speed ($m\,s^{-1}$), from a weather station on Blackford Hill (Figure 2.3 on page 25; Elevation: 134 m; OS Grid Reference: NT258706) in Edinburgh, were obtained from the BADC archive for the period 20 August 2008 – 21 April 2010. These data were averaged to daily means for comparison with the Partisol PM_{10} concentrations. Care was taken to ensure that the wind direction was vector-averaged. This was done using the 'openair' package [Carslaw and Ropkins, 2011] in R [R Development Core Team, 2011] (with all the wind speed and direction graphs being plotted using this software).

The wind in Edinburgh was predominantly from the west to south-west, between 20 August 2008 and 21 April 2010, with the majority of high wind speeds being associated with the south-westerly direction (Figure 2.29a). In Figure 2.29b it can be seen that most of the highest PM_{10} concentrations (25–58 $\mu g\,m^{-3}$) in Edinburgh (Urban Background) were when the wind was coming from the west or north-east. It is not clear if the sources of this pollution were close to, or far away from, the monitoring site. There are busy main roads to the west and east so local traffic sources could be the source of the higher PM_{10} levels. There is no obvious PM_{10} source to the north-east of the site but analysis of PM_{10} episodes in Section 2.4.4 showed the potential for long-range transport of PM from Europe. Nearer to Edinburgh, sea-spray is a potential source, as it could be carried in from the Firth of Forth to the north-east of the city. The westerly winds could transport PM_{10} from the more industrial areas of Glasgow (a city in Scotland's west central lowlands with a population of ~ 2.5 million) and the Central Belt (area of relatively high population density between Edinburgh and Glasgow).

The wind roses are plotted separately according to the level of PM_{10} pollution in Figure 2.30. The lowest PM_{10} concentrations (top left of Figure 2.30) were associated with south-westerly winds. This is to be expected, as the PM_{10} levels were generally low in Edinburgh and this was the predominant wind direction. The highest PM_{10} concentrations (bottom right of Figure 2.30) were associated with west to south-westerly and north-easterly winds, which has already been seen. What can also be seen is that high PM_{10} levels were associated with the lowest wind speeds (0–2 $m\,s^{-1}$). This shows that calm conditions prevented the dispersion of PM from the city and led to an increase in concentrations.

Another useful way of viewing this data is a bivariate polar plot of concentrations by wind speed and wind direction (Figure 2.31a). This plot is shown as a continuous smoothed surface, as described by Carslaw and Ropkins [2011]. As might be expected,

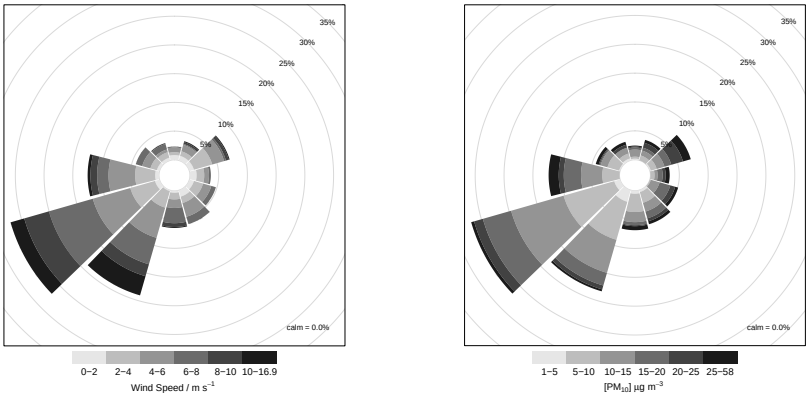

(a) Wind rose of wind speed and wind direction.

(b) Pollution rose of Urban Background PM_{10} concentration variation with wind direction.

Figure 2.29: Wind and pollution roses using wind data from Blackford Hill (20 August 2008 – 21 April 2010). Rings show the proportion in 5 % intervals.

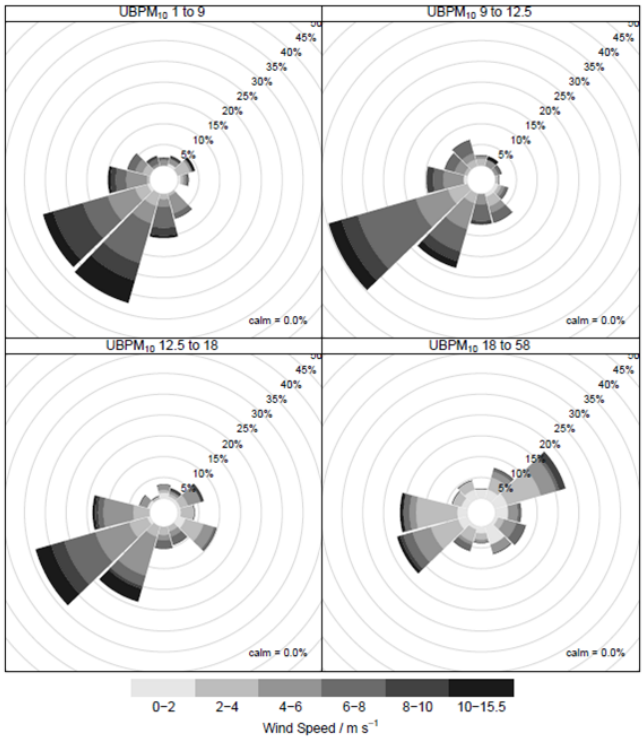

Figure 2.30: Wind roses of the wind speed and wind direction from Blackford Hill plotted according to the PM_{10} concentration at the Urban Background site. From top-left to bottom-right: 1 to 9 $\mu g\,m^{-3}$; 9 to 12.5 $\mu g\,m^{-3}$; 12.5 to 18 $\mu g\,m^{-3}$; 18 to 58 $\mu g\,m^{-3}$. Rings show the proportion in 5 % intervals.

increasing wind speed was generally associated with lower concentrations. This is likely to be due to dilution through advection and increased turbulence. The highest PM_{10} concentrations, therefore, were associated with low wind speeds regardless of wind direction. In these conditions the particle concentration in the air can increase over time without being removed from the city. This suggests that the main source of high PM_{10} in Edinburgh was the build-up of regional emissions. However, there also seems to be a clear source of PM_{10} from the east at higher wind speeds. This could be from the re-suspension of road dust from the nearest main road (a busy road running into the city centre and out to the south), the generation of sea spray (which could be carried in from the Firth of Forth to the east of the city), or long-range transport from mainland Europe.

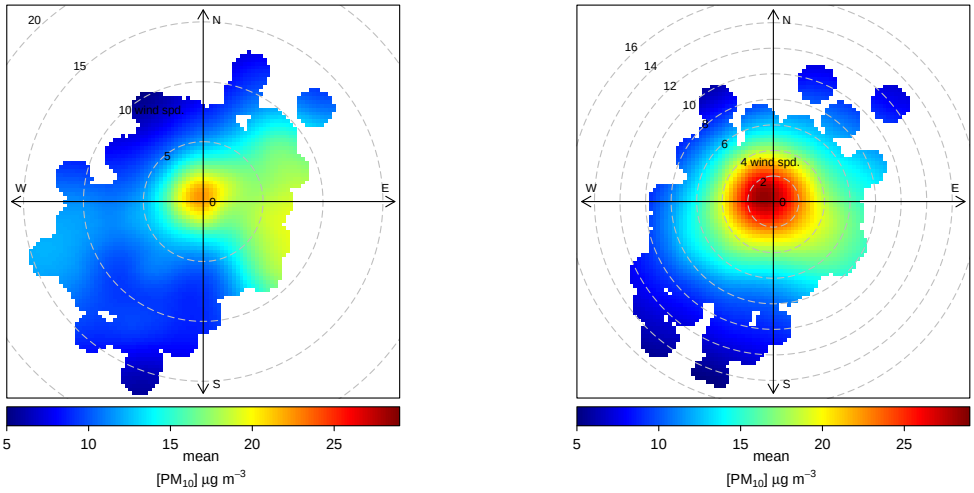

(a) Urban Background; 20 August 2008 until 21 April 2010.

(b) Roadside; 10 September 2009 until 21 April 2010.

Figure 2.31: Bivariate polar plots of PM_{10} concentrations shown to vary by daily wind speed and wind direction.

The source from the east is not as clear from the Roadside data (Figure 2.31b) but this may just be due to the different PM_{10} concentration scale. The nearest main roads are to the north and west of the Roadside Site. If re-suspension of road dust was a major PM_{10} source evidence of this should be seen in Figure 2.31b, which is not the case. Also, if sea spray were being measured at the Urban Background site when wind speeds were relatively high the same should be seen at the Roadside site. One reason that this may not happen is that the Roadside site is within a street canyon, with buildings to the north and south-east of the Partisol monitor, which could lead to the dependence of concentrations on wind speed being complex. Another reason is the period of time of the Urban Background and Roadside measurements. The emissions

from the source in the east may have occurred when the Roadside monitor was not in operation. However, what is clear from these data (Figure 2.31b) is that the highest Roadside PM_{10} concentrations also occur when the wind speeds are the lowest, regardless of wind direction. As with the Urban Background site, calm conditions would lead to the build-up of PM, especially close to busy roads. The higher PM_{10} concentrations for the Roadside site (Figure 2.31b) are evidence of this.

Although this type of analysis between PM_{10} concentrations, wind speed and wind direction can be useful in identifying sources of pollution, and reasons for high PM levels, some caution should be exercised:

- The wind data used in this analysis is from a source distanced from the monitoring locations (see Figure 2.3) and so may not be representative.

- For the bivariate polar plots, the assumptions used in the modelling, and different scales displayed, may lead to incorrect interpretations. For example, a high PM_{10} concentration in the plot may be the result of a single value and not representative of a trend in the data.

Another potential issue with the results presented in Figure 2.31 is that the hourly wind direction and wind speed data were averaged to daily means for comparison with the daily PM_{10} concentrations. This type of averaging can lead to a loss of detail, even if it is possible to indicate some of the upwind source locations quite well [Cosemans et al., 2008]. Cosemans et al. [2008] presented a computational scheme to obtain pollutant roses from daily averaged concentrations that were comparable to those made with half-hourly concentrations. It is beyond the scope of this work to do the same but it is possible to increase the level of detail in the bivariate polar plots. Daily PM_{10} concentrations were expanded to hourly values and these were matched with the hourly meteorological data (i.e., each hour in a 24 h period was assigned the concentration from that day). Hourly bivariate polar plots are shown in Figure 2.32 and these have clearer features than the daily ones in Figure 2.31. There could still be inaccuracies in Figure 2.32 since the variation in PM_{10} concentration throughout the day is not represented. Although it was not done here, an estimate of a typical diurnal profile for PM_{10} measurements, using a TEOM-FDMS for example, would improve the accuracy of bivariate polar plots further.

A local PM_{10} source close to the Urban Background (Figure 2.32a) and Roadside (Figure 2.32b) monitoring sites, at low wind speeds, is still seen for the hourly data. The easterly source in the daily Urban Background concentrations (Figure 2.31a) is split into three components in the hourly analysis (Figure 2.32a). The exact reason for

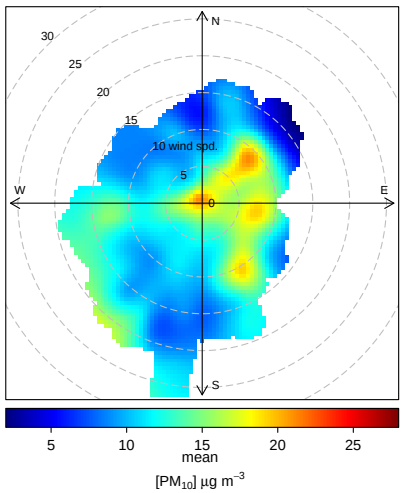

(a) Urban Background; 20 August 2008 until 21 April 2010.

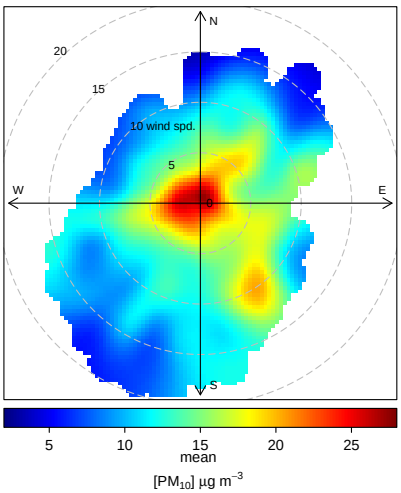

(b) Roadside; 10 September 2009 until 21 April 2010.

Figure 2.32: Bivariate polar plots of PM_{10} concentrations shown to vary by hourly wind speed and wind direction.

this split is not known but it could be due to different sources: sea-spray from the Firth of Forth to the north-east; traffic on the road to the east of the site; and a continental influence from the south-east. The likely continental source to the south-east is clearly shown in the Roadside plot (Figure 2.32b). There is an indication of higher PM_{10} concentrations coming from the west of the Urban Background site in Figure 2.32a (also shown in Figure 2.29b), which could be from a busy local road or longer-range transport from industrial areas of Glasgow and/or the Central Belt. Further detail of the local PM_{10} source at lower wind-speeds is seen in the hourly Roadside plot (Figure 2.32b). Relatively high PM_{10} concentrations to the west and north-east are most likely from the roads adjacent to the monitoring site (Figure 2.6).

2.5 Monitor inter-comparison

Comparison of data from collocated monitoring devices can provide reassurance in the monitoring methods being used, or highlight discrepancies that require further investigation. A report published in 2006 presented the results of a series of tests carried out in the UK to determine the overall performance of a number of 'candidate' particulate matter samplers with that of the EU reference method for PM_{10} [Harrison et al., 2006]. The tests assessed the achievement of the criteria of the Data Quality Objectives in Annex 1 of the Ambient Air Quality Directive 2008/50/EC [European

Union, 2008], as a programme of 'equivalence' must be undertaken if a monitoring method outside of the reference method is to be used. The Guide to Demonstration of Equivalence (GDE) was updated in January 2010 and the data from Harrison et al. [2006] was reprocessed accordingly [Bureau Veritas, 2010]. The results showed that both Partisol 2025 and TEOM-FDMS monitors, as deployed in the original tests, still met the equivalence criteria and their use in the UKs AURN was justified.

The test criteria set out in the GDE are rigorous, with the following requirements being adhered to as closely as possible in the UK equivalence programme (taken from Harrison et al. [2006]):

- Test sites shall be representative of typical conditions for which equivalence will be claimed including possible episodes of high concentrations.
- A minimum of four comparisons shall be performed with particular emphasis on the following variables, if appropriate:
  - Composition of the PM fraction, notably high and low fractions of semi-volatile particles, to cover the maximum impact of losses of semi-volatiles.
  - Air humidity and temperature (high and low) to cover any conditioning losses of semi-volatiles during the sampling process.
  - Wind speed (high and low) to cover any dependency of inlet performance due to deviations from ideal behaviour as dictated by mechanical design, or deviations from the designated sampling flow rate.
- A minimum of 40 measurement results each averaged over at least 24-hour per comparison shall be collected.
- Samplers and instruments shall be positioned in such a way that the effect of spatial inhomogeneities of the compound concentration in the sampled air are negligible in comparison with other uncertainty contributions
- Between-sampler uncertainty of both reference and candidate samplers should be determined.

A weakness of this approach could be that only 40 days of measurement were required for the comparison. Depending on the site, 39–58 between-sampler measurements were made for Partisols during the UK Equivalence Programme [Harrison et al., 2006]. Over this relatively short period of time some of the other requirements of the GDE (i.e., variation in PM composition and meteorological conditions) may have been missed. This could be improved by taking measurements over a longer time period.

2.5.1 FDMS versus Partisol

One of the advantages of using the AURN's Urban Background site at St Leonards in Edinburgh for Partisol PM_{10} measurements in this project was the presence of a PM_{10} TEOM-FDMS. For the Urban Background Partisol, 576 valid daily measurements were made between August 2008 and April 2010 (Table 2.10), giving the potential for many more than the GDE's required minimum of 40 days of inter-comparison between the Partisol and TEOM-FDMS. The TEOM-FDMS data were obtained from the Data Archive section of Defra's air pollution website (`http://uk-air.defra.gov.uk/data/`). The Partisol PM_{10} concentrations are compared with the values from the PM_{10} FDMS in Figure 2.33.

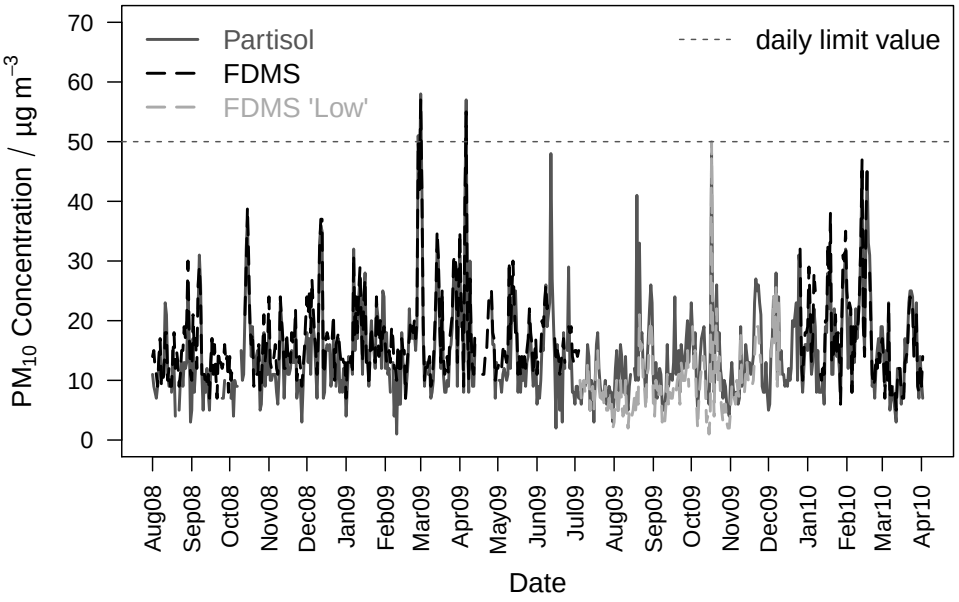

Figure 2.33: Time series of daily mean PM_{10} measurements from the Partisol and TEOM-FDMS monitors at the Urban Background site. The "FDMS 'Low'" line is for the period that a dryer changed caused the measured PM_{10} concentrations to be lower than expected.

At the end of July 2009, the dryer on the TEOM-FDMS was changed to a B-type dryer. This resulted in a step-change in the PM_{10} concentrations: the FDMS values were noticeably lower than those from the Partisol and are labelled as "FDMS 'Low'" in Figure 2.33. The TEOM-FDMS was repaired in January 2010 and this is where the "FDMS 'Low'" dataset ends. FDMS data collected during this period were subsequently removed from the national data archive following data ratification discussions.

The graphs in Figure 2.34 show more clearly the effect of the FDMS dryer change. Figure 2.34a shows a comparison of daily mean PM_{10} concentrations between the Partisol and FDMS without the "FDMS 'Low'" values. There is a good linear agreement between the monitors ($r^2 = 0.88$), with a major axis relationship that is close to the ideal $1:1$ ($y = 0.92x + 3.14$) but with a positive intercept of $\sim 3\,\mu g\,m^{-3}$. This appears to be caused by the tendency of the FDMS to give higher values than the Partisol at low PM_{10} concentrations. The two monitors are measuring the same quantity so it would be expected that they agree.

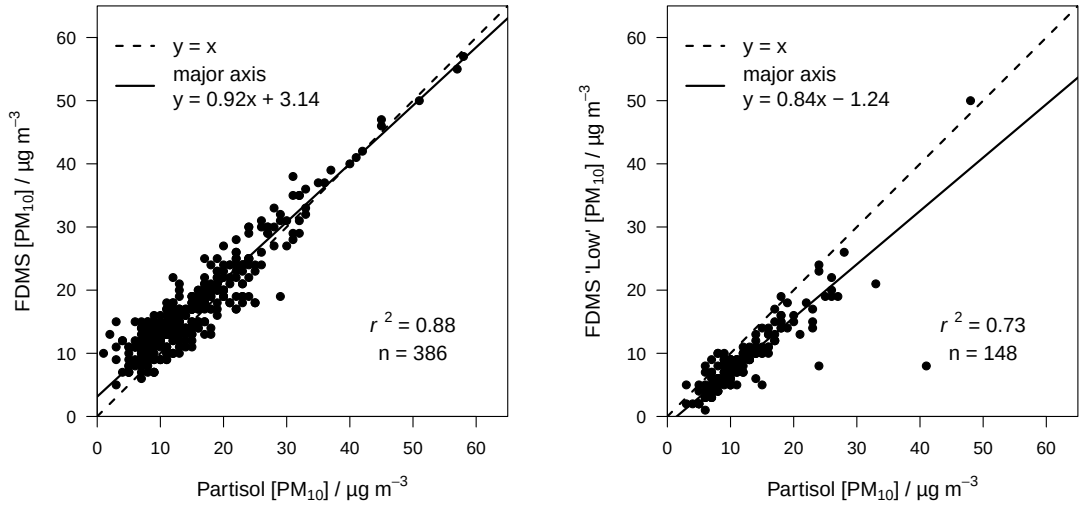

(a) Not including "FDMS 'Low'". **(b)** "FDMS 'Low'".

Figure 2.34: Comparison of daily mean Urban Background PM_{10} concentrations between the Partisol and TEOM-FDMS.

The plot for the period between the dryer change and the problem being resolved (Figure 2.34b) shows that the linear agreement between the two monitors was reduced during this time ($y = 0.84 - 1.24$; $r^2 = 0.73$). Most of the values are below the $y = x$ line showing that the FDMS was generally giving lower readings throughout this period.

At the time of the FDMS dryer change it was not clear that this had caused the step-change in measured PM_{10} concentrations. The SOs who were responsible for the

FDMS monitor were certain that the routine dryer change had not caused a problem and everything was running as it should. Nothing had changed with the operation of the Partisol sampler during this period, and no step-changes in Partisol or filter weighing performance were highlighted during any of the regular checking procedures (previously described), so there were was no reason to doubt the Partisol PM_{10} concentrations. It was not until City of Edinburgh Council staff noticed that some FDMS $PM_{2.5}$ concentration values from the same site were higher than the FDMS PM_{10} concentrations, which is technically impossible (as $PM_{2.5}$ is a subset of PM_{10}), that the FDMS SOs agreed to look more closely at the instrument that appeared to have a problem. After detailed investigation, it was decided to convert the $PM_{2.5}$ analyser to PM_{10} for a two-week period in December to check for acceptable agreement between the two analysers [Eaton and Stacey, 2010]. As a result of this, the PM_{10} sensor and control units were replaced on 13 January 2010, and measured concentrations returned to levels similar to those prior to the dryer change. The data for the period 24 July 2009 to 13 January 2010 will therefore not be used for subsequent FDMS and Partisol PM_{10} concentration comparisons.

An outcome of the above is that 148 days of FDMS PM_{10} concentration data were lost at the St Leonards site for reporting as part of the AURN. As the AURN has many sites in the UK this was probably not a significant issue for the reporting of national PM levels, but St Leonards is a major site used by the City of Edinburgh Council in their annual report on air pollution, and nearly one half of the PM_{10} concentration data for the year 2009 were lost. As they had helped with the set-up and operation of this project's Partisol sampler, at St Leonards, they were aware of the level of accuracy and precision of the results, as well as the level of agreement with the FDMS before the dryer change. With due acknowledgement, the City of Edinburgh Council were able to use the Partisol PM_{10} concentration data in their reporting and vastly increase their level of data capture.

2.5.2 Grubbs' outlier test

The Partisol and FDMS samplers were compared using the the same methods as the UK Equivalence Programme [Harrison et al., 2006]. A Grubbs' Outlier Test [Grubbs, 1969], at the 99 % Confidence Level, was used to remove a maximum of three outliers. Δ_i was calculated and $\Delta_{i=\max}$ identified:

$$\Delta_i = |x_{i,1} - x_{i,2}| \tag{2.5.1}$$

$$\Delta_{i=\max} = |x_{i,1} - x_{i,2}|_{i=\max} \tag{2.5.2}$$

where

Δ_i is the absolute difference between data-pairs

$\Delta_{i=\max}$ is the maximum absolute difference between data-pairs

$x_{i,1}$ and $x_{i,2}$ are parallel measurements for a single 24-hour period i

i =max is the data-pair with the largest absolute difference

R statistical software [R Development Core Team, 2011] was then used to perform Grubbs' test on $\Delta_{i=\max}$. This value was found to be an outlier ($p < 0.01$) so the associated data were removed. The test was then repeated with a new $\Delta_{i=\max}$. This value was also found to be an outlier ($p < 0.01$) and the associated data were, therefore, removed. The test was repeated, again, for a third $\Delta_{i=\max}$ and this was not found to be an outlier ($p > 0.01$). A scatter plot of the comparison between the TEOM-FDMS and the Partisol is shown in Figure 2.35. The outliers removed by Grubbs' test are highlighted in grey. Data for the period where there was a problem with the FDMS dryer have also been removed from the inter-comparison.

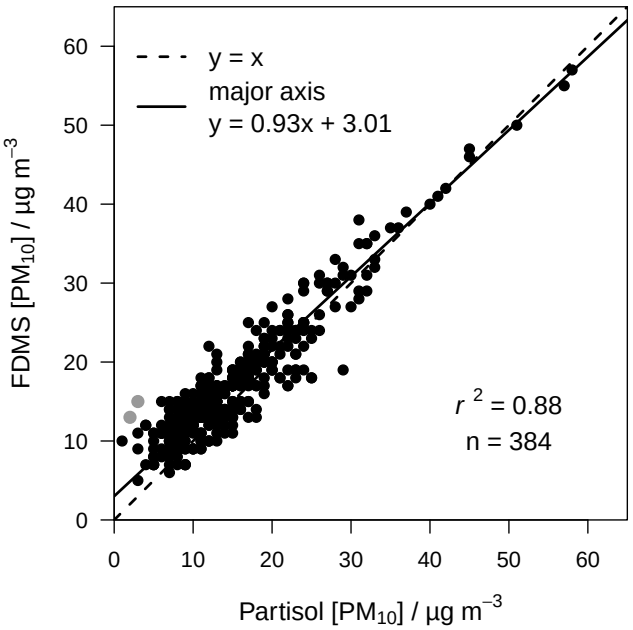

Figure 2.35: Comparison of daily mean Urban Background PM_{10} concentrations between the Partisol and TEOM-FDMS. Paired data were removed where: 1) the FDMS values were low due to a problem with the dryer; 2) they were shown to be outliers by Grubbs' test (points shown in grey).

2.5.3 Equivalence test

The following describes a non-standard use of CEN equivalence testing [CEN, 2005] as a useful method of demonstrating the level of agreement between a Partisol and TEOM-FDMS. The original CEN document [CEN, 2005] uses between-sampler uncertainty (u_{bs}) to test identical monitors, and the slope (b) and intercept (a) of the major axis line ($y = a + bx$) to determine the performance of a 'candidate' PM_{10} instrument against that of the EU reference method.

Two identical candidate samplers and two identical reference samplers were not available, as required by the CEN [2005] method, so the between-sampler uncertainty (u_{bs}) was not determined. The next stage of the equivalence test, which looks at the uncertainty between candidate and reference samplers, was used. Slope (b) and intercept (a) of the major axis line ($y = a + bx$) were calculated (by orthogonal regression) and this line is shown in Figure 2.35. For the instruments to be considered equivalent the following criteria must be met:

1. The uncertainty in the slope (u_b) must not be significantly different from 1, using the criterion: $|b - 1| > 2.u_b$

2. The uncertainty in the intercept (u_a) must not be significantly different from 0, using the criterion: $|a| > 2.u_a$

Calculated by:

$$u_b = \sqrt{\frac{S_{yy} - \left({S_{xy}}^2 / S_{xx}\right)}{(n_{bs} - 2) \cdot S_{xx}}} \tag{2.5.3}$$

$$u_a = \sqrt{{u_b}^2 \cdot \frac{\sum_{i=1}^{n_{bs}} x^2}{n_{bs}}} \tag{2.5.4}$$

where

$$S_{xx} = \sum_{i=1}^{n_{bs}} (x_i - \bar{x})^2$$

$$S_{yy} = \sum_{i=1}^{n_{bs}} (y_i - \bar{y})^2$$

$$S_{xy} = \sum_{i=1}^{n_{bs}} (x_i - \bar{x}) \cdot (y_i - \bar{y})$$

The above equations give a slope of $b = 0.93 \pm 0.03\,\mu g\,m^{-3}$ ($b \pm 2.u_b$) and intercept $a = 3.01 \pm 0.57\,\mu g\,m^{-3}$ ($a \pm 2.u_a$). This means that the major axis line is significantly different from the ideal $y = x$ relationship and these instruments failed the equivalence test (used by Harrison et al. [2006]) at the Urban Background site from August 2008 to April 2010.

As the Partisol and TEOM-FDMS were shown to be equivalent to the reference method during the UK Equivalence Programme [Harrison et al., 2006], and subsequent re-working of the results [Bureau Veritas, 2010], this result is unexpected. There could be a number of different reasons for the failure of the major axis relationship to meet the equivalence criteria:

- The GDE sets out a procedure for determining if a 'candidate' instrument is equivalent to the reference method. The work carried out in this project was testing the agreement between two instruments that have already been shown to be equivalent to the reference method. It is possible that if one 'equivalent' instrument had a positive (but insignificant) deviation from the reference method, and another 'equivalent' instrument had a negative (but insignificant) deviation from the reference method, that the difference between the two 'equivalent' instruments could be significant. However, even taking this into account, the intercept of $3.01 \pm 0.57\,\mu g\,m^{-3}$ found in this test seems to be too high.

- Because the GDE is about determining if a 'candidate' instrument is equivalent to the reference method, the equations used may not be relevant for the inter-comparison carried out in this project.

- The maximum number of between-sampler measurements (for Partisols or FDMSs), during the UK Equivalence Programme [Harrison et al., 2006], was 58. This may not have been enough days to get the necessary variation in PM composition and meteorological conditions. It is possible that these instruments may not have met the equivalence criteria if a longer sampling period was used. The test undertaken in this project was for 384 days and this could be the reason for the lack of agreement between instruments.

- The relatively-large positive intercept ($3.01 \pm 0.57\,\mu g\,m^{-3}$), and slope of < 1, shows that the FDMS was giving higher readings than the Partisol for PM_{10} at lower concentrations. One possible reason for the lower PM_{10} concentrations measured by the Partisol is the loss of semi-volatile PM from the filters after sampling. The filters were left for at least 2 weeks, in ambient conditions, after sampling, which could be long enough for this loss to occur. The loss of material from sampled

filters would not be compensated for by the Machine Blank correction, as no PM_{10} was collected on the Machine Blanks. However, since the agreement between the monitors appears to be good at high concentrations, it is likely that something else is responsible for the difference.

2.6 Conclusions

Despite initial problems getting the Partisol-Plus 2025 Sequential Air Samplers to operate satisfactorily they performed well during this project. Once the monitors were repaired and operational, and the filter-exchange issue was solved, the data capture was high. Over 610 days of sampling, the Urban Background monitor had a 94 % success rate. Over a total of 280 combined days at the Rural and Roadside locations, the other monitor had 92 % success. The error in the flow-rate of both monitors was low. The standard deviation of the flow-rate was less than 0.5 % of the mean, for both samplers.

The precision of the balance used for weighing filters was shown to be high. For the 20 mg calibration mass, the standard deviation of 46 individual means was 0.005 % of the overall mean. For the 200 mg calibration mass, the standard deviation of 46 individual means was 0.004 %. The accuracy of the balance was also shown to be high, with the maximum difference from another balance being 3 µg (which is less than 0.002 % of the mass being measured).

The quartz filters used to collect PM_{10} were shown to change mass with changes in ambient RH. As it was not possible to condition the filters in a way that would prevent this mass change, Machine Blank filters were used to correct for this. The correction was successful, with good agreement attained between the Partisol and a TEOM-FDMS instrument at the same monitoring site. However, this agreement was not perfect, with a noticeable difference shown between the two monitors at low PM_{10} concentrations. The reason for this small difference is unclear.

The general levels of PM_{10} measured in this monitoring campaign indicate that the air in Edinburgh was relatively clean. The measured concentrations were well below the EU determined limit value requirements. The main factor causing exceedance of the daily limit value was shown to be transport of PM_{10} from areas of mainland Europe. High PM_{10} concentrations were also strongly associated with calm weather conditions in Edinburgh, which allow the build-up of particulate pollution over time.

Chapter 3

The black carbon component of PM

3.1 Introduction

Soot is a black substance formed from the incomplete combustion of fossil fuels and various types of biomass burning, and contains particles of carbon in its elemental form. It is a component of particulate air pollution that has been systematically measured in the United Kingdom (UK), as black smoke (BS), since the 1920s [Quincey, 2007]. Air is drawn through a filter and the darkness of the stain produced by light-absorbing particulate matter (PM) is measured as the reflectance of white light relative to the reflectance of a clean filter. The BS standard [ISO 9835, 1993] uses the principal of the Beer-Lambert law, which states that equal fractions of the incident radiation are absorbed by successive layers of equal thickness of the light absorbing substance:

$$I = I_0 \exp(-\alpha l) \tag{3.1.1}$$

where

I is the intensity of transmitted light

I_0 is the intensity of the incident light

α is the absorption coefficient of the sampled air

l is the length of the sampled air column

i.e.,

$$l = V/A \tag{3.1.2}$$

where

V is the volume of air sampled

A is the exposed filter area

In ISO 9835 [1993] it is assumed that the surface of the filter material underlying the deposited PM acts as a mirror so the result is a measure of light absorbed after passing twice through the absorbing layer. This leads to a working absorption coefficient being derived from Equation (3.1.1) and Equation (3.1.2):

$$\alpha' = \frac{A}{2V} \ln\left(\frac{R_0}{R}\right) \tag{3.1.3}$$

where

α' is the working absorption coefficient in units of m^{-1} if A and V in units of m^2 and m^3, respectively

R_0 is the intensity of the light reflected from a clean filter

R is the intensity of the light reflected from a sampled filter

A table is provided in ISO 9835 [1993] that can be used to convert α' into a Black Smoke Index (BSI) ($\mu\mathrm{g}\,\mathrm{m}^{-3}$), in line with the Organization for Economic Co-Operation and Development (OECD) and European Economic Community (EEC) reference methods. The BSI should be a measure of the concentration of BS in the air but the quantity and composition of PM has changed since the original conversion from reflectance was determined. The interpretation of BSI as a total mass concentration is therefore no longer valid, although it can be used as a measure of variation of BS in the atmosphere. This is useful in health studies as long-term exposure to BS, as a measure of traffic-related air pollution, may shorten life expectancy [Hoek et al., 2002].

Measurement of black carbon (BC) is another optical method of estimating the level of airborne soot. As part of Department for Environment, Food and Rural Affairs (Defra)'s long-running national network (reduced to 20 sites across the UK in 2006), an automatic instrument (aethalometer) was deployed at each site in 2008 to measure BC using a real-time optical transmission technique [Bower et al., 2009] (prior to this BS was measured in the UK network). Similarly to the BS technique, air is drawn through a filter and the darkness of the stain produced is measured as the intensity of light transmitted through the sample relative to a clean filter. The absorption coefficient is

derived from Equation (3.1.1) and Equation (3.1.2) to give:

$$\alpha = \frac{A}{V} \ln\left(\frac{I_0}{I}\right) \tag{3.1.4}$$

where

α is the absorption coefficient in units of m^{-1}
if A and V in units of m^2 and m^3, respectively

This can then be converted to BC concentration ($\mu\mathrm{g}\,\mathrm{m}^{-3}$) using:

$$\mathrm{BC} = 10^6 \alpha / \alpha_{atn} \tag{3.1.5}$$

where

α_{atn} is the mass extinction coefficient for BC, in units of $\mathrm{m}^2\,\mathrm{g}^{-1}$

Magee AE21 Aethalometer instruments are used in the UK network and the manufacturers recommend that the value of $\alpha_{atn} = 16.6\,\mathrm{m}^2\,\mathrm{g}^{-1}$ should be used. This leads to a final relationship of:

$$\mathrm{BC} = 6.02 \times 10^4 \alpha \tag{3.1.6}$$

As with the BSI, the BC concentration value may not be accurate since the value of α_{atn} depends on the particle composition and size. As the value of α_{atn} recommended by Magee was chosen to agree most closely with independently determined elemental carbon (EC) concentrations (determined by thermo-optical methods) [Quincey, 2007], BC is likely to be more accurate than BSI (although α_{atn} will vary spatially and temporally). Despite the potential unreliability of BC mass concentration values, BC concentration is still a useful metric for determining the variation of levels of airborne soot and the potential health effects of airborne PM.

3.1.1 Shadowing correction

Another source of inaccuracy in measurements of BC concentration comes from the fact that the rate of change of light transmission is not linear [Virkkula et al., 2007]. One reason for this is that both scattering and absorbing particles collected on the filter alter the internal reflections in the PM/filter combination. The consequence is that as

the filter gets darker, and the transmission of light decreases, the BC concentration gets underestimated. Virkkula et al. [2007] derived a simple method for correcting for the loading effects (often called 'shadowing') of aethalometer BC data:

$$\mathrm{BC}_{\mathrm{CORRECTED}} = (1 + k \cdot ATN) \cdot \mathrm{BC}_{\mathrm{NONCORRECTED}} \tag{3.1.7}$$

where

k is an empirical constant

ATN is the attenuation of the filter, defined as $-\ln(I/I_0)$

The constant, k, should be derived from appropriate experimental data (which can vary depending on the quantity and composition of BC within the PM, which can itself vary with time and space).

3.2 BC in PM_{10} samples

As described in Chapter 2, PM_{10} samples were collected from an Urban Background, Rural and Roadside sites in Edinburgh. The BC concentration ($\mu g\, m^{-3}$) of these samples can be determined by measuring the reflectance of the filters relative to the reflectance of the Machine Blanks. One of the benefits of using Partisol Samplers for making PM_{10} measurements is the availability of the filters afterwards for further analysis. If this method of determining BC concentration works, it would increase the potential number of measurement sites in the UK (where Partisols are present), as BC concentration is usually only measured with dedicated instrumentation (e.g., aethalometers); i.e., if a Partisol sampler was operational at a particular site, but no BC or BS equipment was running, it would still be possible to determine daily BC concentrations by conducting reflectance measurements on the filter samples.

An aethalometer was operational at the Urban Background site at the same time PM_{10} was being sampled for this project, from 29 October 2008 to 21 April 2010. Although BC can, in principle, be determined for all of the filters collected at the three sites, only the Partisol-derived BC values from the Urban Background site can be compared with independently-derived BC concentrations from an aethalometer. However, a relationship established between the Partisol and aethalometer BC values from the Urban Background site could be used to determine aethalometer-equivalent BC concentrations at the Rural and Roadside sites.

3.2.1 Reflectance measurements

Reflectance measurements were carried out using an EEL MD43 Smokestain Reflectometer (Figure 3.1a). The protocol was based on that used in the UK BS network, which, in turn, was based on ISO 9835 [1993]. Low lighting was used in the laboratory in which the measurements were made.

3.2.1.1 Setting up the Reflectometer

The meter was switched on, with the head disconnected, and the reading was set to 0.0 using the ZERO control on the front of the meter. The black plastic mask, with a central hole, was placed on the white part of the reference tile (the central hole was placed approximately in the middle for all measurements). The mask and tile had previously been wiped free of dust with a lens tissue, cleaned with MeOH (LC-MS), and left to dry. The reflectometer head was reconnected and placed face down on the mask (Figure 3.1a). To warm the instrument up, it was switched on and left for 30 min. With the light source and mask on the white part of the reference tile, the reading was adjusted to 100.0 ± 0.2, using the COARSE and FINE controls. The light source and mask were then moved onto the dark part of the reference tile, and the reading adjusted using the ZERO control to read 33 ± 1.5. The light source was moved between the white and dark part of the reference tile, and the values re-adjusted as necessary until consistent readings were obtained (demonstrating linearity of response).

3.2.1.2 Measuring sample reflectance

The daily samples of PM_{10} were collected on quartz fibre filters, as described previously in Chapter 2 (Figure 3.1b). The filters were handled with plastic tweezers, which had been pre-cleaned with deionised water (18 MΩ) and MeOH, and left (covered) to dry. Once the reflectometer was set up, a Machine Blank filter was placed on the white part of the reference tile, the mask and light source were placed on the filter, and the reading was adjusted to 100.0 ± 0.2, using the COARSE and FINE controls. The mask and light source were removed from, then replaced on, the filter and the reading checked to see if it was still 100.0 ± 0.2. This was readjusted if necessary and the process repeated until a stable reading was obtained. The sample filters were measured by placing a filter on the white part of the reference tile, moving the mask and light source onto the filter, and recording the value obtained. Each sample filter was measured twice and the mean of the duplicate readings was used. The Machine Blank was re-checked after 6 sample

(a) EEL MD43 Smokestain Reflectometer (back), with light-source placed on the reference tile (centre). Pre-cleaned plastic tweezers are resting on a PetriSlide® (front). The instrument was operated in a dark corner of the laboratory with the lights turned off.

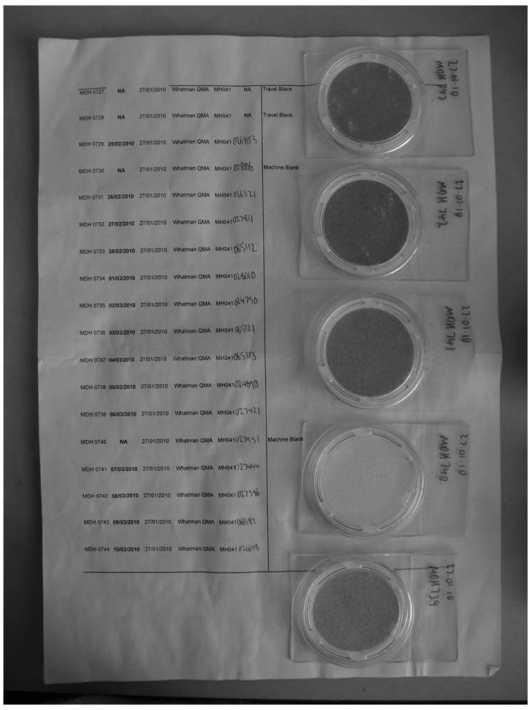

(b) Quartz filters, with collected PM_{10}, prior to reflectance measurements. A 'clean' Machine Blank filter is also present. The darker the stain on the filter, the higher the concentration of BC.

Figure 3.1: Pictures from the Edinburgh laboratory, where reflectance measurements took place.

filters and the reading readjusted to 100.0 ± 0.2 if necessary. To check the consistency of the filters used, both Machine Blanks were measured as if they were samples (each two-week batch of 14 samples contained two Machine Blank filters).

3.2.2 Calculating BC concentration

The reflectance of the Partisol filters was converted to the working absorption coefficient (α' in m^{-1}) using Equation (3.1.3). A (the exposed area of the Partisol filter) was $0.0011946\,\mathrm{m}^2$. V (the volume of air sampled in 24 h) varied from day-to-day but was $\sim 24\,\mathrm{m}^3$ on average. A value of 100 was always used for R_0. Equation (3.1.3) assumes a perfect optical double pass through the particles on the filter. In a perfect reflection measurement, the value of α' would be the true sample absorption coefficient (α). This would only occur when monochromatic light was used and the PM only collected on the surface of the filter. ISO 9835 [1993] states that $\alpha \approx 2\alpha'$, to account for the use of

white light and for the penetration of the particles into the filter paper. Assuming the factor of 2 conversion is accurate, then Equation (3.1.3) becomes the following:

$$\alpha = \frac{A}{V} \ln\left(\frac{R_0}{R}\right) \tag{3.2.1}$$

Using Equation (3.1.6) to convert α, BC concentration ($\mu g\, m^{-3}$) was calculated as:

$$\mathrm{BC} = 6.02 \times 10^4 \times \frac{A}{V} \ln\left(\frac{R_0}{R}\right) \tag{3.2.2}$$

As with the aethalometers in the UK network, a value of $\alpha_{atn} = 16.6\, m^2\, g^{-1}$ was used.

3.2.2.1 Partisol versus Aethalometer

The National Physical Laboratory (NPL) provided hourly aethalometer data measured at the Urban Background site, from 29 October 2008 to 21 April 2010, which were averaged to daily BC concentrations ($\mu g\, m^{-3}$). The time series of these data in Figure 3.2 appears to show a good agreement between both instruments, with common trends of BC concentration being followed. The scatter plot in Figure 3.3 confirms the good linear agreement between the monitors ($r^2 = 0.85$), although this isn't a perfect $1:1$ relationship ($y = 0.82x + 0.45$). At lower BC concentrations ($< 3\, \mu g\, m^{-3}$) the relationship appears to be close to the ideal $1:1$, but at higher concentrations ($> 3\, \mu g\, m^{-3}$) the aethalometer tends to give higher readings than the Partisol. This is because the Partisol-derived BC values have not been corrected to account for shadowing (NPL indicated their supplied aethalometer BC values were already corrected).

The shadowing correction was undertaken using the Virkkula et al. [2007] approach (Equation (3.1.7)) of assuming a correction that is linear in filter ATN (where $ATN = \ln(R_0/R)$):

$$\mathrm{BC}_{\mathrm{CORRECTED}} = (1 + k \cdot \ln(R_0/R)) \cdot \mathrm{BC}_{\mathrm{NONCORRECTED}} \tag{3.2.3}$$

Using the Virkkula et al. [2007] average value of $k = 0.5$, the scatter plot relationship shown in Figure 3.4a was obtained. The linearity at the highest BC concentrations was improved by the shadowing correction ($r^2 = 0.88$) but the values derived from the Partisol filters tended to be $\sim 45\,\%$ higher than the aethalometer data. This inaccuracy is most likely due to the limitations of the various correction factors used: $\alpha_{atn} = 16.6\, m^2\, g^{-1}$; $\alpha = 2\alpha'$; and $k = 0.5$. These values can vary according to the exact make-up of the PM being sampled (and, therefore, the time and place of sampling),

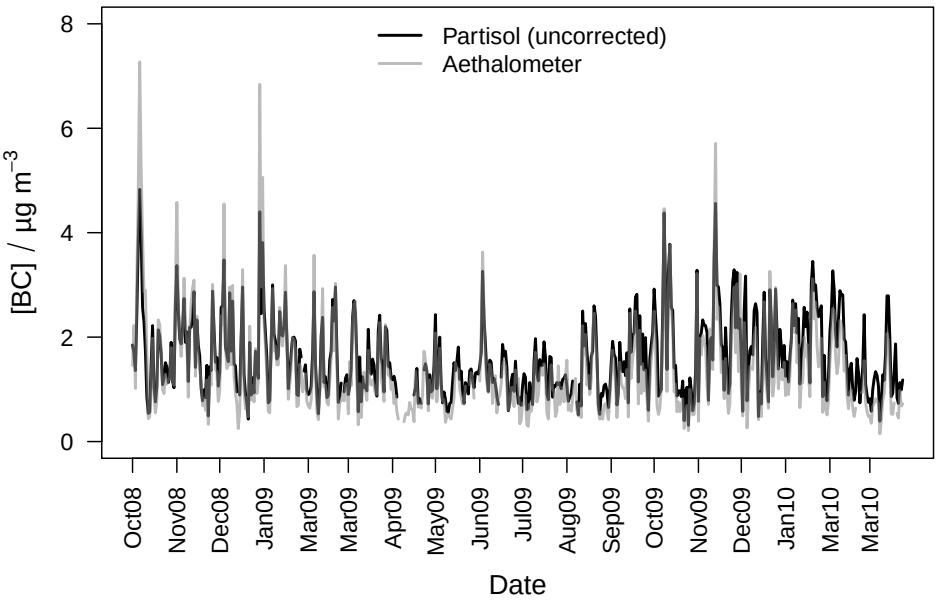

Figure 3.2: Time series of daily mean Urban Background BC measurements from a Partisol and an Aethalometer.

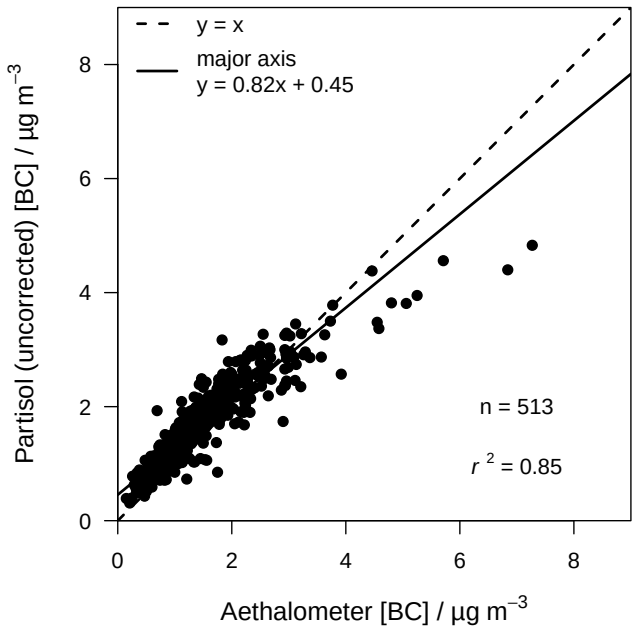

Figure 3.3: Comparison of daily mean Urban Background BC concentrations between the Partisol and Aethalometer.

the reflectance of the filters used for particle collection, the depth of penetration of particles into the filter, and the type of light used in the analysis. Some form of duplicate correction appears to have been introduced into the calculations leading to the reflectance-derived BC concentration values being too high. Since the value of $\alpha_{atn} = 16.6\,\mathrm{m^2\,g^{-1}}$ is used in both the reflectance and aethalometer methods, it is likely that the over-reading of the Partisol reflectance method is due to the factor 2 in the correction of α' to α being too high (and this factor 2 already including aspects of the k correction), and/or the value $k = 0.5$ not being representative of the BC collected in this project.

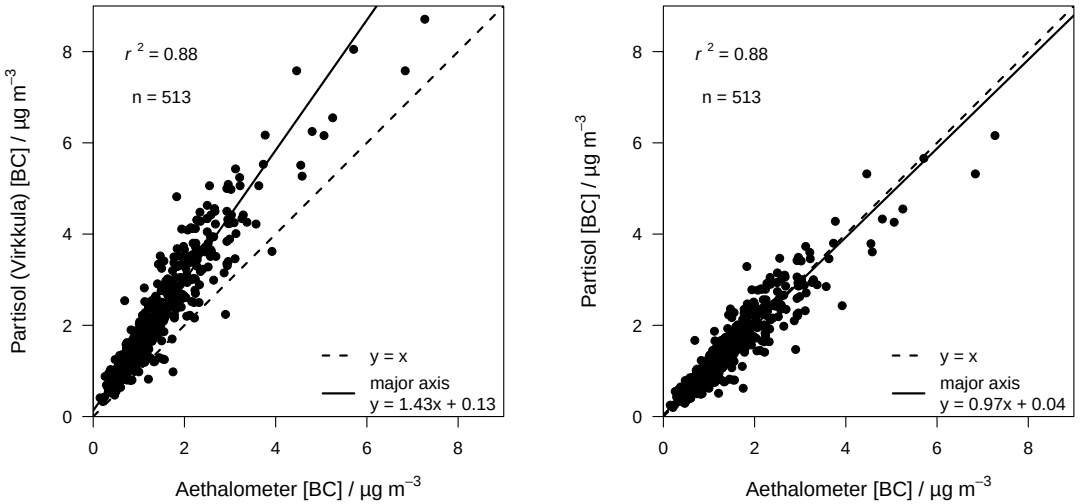

(a) Partisol data were corrected for shadowing using the Virkkula et al. [2007] approach with factors $K = 2$ and $k = 0.5$. Aethalometer data were corrected for shadowing by NPL.

(b) These data have been corrected (using $K = 1.2$ and $k = 0.7$) to give a high level of agreement between the two instruments.

Figure 3.4: Scatter plots of Partisol versus aethalometer BC values from the Urban Background site.

A more direct approach is to undertake correction of the working absorption coefficient (α') in one step, to give a potentially more accurate absorption coefficient (α_{cor}). For the simple model of a correction that is linear in ATN, this is given by:

$$\alpha_{cor} = \alpha' \cdot K(1 + k \cdot \mathrm{ATN})$$

For the reflectance measurements on the Partisol filters the appropriate formula is:

$$\alpha_{cor} = \alpha' \cdot K\left(1 + k \cdot \ln\left(\frac{R_0}{R}\right)\right) \tag{3.2.4}$$

Here K is the correction factor as $R \to R_0$ (ATN $\to$ 0), i.e., a fixed correction for underestimation of α' by the reflectance method. From this the relationship $\alpha = K\alpha'$ can be inferred. The constant k describes the sensitivity of the reflectance underestimation as filter darkness (strictly filter ATN) increases (this is the same k as introduced by Virkkula et al. [2007]). For the data displayed in Figure 3.4a the values of $K = 2$ and $k = 0.5$ were effectively used.

Applying the expression for α' (Equation (3.1.3)) to Equation (3.2.4) leads to the following algebraic expression for α_{cor}:

$$\alpha_{cor} = \frac{A}{2V} \ln\left(\frac{R_0}{R}\right) K \left(1 + k \cdot \ln\left(\frac{R_0}{R}\right)\right) \tag{3.2.5}$$

This can then be converted to a corrected BC concentration using Equation (3.1.5):

$$\mathrm{BC_{CORRECTED}} = 10^6 \cdot \frac{A}{\alpha_{atn} 2V} \ln\left(\frac{R_0}{R}\right) K \left(1 + k \cdot \ln\left(\frac{R_0}{R}\right)\right) \tag{3.2.6}$$

This is a quadratic equation in the variable $\ln(R_0/R)$. Using the aethalometer BC concentrations and Partisol reflectance values from the Urban Background site (shown in Figure 3.5) the following best-fit quadratic relationship exists:

$$\mathrm{BC_{AETHALOMETER}} = 1.23 \cdot \left(\ln\left(\frac{R_0}{R}\right)\right)^2 + 1.80 \cdot \ln\left(\frac{R_0}{R}\right) \tag{3.2.7}$$

From the quadratic coefficients above, values of $K = 1.2$ and $k = 0.7$ (as opposed to the $K = 2$ and $k = 0.5$ values used before) were derived to give the best-fit between Partisol and aethalometer BC concentrations at the Urban Background site. The data is plotted in Figure 3.4b and an almost perfect linear 1 : 1 agreement now exists (the small derivation from the ideal $y = x$ line is due the the constants being rounded to 1 decimal place). The linearity between the data-pairs in Figure 3.4a and Figure 3.4b has not changed ($r^2 = 0.88$ for both plots) since it is only the constants in the shadowing correction that have been altered.

Now that the relationship has been established, aethalometer-equivalent BC concentrations can be derived for the Rural and Roadside Partisol data, using constants $\alpha_{atn} = 16.6\,\mathrm{m^2\,g^{-1}}$, $K = 1.2$ and $k = 0.7$ in Equation (3.2.6). This approach assumes that the values of K and k derived for Partisol reflectance measurements on Urban Background PM_{10} also apply to reflectance measurements on the Rural and Roadside PM_{10}. Since the value of K is likely to depend more on the sample collection method, which remains constant, than on reflectance differences in the PM mix (i.e., it contains an element of correction for the limitations in the presumed double-path through the sample of

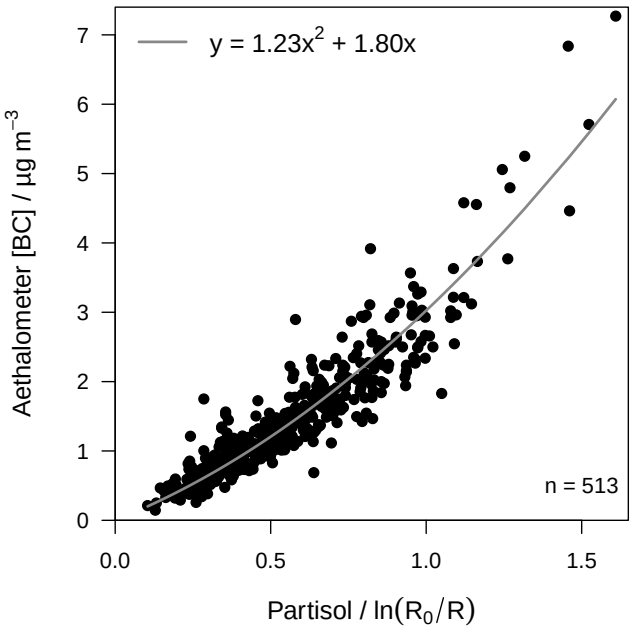

Figure 3.5: Aethalometer BC versus $\ln(R_0/R)$ from the Urban Background site. The quadratic best-fit line (shown in grey) was used to derive Equation (3.2.7)

the reflectance configuration and for the broadband light source), this is likely to be a reasonable assumption. However, the value of k can vary according to sampling location, season, and PM composition and age [Park et al., 2010].

Values of k obtained by Virkkula et al. [2007] and Park et al. [2010] varied with time, as expected. The average of $k = 0.005$ over the whole measurement period was reported by Virkkula et al. [2007] who expressed ATN as a percentage. This becomes $k = 0.5$ when expressed in ATN units directly and is lower than the value of $k = 0.7$ derived here. As the k factor increases so does the contribution of BC to the total PM_{10} mass [Virkkula et al., 2007]. The higher value reported here for Edinburgh suggests that the sampled PM_{10} contains BC that is less aged than in the samples collected by Virkkula et al. [2007] and Park et al. [2010]. If the data were available, it would be useful to see the k values derived by NPL for the aethalometer at the Urban Background site. They could help confirm the validity of the approach used to obtain $k = 0.7$ for the Partisol samples, and determine if it was appropriate to used a fixed value of k for all samples.

Another interesting outcome is that the $K = 1.2$ value reported here is lower than the $K = 2$ assumed in ISO 9835 [1993]. This indicates that the value of $K = 2$ is too high, as it includes an element of the correction for optical shadowing by particles on the filter that the factor k is already correcting for. The reflectance-derived BC values in Figure 3.4a being too high can be explained by this discrepancy.

3.2.3 Measurement errors

Errors in flow rate ($\mathrm{l\,min^{-1}}$) and the volume of air sampled (V, $\mathrm{m^3}$) were discussed in Section 2.2.2.3 and Section 2.3.2. The maximum expected difference in flow rate between the value measured by the Partisol monitor and the National Institute of Standards and Technology (NIST)-traceable Flow Transfer Standard (FTS) was 2.1% (with 95% confidence). The 95% confidence interval of daily air volume measurements was ±0.05% (for the worst case scenario at the Rural site).

The use of Machine Blank filters to set up the Reflectometer, re-check and adjust the set up, and test for consistency is discussed in Section 3.2.1.2. Both Machine Blanks in each 14-day batch of filters were measured, in duplicate, as samples. For all batches from the Urban Background, Rural and Roadside sites a total of 248 Machine Blank reflectance measurements were made, with a mean of 100.2 and standard deviation of 0.3. This standard deviation is larger than the allowed tolerance of ±0.2 in the Reflectometer set up. At the 95% confidence level the value of R_0 used in Equation (3.2.6) should have been 100.2 ± 0.0, instead of the value of 100.0 actually used (although this is within the measurement tolerance of 100.0 ± 0.2). Using Equation (3.2.6) with values of $A = 0.0011946\,\mathrm{m^2}$, $\alpha_{atn} = 16.6\,\mathrm{m^2\,g^{-1}}$, $V = 24.0\,\mathrm{m^3}$, $R = 20.0$, $K = 1.2$, and $k = 0.7$, the difference in BC concentration going from $R_0 = 100.0 \rightarrow 100.2$ is $0.01\,\mathrm{\mu g\,m^{-3}}$. As $R = 20.0$ was the lowest reflectance value measured, this can be viewed as the maximum error introduced by the mean reflectance values of the Machine Blank filters being greater than $R_0 = 100.0$. As R increases the magnitude of this error is reduced.

Another potential source of error was in the set up of the Reflectometer to read 33 ± 1.5 on the dark part of the reference tile. The difference in BC concentration going from $R = 31.5 \rightarrow 34.5$ is $0.4\,\mathrm{\mu g\,m^{-3}}$ (using Equation (3.2.6) as above), which is an error of ±6% from the median value of $R = 33.0$. During this work the Reflectometer was always set to 31.5 and any error in relation to the reference tile was therefore consistent (i.e., if another laboratory set up the Reflectometer to $R = 34.5$ the systematic error between their work and the results presented here would be predictable and remain the same). Considering the level of uncertainty introduced by the constants α_{atn}, K and k, the uncertainty in the measurements in this work is likely to be negligible.

3.3 Results and discussion

The daily BC concentrations (in $\mu g\,m^{-3}$ and corrected for shadowing) were calculated using Equation (3.2.6) and the following values:

$A = 0.0011946\,m^2$

$\alpha_{atn} = 16.6\,m^2\,g^{-1}$

V as measured by the Partisol sampler in units of m^3

$R_0 = 100.0$

R as the mean of duplicate Reflectometer measurements

$K = 1.2$

$k = 0.7$

3.3.1 Data capture

The 2009 data capture for Aethalometer measurements in the UK BC Network was 91% [Butterfield et al., 2010]. Butterfield et al. [2010] reported this as showing a good performance for the network in its first full year of operation and comparable with other automatic networks. The data capture at all of the sites for the Partisol BC measurements was the same as for PM_{10}, as summarised in Table 2.9. At the longer running Urban Background and Roadside sites this was $> 90\%$, which is comparable with the UK BC Network and can be classed as satisfactory.

3.3.2 Mass concentration

A summary of the BC mass concentration ($\mu g\,m^{-3}$), from all of the sites, is shown in Table 3.1.

BC concentrations are reported to the nearest 0.1, as this is the level of precision used in reporting from the UK BC Network. Taking into consideration the level of precision and accuracy in the measurements, and the overall magnitude of BC concentrations, this seems an appropriate level of precision.

The BC calculation was carried out on the 248 Machine Blank filter R values to give a mean concentration of $-0.003\,\mu g\,m^{-3}$ with a standard deviation of 0.006. The limit of

Table 3.1: Overview of BC mass concentrations at all of the monitoring sites.

BC Concentration	Urban Background	Rural	Roadside
Mean / $\mu g\,m^{-3}$	1.4	0.5	3.4
SD / $\mu g\,m^{-3}$	0.9	0.5	2.0
Minimum / $\mu g\,m^{-3}$	0.2	0.1	0.3
Maximum / $\mu g\,m^{-3}$	6.2	2.0	11.1
n	576	48	209

detection (LOD) was calculated as 0.02 $\mu g\,m^{-3}$ (3 $\times$ standard deviation). All of the BC concentrations reported in this work are above the LOD.

For the UK BC Network in 2009 the median concentration of the means of the two Roadside sites was 6.3 $\mu g\,m^{-3}$, and the median concentration of the means of the eleven Urban Background sites was 1.5 $\mu g\,m^{-3}$ [Butterfield et al., 2010]. The mean Edinburgh Partisol BC concentrations, measured in this work, were lower than the UK-wide median values at the Roadside site (3.4 $\mu g\,m^{-3}$ versus 6.3 $\mu g\,m^{-3}$) and Urban Background site (1.4 $\mu g\,m^{-3}$ for the whole period of measurement, and 1.3 $\mu g\,m^{-3}$ for 2009 only, versus 1.5 $\mu g\,m^{-3}$). The mean Edinburgh Rural BC concentration of 0.5 $\mu g\,m^{-3}$, from this work, was slightly higher than the 0.4 $\mu g\,m^{-3}$ reported for the UK Network by Butterfield et al. [2010]. Although exactly the same periods of are not being compared, BC concentrations in Edinburgh appear to be lower, in general, than the national average.

3.3.3 Site inter-comparison

The daily BC concentration was variable over time at all of the sites with the following general trend in magnitude: Rural < Urban Background < Roadside (Table 3.1 and Figure 3.6). As there is a relatively relatively low level of heavy industry in Edinburgh, and biomass burning is not a common method of space heating within homes, road traffic is likely to be the main source of BC in the city and the reason why mean BC concentration was highest at the Roadside site.

There was a reasonable linear agreement between the BC concentrations at the Rural and Urban Background sites ($r^2 = 0.68$), showing that common trends in BC concentration were being followed, i.e., a high concentration at one site tended to coincide with a high concentration at another (Figure 3.7a). This suggests some commonality of sources and

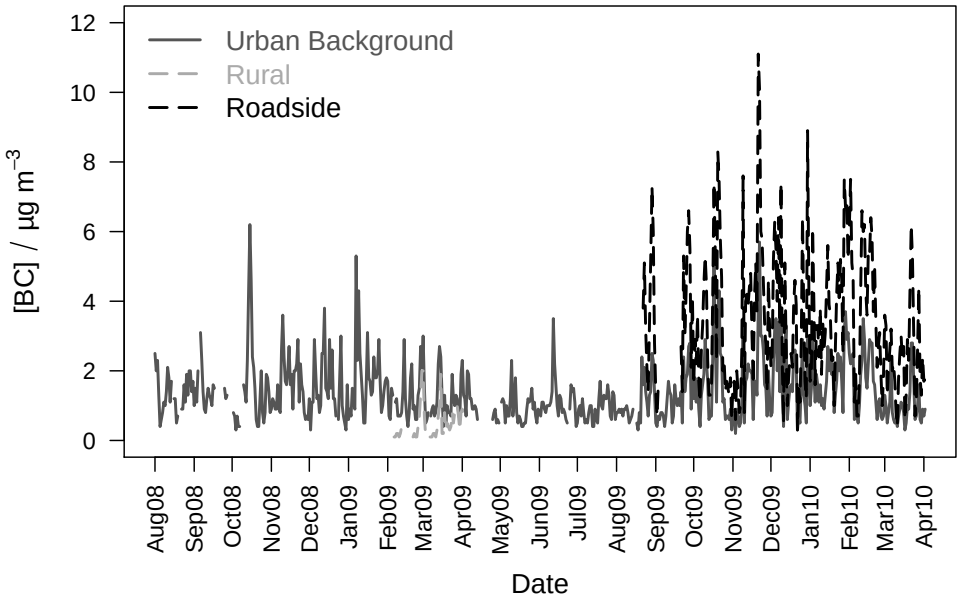

Figure 3.6: Time series of daily BC concentration at the Urban Background, Rural and Roadside sites (20 August 2008 – 21 April 2010).

meteorology at the sites. The BC detected at the Rural site could have come from the city of Edinburgh, which would explain the good agreement. However, only 46 days of measurements were made so not too much should be read into this agreement. PM from exhaust emissions was expected to be the major source of BC so less BC should be detected at the Rural location, which is further removed from busy roads than the Urban Background site [Lenschow et al., 2001]. This is seen in Figure 3.7a, in which all data, and the major axis line, are below the $y = x$ relationship. The average of the daily Urban Background BC increments (Urban Background – Rural) of 0.7 µg m^{-3} is an indication of the amount of BC, on average, that came from urban sources in Edinburgh, which is about half of the mean Urban Background BC concentration.

There was a good linear agreement ($r^2 = 0.82$) between the BC concentrations at the Urban Background and Roadside sites (Figure 3.7b). Again, this shows that the general trend in BC concentration was being followed regardless of location (due to common sources and meteorology). The better linear agreement between these sites ($r^2 = 0.82$), compared with Rural versus Urban Background ($r^2 = 0.68$), can be explained by: 1) these sites being closer to each other and more likely to experience the same weather; and 2) these sites being closer to urban sources of BC [Lenschow et al., 2001]. The influence of direct traffic emissions at the Roadside site is demonstrable by the concentrations of BC being more than twice those at the Urban Background site (major axis slope of 2.21 in Figure 3.7b). The average of the Roadside BC concentration increments

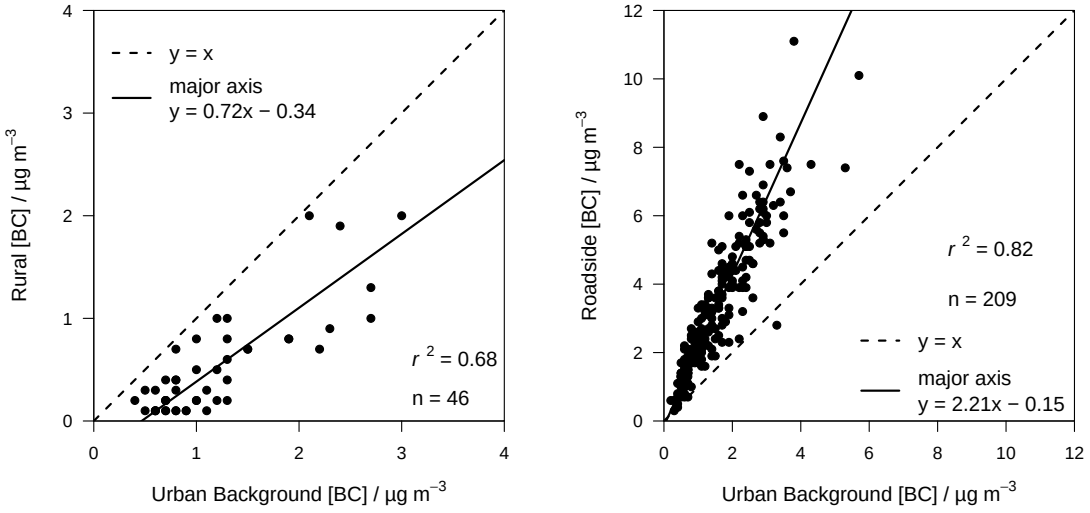

(a) Rural versus Urban Background **(b)** Roadside versus Urban Background

Figure 3.7: Scatter plots of daily BC measurements from the three monitoring sites.

(Roadside − Urban Background) of $1.8\,\mu g\,m^{-3}$ is an indication of the amount of BC, on average, that came from direct traffic emissions, which is about half of the mean Roadside BC concentration.

3.3.4 BC versus PM_{10}

The time series of Urban Background PM_{10} and BC shows that BC was a relatively small fraction of PM_{10} (Figure 3.8). There is also a suggestion that peaks in PM_{10} were matched by peaks in BC. This apparent relationship can be more closely analysed by examining the scatter plot of the data in Figure 3.9a. In fact, the linear agreement was not particularly good ($r^2 = 0.36$), which shows that the variations in concentration of BC were largely independent of changes in PM_{10}. The major peaks in BC concentration were, in general, not matched by those of PM_{10}, highlighting some differences in source influence of the two PM metrics. According to the major axis relationship BC contributed $\sim 7\,\%$, on average, to PM_{10}. As BC was a small proportion of PM_{10} mass, changes in local emissions (most likely traffic-related) of BC did not greatly influence PM_{10}. Another driver for the difference could be that BC was affected differently by local meteorological conditions compared with the other portion of PM_{10}. BC concentrations are likely to be reduced by high wind speeds due to dilution through advection but these same conditions could lead to an increase in PM_{10} concentrations through the re-suspension of road dust.

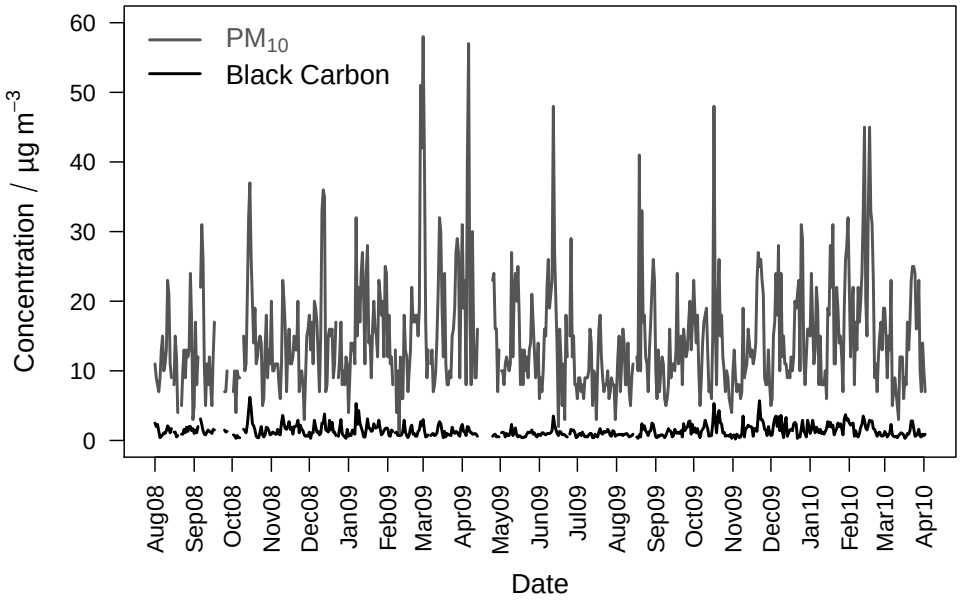

Figure 3.8: Time series of daily mean Urban Background PM_{10} and BC measurements from a Partisol monitor.

There was a good linear relationship ($r^2 = 0.76$) between BC and PM_{10} at the Rural site (Figure 3.9b), with the peaks in BC concentration being matched by the peaks in PM_{10}. This is likely to be the result of the Rural monitor sampling general "background" air that has common sources of BC and PM_{10}. The Rural site was far enough from the nearest busy road that direct traffic emissions would not be measured here, but diluted BC from Edinburgh could be detected. The major axis relationship indicates that Rural BC contributes, on average, $\sim 4\,\%$ to PM_{10} at this site. This lower contribution than at the Urban Background site can be explained by the lack of immediate sources of particles from vehicle exhausts, and could be viewed as the general "background" level of BC.

As at the Urban Background site, Roadside BC had a relatively low linear correlation ($r^2 = 0.47$) with PM_{10} (Figure 3.9c), with the major peaks of both occurring at different times. Since high levels of BC were not always associated with high PM_{10} the sources are likely to be different. $\sim 65\%$ of the average Roadside PM_{10} increment is explained by the average Roadside BC increment, i.e., $\sim 65\%$ of the traffic source of PM_{10} was BC. $\sim 35\%$ of the average Roadside PM_{10} increment is therefore explained by other traffic sources, i.e., the re-suspension of road dust, or brake and tyre wear. The influence of traffic emissions at this site is revealed by the relatively high major axis slope (Figure 3.9c); on average BC was $\sim 16\,\%$ of PM_{10}. This contribution is more than

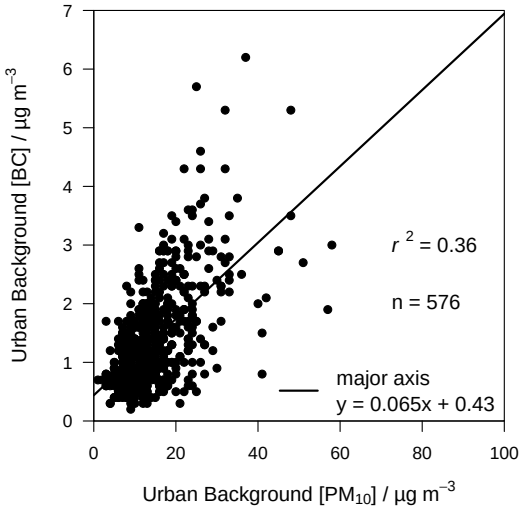

(a) Urban Background

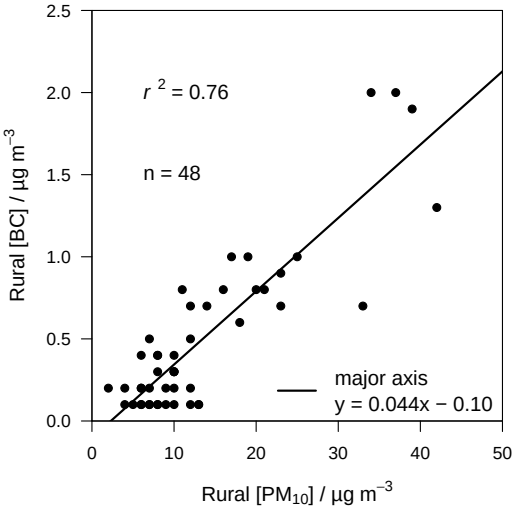

(b) Rural

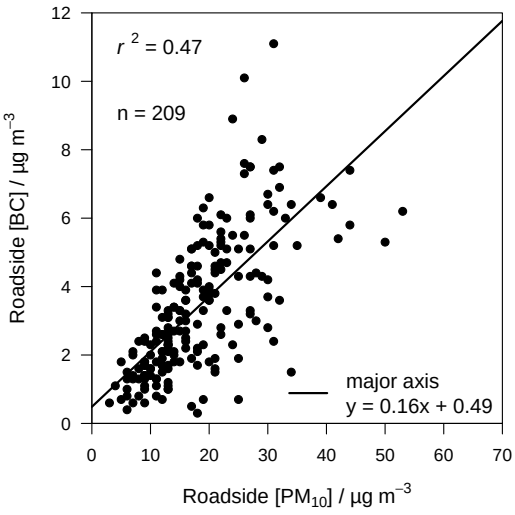

(c) Roadside

Figure 3.9: Scatter plots of daily BC versus PM_{10} measurements from the three monitoring sites.

twice that observed at the Urban Background site. Exposure to BC in the Edinburgh urban area will therefore be higher at locations close to busy roads.

The results found in this work support those from Heal et al. [2005] who reported that the "background" component of BS, influenced by long-range transport, was a minor source compared with BS generated in the local vicinity of the urban area of Edinburgh.

3.3.5 Comparison with wind data

More insight about the possible sources of BC is obtained by examining how concentrations vary according to wind speed and wind direction (Figure 3.10). The high values centred around low wind speeds, in Figure 3.10, suggest that BC sources were close to the Urban Background and Roadside monitoring sites. Both sites were close to roads so vehicle exhaust emissions were likely to be the main contributors to BC in Edinburgh. During periods of low wind speed, concentrations were able to build up; high winds would lead to dispersion and lower BC concentrations. The same pattern was also observed at the Rural site (high BC concentrations at low wind speeds and low BC concentrations at high wind speeds) but this is not plotted due to the lack of data points. There is no evidence in Figure 3.10 of a source of high BC outside of the city, unlike the easterly source seen for PM_{10} (which was likely to be from the re-suspension of road dust, generation of sea spray, or long-range transport from Europe), confirming the conclusion that relatively low concentrations of BC were locally emitted and less affected by regional scale meteorology [Buchanan et al., 2002].

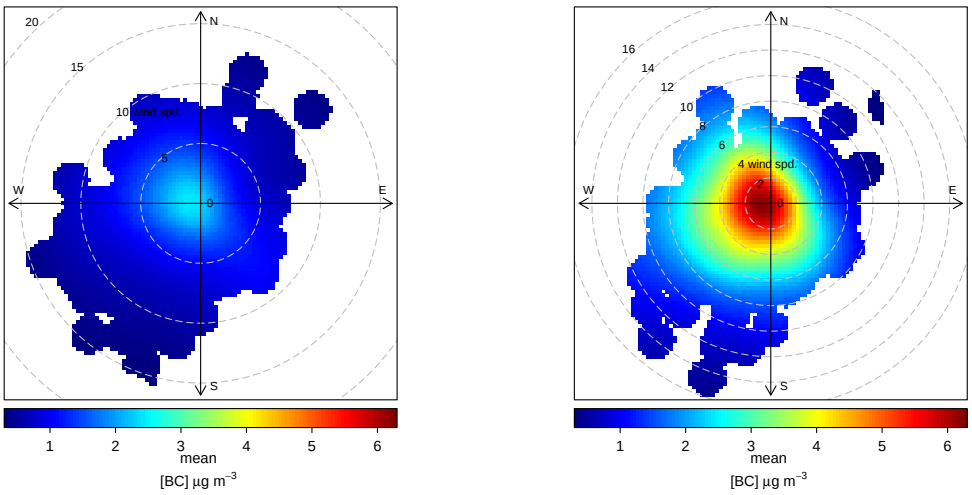

(a) Urban Background **(b)** Roadside

Figure 3.10: Polar plots to show how BC concentration varies with daily wind speed and wind direction.

However, comparing BC concentrations with hourly wind data (Figure 3.11) demonstrates that there was a source to the south-east with higher speeds, which is consistent with transport from continental Europe (also seen for PM_{10}). This is shown most clearly at the Roadside site (Figure 3.11b) but why it is not as obvious at the Urban Background site (Figure 3.11a) is unclear. As would be expected with BC, the hourly polar plots in

Figure 3.11 confirm a very local source to the monitoring site during periods with little wind speed. The shape of the plot in Figure 3.11b shows this as exhaust emissions from traffic on the roads directly to the north and west of the Roadside site.

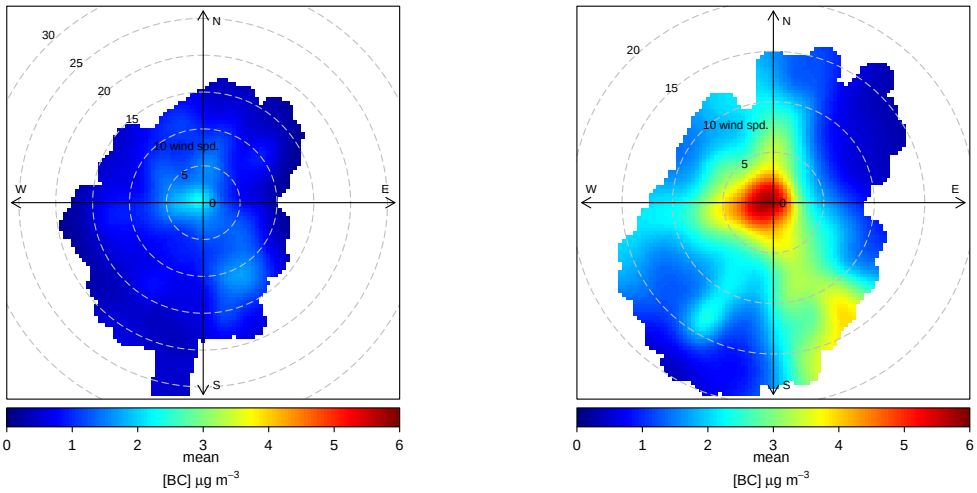

(a) Urban Background

(b) Roadside

Figure 3.11: Polar plots to show how BC concentration varies with hourly wind speed and wind direction.

3.3.6 Seasonal trend

A seasonal trend in EC was observed by Kiss et al. [2002] and Duarte et al. [2007] with maximum values during autumn and winter, and minimum concentrations during warmer periods. It was suggested that the increase of concentrations during autumn and winter was related to an increase in domestic heating, and lower ambient temperatures shifting the semi-volatile organic compounds from the gas phase into the particulate phase. Looking at the BC data in Figure 3.12 a similar trend was observed at the Urban Background site in Edinburgh. Although there is a lot of variation in the data there does appear to be a dip in BC concentration during the warmer summer months. As wood burning is not a common method of domestic heating in Edinburgh this is more likely to be related to the phase shift of semi-volatile compounds according to changes in ambient temperatures.

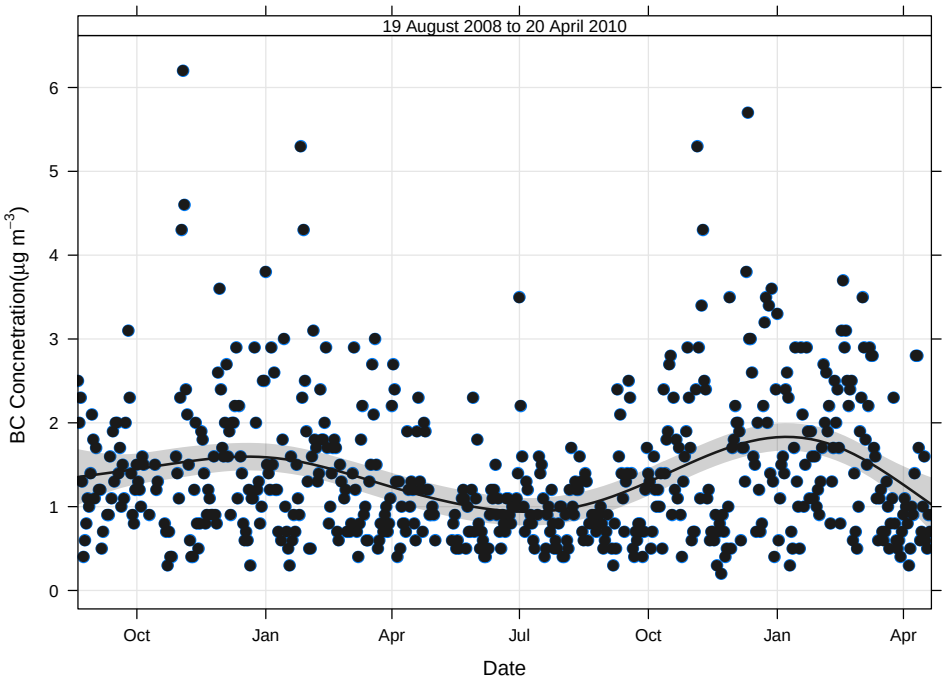

Figure 3.12: Time series of BC concentrations at the Urban Background site to highlight the seasonal trend. The trend line is a spline calculated using a generalized additive model [Carslaw and Ropkins, 2011]. 95% confidence intervals are shown in grey.

3.4 Conclusions

It has been shown that it is possible to determine aethalometer-equivalent daily concentrations of BC by measuring the optical reflectance of the PM_{10} filters from the Partisol samplers. However, as the conversion of reflectance values to BC concentrations is reliant on a number of correction factors, which vary according to the nature of the PM sampled, the accuracy of the results with variations in time and location are not assured. This is an issue with all BC and BS measurements that rely on fixed values of these correction factors.

The concentration of BC in Edinburgh was shown to be relatively low, with the daily variation being controlled by local emissions and meteorology. BC as a proportion of PM_{10} increased with sampling location in the order: Rural < Urban Background < Roadside. Predominantly traffic-related BC concentrations increased during periods of low wind speed and were not greatly influenced by long-range transport of PM (although there was a possible continental source). The local and anthropogenic nature of BC should make it more amenable to control than the larger natural and long-range portions of PM_{10}. It could be seen as beneficial to human health if European legislation moved

more towards the monitoring and reduction of harmful BC compared with the current Directives [European Union, 2004, 2008] that focus on PM_{10}.

Chapter 4

The water-soluble organic matter component of PM

4.1 Introduction

Carbonaceous material is an important part of particulate matter (PM). Approximately one-third on average of urban background PM_{10} in the United Kingdom (UK) is comprised of black carbon (BC)/elemental carbon (EC) and organic matter (OM) [AQEG, 2005]. It was shown in Chapter 3 that up to $\sim 16\%$ of PM_{10} in Edinburgh was BC, with the majority of this likely to be due to direct emissions from anthropogenic fossil fuel burning in vehicles. Any remaining carbonaceous material in the PM_{10} samples collected for this project should be OM.

There are a number of potential sources of the organic fraction of PM: direct emissions from fossil fuel and biomass burning; and indirect gas-to-particle conversion of organic vapours, which can be anthropogenic (for example, petrol and solvents) or natural (vegetation). This leads to a complicated mixture of organic compounds in PM that presents a considerable analytical challenge to characterise. One approach to the characterisation of this material is by detailed organic speciation, usually by gas chromatography mass spectrometry (GC-MS). Although hundreds of organic compounds have been detected using this technique, even in the most comprehensive investigations only 10–40 % of the OM were unambiguously identified on a molecular level [Pöschl, 2005]. Even if the speciation techniques cannot provide information on the concentration and properties of the organic PM as a whole, they can be used to detect specific target compounds that are potentially toxic, or source tracers, or both [Gelencser, 2004].

Another approach is to look at the bulk properties of the sampled aerosol particles. Mass concentrations of PM can be determined by different techniques. In this work

it was done gravimetrically for PM_{10} (Chapter 2) and by using reflectance for BC (Chapter 3). A common method for the determination of total carbon (TC), EC and organic carbon (OC) (where TC = EC + OC) is by thermochemical oxidation and evolved gas analysis (CO_2 detection) of a filter sample by controlling the temperature and atmosphere in the instrument used (for example, Birch and Cary [1996]). Although the TC measurements usually have good enough sensitivity and accuracy, the division between OC and EC has inherent uncertainty because of a continuous change in thermochemical refractiveness, rather than a sharp boundary [Gelencser, 2004; Pöschl, 2005]. BC and EC are both methods of detecting soot carbon in PM but can give different results because of the different properties they measure (optical reflectance and chemical refractiveness, respectively). The question of what is actually being measured will be looked at in Chapter 6.

Organic species contain other elements besides carbon so a conversion factor needs to be used to determine the mass of OM present from the results of OC analysis. A recent study in the UK [Yin and Harrison, 2008] used previously determined factors [Harrison et al., 2003] of 1.4 (urban background) and 1.3 (roadside) to convert the mass of OC to a mass of OM in PM samples. These values were based on the assumptions that: 1) the major contributor to OM was primary emissions predominantly from road traffic, with a contribution, especially in the summer months, from secondary organic carbon; and 2) traffic emissions (mainly diesel) were likely to have a ratio of about 1.2. Yin and Harrison [2008] found the mean composition of PM_{10} at a UK urban background site to contain $\sim 8\%$ EC (comparable to the $\sim 7\%$ of BC found in Chapter 3 of this work) and $\sim 24\%$ OM. A review by Heintzenberg [1989] showed the average mass of global tropospheric urban PM to have a similar composition: $\sim 9\%$ EC and $\sim 31\%$ OM. Despite the good agreement, there will be uncertainty in these values due to the estimation of the factors used to derive them.

It is possible to determine the concentration of water-soluble organic matter (WSOM) in aerosol by extracting filter samples with water and measuring the amount of dissolved organic carbon (DOC) in the aqueous extracts. Duarte et al. [2007] found that rural-coastal WSOM in Portugal contributed $\sim 8\%$ to $PM_{2.5}$ and followed a seasonal trend (along with TC, OC and EC) with maximum values during autumn and winter, and minimum concentrations during warmer periods. This trend was similar to that seen by Kiss et al. [2002] who suggested the increase of concentrations during autumn and winter in rural Hungary may be related to an increase in domestic heating, and lower ambient temperatures shifting the semi-volatile organic compounds from the gas phase into the particulate phase.

Once in the aqueous phase, the composition of WSOM can be investigated by a number of sophisticated chemical analytical techniques. For example, Duarte and Duarte [2005] used ultraviolet-visible (UV-Vis), synchronous fluorescence (with $\Delta\lambda = 20$ nm), Fourier transform infrared (FT-IR) and cross polarization and magic angle spinning (CPMAS)-^{13}C nuclear magnetic resonance (NMR) spectroscopies to show that WSOM was dominated by a high content of aliphatic structures, carboxyl groups and aliphatic carbons single bonded to one oxygen or nitrogen atom. They also determined that autumn samples exhibited a higher aromatic content than summer samples, which they attributed to lignin breakdown products most likely released during wood combustion processes (i.e., biomass burning processes in domestic fireplaces during low temperature conditions).

Although a large proportion of OC in aerosol is WSOM, and investigation of the amount and nature of this fraction of atmospheric particles has been an active research area over the last 10–20 years, information on the constituents of WSOM is still relatively poor. This chapter aims to add to the available data by presenting results from the analysis of WSOM concentrations measured at the Urban Background, Rural and Roadside sites in Edinburgh. The following chapter (Chapter 5) investigates the nature of the Edinburgh WSOM with UV-Vis spectroscopy.

4.2 DOC measurement

All sample preparation was carried out in the School of Chemistry at the University of Edinburgh. Laboratory surfaces and equipment were wiped before use to remove dust. Gloves (purple nitrile or powder-free latex) were worn at all times in the laboratory to prevent contamination of the samples. Glass sample vials (15 ml), test tubes and storage bottles were cleaned by rinsing with deionised water (10 MΩ followed by 18 MΩ), baking at 500 °C for 1 h and drying in a desiccator. The plastic lids were cleaned by soaking in deionised water (10 MΩ for 1 h), rinsing with deionised water (18 MΩ) and drying under a stream of N_2. Plastic items used for the handling, storage and transport of filters would be cleaned with deionised water (18 MΩ) and methanol (LC-MS), and dried overnight, before use.

4.2.1 Method validation

The first step in the analysis of DOC was to test the TOC-Analyser with different concentrations of the following two National Institute of Standards and Technology (NIST) standard reference material (SRM)s:

1648 **Urban Particulate Matter** Consists of natural atmospheric PM collected in an urban location (St Louis, MO, USA) in a baghouse specially designed for this purpose.

1649a **Urban Dust** An atmospheric particulate material collected in an urban area (Washington DC, USA) in 1976–1977 using a baghouse specially designed for the purpose. It is the same particulate material that was issued previously in 1982 as SRM 1649 but it has been re-bottled.

Both SRMs are intended for use as control materials in the evaluation of methods used in the analysis of atmospheric PM. The particulate material was collected over a period of 12 months and, therefore, represents a time-integrated sample. The PM was removed from the baghouse filter bags by a specially designed vacuum cleaner and combined into a single lot. This lot was passed through a 125 µm (120 mesh) sieve to remove bag fibres and other extraneous materials. The sieved material was then thoroughly mixed in a V-blender and bottled. While the sample is not intended to be representative of the area in which it was collected, it should generally typify atmospheric PM obtained from an urban area. The SRMs were provided in amber glass bottles and stored away from direct sunlight at fridge temperature. To ensure equilibration to ambient conditions, they were removed from the fridge at least 2 h before analysis.

4.2.1.1 SRM sample preparation

Before use, the 4-figure laboratory balance was levelled, switched on and left to warm up for 30 min. To equilibrate the balance to laboratory conditions, the draft shield was opened and closed 3 times. A 100 g calibration mass was weighed 3 times, without recording the result, to exercise the balance. The calibration mass was always handled with clean tweezers to prevent any contamination that would alter its mass. When not being used it was stored in a wooden container. The balance was calibrated with the 100 g calibration mass. After calibration the empty balance was tared and the calibration mass was weighed. If the mass was outside 100.0000 ± 0.0002 g the balance was re-calibrated until the mass was within this range.

The required quantity (~ 0.01 g) of SRM 1648 (0.0101 g) and 1649a (0.0075 g), to make up $\sim 1\,\mathrm{mg\,ml^{-1}}$ stock solutions, was weighed directly into a glass sample vial. 10 ml of deionised water (18 MΩ) was added to each sample, and a blank was made that contained no SRM. Plastic lids were placed on the vials and they were shaken using a laboratory shaker for 30 min. After standing for a further 30 min each solution was filtered through a sterile 0.22 µm Millex syringe filter (Millipore, Billerica, USA) into a fresh vial and covered with a fresh lid. The syringe filter was rinsed with 10 ml of deionised water (18 MΩ) immediately before use, to remove any potential soluble contaminants. Dilutions of the aqueous SRM samples were made, to create samples of different concentrations, as follows: 5 ml of sample was added to a fresh vial; 5 ml of deionised water (18 MΩ) was added to the sample; a fresh lid was added to the vial and the sample was shaken for 5 min on the laboratory shaker. Four dilutions of each of the aqueous SRM solutions was made giving five different sample concentrations and one blank with 'zero' concentration. The samples were stored in the freezer ($-30\,^{\circ}$C) until further use and defrosted overnight in a refrigerator the night before analysis. The defrosted samples were mixed with a Whirlimixer before analysis, to ensure homogeneity.

4.2.1.2 Preparation of 2000 ppmC standard

The volumetric flasks and stoppers were subjected to the following cleaning procedure (similar to that used by Hibbs [2002]): 24 h in 10 % v/v Decon 90 in 10 MΩ deionised water; 24 h in 10 % v/v Aristar grade HCl in 10 MΩ deionised water; 24 h in 10 % v/v HPLC grade methanol in 10 MΩ deionised water; 24 h in 10 MΩ deionised water; followed by rinsing with 18 MΩ deionised water. After cleaning, volumetric flasks and stoppers were covered and left to dry overnight (an image of the drying tray is shown in Figure 2.12a).

425 mg of potassium hydrogen phthalate (99.5%, Sigma Ultra), which had been dried to a constant mass, was weighed into a 100 ml volumetric flask and mixed with ~ 50 ml of 18 MΩ deionised water. 100 µl of ortho-phosphoric acid (puriss. p.a. for HPLC, 85%, Fluka) was added to the mixture and the flask was shaken until all of the solid material had dissolved. The volume was then made up to 100 ml with 18 MΩ deionised water. The solution was transferred into a pre-cleaned amber coloured glass storage bottle, which was stored under refrigeration and replaced on a monthly basis.

4.2.1.3 Preparation of 10 ppmC standard

Fresh 10 ppmC standards were made up for each daily set of DOC measurements. Two standards were made by introducing 1 ml of the 2000 ppmC standard into two separate 200 ml volumetric flasks. The volume was made up to 200 ml with 18 MΩ deionised water and the contents of the flasks were thoroughly mixed with shaking.

One of the 10 ppmC standards was used to calibrate the analyser to 10.00 ppm ($\equiv$ 10.00 mg l^{-1}). The instrument used was a DC-80 Total Organic Carbon Analyser (Tekmar-Dohrmann, Cincinnati, USA) based at the Scottish Agricultural College (SAC) in Edinburgh. Aqueous samples were injected into the reaction vessel, filled with a persulfate solution (which magnifies the oxidation power of the reaction), and exposed to UV radiation. The UV light oxidized the carbon within the sample to produce CO_2, which was then detected by an infrared (IR) analyser. The instrument was switched on 30 min before use to warm up. 1 ml of the standard was injected into the instrument and the Start button depressed. Once a DOC value (in ppm) was obtained the Calibrate button was depressed to calibrate the instrument to 10.00 ppm. This process was repeated for three injections to obtain a consistent calibration. The system was rinsed with deionised water (18 MΩ) and then replicate injections of the water were analysed. The system blank was determined by injection of freshly withdrawn reactor solution. The volume of deionised water (18 MΩ) to be added to the unused 10 ppmC standard, to compensate for any DOC in the water, was calculated as follows:

$$\text{Volume (ml)} = 20X + 2X^2 \tag{4.2.1}$$

where

X = the average DOC concentration (mg l^{-1}) of the deionised water (18 MΩ) sample after subtraction of the system blank

This was done by one of the SAC technicians using a volume of 5.7 ml. The system was recalibrated from three injections of the diluted 10 ppmC standard. Assuming consistency in the system blank and water used, this dilution was used for all subsequent 10 ppmC standards.

4.2.1.4 DOC concentration

The DOC concentration (mg l^{-1}) of the SRM samples was measured by injecting 1 ml aliquots into the analyser (one sample was lost due to the glass vial cracking in the

freezer). The mean of duplicate injections was used and the results of this analysis are shown as "total carbon" in Figure 4.1. The instrument showed an excellent linear response for the measurement of DOC in the SRMs ($r^2 \geq 0.99$), validating its suitability for measuring the DOC concentration of PM_{10} collected in Edinburgh.

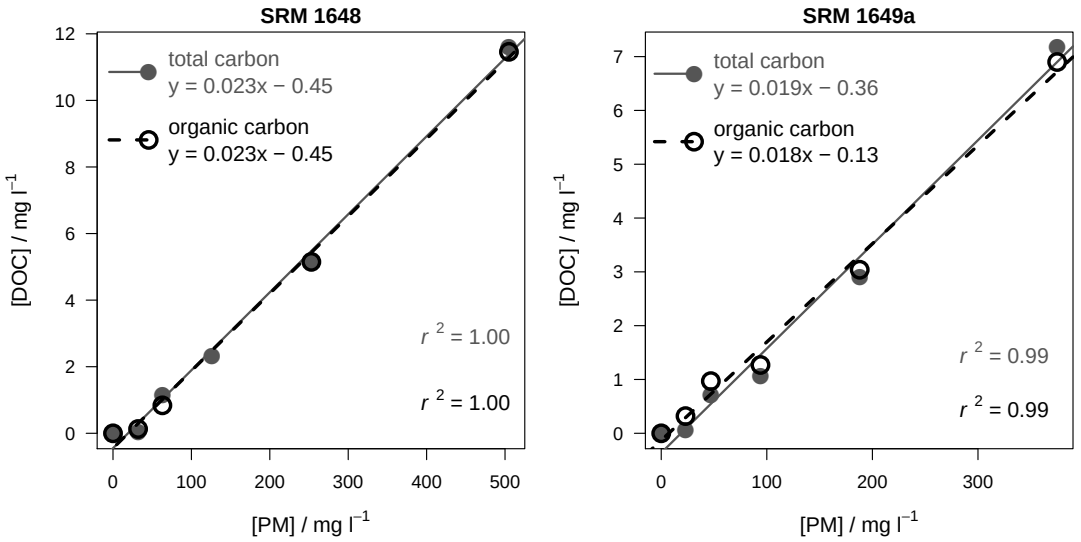

Figure 4.1: DOC concentration against different concentrations of two NIST SRMs (1648 and 1649a). Grey points and lines are from samples that have not been acidified, i.e., they contain inorganic and organic carbon. Black points and lines are from samples that have been acidified, i.e., they contain organic carbon only. OLS regression lines are shown.

The samples were acidified (pH $\sim$ 2) with 50 µl of ortho-phosphoric acid and sparged for 5 min immediately prior to analysis with the same ultra-high purity oxygen that was used as a carrier gas in the total organic carbon (TOC) analyser. Inorganic (carbonate; CO_3^{2-}) carbon reacts with the acid to form CO_2 that is subsequently removed from the sample. These samples were analysed as before and the results shown as "organic carbon" in Figure 4.1. There is no indication of the presence of carbonate carbon in SRM 1648 as the regression equations are the same. Although there appears to be a difference in results for SRM 1649a, the regression equation for "organic carbon" is within the 95 % confidence intervals of the "total carbon" regression model. Therefore, there is no evidence for the presence of carbonate carbon in SRM 1649a and if it is present the quantity is negligible (i.e., undetectable). The linear regression slopes in Figure 4.1 show that, on average, $\sim$ 2 % of these PM SRMs was DOC, which is $\sim$ 15% of the certified OC contents.

4.2.2 Aqueous filter extraction

One batch of filter samples (14 daily samples and 2 Machine Blanks) was extracted per day in the laboratory. Filters from Partisol monitors at the Urban, Roadside and Rural sites (Section 2.2) were placed, sampled side facing inwards, into glass test tubes. 15 ml of deionised water (18 MΩ) was added to each test tube (to ensure that the filters were completely submerged), the samples were covered with aluminium foil, and subjected to 30 min of sonication to dissolve the WSOM. After a further 30 min of standing, the aqueous extracts were filtered through 0.22 µm syringe filters (previously rinsed with 10 ml of deionised water (18 MΩ)) into cleaned glass sample vials to remove insoluble compounds. Cleaned plastic lids were screwed onto the vials and the samples were stored in the freezer (−30 °C) until further use.

4.2.2.1 Solid phase extraction

The purpose of the silica-based solid phase extraction (SPE) procedure (reversed phase) was to isolate WSOM from aqueous samples without the presence of inorganic constituents that could interfere with further chemical characterisation (e.g., UV-Vis analysis). The method used was based on that of Varga et al. [2001]. After defrosting, the aqueous extracts were acidified (pH ∼ 2) with 50 µl of 1 M phosphoric acid and then mixed with swirling. In order to minimise acid hydrolysis of the organic compounds, the aqueous extracts were acidified just before starting the procedure. HyperSep C18 SPE Columns (Thermo Fisher Scientific, Waltham, USA) with a 200 mg bed weight and 3 ml column volume were used for the extraction. Material was drawn though the columns under vacuum at a rate of ∼ 1 ml/min. The process was carried out as shown in Table 4.1.

Table 4.1: Different stages of the SPE procedure shown in order. LC-MS grade methanol obtained from Fisher Scientific was used.

Stage	Description	Material	Volume
1	Activation	Methanol	2 × 2.5 ml
2	Equilibration	Phosphoric acid (0.01 M)	2 × 2.5 ml
3	Loading	Sample	2 × 2.5 ml
4	Washing	Deionised water (18 MΩ)	2 × 2.5 ml
5	Elution	Methanol	2 × 2.5 ml

The effluent from stages 1–4 was discarded. The eluate from stage 5 was collected in a fresh sample vial, transferred to a cleaned Quickfit® glass test tube and evaporated to dryness using a rotary evaporator (BÜCHI Labortechnik AG, Switzerland) to remove the bulk of the methanol. An initial test tube containing only methanol (5 ml) was run on the rotary evaporator to clean the instrument, prior to evaporation of the samples. Some methanol remained in the samples after rotary evaporation (as shown by initial DOC measurements, which overloaded the instrument) so the WSOM was redissolved in 10 ml of deionised water (18 MΩ), transferred to a fresh sample vial, frozen at −30 °C for at least 24 h, and freeze dried over a period of 48 h. Freeze drying took place in a laboratory at the Grant Institute (School of GeoSciences, the University of Edinburgh). After freeze drying, the sample vials containing methanol-free (solid) WSOM were stored in the freezer (−30 °C) until further use. The samples were removed from the freezer on the day of analysis, left to equilibrate to ambient conditions for 1 h and then redissolved in 10 ml of deionised water (18 MΩ).

4.2.3 Sample concentration

Two batches of aqueous samples were measured per day using the Total Organic Carbon Analyser, which was switched on 30 min before use to warm up. Samples were defrosted overnight in the refrigerator (if necessary) the day before analysis. The defrosted samples were mixed by Whirlimixer to ensure homogeneity. The instrument was calibrated and samples measured as described in Section 4.2.1. Due to time constraints only single sample measurements were made to give DOC concentrations in $\mathrm{mg\,l^{-1}}$ (but the Machine Blanks were measured in duplicate). Re-calibration was carried out after every 9 sample injections. Duplicate measurements of the deionised water (18 MΩ) were taken after the initial calibration, and single measurements of the water carried out after each subsequent re-calibration. This was to check for consistency and aid with the calculation of the limit of detection (LOD). A 'zero' measurement (i.e., running the instrument without injecting a sample) was also taken after each calibration to test for any offset or drift in the instrument and/or reactor solution. The mean Machine Blank value was subtracted from each sample concentration to correct for any carbon introduced during the sampling, extraction and measurement procedure.

4.3 Results and discussion

The DOC concentration ($\mathrm{mg\,l^{-1}}$) of the daily aqueous PM_{10} extracts was calculated as shown in the following equation (each 14 day batch of samples had 2 Machine Blanks associated with it):

$$\text{Aqueous DOC} = \text{Sample DOC} - \text{Mean Machine Blank DOC} \tag{4.3.1}$$

For comparison with other daily PM metrics, the value of interest is the daily concentration of WSOM in the sampled air (in units of $\mu\mathrm{g\,m^{-3}}$). To derive this, the aqueous DOC concentration ($\mathrm{mg\,l^{-1}}$) was converted to an atmospheric DOC concentration ($\mu\mathrm{g\,m^{-3}}$) using the following calculation:

$$\text{Atmospheric DOC} = \text{Aqueous DOC} \times W/V \tag{4.3.2}$$

where

W = volume of water used to extract WSOM from the PM_{10} filters, in units of ml

V = volume of air sampled during daily PM_{10} collection, in units of $\mathrm{m^3}$

In Section 4.1 it was stated that organic species contain other elements besides carbon. To get from atmospheric DOC to WSOM mass concentration in the sampled PM_{10} a conversion factor needs to be used. Kiss et al. [2002] (using elemental analysis) and Sun et al. [2011] (using a High-Resolution Time-of-Flight Aerosol Mass Spectrometer (HR-ToF-AMS)) determined an average OM to OC mass ratio of 1.9 (with a relative standard deviation (SD) $\leq 6\%$) for WSOM. As this value did not vary considerably during sampling at different locations (urban and rural), over different time periods (summer and winter), it seems appropriate to use it in this work. The WSOM concentration ($\mu\mathrm{g\,m^{-3}}$) was therefore calculated as follows:

$$\text{WSOM Concentration} = \text{Atmospheric DOC} \times 1.9 \tag{4.3.3}$$

4.3.1 Errors in the determination of WSOM concentration

Errors related to the sampling of PM_{10} have already been discussed in Chapter 2 so this section mainly considers errors in the aqueous extraction and measurement of WSOM. It is possible that not all of the water-soluble (WS) material was extracted from the filters

so WSOM is operationally defined here as the material that was dissolved by water, and passed through the 0.22 µm syringe filter, in the method described in Section 4.2.2.

Three variable volume Fisherbrand pipettors (Thermo Fisher Scientific, Waltham, USA) were purchased at the start of the project. The pipettors were supplied with certified values (%) of inaccuracy and imprecision at specific volumes, and were tested and re-calibrated periodically. Testing and re-calibration was performed by weighing the specified volumes of deionised water (10 MΩ) in triplicate on the laboratory balance. To accurately calibrate the equipment, consideration was given to the "buoyancy effect" caused by the difference in mass of air, the water displacing it, and the mass of the balance weights. The correction factors used are shown in Table 4.2. The pipettors were adjusted, if necessary, to dispense the correct mass of water (the temperature of the water was determined before measurement). The inaccuracy and imprecision were calculated as follows:

$$\text{Inaccuracy} = \frac{|MM - TM|}{TM} \times 100\% \tag{4.3.4}$$

$$\text{Imprecision} = \frac{SD}{TM} \times 100\% \tag{4.3.5}$$

where

MM = mean of the triplicate mass measurements, in units of g

TM = theoretical mass of the specified volume, according to the correction factor, in units of g

SD = standard deviation of the triplicate mass measurements, in units of g

The results of the pipettor testing are shown in Table 4.3. The method used for calculating the certified inaccuracy and imprecision is not shown on the certificate but Equation (4.3.4) and Equation (4.3.5) are logical estimates. The measured inaccuracy was lower than the certified value, whereas measured imprecision was higher. This shows there may have been some scope for improving pipetting technique. Regardless of this, all the pipettor errors were $< 0.5\%$. The 15 ml of water used to extract the filters was measured as 3×5 ml, with a maximum error of 0.27% ($3 \times 0.09\%$). Errors due to pipetting can, therefore, be viewed as small, and the measurement of water volume accurate and precise. These relatively small pipetting errors will also impact on the SPE procedure and the redissolving of WSOM after freeze drying.

Table 4.2: Correction factors for volumetric calibration using water. Factors are based on water density and are corrected for buoyancy. Data from Harris [1996].

Temperature (°C)	Correction Factor ($mg\,l^{-1}$)
19	1.0027
20	1.0029
21	1.0031
22	1.0033
23	1.0035
24	1.0038

Table 4.3: Results of testing the three pipettors and the certified values provided by the manufacturer. Measured values were calculated according to Equation (4.3.4) and Equation (4.3.5), and are means of all the tests ($n = 8$). CIA = certified inaccuracy; MIA = measured inaccuracy; CIP = certified imprecision; MIP = measured imprecision.

Volume Range	Certified Volume	CIA %	MIA %	CIP %	MIP %
1–5 ml	1 ml	0.50	0.04	0.03	0.09
100–1000 µl	200 µl	0.22	0.16	0.06	0.12
20–200 µl	50 µl	0.52	0.26	0.11	0.43

Chemicals and columns used in the extraction procedure could have introduced contamination into the samples, despite care being taken to avoid this. These systematic errors should be corrected (at least to some degree) by the use of Machine Blanks. It is also likely that semi-volatile material (if present) was lost during rotary evaporation and/or freeze drying.

Some error will be present in the production of the 2000 ppmC and 10 ppmC standards due to: weighing of the potassium hydrogen phthalate; accuracy and precision in use of volumetric flaks; quantity of material dissolved; ageing stability; pipetting; and dilution of the 10 ppmC standard to compensate for any DOC in the water. Only the pipetting errors were quantified and these have already been described.

Checks were made on the TOC analyser, as mentioned in Section 4.2.3, and the results of these are summarised in Table 4.4. The instrument 'zero' of 0.01 ± 0.01 ($\pm\sigma$) shows that some carbon was 'detected' by the instrument. Whether this was from carbon

present in the reactor solution or drift in the detector is unclear. A 'zero' value of $0.02\,\mathrm{mg\,l^{-1}}$ is only 0.2% of 10 ppm so can be considered as being relatively small. If the SD of the deionised water (18 MΩ) measurements is considered as the measurement blank, the LOD was $0.22\,\mathrm{mg\,l^{-1}}$ (3σ). At $> 2\%$ of 10 ppm, the mean water value is higher than ideal (although it is equal to the LOD). This could be due to inadequate purification of the deionised water (18 MΩ) by the purification system (EASYpure$^{\mathrm{TM}}$ UV, Barnstead | Thermolyne, Dubuque, USA), contamination in the glassware used to transport and store the water, or contamination in the needle used to inject the sample. The accuracy and precision in the determination of the concentration of the 10 ppm standard were 0.47% and 1.78%, respectively (calculated according to Equation (4.3.4) and Equation (4.3.5), respectively). The maximum error in measurement of the 10 ppm standard was therefore $< 2\%$.

Table 4.4: Summary of checks carried out on the TOC analyser.

DOC	Instrument Zero	Deionised Water	10 ppmC Standard
Mean / $\mathrm{mg\,l^{-1}}$	0.01	0.22	10.05
SD / $\mathrm{mg\,l^{-1}}$	0.01	0.07	0.18
n	167	213	254

Each sample concentration was corrected by subtracting the concentration obtained from the mean of 2 Machine Blanks (Equation (4.3.1)). The importance of making Machine Blank corrections was discussed in Chapter 2. The PM_{10} blank was explained by changes in filter mass over time being correlated with changes in ambient relative humidity (RH). Increases in PM_{10} blank mass were most likely due to the absorption of moisture onto the filters. This common systematic error with the Partisol PM_{10} concentrations was successfully corrected, as shown by the good agreement with Tapered Element Oscillating Microbalance Filter Dynamics Measurement System (TEOM-FDMS) concentrations (Section 2.5.1). The DOC blank masses are shown in Table 4.5. As the quartz filters should have been carbon-free after baking at 500 °C, there is some parallel here with the mass increase over time observed during filter weighing (Chapter 2), i.e., there seems to have been some increase in the amount of DOC in the filters over time. DOC is known to be a constituent of fog-water [Kiss et al., 2001] and rainwater [Camposa et al., 2007] so there could have been some carbon in the moisture absorbed by the filters. As the filters were out of storage for six weeks (i.e., four weeks of conditioning and weighing, and two weeks in the Partisol samplers), there was enough time for the absorption of semi-volatile organic vapours to occur, which is a more likely explanation

for some of the DOC observed in the Machine Blank filters. Salma et al. [2007] have shown that the organic species that cause adsorptive sampling artefacts are generally more water-soluble (more polar) than the OM collected on the filters.

Table 4.5: Summary of Machine Blank DOC masses.

Machine Blank Mass	Urban Background	Rural	Roadside
Mean / g	0.000019	0.000018	0.000017
SD / g	0.000004	0.000003	0.000003
n	34	3	15

The deionised water (18 MΩ) was responsible for $\sim$ 20%, on average, of the Urban Background DOC blank (using values from Table 4.4 and Table 4.5). Other potential sources of contamination exist throughout the process and have already been mentioned. A stage yet to be mentioned is the cleaning of the glassware through rinsing with deionised water (10 MΩ followed by 18 MΩ) followed by baking at 500 °C for 1 h. The glassware was soaked in deionised water (10 MΩ) for at least 12 h before rinsing. It is possible that this cleaning procedure could have been made more effective by baking the glassware for a longer period of time, although Camposa et al. [2007] found relatively high residual DOC concentrations after baking at 500 °C for at least 5 h. In the Camposa et al. [2007] study, the average concentration for residual DOC was surprisingly high — five times higher than the control water. This is similar to the value found in this study where the average DOC concentration of the Urban Background Machine Blank was six times higher than the control water. Regardless of the source of this residual DOC, the same procedure was used to correct for this systematic error that was successfully used for PM_{10} so it should not unduly effect the reliability of the DOC concentrations obtained.

The conversion factor of 1.9 used to determine the concentration of WSOM from the measured DOC (Equation (4.3.3)) is only an estimate and subject to both uncertainty and sample-to-sample variability. To determine the concentration of WSOM in the daily PM_{10} samples collected in Edinburgh, which is of interest, this estimation is unavoidable unless much more is known about the composition of the PM sampled. This situation is similar to that made in the measurement of BC (Chapter 3) where a number of factors were used in converting reflectance measurements to concentrations. An example of a study that determined the OM to OC ratio is the work of Kiss et al. [2002]. They measured the elemental composition of the WS fraction isolated from atmospheric PM (collected at a rural site in Hungary from January to September 2000) and used

this to calculate an average OM to OC mass ratio of 1.93 (with a relative SD of 2%). Another study, by Sun et al. [2011], used HR-ToF-AMS measurements of WSOM in particles collected at one rural and three urban sites (in 2004 and 2005). They directly determined the OM to OC mass ratio to be 1.93 ± 0.12 (average $\pm 1\sigma$). Although both of these studies found the same ratio despite being measured at different locations over different time periods, and the ratio was found to have a low level of variability, the value of 1.93 may not be ubiquitous. The estimate of 1.9 was used in this work with the acceptance that the level of error introduced is uncertain.

4.3.2 Data capture

The data capture for the WSOM measurements is shown in Table 4.6. Complete data capture did not occur for the PM_{10} sampling part of the project (Table 2.9) so $< 100\%$ of the daily filters were available for aqueous extraction. The data capture for WSOM at the Urban Background site is lower than for PM_{10} (80% against 94%). The main reason for this is that the first few batches of filters were used for developing the water extraction procedure and these results are therefore not used. A big issue encountered during the development stage was that the glass of the glass vials used for sample storage was so thin that it would easily crack under freezing ($-30\,^{\circ}C$) and a lot of samples were lost. This problem was solved by moving to vials with thicker glass, although a vial would still occasionally break. The first PM_{10} sample was collected on 20 August 2008, whereas the first DOC result is only available from 23 October 2008.

Table 4.6: Record of WSOM data capture at the three monitoring locations.

	Urban Background	Rural	Roadside
Days Sampling	610	56	224
Number of Samples	491	40	206
Data Capture %	80	71	92

For practical reasons, if too many filter samples were missing from a batch it was decided that no filters from that batch would be extracted. This had a large impact on the WSOM data capture from the Rural site as the first batch of filters was not extracted and the sampling period was only short. By the time it came to extract the filters from the Roadside site the procedure was well developed and the WSOM data capture was almost as good as with PM_{10} (92% against 93%).

WSOM concentrations of $< 0\,\mu g\,m^{-3}$ were removed from the dataset.

4.3.3 Mass concentration

A summary of the WSOM mass concentration ($\mu g\,m^{-3}$; calculated using Equation (4.3.3)), from all of the sites, is shown in Table 4.7.

Table 4.7: Overview of WSOM mass concentrations at all of the monitoring sites.

WSOM Concentration	Urban Background	Rural	Roadside
Mean / $\mu g\,m^{-3}$	1.6	1.6	1.8
SD / $\mu g\,m^{-3}$	1.2	1.4	1.1
Minimum / $\mu g\,m^{-3}$	0.0	0.2	0.2
Maximum / $\mu g\,m^{-3}$	10.8	4.9	6.1
n	491	40	206

As with BC, the WSOM concentrations are reported to the nearest $0.1\,\mu g\,m^{-3}$. Taking into consideration the level of precision and accuracy in the measurements, and the overall magnitude of WSOM concentrations, this is an appropriate level of precision.

The LOD calculated according to DOC measurements of deionised water (18 MΩ) is $0.22\,mg\,l^{-1}$. This is equivalent to a WSOM concentration of $0.26\,\mu g\,m^{-3}$. It should be borne in mind that this LOD only relates to the precision of the TOC analyser in measuring a deionised water (18 MΩ) blank and does not take into account other aspects of the analytical procedure, i.e., PM_{10} sampling and aqueous filter extraction. Due to the magnitude of the Machine Blank concentration it was not used for calculation of the LOD (this is the reason why no PM_{10} LOD was calculated).

A decision has to be made about what should be done with values that fall below the LOD. Brown [2008] described five possible courses of action for reporting of these values:

1. Not detected
2. < LOD
3. Zero

4. A fraction of the LOD, such as "LOD/2"

5. The result recorded together with a statement of its uncertainty

The first two options provide very little information and do not produce a value that can be used properly in descriptive statistics. The use of "zero" is misleading and will bias values of means and standard deviations, for example. Although using a fraction of the LOD gives some information about the range in which the results may lie and produces a value that can be used in descriptive statistics, the arbitrary nature of the value is likely to bias these statistics. Brown [2008] recommends that LODs are not employed, but the result obtained and its uncertainty quoted instead. The errors already discussed in this chapter, and the quoted LOD, provide a description of the level of uncertainty in the results. Values that fall below the LOD have been left in to avoid bias in the descriptive statistics. Only WSOM concentrations of 0.0, 0.1 and 0.2 $\mu g\,m^{-3}$ would fall below the LOD. This equates to 17 samples (4% of measured values) at the Urban Background site, 1 sample (3%) at the Rural site and 4 samples (2%) at the Roadside site.

The mean WSOM concentrations at the three sites are similar (Table 4.7), with a slightly higher value being observed at the Roadside site. This hints at a minor contribution to WSOM from direct traffic emissions. What is also interesting is the much higher maximum concentration (10.8 $\mu g\,m^{-3}$) measured at the Urban Background site, which deserves closer consideration. A time series of the concentration data is shown in Figure 4.2. The daily variations and magnitudes appear to be well matched at all of the sites (suggesting similar meteorology and source contributions) apart from the Urban Background peak on 3 January 2010. Considering the good agreement between the results on all other days this result appears to be anomalous. This is clearly obvious in scatter plots of the data (Figure 4.3).

There is an excellent linear agreement ($r^2 = 0.90$) between the concentrations at the Rural and Urban Background sites, as shown in Figure 4.3a, which suggests that most of the WSOM is from the same (background) sources outside of the city. A small fraction ($\sim 10\,\%$) of the WSOM appear to come from inside the city, as indicated by the major axis line of gradient 0.89 (Figure 4.3a).

All of the points in Figure 4.3b, apart from one, appear to lie relatively close to the $y = x$ line. The apparent outlier is from 3 January 2010, as mentioned above. It is so far removed from all of the other data points that it seems reasonable to apply Grubbs' Outlier Test [Grubbs, 1969] (at the 99% confidence level), as used in Section 2.5.2 with Equation (2.5.1) and Equation (2.5.2). This value was found to be an outlier ($p < 0.01$)

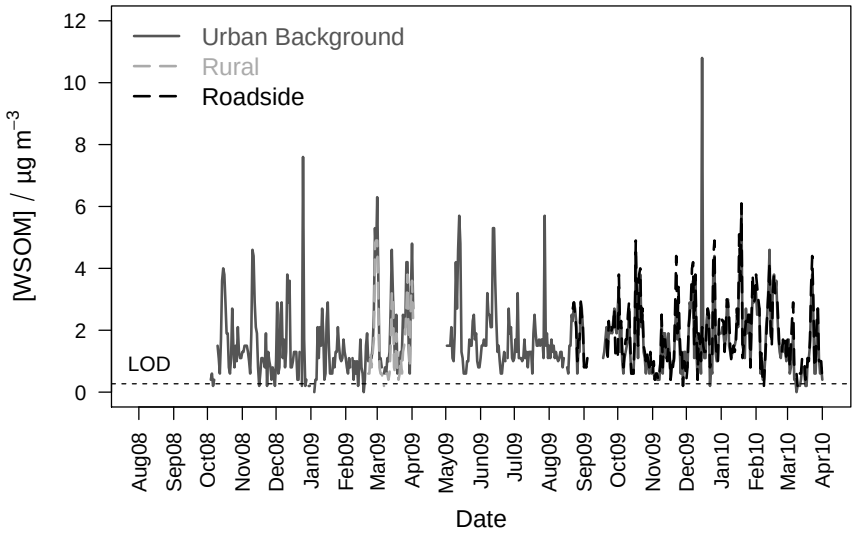

Figure 4.2: Time series of daily WSOM concentration at all of the sites. The LOD is indicated by a horizontal dashed line.

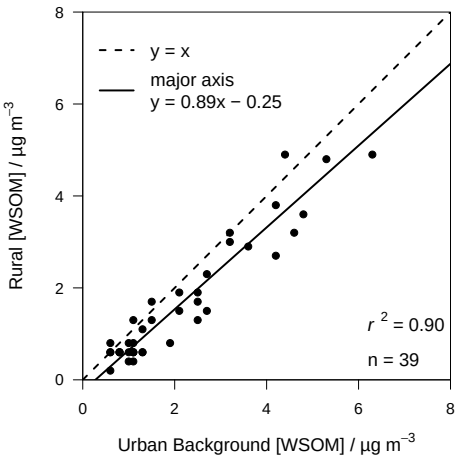

(a) Rural versus Urban Background

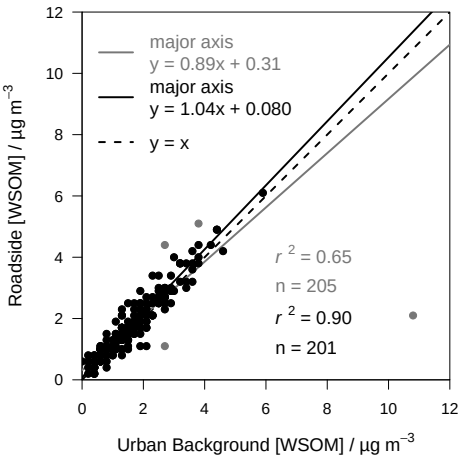

(b) Roadside versus Urban Background (potential outliers and associated data are shown in grey)

Figure 4.3: Scatter plots of daily WSOM concentrations.

so the associated data were removed. The reason for this exceedingly high WSOM concentration in the Urban Background data is not known but it is likely to come from contamination introduced into the sample during collection or extraction, and not be a genuine result. As Grubbs' test was used to remove this value it was applied to the rest of the data and 3 more data points were removed. This is according to the method reported in the UK Equivalence Programme for Monitoring of Particulate Matter [Harrison et al., 2006] where a maximum 5% of data pairs were removed. The 4 data points removed in this work were 2% of the dataset (Figure 4.3b). Due to the potential for false positives in a statistical test of this nature, data with (grey) and without (black) the outliers have been plotted in Figure 4.3b. With the potential outliers removed, a much better linear agreement from ($r^2 = 0.65$ to $r^2 = 0.90$) is seen between the concentration of WSOM at the Roadside and Urban Background sites (Figure 4.3b). Again, this linear agreement suggests that the WSOM are mainly from the same (background) sources outside of the city. The major axis line fitted to this data has a gradient of 1.04. This is taken to mean that $\sim 5\,\%$ of the WSOM is from direct traffic sources, which also explains why the Urban Background concentrations are slightly higher than at the Rural site (i.e., the Urban Background site is closer to traffic-related sources). As a logical trend in WSOM concentration is followed across the sites there is some confirmation that removing the outliers has not badly affected the results. In comparison, the data containing all of the values suggests lower concentrations at the Roadside site (gradient of 0.89 in Figure 4.3b), which is difficult to explain.

4.3.4 WSOM in PM_{10}

The time series of PM_{10} and WSOM concentration at the Urban Background site (Figure 4.4) clearly shows WSOM as a subset of PM_{10}. The nature of the relationship between WSOM and PM_{10} is investigated by looking at scatter plots of the data (Figure 4.5).

The mean concentrations shown in Table 4.7 go some way to suggesting a background source of WSOM at the monitoring sites in this work, with only a slightly higher concentration measured at the Roadside site. As the majority of the PM_{10} mass is not expected to be of local origin (Chapter 2), WSOM and PM_{10} should be well correlated. This was certainly the case at the Rural site ($r^2 = 0.81$ in Figure 4.5b), which is the location least influenced by local sources. The linear relationship was not as good at the Urban Background ($r^2 = 0.49$ in Figure 4.5a) and Roadside ($r^2 = 0.61$ in Figure 4.5c) sites (similar relationships are seen for data including potential outliers, which are shown

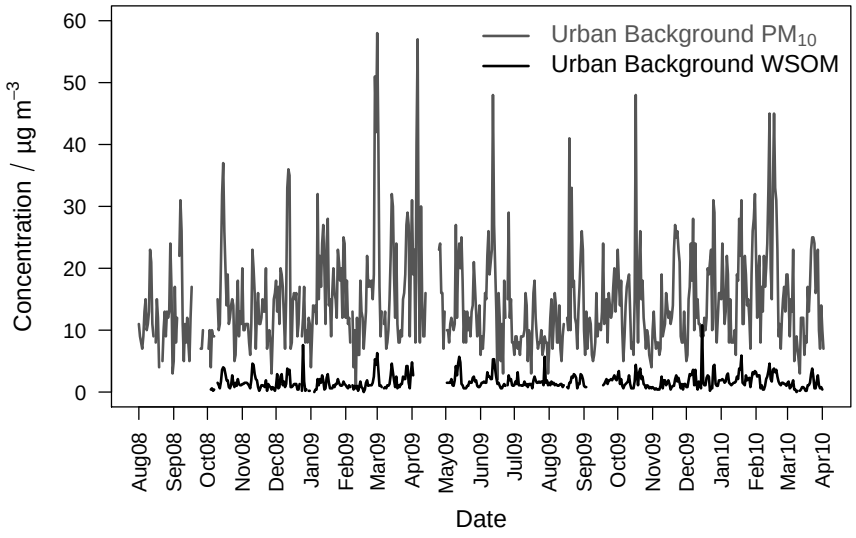

Figure 4.4: Time series of daily Urban Background PM_{10} and WSOM concentrations. The potential WSOM outliers are included.

in grey in Figure 4.5). The lower correlations at the urban sites are likely to be due to small contributions to WSOM from local sources and the longer monitoring periods.

The gradients of the major axis slopes in Figure 4.5 provide an estimate of the average contribution of WSOM to PM_{10} mass of 10–12%. Further support is given to the idea of a background source of WSOM by the highest contribution to PM_{10} occurring at the rural site (Figure 4.5b).

4.3.5 WSOM versus BC

Figure 4.6 shows the time series of WSOM with BC at the Urban Background site. It appears that on the majority of days WSOM concentration was higher than BC concentration. Analysis of the scatter plot of the data (Figure 4.7a) confirms this, with WSOM being ~ 1.5 times higher than BC, on average, at the Urban Background site. The linear relationship between the two is relatively weak ($r^2 = 0.38$) showing that on most days different factors were affecting WSOM and BC concentrations. This observation is expected since the majority of carbonaceous material identified as BC by the optical reflectance measurements (Chapter 3) is unlikely to be water-soluble. WSOM and BC components of PM_{10} are therefore anticipated to independent quantities, except on occasions where they may be derived from similar sources (for example, biomass burning).

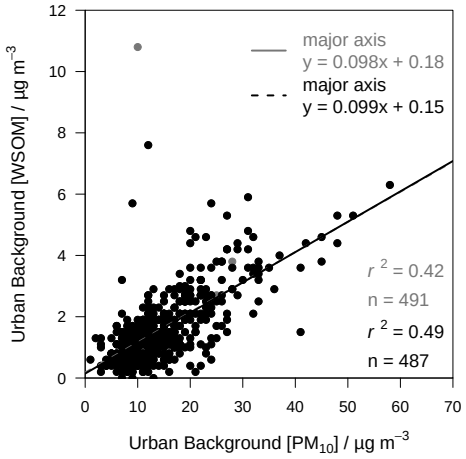

(a) Urban Background (data containing potential outliers is shown in grey)

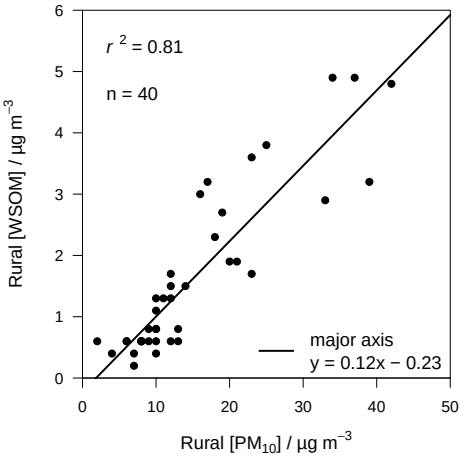

(b) Rural

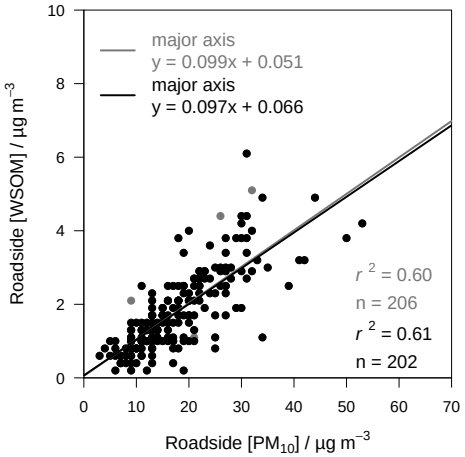

(c) Roadside (data containing potential outliers is shown in grey)

Figure 4.5: Scatter plots of daily WSOM versus PM_{10} concentrations from the three monitoring sites.

There is a much better linear relationship ($r^2 = 0.80$) between WSOM and BC at the Rural site (Figure 4.7b). This is because the air sampled here was remote from any direct sources so the composition of the particles collected here is likely to remain relatively stable over time, i.e., the contribution of WSOM and BC to PM_{10} in background air was fairly constant. It should be mentioned that this may be due to only 40 daily samples being compared and a longer time period may have led to a greater variety in relative concentrations. WSOM concentration was almost 3 times higher than BC concentration at the Rural site. This shows the greater contribution that WSOM makes to PM in general background air. The difference between the levels of WSOM and BC may be due, in part, to the Rural site being close to potential sources of WSOM particles (for

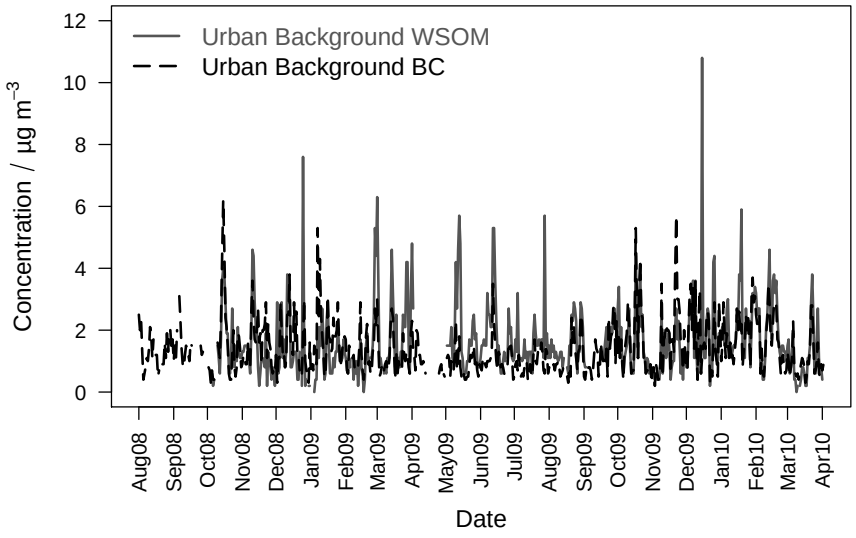

Figure 4.6: Time series of daily Urban Background WSOM and BC concentrations. The potential WSOM outliers are included.

example, natural emissions from vegetation) and removed from potential sources of BC (for example, traffic emissions).

As at the Urban Background site, the linear correlation between WSOM and BC at the Roadside site is poor ($r^2 = 0.47$ in Figure 4.7c). This can be explained by the dominant traffic source of BC, which is not a major contributor to WSOM, and confirmed by the gradient of the major axis line in Figure 4.7c (0.43) showing that BC concentration was more than twice as high, on average, than WSOM concentration. Most of the WSOM should already be present in the background air transported into the city, whereas BC came from vehicle emissions from traffic passing close to this site.

4.3.6 Comparison with wind data

More insight about the possible sources of WSOM is obtained by examining how concentrations vary according to hourly wind speed and wind direction as shown in Figure 4.8 (there is no plot from the Rural site due to insufficient data). The highest concentrations in the polar plots (up to about 3.0 µg m^{-3}) are not as high as the peaks in WSOM concentration (up to about 7.5 µg m^{-3}) because mean concentrations of cells split according to wind speed and wind direction were used, and continuous surfaces were calculated through modelling using smoothing techniques [Carslaw et al., 2006; Carslaw and Ropkins, 2011]. Both plots in Figure 4.8 show a similar pattern, with the highest concentrations being associated with relatively low wind speeds from all

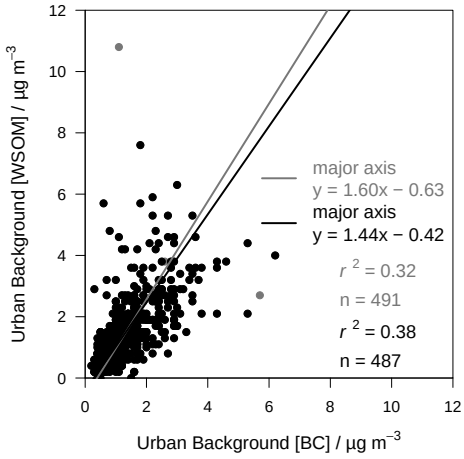

(a) Urban Background (data containing potential outliers is shown in grey)

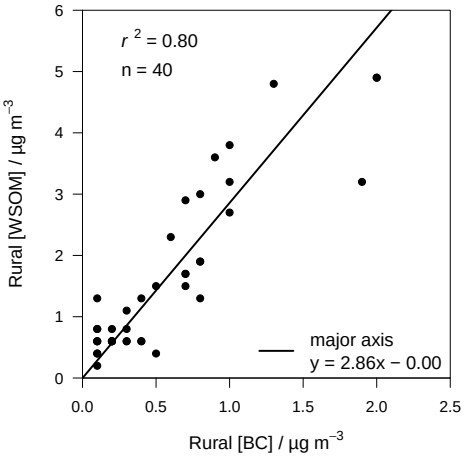

(b) Rural

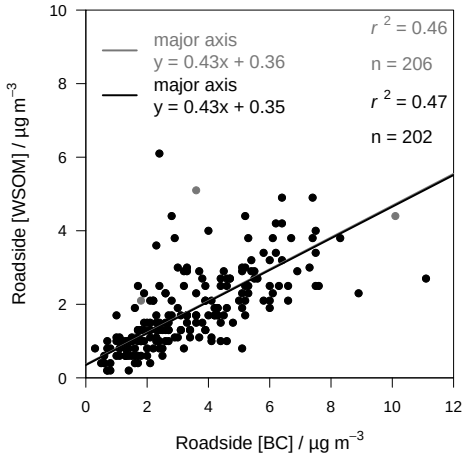

(c) Roadside (data containing potential outliers is shown in grey)

Figure 4.7: Scatter plots of daily WSOM versus BC concentrations from the three monitoring sites.

directions and an influence coming from the south-east at higher wind speeds. The mainly lower concentrations at higher wind speeds can be explained by dilution through advection and increased turbulence.

The source from the south-east with higher wind speeds is almost certainly long-range OM from continental sources, most particularly secondary organic aerosol (SOA) from the oxidation of biogenic volatile organic compound (BVOC) emissions [Heal et al., 2011]. It was reported by Heal et al. [2011] that about half of the average urban background $PM_{2.5}$ carbon in the UK was of contemporary (i.e., non-fossil fuel) origin. As well as the largest component of the contemporary carbon coming from BVOC-derived secondary

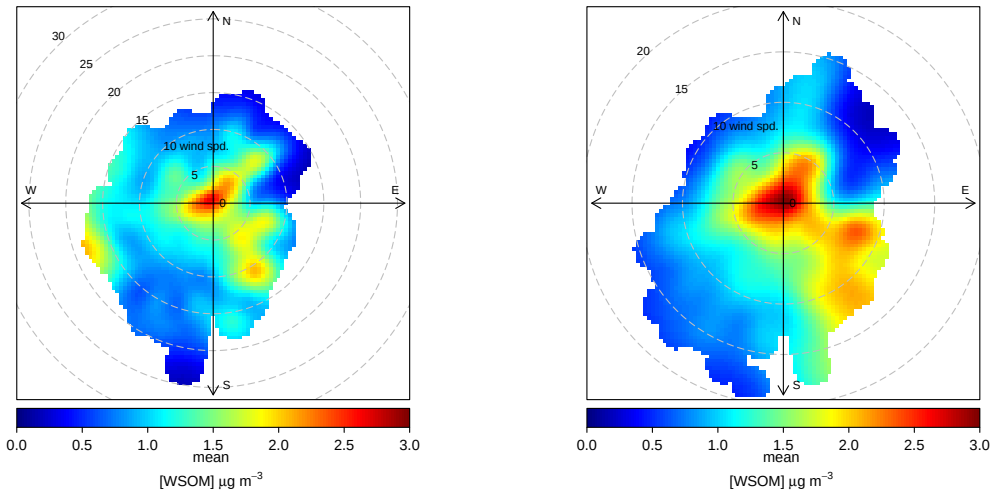

(a) Urban Background **(b)** Roadside

Figure 4.8: Polar plots to show how WSOM concentration varied with hourly wind speed and wind direction.

organic carbon (SOC), there was also a proportion of primary organic carbon (POC) from anthropogenic combustion of biofuel/biomass and some non-combustion sources. SOC/TC ratio was observed by Heal et al. [2011] to be significantly higher with easterly and southerly air-mass trajectories, which agrees with the higher WSOM concentrations observed with south-easterly winds in this work (Figure 4.8). A pollution episode was described in Section 2.4.4, which European particulate forecasting models suggested was due to long range transport of a combination of secondary pollution from Europe and smoke from agricultural fires in western Russia [Griffin et al., 2010]. This also shows that secondary pollution and smoke, from Europe and Russia, were likely to be responsible for elevated levels of WSOM in Edinburgh.

Elevated WSOM concentrations of $> 6\ \mu g\, m^{-3}$ occurred on three occasions (not including potential outliers): Urban Background on 13 January 2009 and 20 March 2009; Roadside on 7 February 2010. The peak on 20 March 2009 coincided with a PM_{10} exceedance and has already been described in Section 2.4.4. Analysis of air mass back-trajectory plots, and data from Griffin et al. [2010], showed that the air arriving at the Urban Background site had passed over the north of France and Benelux and picked up PM that had built up over these regions. The re-circulation of air over the UK at this time helped prolong elevated levels of PM_{10}. It appears from this that the PM in the air picked up over France and Benelux contained relatively high concentrations of WSOM.

Air mass back trajectories for 12 and 13 January 2009 are shown in Figure 4.9. The air arriving in Edinburgh on the day before the peak in WSOM (12 January 2009) had come from the west in a trajectory over the Atlantic Ocean. This air would be expected to be clean, apart from any particles picked up over land immediately before arrival in Edinburgh but previous analysis in this work has not highlighted any local WSOM sources to the west of Edinburgh. The WSOM concentration on this day was low at 0.2 $\mu g\,m^{-3}$ (which is below the LOD). A sharp increase to 7.6 $\mu g\,m^{-3}$ was seen on the following day, associated with air that had followed a trajectory south-west over the landmasses of Svalbard (a Norwegian archipelago in the Arctic) and Iceland, before turning south east to arrive in Edinburgh (over the Atlantic Ocean from the west). This suggests that elevated levels of WSOM were picked up over Iceland (or possibly Svalbard) and transported to Edinburgh, but these northerly landmasses acting as sources of WSOM in midwinter seems very unlikely. A more likely explanation for this unusually high WSOM value is some form of measurement error (e.g., accidental contamination during water extraction), particularly since neither PM_{10} or BC concentration were especially high on this day. High WSOM at another site could have validated this result but no other PM_{10} samples were collected on this day.

Also shown in Figure 4.9 are trajectories for 6 and 7 February 2010. On both days the air arrived in Edinburgh from the east after travelling over Benelux and France, and on both days the WSOM concentrations were relatively high (3.6–6.1 $\mu g\,m^{-3}$). The air mass arriving on 5 February 2010 had also followed a similar trajectory and resulted in another high WSOM concentration (5.1 $\mu g\,m^{-3}$). There is confidence in these peaks detected at the Roadside site being real as relatively high values were also measured at the Urban Background site. As with the PM_{10} and WSOM event in March 2009, air passing over France and Benelux appears to be responsible for high WSOM concentrations in Edinburgh on 7 February 2010. The reason for these elevated levels in Europe at this time is not known but the build up of SOA, and/or the release of biogenic smoke (probably biomass heating), are the most likely contributors to WSOM. Fires in western Russia, and secondary contributions from European anthropogenic pollution and pollen released in northern Europe, were linked with unusually high PM_{10} levels in the UK [Witham and Manning, 2007]. Russian wild fires were unlikely to be a source of PM in February, so it is other organic PM that seems to be causing the higher WSOM concentrations in Figure 4.8 at higher wind speeds from the south-east. The results presented here are consistent with those from the rest of Europe and support the conclusion of a significant contribution from biogenic sources to the carbon in terrestrial PM [Heal et al., 2011].

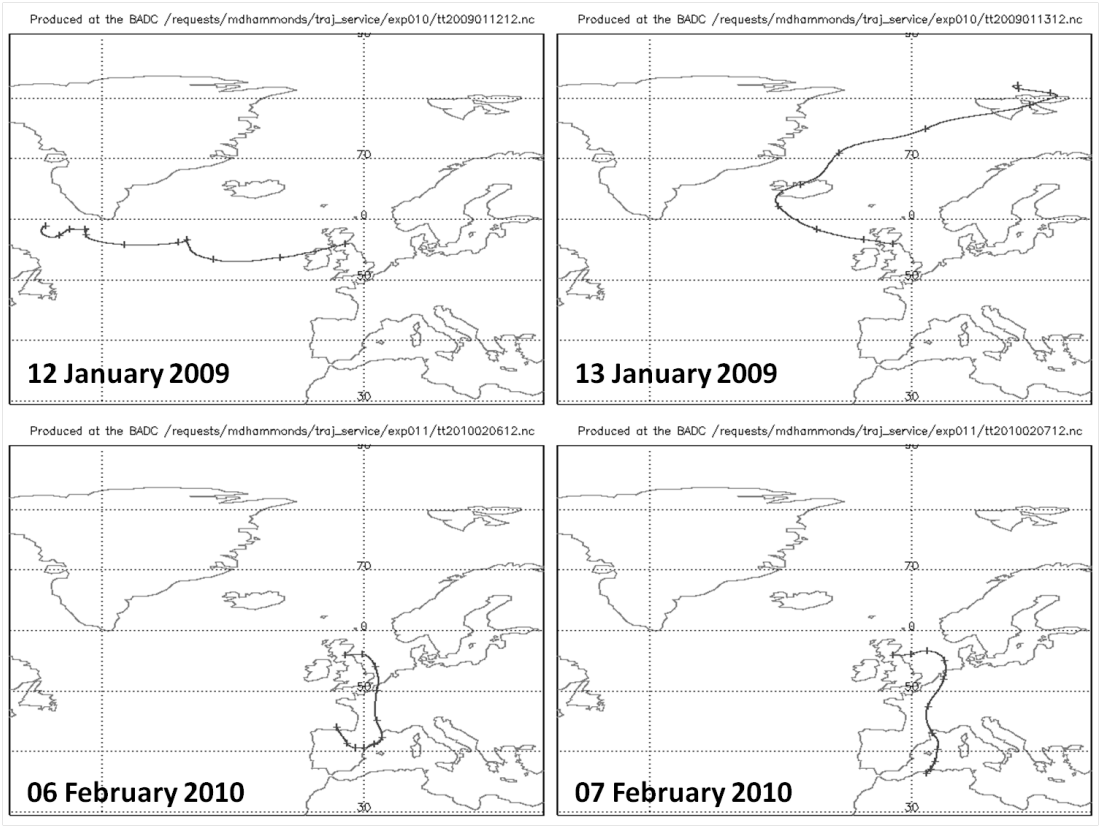

Figure 4.9: 5-day air-mass back trajectories for midday arrival in Edinburgh at the 900 hPa level, from 12–13 January 2009 and 6–7 February 2010. Markers are at 12 h intervals. Data from the BADC Trajectory Service (`http://badc.nerc.ac.uk/community/trajectory/`)

4.3.7 Hydrophobic WSOM

Although the term hydrophobic water-soluble organic matter (HWSOM) appears contradictory, the material recovered from the SPE procedure was the more hydrophobic fraction of the WSOM in the aqueous filter extracts. When the aqueous samples were passed through the columns, the more hydrophobic organic compounds interacted with the silica packing and were retained, whereas the more hydrophilic organic compounds passed through. Inorganic ions also passed through with the hydrophilic compounds and were discarded. The HWSOM thus isolated was then recovered for analysis. During the SPE procedure a brown-yellow band was observed to form on the top of the column, which was representative of the most strongly retained compounds. The colour changed going down the stationary phase to a lighter yellow, representing the more weakly retained compounds. During elution this colour would disappear indicating the recovery of these compounds. The SPE process used in this work was based on that of Varga et al. [2001] who determined that the eluted fraction of the columns consisted of compounds possessing polyconjugated structures.

Initial attempts at isolating the HWSOM from the daily aqueous samples were not successful. Most of the results were below the DOC LOD indicating that insufficient material was being recovered. The combination of the relatively low volume sampling rates of the Partisols ($1\,m^3\,h^{-1}$) and the relatively low PM_{10} levels in Edinburgh contributed towards this. Other studies involved in the analysis of WS compounds extracted from PM have tended to use high volume samplers and longer sampling periods to allow an adequate quantity of material to be collected. For example, Varga et al. [2001] sampled at $40\,m^3\,h^{-1}$ over a period of 2–5 days, and Duarte et al. [2005] sampled at $68\,m^3\,h^{-1}$ over 7 days. The difficulty in the analysis of the daily samples caused by the low level of material collected could be compounded by the following:

- The small portion ($\sim 10\%$) of the PM_{10} sampled that was extracted from the filters as WSOM;
- The small portion of WSOM that was hydrophobic and therefore retained on the columns;
- Failure to recover all the HWSOM retained on the columns;
- Loss of the more volatile compounds in the HWSOM fraction during the removal of methanol.

To increase the amount of material retained on the SPE columns in this project, it was decided to pass a batch of samples (i.e., 14 daily samples) through one column. This allowed enough material to be isolated for measurement by the TOC analyser. All other steps in the procedure were carried out in the same way as for the daily samples. Means of duplicate measurements were calculated and corrected using the means of the Machine Blanks to give an aqueous DOC concentration (Equation (4.3.1); $mg\,l^{-1}$). Aqueous DOC was then converted to a daily equivalent HWSOM concentration ($\mu g\,m^{-3}$) using the following equation:

$$\text{HWSOM} = \frac{\text{Aqueous DOC} \times w1 \times w2 \times 1.9}{w3 \times S \times V} \tag{4.3.6}$$

where

$w1$ = volume of water used to redissolve the solid material after freeze drying, 10 ml

$w2$ = volume of water used to extract WSOM from a PM_{10} filter, 15 ml

$w3$ = volume of water passed through an SPE cartridge per sample, 5 ml

S = number of samples passed through an SPE cartridge, usually 14 but was less in some batches

V = volume of air sampled for a daily PM_{10} sample, assumed to be 24 m^3

A summary of the HWSOM mass concentration ($\mu g\,m^{-3}$; calculated using Equation (4.3.6)), from all of the sites, is shown in Table 4.8. Data are reported to 2 decimal places in order to discern the difference between the relatively low concentrations observed. The mean concentration of HWSOM was highest at the Roadside site. As with WSOM, this is indicative of a minor traffic source of HWSOM within the city. Most of the HWSOM was an inherent part of the background air. On average, $\sim 30\%$ of the WSOM extracted from the PM_{10} filters was isolated as HWSOM. This is a lower proportion than the $\sim 60\%$ proportion reported by Varga et al. [2001].

Table 4.8: Summary of HWSOM mass concentrations at the three monitoring sites.

HWSOM Concentration / $\mu g\,m^{-3}$	Urban Background	Rural	Roadside
n	35	3	15
Mean	0.50	0.51	0.58
Standard Deviation	0.18	0.22	0.18
Minimum	0.11	0.27	0.29
Maximum	0.88	0.71	0.88

Although the mean HWSOM concentrations at the sites differed slightly, the temporal trends were similar at the three sites as shown in Figure 4.10. As with WSOM, this general agreement of HWSOM concentrations over time suggests a predominantly background source. When viewed as a scatter plot (Figure 4.11) the linear agreement between the Roadside and Urban Background sites ($r^2 = 0.43$) is not as good as it may

appear on the time series. The possible traffic source of HWSOM at the Roadside site giving some higher values is likely to be responsible for this. The major axis line fitted to this data has a gradient of 1.26, which is taken to mean that $\sim 25\,\%$ of the HWSOM were from direct traffic emissions. This is $\sim 20\,\%$ higher than the value determined for WSOM (Section 4.3.3; Figure 4.3b). Exhaust PM is likely to be less oxygenated than other sources of WSOM, and it is sampled close to emissions, so there is less time for the transformation of organic aerosol species into more oxidized (more polar, and thus more water soluble) forms. This means exhaust PM will be present in the more hydrophobic portion of WSOM [Salma et al., 2007]. However, a recent study by Glasius et al. [2011] observed that concentrations of non-fossil carbon were higher at roadside locations than at urban background sites. The most likely of the reasons suggested by Glasius et al. [2011] for these higher roadside concentrations are: more tyre wear in re-suspended road dust at roadside locations; and anthropogenic enrichment of biogenic SOA. The possibility of higher concentrations of non-fossil HWSOM at the Roadside site in Edinburgh means there is some uncertainty in the reason for higher HWSOM concentrations, on average, seen in Figure 4.11.

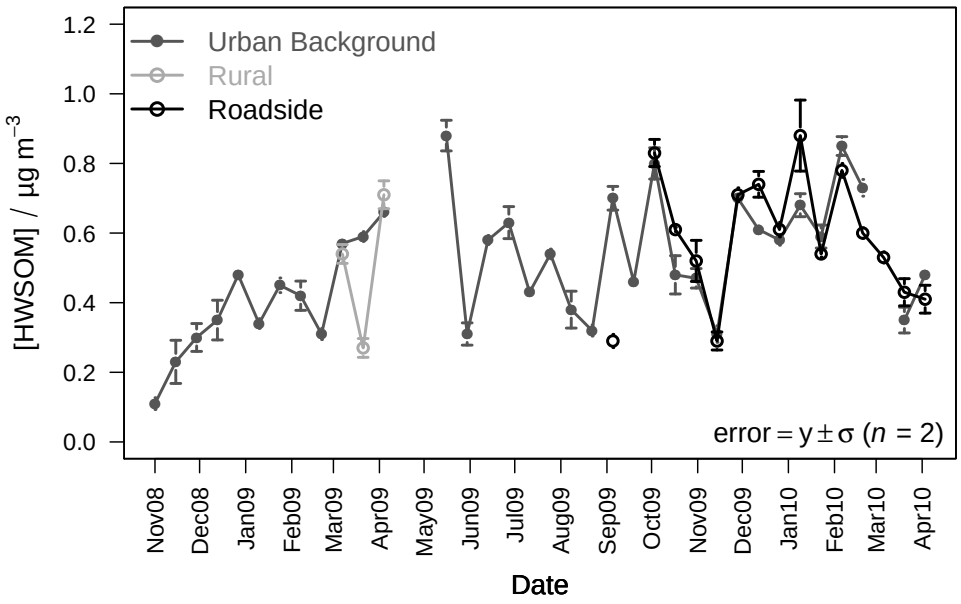

Figure 4.10: Time series of daily equivalent HWSOM concentration at all of the sites. Points are plotted on the first day associated with the 14 day batch.

4.3.7.1 Seasonal trend

A seasonal trend in WSOM was observed by Kiss et al. [2002] (in rural Hungary), Duarte et al. [2007] (in rural-coastal Portugal) and Baduel et al. [2010] (in urban France)

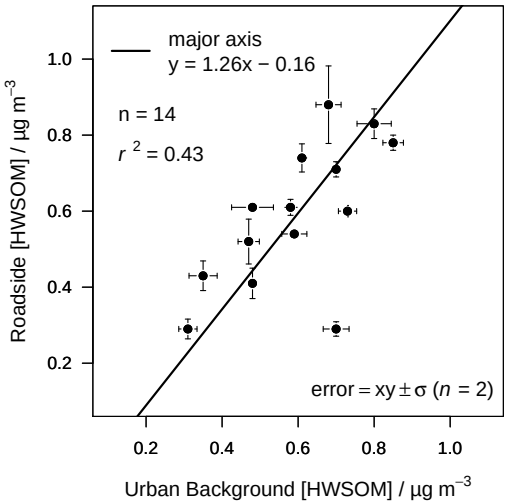

Figure 4.11: Scatter plot of daily equivalent HWSOM concentrations from the Roadside and Urban Background sites.

with maximum values during autumn and winter, and minimum concentrations during warmer periods. It was suggested that the increase of concentrations during autumn and winter was related to an increase in domestic heating, and lower ambient temperatures shifting the semi-volatile organic compounds from the gas phase into the particulate phase. Evaluation of the HWSOM data in Figure 4.12 shows that a similar trend was observed at the Urban Background site in Edinburgh. Although there is a lot of variation in the data there does appear to be a dip in HWSOM concentration during the warmer summer months. As wood burning is not a common method of winter domestic heating in Edinburgh, the dip is more likely to be related to the phase shift of semi-volatile compounds according to changes in ambient temperatures (i.e., less semi-volatile PM in the summer). The lack of a biomass burning source of HWSOM in Edinburgh means that the seasonal trend is not especially pronounced since the winter concentrations are relatively low. Peaks in the concentration trend actually occur in spring and are most likely related to a build up during stable conditions, or long range transport of SOA and biomass smoke arriving from the east (as discussed in Section 4.3.6).

4.3.8 Contribution to PM_{10}

The average contribution to PM_{10} of the different aerosol components measured, calculated from the mean values, is shown in Figure 4.13a. A large proportion of the PM_{10} (up to 84%) remains uncharacterised. This fraction of the PM_{10} collected contains iron rich dust, calcium sulphate, sodium chloride, sodium nitrate, ammonium sulphate, bound water, and water-insoluble OM [AQEG, 2005]. It was reported by

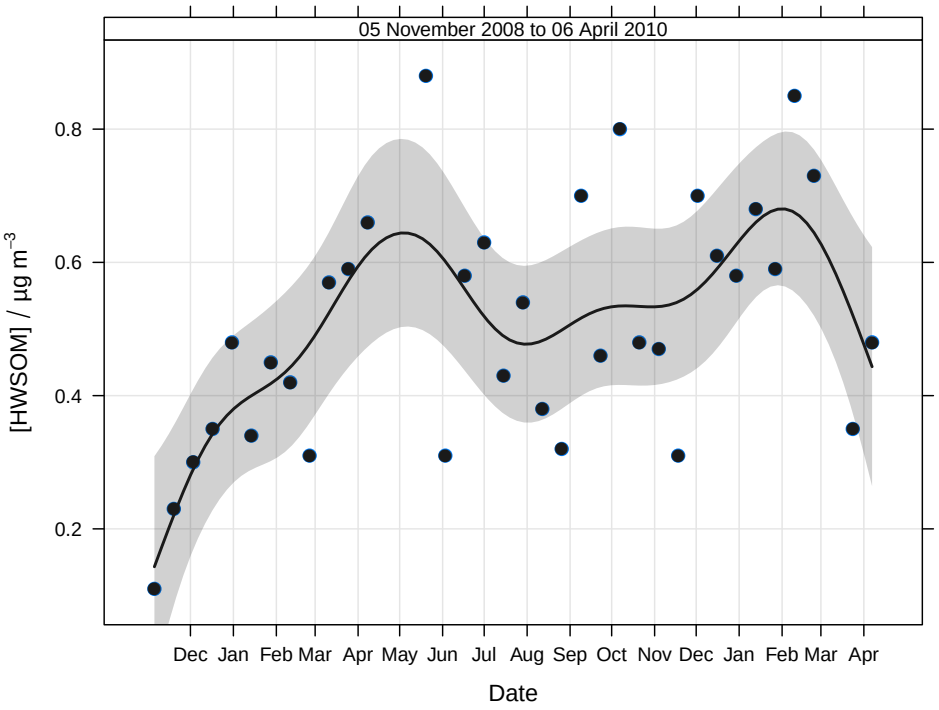

Figure 4.12: Time series of HWSOM concentrations at the Urban Background site to highlight the seasonal trend. The trend line is a spline calculated using a generalized additive model [Carslaw and Ropkins, 2011]. 95% confidence intervals are shown in grey.

AQEG [2005] that the broad chemical composition of UK urban PM, as determined by traditional filter-based chemical analyses, was:

22% organic compounds

18% iron rich dust

14% ammonium sulphate

14% sodium nitrate

10% elemental carbon

8% bound water

8% sodium chloride

6% calcium sulphate

Similar compositions of the carbonaceous fraction of PM were found in other studies already mentioned: ∼ 8% EC and ∼ 24% OM by Yin and Harrison [2008]; ∼ 9% EC and ∼ 31% OM by Heintzenberg [1989].

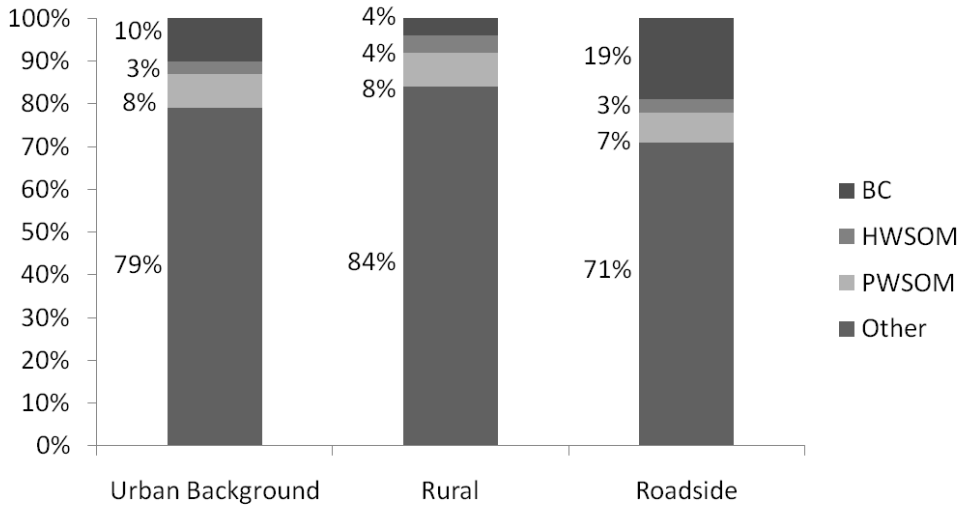

(a) Average relative contributions

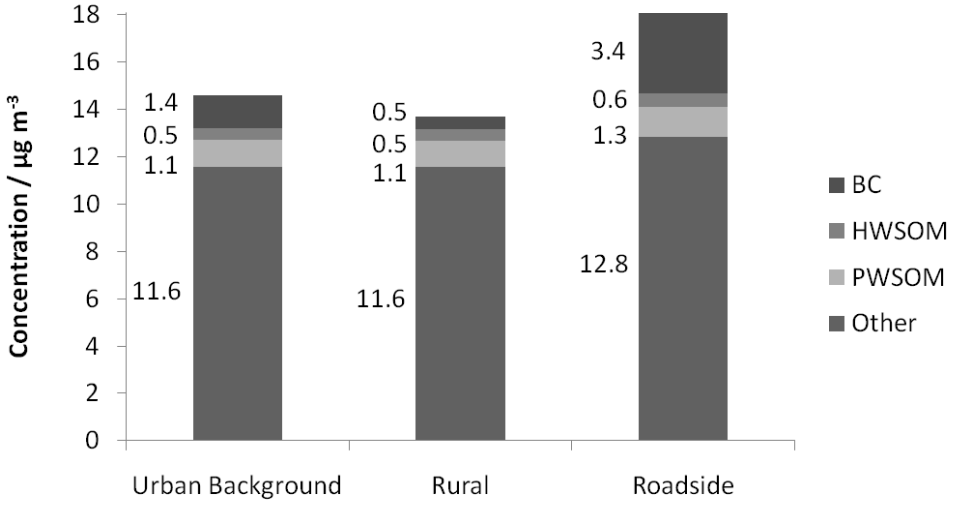

(b) Average absolute concentrations

Figure 4.13: Distribution of the different components of PM_{10} measured at the three Edinburgh sites (BC — black carbon; HWSOM — hydrophobic water-soluble organic matter; PWSOM — hydrophilic water-soluble organic matter; Other — components that were not characterised).

The contribution of BC found at the Urban Background site (Figure 4.13a) matched the broad UK composition (which was measured as EC). Rural BC contribution to PM_{10} was less than half the Urban Background contribution, with Roadside being almost twice Urban Background. The contributions of WSOM to PM_{10} were much

more consistent. As the UK urban PM_{10} contains $\sim 22\%$ OM, it appears that about half of the Edinburgh OM was water-soluble (with the remaining half of insoluble OM not being characterised). About one-seventh of the likely OM content of Edinburgh PM_{10} was isolated by the SPE procedure.

In terms of the average absolute concentrations, shown in Figure 4.13b, Urban Background and Rural PM_{10} had similar compositions, with higher concentrations at the Urban Background site being due to local emissions of BC. All of the measured PM_{10} metrics had higher concentrations at the Roadside site, which shows a traffic source of both BC and WSOM in Edinburgh.

4.4 Conclusions

The DOC concentration of aqueous NIST SRM solutions increased linearly according to the amount of PM in the solution. This validated the required linear response of the TOC analyser and showed that $\sim 4\%$ ($2\% \times 1.9$) of the PM in the SRMs was WSOM, which is less than half the amount of WSOM found in the Edinburgh PM_{10}. This difference could be due to a different sampling method and size fraction of PM being collected, or different source contributions and meteorological effects in the cities where the material was sampled. The difference could possibly be attributed to a reduction in anthropogenic PM emissions in urban areas over recent decades leading to an increase in the relative contribution from biogenic sources.

Despite initial problems with the extraction technique, and relatively low levels of PM_{10} being collected, WSOM was obtained from the filter samples and mass concentrations were measured. About 11% on average of the Edinburgh PM_{10} was WSOM. The majority of this WSOM seems to have originated from air masses outside of the city, although there does appear to be a minor contribution from urban traffic sources. The SPE procedure isolated about one-third of the WSOM as hydrophobic compounds and revealed a relative increase in the amount of less oxygenated material from traffic sources.

Higher than average WSOM concentrations were strongly associated with calm weather conditions that allowed the transient build-up of particle concentrations. Some of the peaks in WSOM concentration were related to the transport of air masses from areas of mainland Europe where biogenic SOA and biomass burning were likely sources. This is consistent with results from elsewhere in Europe that show a significant proportion of terrestrial PM to be biogenic.

Chapter 5

UV-Vis absorption spectroscopy analysis of the WSOM component of PM

5.1 Introduction

Chapter 4 described the extraction of water-soluble organic matter (WSOM) from PM_{10} on filters sampled at Urban Background, Rural and Roadside sites in the Edinburgh area. A fraction ($\sim 30\%$) of this WSOM was recovered from the solid phase extraction (SPE) procedure that was employed to remove inorganic constituents from the aqueous samples. This recovered portion consisted of the most hydrophobic organic molecules and was termed hydrophobic water-soluble organic matter (HWSOM). Isolation of HWSOM on C18 SPE packings was based on the method of Varga et al. [2001]. These authors found that $\sim 60\%$ of the WSOM desorbed from the cartridges in MeOH and this fraction contained $\sim 70\%$ of the Ultraviolet (UV) activity of the total WSOM fraction. The UV analysis by Varga et al. [2001] showed similarities in the spectroscopic behaviour of the eluates from different types of columns, indicating that the retained fractions consisted of the same group of compounds possessing polyconjugated structures.

A number of other studies have measured ultraviolet-visible (UV-Vis) spectra for bulk WSOM derived from aerosol and fog, for example: Havers et al. [1998]; Zappoli et al. [1999]; Krivacsy et al. [2000]; Kiss et al. [2001]; Krivacsy et al. [2001]; Kiss et al. [2002]; Duarte et al. [2005]; Baduel et al. [2010]; Ofner et al. [2011]. The resultant spectra share the same properties of being generally featureless curves with steadily increasing absorptivity towards shorter wavelengths. As with the work of Varga et al. [2001], absorbance above 300 nm in these spectra indicates the presence of polyconjugated

systems (either aromatic rings or aliphatic chains) as building blocks of the WSOM present.

The resemblance of these spectra to typical UV-Vis spectra of terrestrial and aquatic humic acids has led to these substances isolated from atmospheric aerosol being termed HUmic-LIke Substances (HULIS) [Havers et al., 1998]. Despite the similarity of the UV-Vis spectra, different techniques were used for the extraction and isolation of HULIS. For example, Havers et al. [1998] extracted with 0.1 m NaOH and isolated by ion exchange; Zappoli et al. [1999] extracted with water and isolated by size-exclusion chromatography (SEC); Kiss et al. [2001] isolated by liquid chromatography (LC); Krivacsy et al. [2001] extracted with water and isolated by C18 SPE; and Duarte et al. [2005] extracted with water and isolated by adsorption onto XAD-8 and XAD-4 resins in series. Humic acids are base soluble so techniques focusing on water solubility are more likely to extract compounds similar to fulvic acids. A review by Graber and Rudich [2006] concluded that: 1) the polyacidic nature of HULIS, including the number of COOH groups out of total OC groups, is similar to that of fulvic acids; and 2) humic acids are not good models for HULIS. UV-Vis spectra of HULIS tend to display relatively more absorbance in shorter wavelength regions (< 300 nm), and less in the longer wavelength regions (> 300 nm), as compared with terrestrial and aquatic humic substances, i.e., HULIS are not as humic-like as first thought. However, the term HULIS is still used in the literature, and the debate about their exact nature and origin continues.

A useful way of employing UV-Vis analysis of HULIS is by studying the ratio of absorbances at different wavelengths. For aquatic humic substances, Peuravuori and Pihlaja [1997] showed that the quotient E_2/E_3 (absorbances at 250 and 365 nm respectively) had a strong inverse correlation with the total aromaticity and averaged molecular weights of all the humic solutes they analysed. As E_2/E_3 increased the aromaticity and molecular size of the humic substances decreased. Duarte et al. [2005] used this relationship to report that aerosol-derived HULIS from the summer exhibited a lower molecular size and a lower degree of aromaticity than those collected in the autumn in rural Portugal. The results of this study [Duarte et al., 2005] were confirmed by specific fluorescence intensity, Fourier transform infrared (FT-IR) spectroscopy, and cross polarization and magic angle spinning (CPMAS)-^{13}C nuclear magnetic resonance (NMR). A more recent study [Baduel et al., 2010] at urban background locations in France found a smaller E_2/E_3 ratio in winter, attributed to an important contribution of aromatic structures, compared to a higher E_2/E_3 ratio in summer, which was an indication of a more pronounced unconjugated aliphatic character. From their results, Baduel et al. [2010] proposed a seasonal cycle driven by a source change from wood burning in winter

to secondary production in summer as a common feature of most urban environments. As increased conjugation in aliphatic compounds leads to absorption to longer UV-Vis wavelengths [Williams and Fleming, 1973], it could be hypothesised that increasing conjugation, as well as aromaticity, could cause a decrease in the E_2/E_3 ratio.

In this chapter the results of UV-Vis analysis of the inorganic-free HWSOM (which could also be described as HULIS) from the three Edinburgh sites are presented.

5.2 Methods

Samples were prepared as described in Chapter 4. They were removed from the freezer and defrosted overnight in a refrigerator before UV-Vis analysis. A dual beam Lambda 900 UV/VIS/NIR Spectrometer (PerkinElmer, Waltham, Massachusetts, USA) was switched on at least 30 min prior to use to allow it to warm up. UV-Vis spectra were measured in the 220–500 nm range in a 1 cm path length quartz cuvette (volume $\sim$ 3.5 ml) using the following instrumental parameters: 1 nm data interval; 0.04 s integration time; and 750 nm/min scan speed. Deionised water (18 MΩ) was used to calculate the baseline, in single beam mode, before any measurements were taken. The quartz cell was rinsed three times with deionised water (18 MΩ) in between each use.

Samples and Machine Blanks were measured in triplicate using the single beam mode of the spectrometer. Mean absorbances of the triplicate measurements at 250 and 365 nm were used to calculate the E_2/E_3 quotient. Prior to the calculation of E_2/E_3, mean Machine Blank absorbances were subtracted from the sample values. Standard deviations of the triplicate measurements (sample and Machine Blank) were used for error calculations. Periodically, spectra were collected for deionised water (18 MΩ) and the baseline was recalculated.

5.3 Results and discussion

5.3.1 NIST SRM

Before analysing the samples collected at the Edinburgh sites, UV-Vis spectra of four different concentrations of National Institute of Standards and Technology (NIST) standard reference material (SRM) 1648 were taken. The resultant spectra (Figure 5.1a) share the same properties seen for HULIS of being generally featureless curves with

steadily increasing absorptivity towards shorter wavelengths, indicating the presence of polyconjugated systems within the the WSOM. As concentration decreases so does absorbance. For the quotient E_2/E_3 to be useful as a measure of the properties of WSOM it should not be affected by different concentrations. The plot in Figure 5.1b shows that there is some variation in E_2/E_3 for different concentrations but with a relatively low standard deviation (SD) ($< 2\%$ of the mean). This gives some confidence that differences in E_2/E_3 ratio are from different chemical properties rather than concentration effects.

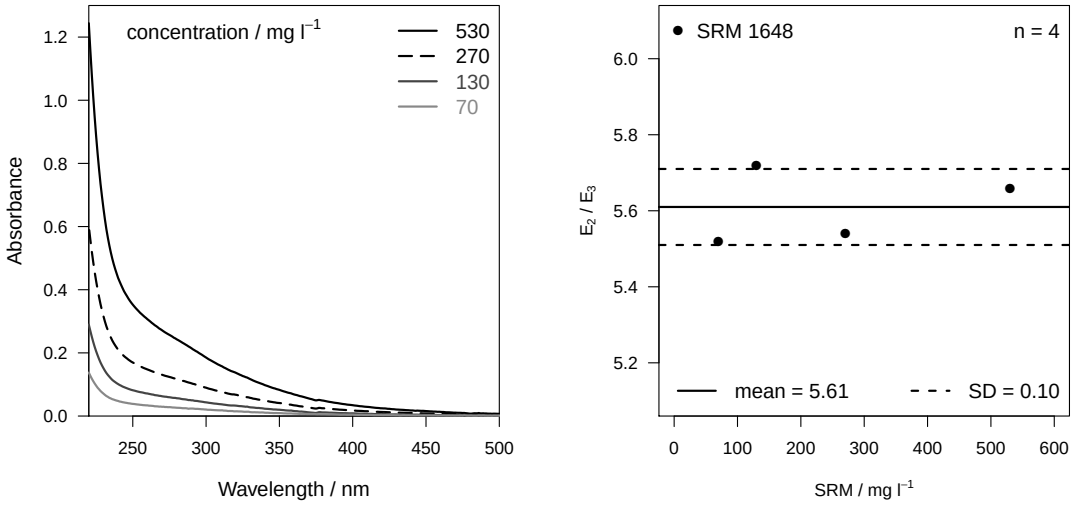

(a) UV-Vis spectra for four different concentrations.

(b) Comparison of the E_2/E_3 ratio at different concentrations.

Figure 5.1: UV-Vis analysis of NIST SRM 1648.

It would be interesting if the E_2/E_3 of ~ 5.6 for SRM 1648 said something about the nature of the particulate matter (PM) collected in St Louis (USA) in the 1970s. Nothing can be inferred seasonally since SRM 1648 was collected over a period of 12 months but the E_2/E_3 ratio can still be compared with results from other studies: 1) Duarte et al. [2005] found E_2/E_3 for rural PM in Portugal to be ~ 8.5 in summer and ~ 6.0 in autumn; and 2) Baduel et al. [2010] found E_2/E_3 for urban background PM in France to be ~ 4.5 in summer and ~ 3.0 in winter. Both studies show a clear seasonal variation in E_2/E_3, which was linked to differences in the chemical structure from the different processes responsible for emissions and formation of HULIS (biomass burning in winter and secondary processes in summer [Baduel et al., 2010]), but with significant differences in the values for the same season. The reason for the difference in absolute E_2/E_3 values for the same season may be due to different sampling, extraction and measurement techniques being employed, and/or the nature of the WSOM in the PM

sampled at the different locations. The lower E_2/E_3 ratios for the urban background PM in France [Baduel et al., 2010] could be due to the samples being collected closer to sources of aromatic emission compounds than the rural sampling location in Portugal [Duarte et al., 2005]. The E_2/E_3 for SRM 1648 (Figure 5.1) was closest to that of rural PM in autumn, which suggests there were fewer biomass burning aerosol sources in St Louis (USA) in the 1970s compared with urban France in 2008.

5.3.2 Measurement errors

A summary of the measurements of absorbances at 250 nm and 365 nm is shown in Table 5.1. The magnitude of absorbances from the Urban Background and Rural sites are similar, with the Roadside values being significantly higher. This is the same as the pattern seen for HWSOM concentrations in Table 4.8, with a higher concentration giving a higher absorbance (Figure 5.1a). The absorbance results for the Machine Blanks and periodic deionised water (18 MΩ) checks are shown in Table 5.2. The limit of detection (LOD) ($3 \times \sigma$) according to the deionised water measurements was 0.005 at 250 nm and 0.004 at 365 nm. There was some absorbance for the Machine Blanks but all the values were below the LOD, apart from the mean at 250 nm for the Roadside site (Table 5.2). Organic compounds that were absorbed onto the quartz filters and show UV-Vis activity could be responsible for the Machine Blank absorbances in the UV-Vis analysis. These compounds were suggested as the possible source of Machine Blank concentrations in the WSOM analysis (Section 4.3.1). Whatever the cause of the Machine Blank absorbances, the same species are likely to be present in the samples and should be corrected for by subtraction of the Machine Blank values.

Table 5.1: Summary of absorbances at 250 nm and 365 nm for the three sampling sites.

Sample	Urban		Rural		Roadside	
Absorbance	250 nm	365 nm	250 nm	365 nm	250 nm	365 nm
Mean	0.085	0.015	0.079	0.015	0.120	0.023
SD	0.040	0.008	0.027	0.005	0.048	0.010
n	32	32	3	3	14	14

Although the baseline was corrected using deionised water (18 MΩ), and periodically recalculated, some signal and variation in the water measurements was still present. For the worst case (365 nm), the relative standard deviation of the water absorbance in relation to the Urban Background mean was $< 8\%$. If the magnitude of absorbance

Table 5.2: Summary of absorbances at 250 nm and 365 nm for the Machine Blanks associated with the three sampling sites, and for deionised water (18 MΩ).

Blank	Urban		Rural		Roadside		Water	
Absorbance	250 nm	365 nm	250 nm	365 nm	250 nm	365 nm	250 nm	365 nm
Mean	0.004	0.001	0.003	0.001	0.007	0.003	0.001	0.000
SD	0.001	0.001	0.001	0.001	0.005	0.004	0.002	0.001
n	32	32	3	3	14	14	76	76

values is large enough, the error in their measurement due to the water should not unduly affect the results of the UV-Vis analysis.

5.3.3 Filter samples

The UV-Vis spectra of HWSOM samples were all similar with decreasing absorbance towards higher wavelengths, indicating the presence of many conjugated systems as seen by other authors for atmospheric HULIS (for example, Duarte et al. [2005]; Baduel et al. [2010]) and for SRM 1648 in this work (Section 5.3.1). This broad absorption pattern at wavelengths > 500 nm is in good agreement with the brown-yellow colour seen for these compounds during the SPE procedure (described in Section 4.3.7 and also noted by Ofner et al. [2011]). Examples of UV-Vis spectra for two different samples from the Urban Background site are shown in Figure 5.2a. The selected spectra represent the highest (29 July 2009) and lowest (16 December 2009) E_2/E_3 ratios (7.0 and 4.9, respectively) calculated for this site. The winter sample should contain more aromatic moieties and have a higher average molecular size than the summer sample, as indicated by the different E_2/E_3 values.

The HWSOM concentration was marginally higher on 16 December (0.61 µg m^{-3}) than on 29 July (0.54 µg m^{-3}). A possible seasonal trend in HWSOM concentrations was highlighted in Section 4.3.7.1 so an inverse correlation between HWSOM and E_2/E_3 might be expected. The points in Figure 5.2b show that no such relationship exists ($r^2 = 0.00$) so E_2/E_3 is independent of the quantity of HULIS extracted from the filters for the period 05 November 2008 – 07 April 2010. A relationship does exist between HWSOM and absorbance at 250 nm if the data are split into winter and summer seasons (as already hinted at by comparing the data in Figure 5.2a with the concentrations on 16 December and 29 July). This is shown for the Urban Background site in Figure 5.2c. Following on from the work of Baduel et al. [2010] the seasons are defined as winter = November–February and summer = May–August. There are clear correlations for

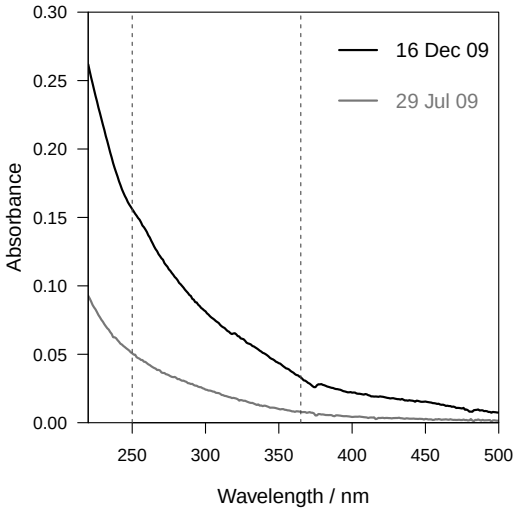

(a) Example UV-Vis spectra of two different HWSOM samples. The date refers to the first day of a 14 day batch. 250 nm and 365 nm wavelengths are shown with dashed lines.

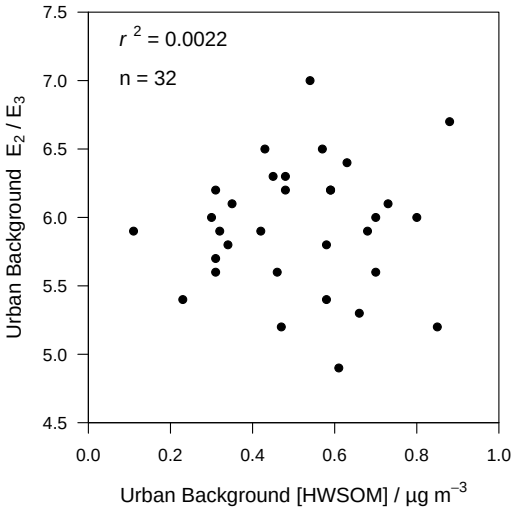

(b) E_2/E_3 versus HWSOM concentration.

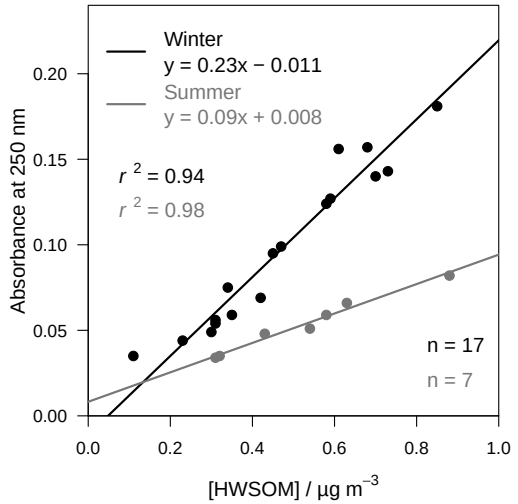

(c) Absorbance at 250 nm versus HWSOM concentration during winter (November–February) and summer (May–August) seasons. Linear relationships were calculated using the standardised major axis model.

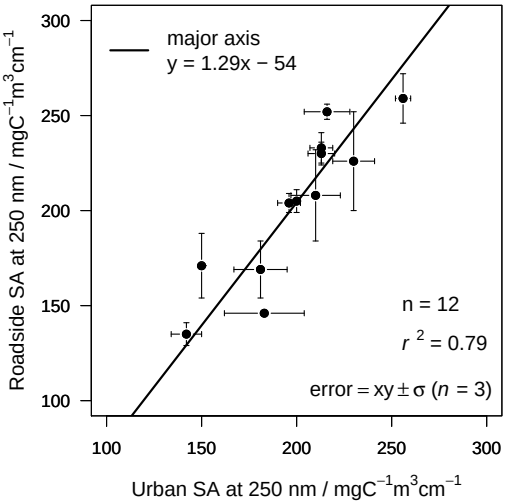

(d) Specific Absorbance at 250 nm for the Roadside and Urban Background sites.

Figure 5.2: Plots of UV-Vis absorption data from the Urban Background site.

the winter ($r^2 = 0.94$) and summer ($r^2 = 0.98$) data, and the different gradients of the best-fit lines for winter (0.23) and summer (0.09) are consistent with seasonal differences in emissions and/or formation processes giving rise to different chemical structures [Baduel et al., 2010]. The low values of both intercepts in Figure 5.2c shows that the extraction procedure was successful at removing inorganic material from the HWSOM.

To eliminate concentration effects from the UV-Vis results the E_2/E_3 quotient or specific absorbance (SA) ($\mathrm{mgC^{-1}\,m^3\,cm^{-1}}$), according to the measured [HWSOM] ($\mu\mathrm{g\,m^{-3}}$) and path length (cm), can be used.

$$\text{Specific Absorbance} = \frac{\text{Absorbance}}{([\text{HWSOM}]/1000) \cdot \text{Path Length}} \tag{5.3.1}$$

The time series of the SA results in Figure 5.3 shows a seasonal trend, with values decreasing towards a summer minimum and then increasing in winter. Horizontal lines representing the mean values and standard deviations show a significant difference between SA values at 250 nm in winter and summer. This matches the trend seen at urban background sites in Grenoble (France) by Baduel et al. [2010], with low values in summer inferred to be from secondary production and the increase in winter attributed to residential wood burning. Duarte et al. [2005] observed an increase in SA for autumn aerosol extracts in rural Portugal, thought to be caused by the presence of compounds with complex unsaturated bond systems with more than two overlapping π-bond orbitals.

SAs at the different sites also appear to be well correlated (Figure 5.3) and this is highlighted by the scatter plot of Roadside against Urban Background SA values (Figure 5.2d). As well as the good linear correlation ($r^2 = 0.79$), the SA is higher, on average, at the Roadside site (Figure 5.2d). SA values have been normalised to avoid concentration dependence so higher HWSOM concentrations at the Roadside site (Figure 4.11) do not explain this result. Electronic π – π^* transitions involving C=C and C=O double bonds are generally associated with absorption at 250 nm [Baduel et al., 2010] so these types of compounds are likely to be more prevalent in the Roadside samples. A relative increase in the quantity of more hydrophobic compounds by the SPE procedure leads to the hypothesis that it is C=C moieties from traffic sources that are being detected. Even without the relative increase in the quantity of HWSOM caused by SPE, traffic emissions would be expected to have a low level of oxidation as this soot-type carbon is sampled close to the source (i.e., there is not enough time for substantial oxidation to take place). However, a recent study by Glasius et al. [2011] observed that concentrations of non-fossil carbon were higher at roadside locations than at urban background sites. The most likely of the reasons suggested by Glasius et al.

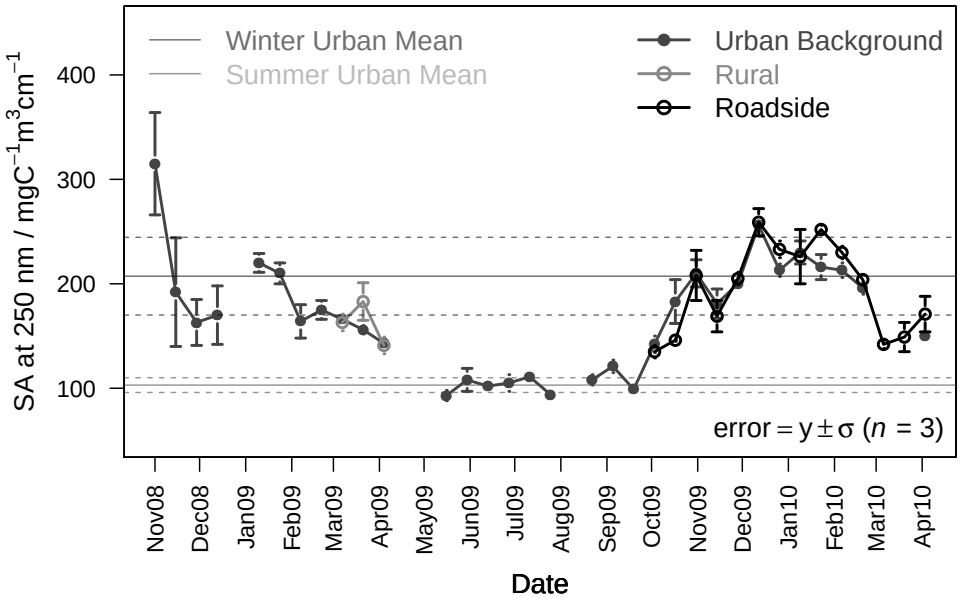

Figure 5.3: Time series of specific absorbance at 250 nm for the Urban Background, Rural and Roadside sites. Horizontal lines represent the winter and summer means and the associated dashed lines are the standard deviations from the mean.

[2011] for these higher roadside concentrations are: more tyre wear in re-suspended road dust at roadside locations; and anthropogenic enrichment of biogenic secondary organic aerosol (SOA). The possibility of higher concentrations of non-fossil HWSOM at the Roadside site in Edinburgh means there is some uncertainty in the reason for higher SA values, on average, seen in Figure 5.2d.

Further evidence of the seasonal change in composition of atmospheric HULIS is given by the trend line in Figure 5.4 for Urban Background E_2/E_3. The smoothed line has the following pattern: an increase in the E_2/E_3 ratio until a summer maximum is reached; a decrease in the E_2/E_3 ratio until a winter minimum is reached; a subsequent increase in the E_2/E_3 ratio towards the summer. This is the same as the pattern observed by Duarte et al. [2005] (rural Portugal), Krivacsy et al. [2008] (urban New Zealand) and Baduel et al. [2010] (urban background France), with a maximum ratio in the summer and a minimum in the autumn/winter. Following the conclusions of the other authors it could be claimed that the samples collected in Edinburgh in winter had a higher aromatic content than the summer samples, and these aromatic compounds were released during wood combustion in domestic fireplaces. There is not expected to be enough biomass burning activity in Edinburgh to have a marked influence on the HULIS concentrations and properties so a wood combustion source, if it exists, would most likely be from long-range transport of PM from mainland Europe. This potential source was seen in the data analysis for PM_{10} (Chapter 2) and WSOM (Chapter 4).

It is possible that at colder winter temperatures, semi-volatile compounds from local traffic emissions are more likely to condense into the particle phase and contribute to an increase in aromaticity and polyconjugation in HWSOM. It is also possible that gaseous precursors adsorb onto the filter surface and HULIS are formed through polymerisation reactions [Krivacsy et al., 2008]. In contrast, the secondary formation processes that dominate in the summer [Samburova et al., 2005a] appear to produce PM with more aliphatic non-conjugated character. Primary production of biogenic HWSOM over the North Atlantic could also be a summer source of oxidized species with extended aliphatic moieties [O'Dowd et al., 2004].

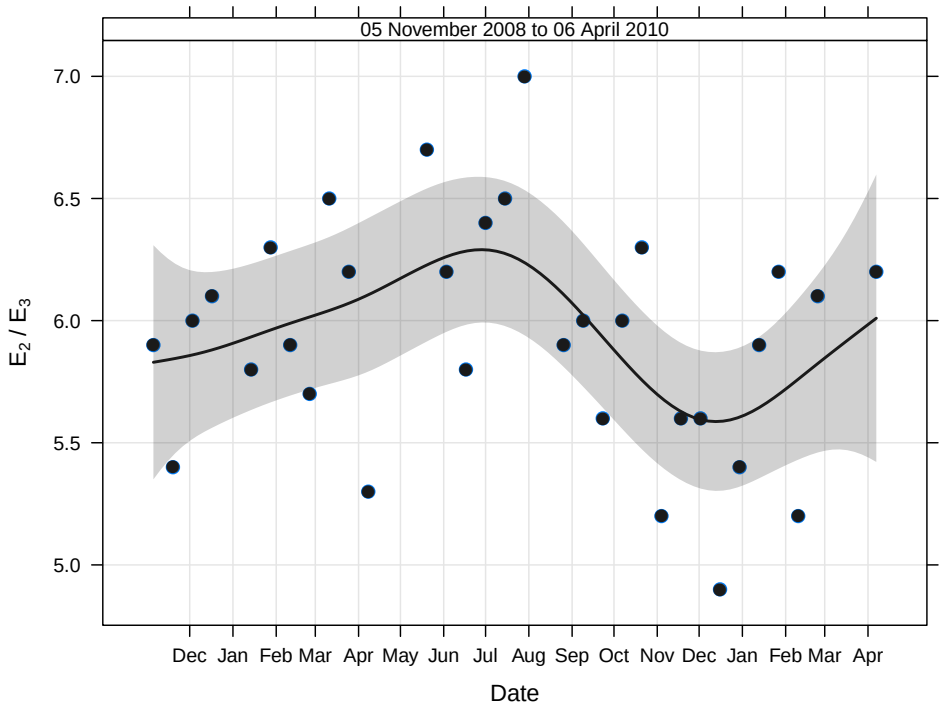

Figure 5.4: Time series of E_2/E_3 ratio for the Urban Background site. The smoothed trend line is a spline (with 95% confidence intervals) calculated using a general additive model in R [Carslaw and Ropkins, 2011].

5.4 Conclusions

Although the low amount of PM_{10} collected in Edinburgh makes the chemical characterisation of the carbonaceous fraction of this PM an analytical challenge, and these low levels could cause problems with the precision and accuracy of this analysis, it was possible to use UV-Vis spectroscopy to show clear seasonal trends in the composition

of HWSOM that are comparable with trends seen elsewhere in Europe. The outcome is that lower molecular weight aliphatic compounds present in the summer tend to be dominated by larger aromatic and polyconjugated compounds in the winter.

There is still some uncertainty about the exact sources of aliphatic compounds in summer, aromatic and polyconjugated compounds in winter, and the prevalence of aromatic and polyconjugated compounds in roadside PM_{10}. Research is still needed to improve our understanding on the nature and origin of the water-soluble compounds in PM.

Chapter 6

Raman microspectroscopy analysis of PM and related materials

6.1 Introduction

Chapter 3 described a method to quantify the amount of black (soot) carbon present in the filter samples from the Edinburgh monitoring sites. It would be useful to be able to analyse the type of carbonaceous species present. One of the issues with black carbon (BC) measurements is that there is not a clear cut-off between carbon that is black (i.e., non-reflective) and reflective species. Because of this range in the reflectance of the carbon present, 'brown carbon' (i.e., carbonaceous material that absorbs some of the light during reflectance measurements) is included in the BC concentration calculations. This problem is well illustrated in Figure 6.1 taken from Pöschl [2005]. Rather than just being a measure of graphitic carbon, the BC technique is also likely to include polycyclic aromatic compounds, biopolymers and compounds similar to humic acid. Andreae and Gelencsér [2006] discussed evidence for the atmospheric presence of brown carbon and the issues that arise with optical (and thermochemical) measurements.

One technique that has the potential to distinguish between the different types of carbon present in atmospheric aerosol is Raman microspectroscopy (RM), where the spatial resolution of an optical microscope is combined with the analytical capabilities of Raman spectroscopy [Ivleva et al., 2007a]. The Raman effect arises through a change of frequency when light is inelastically scattered by molecules [Szymanski, 1967]. The magnitude of the frequency shifts are usually expressed in terms of wave numbers (i.e., Raman shift in cm^{-1}) and are characteristic of the species giving rise to the scattering. When a photon of light strikes a molecule it may transition from the ground state to the excited state and the Raman shifts correspond to vibrational transitions of

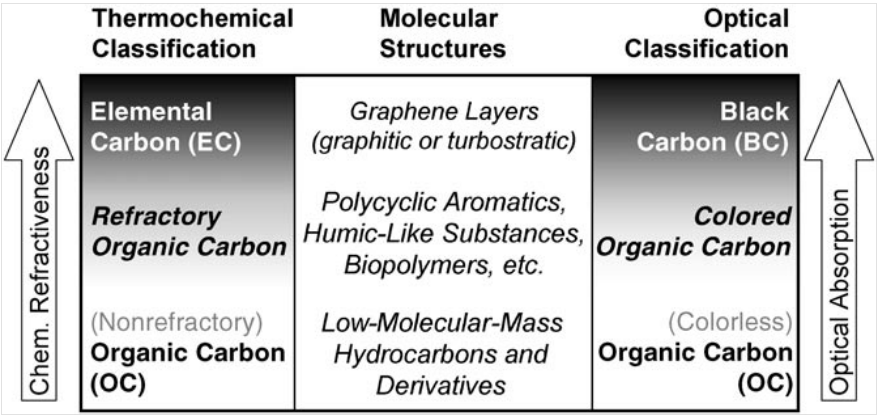

Figure 6.1: "Optical and thermochemical classification and molecular structures of black carbon (BC), elemental carbon (EC), and organic carbon (OC=TC–BC or TC–EC). Depending on the method of analysis, different amounts of carbon from refractory and colored organic compounds are included in OC and BC or EC." [Pöschl, 2005]

the scattering molecule [Szymanski, 1967]. The first use of Raman scattering in the characterisation of particulate matter (PM) was reported by Rosen and Novakov [1977]. They were able to show similarities (and differences) between ambient aerosol, vehicle exhaust, polycrystalline graphite and activated carbon (a form of carbon that has been processed to make it extremely porous). Rosen and Novakov [1977] concluded that physical structures similar to activated carbon were major species in ambient PM, which indicated the presence of graphitic soot (not a surprising conclusion since activated carbon is produced in the combustion process). Raman spectroscopy continues to be used for the analysis of PM [Escribano et al., 2001; Sze et al., 2001; Mertes et al., 2004], and more recent papers have discussed the use of RM to probe individual ambient particles [Batonneau et al., 2006; Potgieter-Vermaak and Van Grieken, 2006; Ivleva et al., 2007a; Deboudt et al., 2010] and soot particles [Sadezky et al., 2005; Ivleva et al., 2007b; Knauer et al., 2009a,b; Schmid et al., 2011]. Interestingly, Ivleva et al. [2005] were also able to demonstrate an RM approach to discriminate between different pollen species.

Graphene is a single layer of carbon atoms bonded together in a hexagonal plane. Regularly stacked layers of graphene form the structure of graphite, as shown in Figure 6.2. A Raman spectrum of an ideal graphitic lattice would contain a very sharp peak around 1580 cm^{-1}, known as the G ("Graphite") band, which corresponds to a lattice vibration mode with E_{2g} symmetry [Tuinstra and Koenig, 1970; Sadezky et al., 2005]. The first-order Raman spectrum of graphite (Figure 6.3) shows the G band but also the presence of another small peak, at around 1350 cm^{-1}, which is known as the D ("Defect") band. This band, which is characteristic of disordered graphite and corresponds to a lattice vibration mode with A_{1g} symmetry, increases in intensity

relative to the G band as the graphitic structure becomes more disordered [Tuinstra and Koenig, 1970; Sadezky et al., 2005].

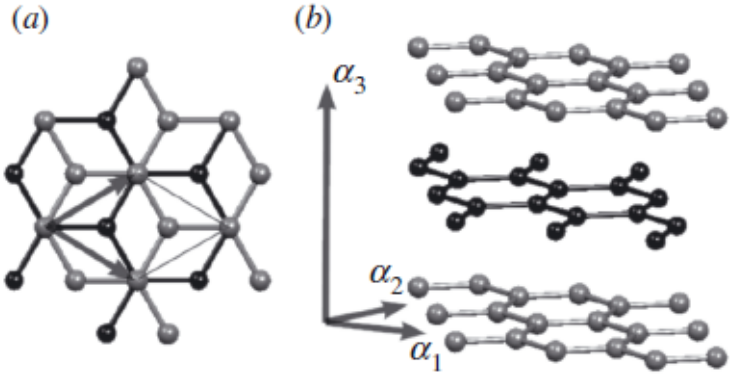

Figure 6.2: "Graphite lattice in (a) top and (b) side view. α_1, α_2 and α_3 span the unit cell of graphite." Taken from Reich and Thomsen [2004]

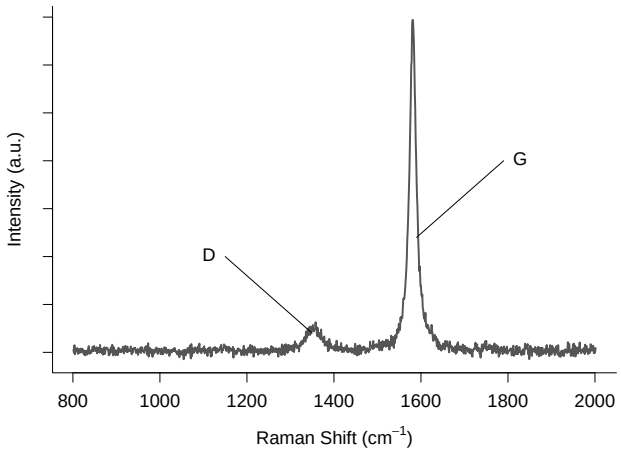

Figure 6.3: Example Raman spectra of highly ordered pyrolytic graphite with $\lambda_0 = 514\,\text{nm}$. The sample and its analysis are described in Section 6.2

A typical soot or PM spectrum looks different to what is observed for graphite, in that there are two peaks with intensity maxima at $\sim$1585 cm^{-1} and $\sim$1360 cm^{-1}, which are broad and strongly overlapping (for example, Figure 6.4). Although the peaks for PM in Figure 6.4 are overlapping and broader than those for graphite in Figure 6.3 they have been labelled as D and G bands, analogous to those of graphite, due to their similar positions. A systematic investigation by Sadezky et al. [2005] attributed the first-order Raman spectra of soot particles (similar in appearance to the PM spectrum in Figure 6.4) to five different bands and these bands were subsequently used by Ivleva et al. [2007a] for the analysis of ambient particle samples. A summary of the bands used by Sadezky et al. [2005] and Ivleva et al. [2007a] (and references therein) follows:

G ~1580 cm^{-1} Ideal graphitic lattice stretching mode (E_{2g} symmetry)

D1 ~1350 cm^{-1} Vibration mode involving graphene layer edges (A_{1g} symmetry)

D2 ~1620 cm^{-1} Vibration mode involving surface graphene layers (E_{2g} symmetry)

D3 ~1500 cm^{-1} Amorphous carbon content of soot (organic molecules, fragments, and functional groups) giving rise to high signal intensities between the two main peaks of the observed spectra

D4 ~1200 cm^{-1} Vibrations of disordered graphite lattices (A_{1g}), sp^2- and sp^3-hybridized carbon bonds, C−C and C = C stretching vibrations of polyenes, and ionic impurities

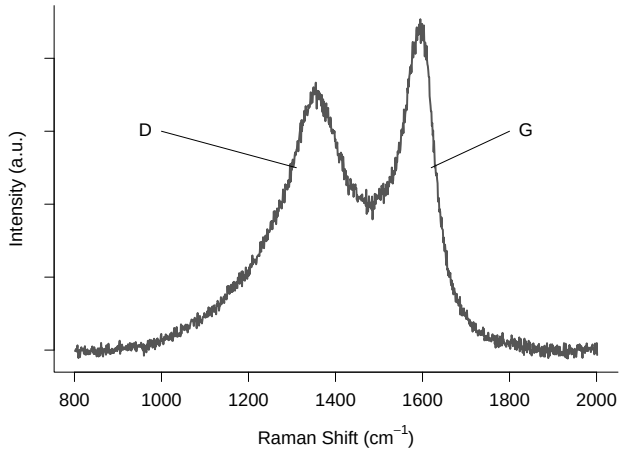

Figure 6.4: Example Raman spectra of PM sample collected in Edinburgh (Roadside; 5 November 2009). $\lambda_0 = 514$ nm. The method of analysis is described in Section 6.2

Ivleva et al. [2007a] fitted these five bands to spectra for reference materials of graphite, soot and HUmic-LIke Substances (HULIS), and used these results to determine the relative abundance and structural order of graphite-like and amorphous carbon in these samples. One finding was that the D1 bandwidth exhibited a near-linear negative correlation with the EC/TC ratio of the reference materials, so as the level of structural order decreased the D1 bandwidth increased. Humic acid was shown to have a greater D1 bandwidth than diesel soot, and the sampled ambient particles were shown to have a D1 bandwidth between these values. It was concluded by Ivleva et al. [2007a] that this technique of RM and band fitting could be used to distinguish soot and HULIS in samples of PM.

Although RM has been shown to be useful in providing some structural information, Sadezky et al. [2005] warned that characterisation is limited by the experimental reproducibility of the spectra and the statistical (and theoretical) uncertainties of the curve fitting procedure. Despite this drawback, the facts that RM can be used as a non-destructive analytical technique prior to further analysis of the filter samples, and has the potential to expand on the reflectance-based BC analysis, are advantageous.

This chapter describes the use of RM for the characterisation of carbonaceous reference materials sampled onto quartz filters, and the comparison of these results with those of PM_{10} samples collected in Edinburgh. Referring back to Figure 6.1, the aim is to try and distinguish between the extent of soot and humic-like structures present.

6.2 Method

6.2.1 Materials

The following solid reference materials were used for the RM analysis and they will be referred to according to the names given below:

HB Pencil graphite from an HB pencil obtained from the Stores in the School of Chemistry, University of Edinburgh

HOPG highly ordered pyrolytic graphite (HOPG) obtained from the research group of Professor Eleanor Campbell, School of Chemistry, University of Edinburgh

MWCNT multi-walled carbon nanotubes (MWCNT) produced by the research group of Professor Eleanor Campbell, School of Chemistry, University of Edinburgh

Bus Diesel exhaust PM (dark solid material) scraped from the inside of the exhaust pipe of a local Edinburgh diesel bus using a clean metal spatula

SRM 1649a National Institute of Standards and Technology (NIST) standard reference material (SRM) 1649a

SRM 1648 NIST SRM 1648

Humic Acid humic acid sodium salt, technical grade, Sigma-Aldrich Corporation, St. Louis, USA

The same pre-baked (500 °C) quartz filters were used for the reference samples as for PM_{10} (Chapter 2). Solid material was distributed across the centre of a filter using a pre-cleaned (with MeOH and water) metal spatula and then pressed down firmly using the base of the spatula. This helped the particles to penetrate between the filter fibres, which prevented the loss of material from the filter surface and partly mimicked the penetration of PM_{10} into the filter during air sampling. Lines of graphite were drawn onto the centre of a filter for the HB Pencil reference. Filters were kept in PetriSlides™ inside a freezer (−30 °C) when not being used.

The PM_{10} samples were those collected onto quartz filters using a Partisol sampler at Urban Background, Rural and Roadside sites in Edinburgh, as described in Chapter 2.

6.2.2 Analysis

Filter samples were analysed with a Raman microscope (Renishaw inVia, Figure 6.5) following the method described by Ivleva et al. [2007a]. The instrument was switched on an hour prior to use to allow it to warm up. Spectra were recorded using laser wavelengths of $\lambda_0 = 514\,\text{nm}$. An optical microscope with 5× and 50× magnification objectives was used. Wavelength calibrations were performed with a silicon wafer (1 s integration time, 50× objective) by utilizing the first order phonon band of Si at $520\,\text{cm}^{-1}$. Instrument control and spectral analysis were performed with the Renishaw WiRE 2.0 software. The quartz filters showed strong Raman signals, making these measurements difficult to perform. Care had to be taken to focus carefully on the particle being measured without the influence of a quartz fibre. Spectra of the samples were recorded over the range of 800–2000 cm^{-1}, 20–30 s integration time, and 8–10 spectral accumulations. The integration time and number of accumulations selected was a balance between achieving a good signal-to-noise ratio without excessive time spent on the instrument. Different laser-microscope configurations were investigated: 5× magnification increased the area of the filter being measured but also increased the magnitude of the background signal from the filter; with 50× magnification only one 'particle' (or agglomeration) could be measured at a time; a fully focused laser beam (at 50× magnification) had a diameter of ≈1–2 µm but defocussing to increase the beam diameter increased the background filter signal; 10% of the source power was used where possible to prevent damage to the material being analysed, and increased if necessary to improve signal strength. Most of the samples were analysed with a laser wavelength

of $\lambda_0 = 514\,\text{nm}$ at 50× magnification, using a fully focused laser beam and 10–50% of the source power.

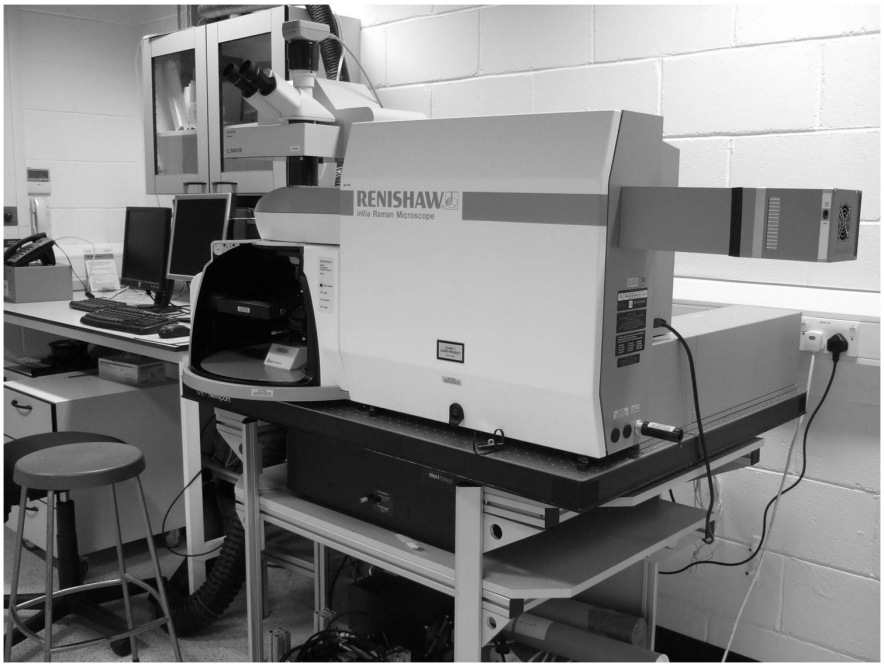

Figure 6.5: The Renishaw inVia Raman microscope at the School of Chemistry, University of Edinburgh.

Filters were removed from the freezer at least an hour before analysis to allow them to equilibrate to ambient conditions. It was possible to analyse a filter whilst still in the PetriSlide™ (with the lid removed) so no filter handling was required. A PetriSlide™ was placed flat on the stage inside the Raman microspectrometer. The stage was operated by remote control and the laser focused onto the sample surface with the use of a video image. Three areas of each filter were analysed, and a single particle (or agglomerate) was selected from each area at random. Even for filters with the highest PM_{10} (or BC) concentrations the coverage of particles appeared rather sparse so the surface had to be scanned until a suitable particle was found.

Although no more than three filters from a fortnight batch of PM_{10} were analysed by RM, the whole batch was removed from the freezer so each filter sample and associated Machine Blanks experienced the same conditions prior to their subsequent water extraction for water-soluble organic matter (WSOM) and ultraviolet-visible (UV-Vis) analysis (see Chapter 4 and Chapter 5).

6.2.3 Curve fitting

The use of a five band fitting procedure by Sadezky et al. [2005] and Ivleva et al. [2007a] to explain the first-order Raman spectra of soot, humic acid and aerosol was described in Section 6.1. Sadezky et al. [2005] tested nine different band combinations for different soot samples and found the combination summarised in Table 6.1 to be the best. One of the most useful outcomes of the Ivleva et al. [2007a] paper was that the D1 band width and the relative intensity of the D3 band were found to be significantly different between humic acid and diesel soot, and this outcome could be used to distinguish between the two different components in ambient particles. The five band fitting procedure summarised in Table 6.1 was therefore used in this work.

Table 6.1: Band combination for curve fitting of first-order Raman spectra used in this work (Sadezky et al. [2005]; Ivleva et al. [2007b,a]).

Band	Initial position (cm^{-1})	Line shape
G	1580	Lorentzian
D1	1360	Lorentzian
D2	1620	Lorentzian
D3	1500	Gaussian
D4	1180	Lorentzian

Due to a high background signal from the quartz filters, a baseline correction was applied to all spectra using the WiRE 2.0 software prior to curve fitting. This used three points in the 800–1000 cm^{-1} region and three points in the 1800–2000 cm^{-1} region. During curve fitting the goodness-of-fit was indicated by the χ^2 statistic. The lower the χ^2 value the better the fit. Values < 3 implied that the fit converged towards the observed spectrum [Ivleva et al., 2007a].

6.3 Results and discussion

6.3.1 Reference materials

Raman spectra of the reference materials on quartz filters are shown in Figure 6.6. Spectra were difficult to obtain due to high background signals from the filters. The laser had to be carefully focussed onto a particle, ensuring that the beam did not come

into the contact with any quartz fibres. This difficulty in avoiding the quartz fibres with the laser beam was due to the three-dimensional structure of the filters and the degree of penetration of the particles.

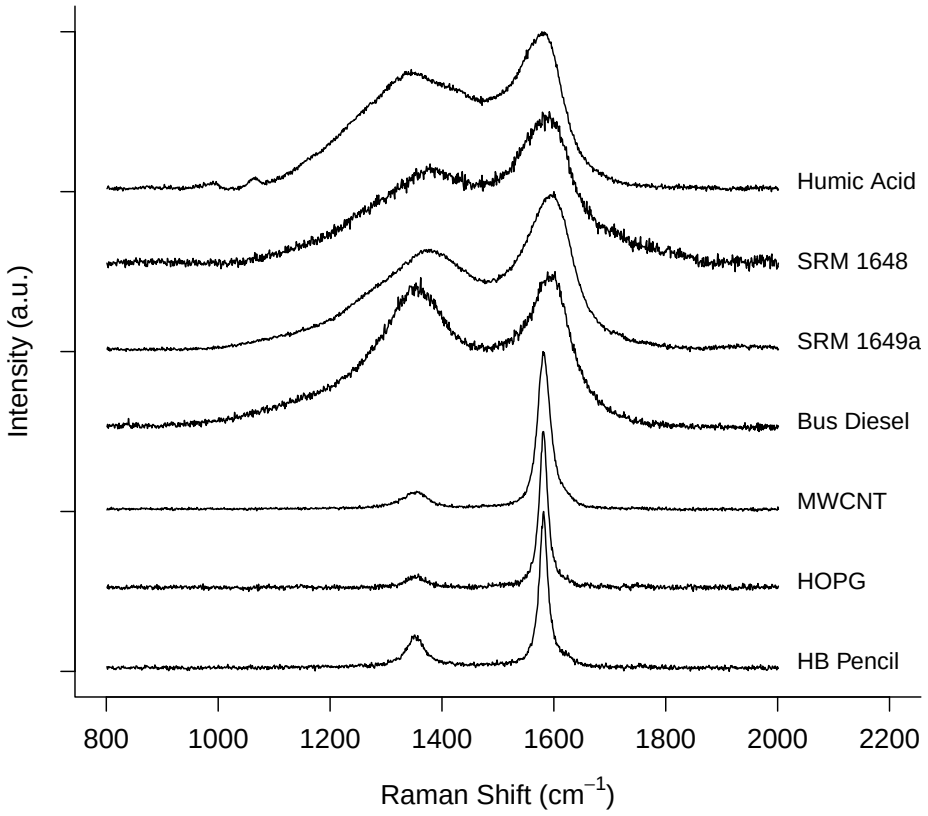

Figure 6.6: Raman spectra ($\lambda_0 = 514\,\text{nm}$) of the reference materials on quartz filters. Lines are offset for clarity.

The Raman spectra of the three graphitic materials (HB Pencil, HOPG, MWCNT) in Figure 6.6 appear similar. This expected result, due to their similar structure, demonstrates the validity of measuring Raman spectra on the substrates used in this work. All spectra show the G band at $\sim 1580\,\text{cm}^{-1}$ that represents the ordered nature of the graphene layers present [Tuinstra and Koenig, 1970; Sadezky et al., 2005]. The graphite in the HB Pencil and HOPG samples is comprised of planar layers of graphene, whereas MWCNT differ slightly in their structure by being layers of graphene rolled into tubes.

Also present in the spectra of the graphene-based materials (Figure 6.6) is the D band at $\sim 1350\,\text{cm}^{-1}$. For HB Pencil graphite, HOPG and MWCNT the D band is relatively weak, which represents a relatively low level of disorder in these materials [Tuinstra and Koenig, 1970; Sadezky et al., 2005]. As the graphitic structure becomes more disordered

the relative intensity of the D band to the G band (i.e., I_D/I_G) increases. The mean $\pm\sigma$ I_D/I_G ratios for the three randomly selected spots of each material were as follows:

HOPG 0.10 ± 0.03

MWCNT 0.12 ± 0.06

HB Pencil 0.15 ± 0.11

These values suggest that the structure of the HOPG had the highest level of order and the HB Pencil graphite the lowest. In fact, HOPG should not show a D band since it is 'highly-ordered' but should appear as large single graphitic crystals with only a G band present [Wang et al., 1990]. Its position as the most ordered reference material is as expected but the origin of the structural defects in the sample are uncertain. As the D band is likely to arise from carbon atoms at the edge of the graphene layers [Wang et al., 1990] it is probably these that are being measured (i.e., there are more edges in the HOPG analysed in this work than would be found in 'perfect' HOPG).

Less care is likely to be taken in the manufacture of pencil graphite so the more disordered nature of the HB Pencil material is no surprise. This is further confirmed by the higher variability (standard deviation (SD)) for the HB Pencil graphite across the three measurements. In comparison, greater homogeneity in the HOPG sample is shown by the lower SD. The details of the production of the MWCNT are not known but the results presented here show it to have an intermediate level of graphitic order when compared with the other reference materials (and an intermediate level of variability between the three measurements).

The presence of another first-order band for the graphitic reference materials is suggested in Figure 6.6 by a small shoulder on the G band at $\sim 1620\,\mathrm{cm}^{-1}$. This band also corresponds to a graphitic lattice mode with E_{2g} symmetry and is denoted as D2 [Sadezky et al., 2005] (leading to the other D band at $\sim 1350\,\mathrm{cm}^{-1}$ being termed D1). Assuming a Lorentzian shape for these bands they can be fitted to the observed spectra using the WiRE 2.0 software (Figure 6.7). Although the G and D2 peaks are coincident in Figure 6.7 for HOPG (suggesting the D2 band is unnecessary to the fit and therefore does not really exist for this sample) the fit closely matches the observed spectrum ($\chi^2 < 1$).

Particles of highly ordered graphitic structure are not generally found in ambient aerosol so of more interest are the Raman spectra of the Bus Diesel exhaust particles and Humic Acid material shown in Figure 6.6. These are representative of the types of carbonaceous

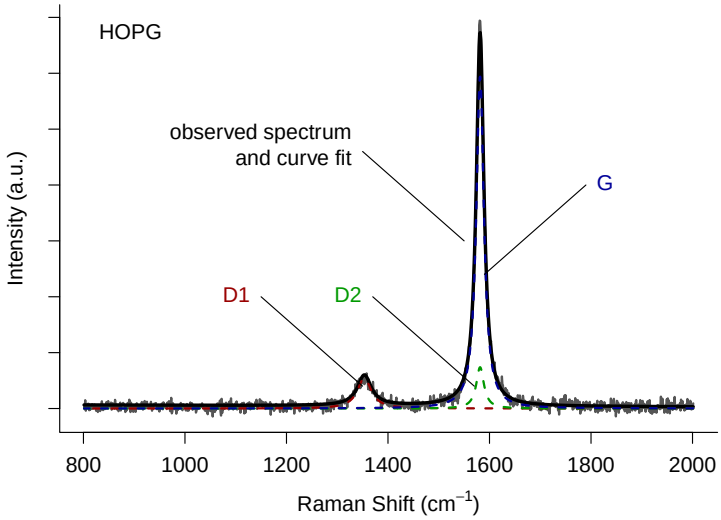

Figure 6.7: Example Raman spectrum ($\lambda_0 = 514\,\text{nm}$) of HOPG. Grey line shows the observed spectrum. Black line shows the fitted spectrum. Dashed black lines are the fitted curves.

materials that could be found in the PM_{10} collected in Edinburgh. The Bus Diesel and Humic Acid spectra are noticeably different from those of the graphitic reference materials (Figure 6.6), with broad and strongly overlapping peaks in the D and G positions. They match closely the spectra for 'SRM 1650 diesel soot' and 'Humic acids' reported by Ivleva et al. [2007a]. The form of the Raman spectra of soot are due to the prevalence of highly disordered graphitic lattices in their various possible structures (the graphite-like crystalline domains are usually made of 3–4 graphene layers irregularly stacked) [Sadezky et al., 2005]. Humic acid has a complicated structure comprising many organic molecules and functional groups (see Chapter 5) and any graphite-like structures are likely to be disordered. The D band of Humic Acid in Figure 6.6 appears broader than that of Bus Diesel, which is most likely due to the less ordered structure of the Humic Acid sample. There is also an unexplained peak in the Humic Acid spectra at $\sim 1050\,\text{cm}^{-1}$, which may have the same origin as the $\sim 1120\,\text{cm}^{-1}$ band in a soot spectrum reported by Ivleva et al. [2007b] and which was explained by the formation (or exposure) of domains containing sp^3-hybridised carbon.

Raman spectra with fitted curves for the Bus Diesel and Humic Acid reference materials are shown in Figure 6.8. To quantify the difference between the two materials the D1 full width at half maximum (FWHM) value is a useful metric. This tends to increase with increasing disorder in the material being measured [Ivleva et al., 2007a]. The following D1 FWHM values were calculated:

Bus Diesel $142 \pm 10\,\text{cm}^{-1}$

Humic Acid $230 \pm 38\,\mathrm{cm}^{-1}$

There is a clear difference between the D1 FWHM values for the Bus Diesel and Humic Acid samples, showing that the the more disordered carbonaceous fraction of humic acid can be distinguished from exhaust soot using RM and quartz filters (i.e., with the equipment and substrates used in this work).

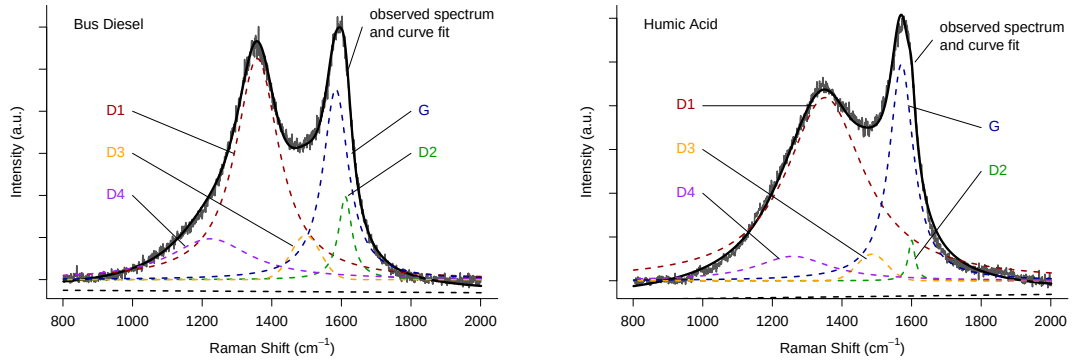

(a) Bus Diesel. **(b)** Humic Acid.

Figure 6.8: Example Raman spectra ($\lambda_0 = 514\,\mathrm{nm}$) with curve fits. Grey lines show the observed spectra. Black lines show the fitted spectra. Dashed black lines are the fitted curves.

The plot in Figure 6.9 (taken from Ivleva et al. [2007a]) illustrates the existence of an inverse relationship between D1 FWHM and elemental carbon (EC) fraction, suggesting that the D1 FWHM value could be a useful measure of the amount of EC in a sample. However, the 'Humic acids' point does not follow the trend as well as the other samples, appearing to have a larger EC/total carbon (TC) ratio than expected. With an origin and structure different to that of soot, humic acid should have a much lower EC content. It is possible to explain this discrepancy as a result of the organic molecules in humic acid being charred during EC measurements and converted into disordered graphite-like structures [Andreae and Gelencsér, 2006]. This highlights the problem with refractory organic carbon (OC) in thermochemical analysis shown in Figure 6.1. A similar problem could also occur with brown carbon in optical analysis but since BC measurements of the reference materials were not made comparisons with the Raman spectra and D1 FWHM values are not possible here. Another potential problem with the relationship shown in Figure 6.9 is that the D1 FWHM values for 'Humic acids' and 'SRM 1650 diesel soot' are relatively close together. Although Ivleva et al. [2007a] report the ability to distinguish between these two materials, the difference appears subtle so some caution should be exercised when interpreting the results. The difference between the D1 FWHM values of Humic Acid and Bus Diesel measured in the current work is larger

but due to potential measurement and calculation errors there is some uncertainty in the values obtained.

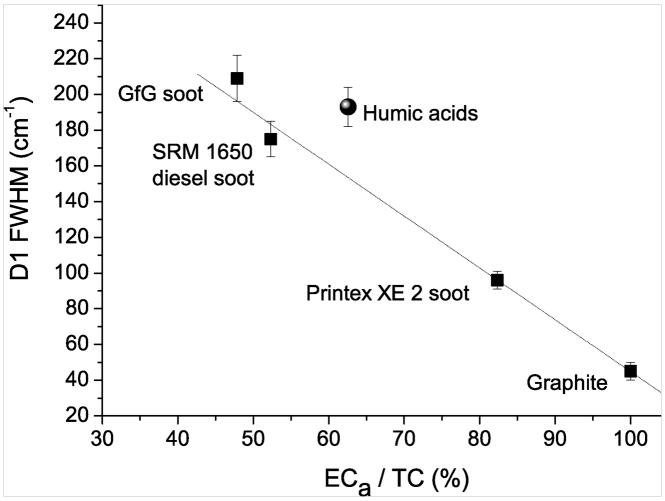

Figure 6.9: "Full widths at half maximum (FWHM) of D1 band vs. apparent elemental carbon (EC_a) fraction of reference materials for soot and humic-like substances (mean values ± standard deviations; linear fit to graphite and soot samples)." Taken from Ivleva et al. [2007a]

It is also interesting to examine the Raman spectra of the PM of the NIST SRMs 1648 and 1649a. Example spectra are plotted in Figure 6.10, together with those of Bus Diesel and Humic Acid (the intensity values are normalised to 1 for the G peak to allow a comparison between the different spectra). All of the spectra appear to have similar G bands apart from the D2 shoulder present in the SRM 1648 spectrum. The signal intensity between the D and G bands is lower for SRM 1649a, suggesting a lower D3 band. The most intense of the D1 bands, from Bus Diesel, is also the narrowest, and the broader D1 band of Humic Acid is also present. SRM 1648 and 1649a spectra have similar but smaller D1 peaks and seem to have D1 widths intermediate between Bus Diesel and Humic acid. This is confirmed by the D1 FWHM values shown in Figure 6.11 (189 ± 21 cm^{-1} for SRM 1648; 200 ± 48 cm^{-1} for SRM 1649a). As a complicated mixture of soot, HULIS and other materials, urban PM would be expected to have D1 widths (and therefore carbonaceous order) between those of Bus Diesel and Humic Acid. SRM 1648 is closer to Bus Diesel and SRM 1649a closer to Humic Acid, suggesting that there is a higher level of soot-type carbon in the particles of SRM 1648 and a higher level humic-like material in SRM 1649a. Relatively large variability in the Humic Acid and SRM 1649a values means there is some uncertainty in the real difference between these samples.

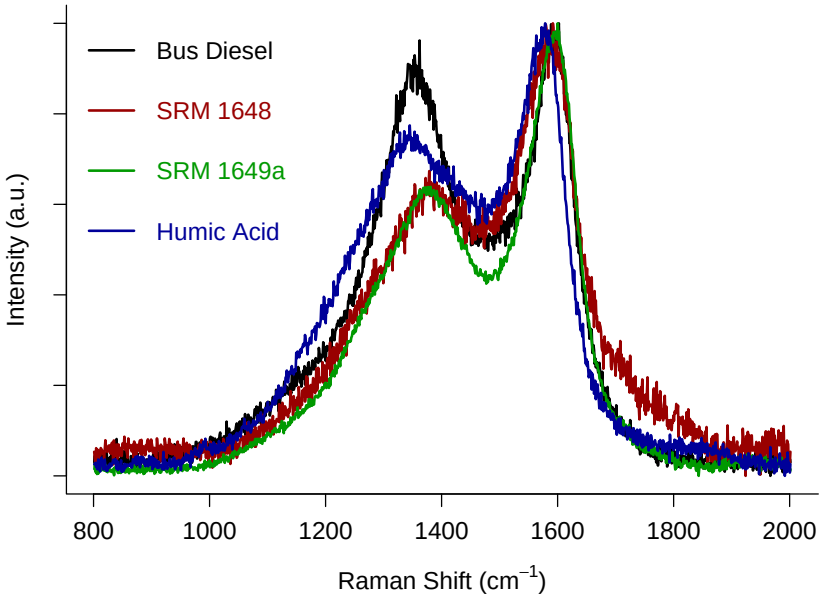

Figure 6.10: Example Raman spectra ($\lambda_0 = 514$ nm) for the reference materials of Bus Diesel, SRM 1648, SRM 1649a, and Humic Acid. Intensity values have been normalised to 1 for the G peak for comparison.

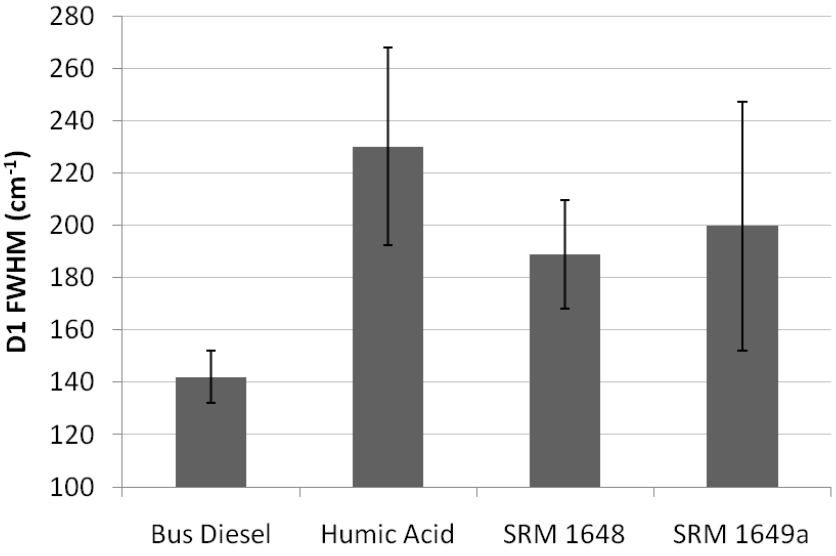

Figure 6.11: D1 band FWHM values of reference materials. Mean ± SD of three measurements.

6.3.2 PM_{10} samples

PM_{10} sample filters were measured with the Raman microscope in the same way as for the reference materials. Three spots on each filter were analysed and minor adjustments were made to the instrument settings to improve the signal-to-noise ratio. The 5 band fitting procedure was applied to the acquired data to obtain fitted spectra as shown in Figure 6.12. These spectra appear similar to those for the NIST SRMs, highlighting the amorphous (rather than crystalline) nature of the carbonaceous materials present.

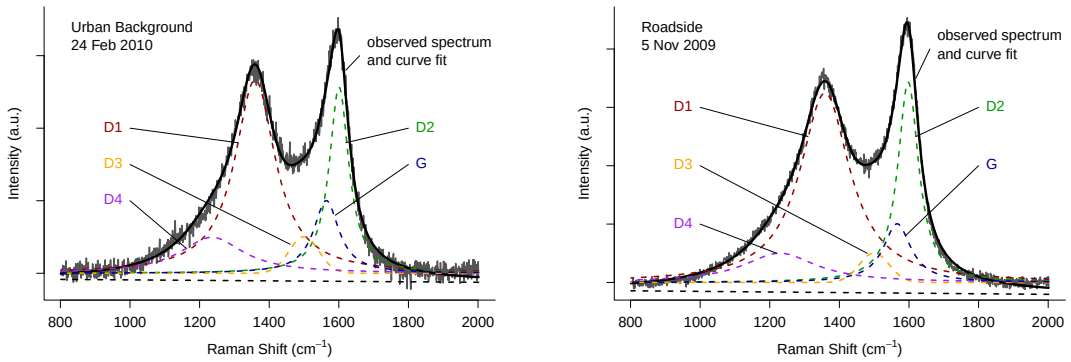

(a) Urban Background. **(b)** Roadside.

Figure 6.12: Example Raman spectrum ($\lambda_0 = 514\,\text{nm}$) of PM_{10} samples with curve fits. Grey lines show the observed spectra. Black lines show the fitted spectra. Dashed black lines are the fitted curves.

The chart in Figure 6.13 shows how the D1 FWHM values varied on three different days at the Urban Background and Roadside sites compared with the reference materials and with their BC concentrations ($\mu\text{g}\,\text{m}^{-3}$). On the two days with the highest BC concentrations the D1 widths were smaller at the Roadside site. This indicates that more soot-like carbon was present in the Roadside samples on these days and is consistent with the previous interpretation that vehicle exhaust emissions were responsible for high BC levels in Edinburgh, especially close to a main road (Chapter 3). However, the average D1 width was not lowest on the day with the highest BC concentrations, suggesting that HULIS may have also contributed to the elevated levels of BC. This is also consistent with the possibility that transport of biomass burning or secondary organic aerosol into Edinburgh caused some days of elevated PM_{10} and WSOM (Chapter 2, Chapter 4 and Chapter 5). The likely reason for organic material influencing elevated BC levels on 5 November 2009 was biomass burning emissions from bonfires in the city, as this date was Bonfire Night.

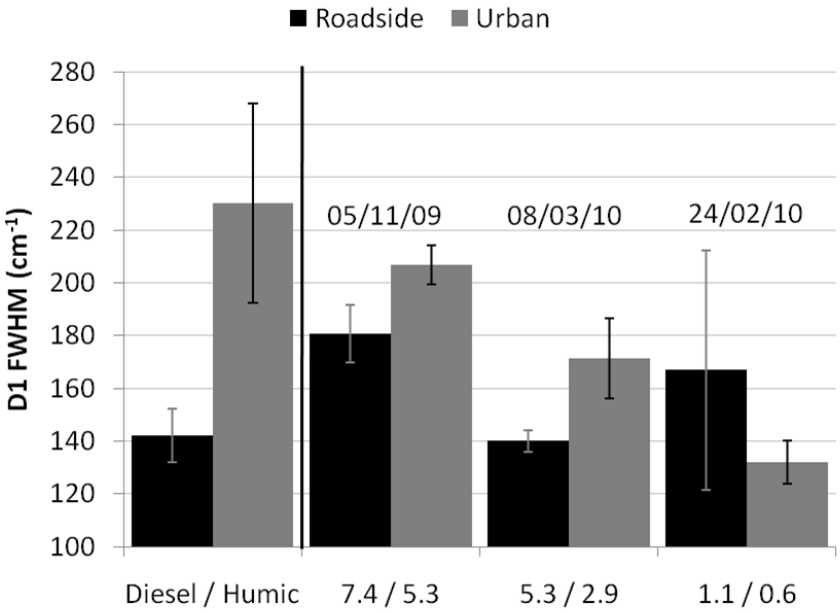

Figure 6.13: D1 band FWHM values for reference materials (Bus Diesel: black; Humic Acid: grey) and PM_{10} samples (dates are shown above the bars). Mean ± SD of three measurements. Values on the x-axis are BC concentration in $\mu g\,m^{-3}$ (Roadside: left; Urban Background: right).

The smaller D1 width at the Urban Background site on the day of lowest BC concentration is indicative of the presence of mainly soot-like carbon from diesel exhausts. As a background level of HULIS should be present (Chapter 4 and Chapter 5) this result is not expected. One explanation could be limitations in the measurement technique. The background organic compounds are generally colourless and therefore do no absorb light in the BC measurements. These same compounds were not measured by RM as it was only the dark particles or agglomerates that were selected. In contrast, organic brown carbon compounds, which occur during PM 'events', absorb light in the BC measurements and were selcted for RM measurements. A similar discrepancy was encountered with 'Humic acids' having a higher EC/TC % than their carbonaceous disorder (as measured by D1 FWHM) would suggest (Figure 6.9), i.e., increased levels of HULIS can lead to increased EC concentrations being measured.

The relatively high SD in the Roadside D1 FWHM on the lowest BC day make it difficult to interpret this result. It actually highlights a potential issue with the measurement technique employed. Two of the spots measured gave D1 FWHM values closer to those of soot carbon (130 and 144 cm^{-1}) and the other spot gave a value closer to that of humic material (222 cm^{-1}). Figure 6.14 shows the different shapes of the Raman spectra that give rise to these different D1 FWHM values.

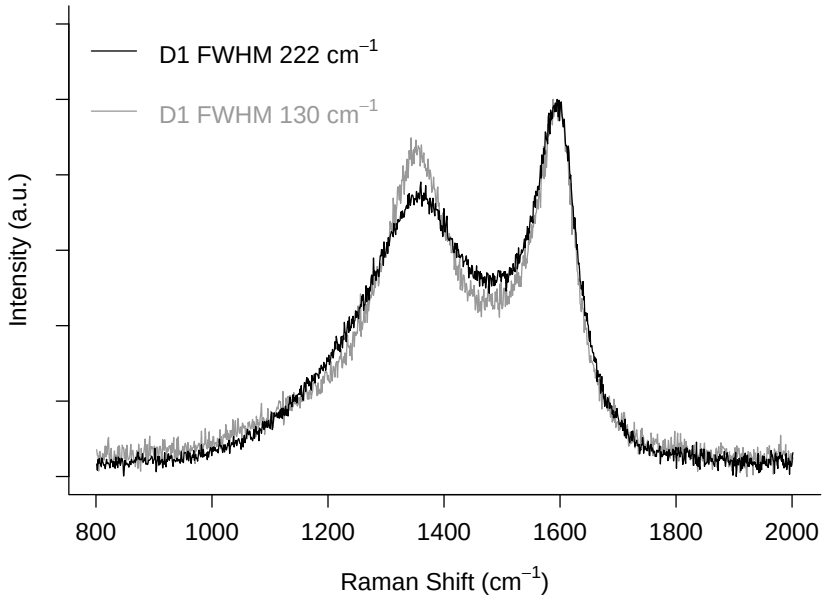

Figure 6.14: Example Raman spectra ($\lambda_0 = 514\,\text{nm}$) for individual particles of the PM_{10} sample collected on 24 February 2010 showing the difference in curve shape associated with different D1 FWHMs. Intensity values have been normalised for comparison.

6.3.2.1 Measurement issues

The previous section showed a potential discrepancy arising from only three different spots on each PM_{10} filter being measured. The number of measurements made was a compromise to allow as many different filters to be measured as possible in the limited time available on the instrument but at the same time still cover different areas of the filter and give statistically meaningful means and SD values. For the graphitic reference materials this was not an issue since all samples gave similar spectra. Similarly, the Bus Diesel and SRM 1648 sample spectra had relatively low D1 FWHM SDs. However, the SD for spectra of Humic Acid and SRM 1649a were larger (Figure 6.11). This issue was also also the case for the Roadside PM_{10} sample collected on 24 February 2010 (Figure 6.13).

Sample heterogeneity could be an issue with this type of analysis [Beyssac et al., 2003]. It is not possible to measure every particle and not all particles are likely to be the same. The question therefore arises as to whether meaningful results can be derived from these RM measurements. The fully focused laser beam (at $50\times$ magnification) used for these analyses had a diameter of ≈ 1–$2\,\mu\text{m}$. Primary particles of soot have diameters of the order of 10–30 nm so, assuming that soot is being measured, at least several hundred primary particles should be probed using the fully focused laser beam [Sadezky et al.,

2005]. If the particles and agglomerates are well-mixed within the sample it is possible that the recorded spectra are fairly representative. Defocussing the laser increases the area being measured, and therefore the number of particles, but useful spectra were not obtained using this technique due to the magnitude of the background signal from the filter.

The uncertainties of the curve fitting procedure may be as limiting as the heterogeneity of the PM samples, especially with noisy spectra. Sadezky et al. [2005] found that spectra with similar appearance gave highly variable spectral parameters (e.g., D1 FWHM). An attempt was made in this work to obtain signal-to-noise ratios as high as possible to allow reliable curve fitting of the Raman spectra. Having three spectra that give D1 FWHM values with a relatively low SD may be enough to give confidence in the results obtained. Ideally, more measurements per filter would have been made.

6.3.2.2 D1 FWHM value versus BC concentration

Accepting that there is some uncertainty in the measurements, the D1 FWHM values are compared with BC concentrations at the Urban Background, Rural and Roadside sites in Figure 6.15. RM could only be applied to a limited number of batches, with three filters usually selected from each batch. These were the two filters with the highest BC concentrations and the filter with the lowest BC concentration. Filters were selected in this way to see if there were any differences in the Raman spectra for particles collected during low and high BC conditions. This approach appears to have provided a reasonable selection of BC concentrations (Figure 6.15). D1 widths tend to fall within the limits of the Bus Diesel and Humic Acid samples showing that the material in the PM_{10} collected over a number of different days at different locations consistently had a carbonaceous order between that of the soot and humic reference materials. More of the samples appear to have D1 widths closer to the mean and SD of the D1 FWHM of the Bus Diesel sample, suggesting a predominance of exhaust soot in the measured samples. To confirm this, the mean D1 FWHM for the Urban Background site is 159 cm^{-1} ($n = 18$), which is much closer to the Bus Diesel value (142 cm^{-1}) than the Humic Acid value (230 cm^{-1}).

Interestingly, the highest BC concentration at the Urban Background site coincides with the highest D1 FWHM (and this value was measured with a relatively low SD). This supports the suggestion that HULIS can affect the results of BC measurements (Figure 6.1) but contradicts the idea of a predominantly traffic-based source of BC in Edinburgh on that day (Chapter 3). However, this one-off result has already been

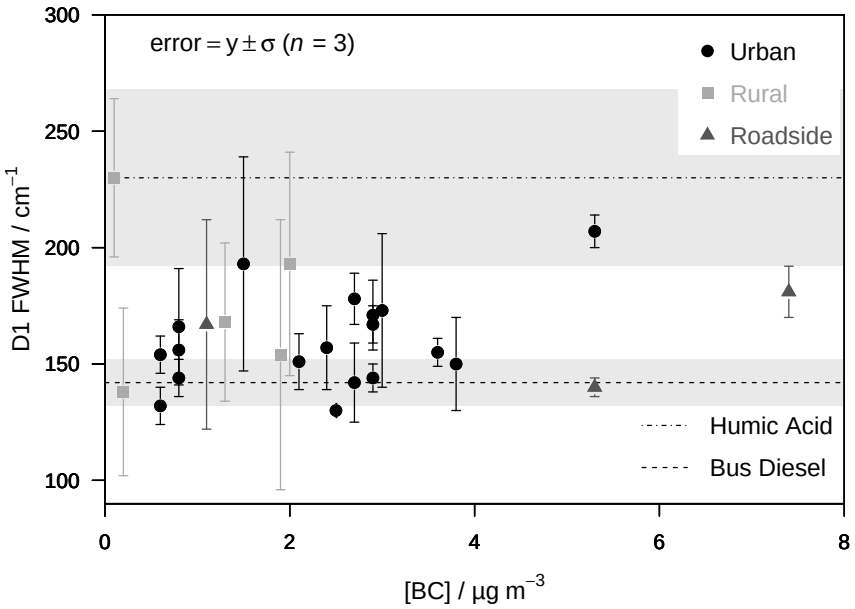

Figure 6.15: D1 FWHM values (mean ± SD) plotted against BC concentrations for PM_{10} samples from the Urban Background, Rural and Roadside sites. Mean D1 FWHMs are shown for the Bus Diesel and Humic Acid references (with ±1 SD variability shaded in grey).

suggested to be from an unusual biomass-burning event in Edinburgh (Bonfire Night; Section 6.3.2) and the Urban Background D1 widths generally tend towards soot-oriented values.

There is no clear pattern of variation in D1 FWHM values with changes in BC, only a tendency for all samples generally to be more soot-like than humic acid-like; the linear correlation for the Urban Background data is rather low ($r^2 = 0.17$; $n = 18$). Linear correlation can be improved by removing the two data with a D1 FWHM SD $> 30\,\mathrm{cm}^{-1}$ ($r^2 = 0.27$; $n = 16$) but this fairly arbitrary correction does not prevent the linear model from being skewed by the highest D1 FWHM value. The resulting line with a positive gradient may not necessarily be representative of the whole of the unmeasured PM sample set.

Results from the Roadside site ($n = 3$) have already been discussed with reference to Figure 6.13. Large measurement errors in all of the Rural samples ($n = 5$) make the results too uncertain to provide any real insight. A lack of homogeneity in these samples is the likely cause of these large errors.

6.4 Conclusions

Raman spectra were obtained for different carbonaceous reference materials. The results of curve fitting for these spectra gave D1 band FWHM values that distinguished between diesel exhaust particles from a local bus and a humic acid sample. This provided a measure for discriminating between soot and HULIS in PM samples, with a more favourable discrimination than in work published previously.

Although some samples had D1 FWHM values with a large variability about the mean, analysis of Edinburgh PM_{10} samples using Raman microscopy showed a variation in the structural order of the carbon compounds present between that of soot and HULIS, with a tendency towards more soot-like material being present. There was no strong relationship between carbonaceous order and BC concentration, showing that coloured organic compounds have the potential to influence reflectance measurements. This means that high BC concentrations do not necessarily equate to high levels of soot particles from exhaust emissions but could be influenced by organic sources, i.e., biomass burning.

The presence of high intensity Raman signals from the quartz filters caused some difficulty in making the measurements and some way of solving this problem would improve the efficiency of the analytical process. More spectra per filter sample is a key way that the results presented here may be improved. However, this would increase the time taken to perform the analysis.

As a routine analytical technique, for the type of sampling methodology used in this work, RM is limited. When hundreds of samples are collected, to allow a daily resolution of results over a number of months, the length of time it takes to analyse a sample is restrictive. Only a fraction of the samples could be analysed in this project. Also, the difficulty in distinguishing between soot and HULIS in ambient samples could lead to high levels of uncertainty in the validity of any results. This difficulty is amplified when taking measurements on quartz fibre filters that are sampled using a low-volume instrument: too few particles are available on the surface of the sample media and a low signal-to-noise ratio is obtained. A low signal-to-noise ratio can increase the level of uncertainty in the accuracy of the fitted curves. RM would therefore be more appropriate for use on samples from a short time-scale measurement campaign, using a high-volume sampler and suitable sample media (e.g., foil).

Chapter 7

Conclusions and future work

7.1 Conclusions

7.1.1 Methods and analysis

The PM_{10} Partisol-Plus 2025 Sequential Air Samplers performed satisfactorily at the Urban Background, Rural and Roadside sites, with $> 90\%$ data capture overall. The error in the flow rate of both samplers was low at $\sim 0.5\%$ of the mean. Accuracy and precision of the balance used for weighing filters was shown to be high. Changes in mass of the quartz filters used to collect PM_{10} were due to changes in ambient relative humidity (RH), and Machine Blank filters were used to correct for this. Good agreement between a Partisol and Tapered Element Oscillating Microbalance Filter Dynamics Measurement System (TEOM-FDMS) instrument at the Urban Background monitoring site demonstrated the success of this correction. However, there was a noticeable difference shown between the two monitors at low PM_{10} concentrations that could not be explained. Because of the general consistency in the Partisol-derived PM_{10} concentrations, the results from this work were used by the City of Edinburgh council to replace missing data in their annual report caused by a fault with their TEOM-FDMS monitor.

Aethalometer-equivalent daily concentrations of black carbon (BC) were determined by measuring the optical reflectance of the PM_{10} filters from the Partisol samplers. A drawback of this technique was the reliance on a number of correction factors to convert reflectance values to BC concentrations. These correction factors can vary according to the nature of the particulate matter (PM) sampled so the accuracy of the results with variations in time and location were not assured. Despite this, there is confidence in the results reported as they are consistent with those found elsewhere in the United Kingdom (UK).

Further investigation of the light-absorbing particles on quartz fibre filters was undertaken by Raman microspectroscopy (RM). Careful focussing of the laser beam and optimisation of the instrumental settings allowed Raman spectra to be obtained for different carbonaceous materials. The results of curve fitting for these spectra gave D1 band full width at half maximum (FWHM) values that provided a measure for discriminating between soot and HUmic-LIke Substances (HULIS) in PM samples.

The combination of aqueous extraction and total organic carbon (TOC) analysis used in this project was validated by measuring the dissolved organic carbon (DOC) concentration of known quantities of water-extracted National Institute of Standards and Technology (NIST) standard reference materials (SRMs). Linearity of the results of these experiments confirmed the approach used. To remove inorganic material from aqueous PM_{10} extracts, a solid phase extraction (SPE) procedure was employed. Initial difficulties with this technique due to relatively low daily PM_{10} concentrations were overcome by combining each fortnight batch of samples into one sample. The SPE process was successful in isolating hydrophobic water-soluble organic matter (HWSOM) and removing water-soluble inorganic compounds. This allowed the subsequent analysis of the chemical characteristics of HWSOM by ultraviolet-visible (UV-Vis) absorption spectroscopy without interference from inorganic ions.

7.1.2 Composition and sources of PM

The concentrations of PM_{10} measured in this monitoring campaign, which were well below the European Union (EU) specified limit value requirements, indicated that the air in Edinburgh was relatively clean. This should be of some benefit to the health of the population of the city. A consequence of the relatively low concentrations of PM_{10} in the Edinburgh area was that the analysis of the water-soluble component of PM in this project (summarised in the previous section) was an analytical challenge. Table 7.1 provides a final summary of PM concentrations and compositional proportions measured at the Edinburgh monitoring sites.

Relatively higher PM_{10}, BC and WSOM concentrations were all associated with calm weather conditions in Edinburgh. Low wind speeds prevented dispersion of PM, therefore allowing the transient build-up of concentrations of all three of the daily-measured PM metrics. No other sources of BC were apparent so the daily variation was shown to be controlled by predominantly traffic-related local emissions and meteorology. The traffic source of BC was highlighted by its proportion in PM_{10} increasing with sampling location in the order: Rural < Urban Background < Roadside.

Table 7.1: Overview of daily PM_{10}, BC and WSOM concentrations, and % proportion of PM_{10}, at all of the monitoring sites. The non-classified fraction of PM_{10} is shown as Other.

Daily	Urban Background		Rural		Roadside	
	$\mu g\,m^{-3}$	%	$\mu g\,m^{-3}$	%	$\mu g\,m^{-3}$	%
PM_{10}	15	100	14	100	18	100
BC	1.4	10	0.51	4	3.4	19
WSOM	1.6	11	1.6	12	1.8	10
Other	12	79	12	84	13	71

Peaks in PM_{10} and WSOM concentrations were related to the transport of air masses from areas of mainland Europe where biogenic secondary organic aerosol (SOA) and biomass burning were likely sources. This is consistent with results from elsewhere in Europe that show a significant proportion of terrestrial PM to be biogenic. Long-range transport is outside of the control of local authorities so this source of peaks in PM concentrations should be taken into consideration when pan-European legislation is being developed.

Although the majority of the Edinburgh PM_{10} and WSOM seems to have originated from air masses outside of the city, there was also a minor contribution from urban traffic sources. More than half of the urban source of PM_{10} can be explained by direct exhaust emissions but the remainder is likely to be from other traffic-related sources, for example, re-suspended road dust. The small quantity of roadside WSOM could be explained by non-fossil carbon in tyre wear or an anthropogenic enrichment of biogenic SOA.

A slight seasonal trend was observed for BC and HWSOM with lower concentrations of both during the warmer summer months. This reduction was most likely related to a shift of semi-volatile compounds from particle to gas phases leading to lower masses of BC and HWSOM particles in the summer. A much clearer seasonal trend was observed for the chemical composition of HWSOM as measured by UV-Vis absorption spectroscopy. This was comparable with trends seen elsewhere in Europe where lower molecular weight aliphatic compounds present in the summer tended to be dominated by larger aromatic and polyconjugated compounds in the winter. The studies from other European cities attributed the aromatic compounds in winter to biomass burning sources but this is an unlikely source of local PM_{10} in Edinburgh (apart from the annual Bonfire Night event on 5 November). Seasonal changes in the aromaticity and polyconjugation

of Edinburgh HWSOM are therefore likely to be controlled by long-range transport of biomass burning PM or local sources of uncertain origin.

RM showed variation in the structural order of the carbon compounds present in Edinburgh PM_{10} between that of soot and HULIS, with a tendency towards more soot-like material being present. The lack of a relationship between carbonaceous order and BC concentration showed that coloured ('brown') organic compounds have the potential to influence reflectance measurements. This means that HULIS may have been mistaken for soot in the BC analysis, as highlighted by the biomass burning source of PM observed in Edinburgh on 5 November 2009 (Bonfire Night).

The combination of the measurement approaches in this thesis have yielded some insight into the nature and variation in carbonaceous PM material with time and sampling location.

7.2 Future work

7.2.1 PM monitoring

An important aspect in the legislation and control of PM pollution is the accurate and precise measurement of atmospheric concentrations. This project demonstrated some of the areas of both agreement and disagreement between different monitoring methods. Whilst there remains a requirement to monitor PM concentrations, and different instrumentation is being used for this purpose, the between-sampler agreement should be improved as far as possible. One area of uncertainty highlighted in this project is the use of fixed correction factors to convert reflectance measurements into BC concentrations. The accuracy of the fixed correction factors is diminished by the fact that there are likely to be spatially and temporally variable. Finding and using correction factors according to the time and place that monitoring is taking place would hopefully improve the accuracy of reported results.

7.2.2 Sources and composition

PM_{10} has been studied extensively by various researchers over many years. Although a great deal is understood about this fraction of PM there are still areas of uncertainty.

One area of research that is still open is in the determination of the exact nature and origin of the carbonaceous fraction of PM.

Further insight into the composition and sources of WSOM would likely be gained through research similar to that reported in this work being carried out over a longer time-scale and by including the collection of $PM_{2.5}$. Simultaneous daily sampling of PM_{10} and $PM_{2.5}$ at the Urban Background, Rural and Roadside locations for a minimum of 2 years is one possibility that would allow a better representation of the spatial and temporal trends in the different PM fractions. Use of a high volume sampler would open up the possibility of analysing daily concentrations of the hydrophobic and hydrophilic fractions of WSOM (only two-weekly concentrations were reported in this work), as well as allowing the use of other analytical techniques, for example, nuclear magnetic resonance (NMR) spectroscopy and Fourier transform ion cyclotron resonance mass spectrometry (FT-ICR-MS).

FT-ICR-MS would complement the chemical information provided by UV-Vis absorption spectroscopy analysis of the seasonal changes in WSOM. The high resolving power and mass accuracy of FT-ICR-MS means that each peak in a mass spectrum represents a chemically distinct component, and the molecular formula of many of these peaks can be determined. An example of an FT-ICR mass spectrum of PM is shown in Figure 7.1 and this highlights the complexity of this sample of PM. Further information on the chemical components of PM in Edinburgh could help determine the winter source of aromatic and polyconjugated compounds.

Analysis of the total carbon (TC) and organic carbon (OC) fractions of PM would add to the information already reported in this project on the BC and WSOM fraction. This could be added to further by measuring the concentrations of metals in the PM samples collected and this may help confirm the source of non-exhaust traffic-influenced PM_{10} and WSOM.

The potential for using RM to distinguish between different types of carbonaceous particles in PM_{10} would be improved by measuring more spectra per filter sample. With this improvement in place the analysis of spatially and temporally variable samples could help further enhance knowledge of the nature and variation in carbonaceous PM material.

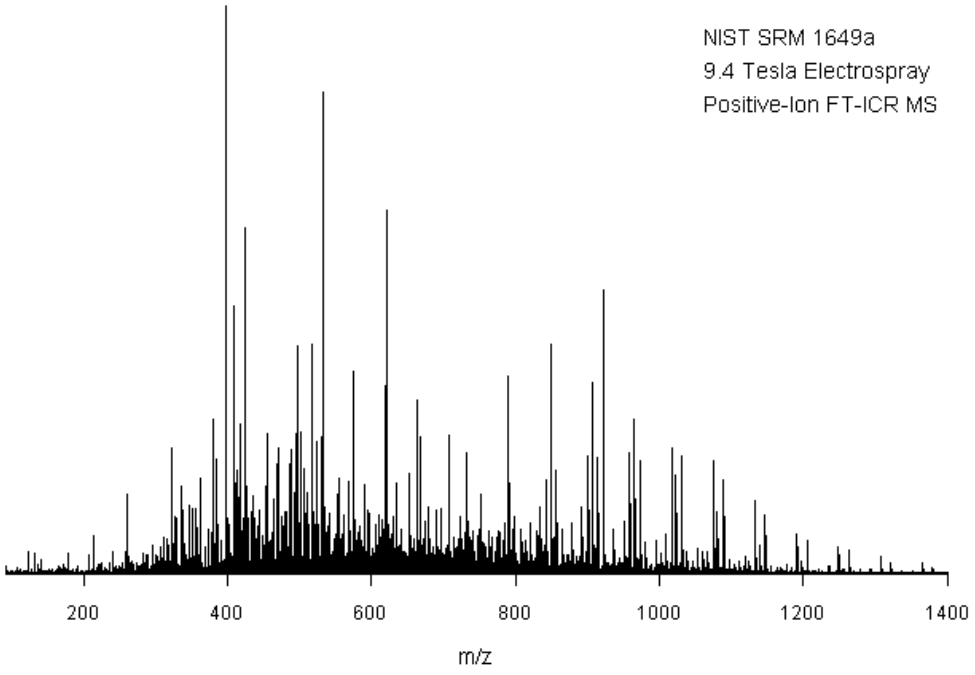

Figure 7.1: Example of an FT-ICR mass spectrum of the WSOM in NIST SRM 1649a. Analysis carried out in the SIRCAMS laboratory, School of Chemistry, University of Edinburgh.

References

Andreae, M. O. and Gelencsér, A.: Black carbon or brown carbon? The nature of light-absorbing carbonaceous aerosols, Atmospheric Chemistry and Physics, 6, 3131–3148, 2006.

AQEG: Particulate Matter in the United Kingdom, Tech. rep., Air Quality Expert Group, Department for the Environment, Food and Rural Affairs, 2005.

Atkinson, R. W., Fuller, G. W., Anderson, H. R., Harrison, R. M., and Armstrong, B.: Urban ambient particle metrics and health, a time-series analysis, Epidemiology, 21, 501–511, 2010.

Ayers, G.: Comment on regression analysis of air quality data, Atmospheric Environment, 35, 2423–2425, 2001.

Baduel, C., Voisin, D., and Jaffrezo, J.-L.: Seasonal variations of concentrations and optical properties of water soluble HULIS collected in urban environments, Atmospheric Chemistry and Physics, 10, 4085–4095, 2010.

Batonneau, Y., Sobanska, S., Laureyns, J., and Bremard, C.: Confocal microprobe Raman imaging of urban tropospheric aerosol particles, Environmental Science and Technology, 40, 1300–1306, 2006.

Beyssac, O., Goffé, B., Petitet, J., Froigneux, E., Moreau, M., and Rouzaud, J.: On the characterization of disordered and heterogeneous carbonaceous materials by Raman spectroscopy, Spectrochimica Acta Part A, 59, 2267–2276, 2003.

Birch, M. E. and Cary, R. A.: Elemental carbon-based method for occupational monitoring of particulate diesel exhaust: Methodology and exposure issues, Analyst, 121, 1183–1190, 1996.

Bland, J. M. and Altman, D. G.: Statistical Methods for Assessing Agreement between Two Methods of Clinical Measurement, Lancet, 327, 307–310, 1986.

Bower, J., Broughton, G., Connolly, C., Cook, A., Eaton, S., Glynn, A., Grice, S., Kent, A., Loader, A., Stedman, J., Targa, J., Telling, S., Tsagatakis, I., Vincent, K., Willis, P., Yap, F., and Yardley, R.: Air Pollution in the UK: 2008, Tech. rep., AEA, 2009.

Brown, A. S., Yardley, R. E., Quincey, P. G., and Butterfield, D. M.: Studies of the effect of humidity and other factors on some different filter materials used for gravimetric measurements of ambient particulate matter, Atmospheric Environment, 40, 4670–4678, 2006.

Brown, R. J.: The use and abuse of limits of detection in environmental analytical chemistry, The Scientific World Journal, 8, 796–801, 2008.

Buchanan, C. M., Beverland, I. J., and Heal, M. R.: The influence of weather-type and long-range transport on airborne particle concentrations in Edinburgh, UK, Atmospheric Environment, 36, 5343–5354, 2002.

Bureau Veritas: Assessment of UK AURN particulate matter monitoring equipment against the January 2010 Guide to Demonstration of Equivalence, Tech. rep., Defra and the Devolved Administrations, 2010.

Butterfield, D. and Quincey, P.: Measurement science issues relating to PM_{10} and $PM_{2.5}$ airborne particles, Tech. rep., National Physical Laboratory, 2007.

Butterfield, D., Beccaceci, S., Sweeney, B., Green, D., Alexander, J., and Grieve, A.: 2009 Annual Report for the UK Black Carbon Network, Tech. rep., NPL, 2010.

Camposa, M., Nogueirab, R., Damettob, P., Franciscob, J., and Coelhoa, C.: Dissolved organic carbon in rainwater: Glassware decontamination and sample preservation and volatile organic carbon, Atmospheric Environment, 41, 8924–8931, 2007.

Carslaw, D. and Ropkins, K.: openair: Open-source tools for the analysis of air pollution data, R package version 0.4-17, 2011.

Carslaw, D. C., Beevers, S. D., Ropkins, K., and Bell, M. C.: Detecting and quantifying aircraft and other on-airport contributions to ambient nitrogen oxides in the vicinity of a large international airport, Atmospheric Environment, 40, 5424–5434, 2006.

CEN: European Standard EN 12341 Air Quality—Determination of the PM_{10} fraction of suspended particulate matter—Reference method and field test procedure to demonstrate reference equivalence of measurement methods., European Committee for Standardization, Brussels, 1999.

CEN: Demonstration of Equivalence of Ambient Air Monitoring Methods, Tech. rep., EC Working group on Guidance for the Demonstration of Equivalence, 2005.

Chow, J. C., Watson, J. G., Chen, L.-W. A., Arnott, W. P., and Moosmüller, H.: Equivalence of elemental carbon by thermal/optical reflectance and transmittance with different temperature protocols, Environmental Science and Technology, 38, 4414–4422, 2004.

Cook, R. L.: Coupling NMR to NOM, Analytical and Bioanalytical Chemistry, 378, 1484–1503, 2004.

Cosemans, G., Kretzschmar, J., and Mensink, C.: Pollutant roses for daily averaged ambient air pollutant concentrations, Atmospheric Environment, 42, 6982–6991, 2008.

Davis, J.: Statistical and Data Analysis in Geology, 2nd Edition, Wiley, New York, 1986.

Deboudt, K., Flament, P., Choël, M., Gloter, A., Sobanska, S., and Colliex, C.: Mixing state of aerosols and direct observation of carbonaceous and marine coatings on African dust by individual particle analysis, Journal of Geophysical Research, 115, D24 207, doi:10.1029/2010JD013 921, 2010.

Decesari, S., Mircea, M., Cavalli, F., Fuzzi, S., Moretti, F., Tagliavini, E., and Facchini, M. C.: Source attribution of water-soluble organic aerosol by nuclear magnetic resonance spectroscopy, Environmental Science & Technology, 41, 2479–2484, 2007.

Dockery, D. W., Pope III, C., Xu, X., Spengler, J. D., Ware, J. H., Fay, M. E., Ferris, B. G., and Speizer, F. E.: An association between air pollution and mortality in six U.S. cities, The New England Journal of Medicine, 329, 1753–1759, 1993.

Duarte, R. M. B. O. and Duarte, A. C.: Application of non-ionic solid sorbents (XAD resins) for the isolation and fractionation of water-soluble organic compounds from atmospheric aerosols, Journal of Atmospheric Chemistry, 51, 79–93, 2005.

Duarte, R. M. B. O., Pio, C. A., and Duarte, A. C.: Synchronous scan and excitation-emission matrix fluorescence spectroscopy of water-soluble organic compounds in atmospheric aerosols, Journal of Atmospheric Chemistry, 48, 157–171, 2004.

Duarte, R. M. B. O., Pio, C. A., and Duarte, A. C.: Spectroscopic study of the water-soluble organic matter isolated from atmospheric aerosols collected under different atmospheric conditions, Analytica Chimica Acta, 530, 7–14, 2005.

Duarte, R. M. B. O., Santos, E. B. H., Pio, C. A., and Duarte, A. C.: Comparison of structural features of water-soluble organic matter from atmospheric aerosols with those of aquatic humic substances, Atmospheric Environment, 41, 8100–8113, 2007.

Eaton, S.: QA/QC data ratification report for the Automatic Urban and Rural Network, July-September 2010, Tech. rep., AEA Group, 2011.

Eaton, S. and Stacey, B.: QA/QC data ratification report for the Automatic Urban and Rural Network, October-December 2009, and Annual Review 2009, Tech. rep., AEA Group, 2010.

Escribano, R., Sloan, J., Siddique, N., Sze, N., and Dudev, T.: Raman spectroscopy of carbon-containing particles, Vibrational Spectroscopy, 26, 179–186, 2001.

European Union: DIRECTIVE 2004/107/EC OF THE EUROPEAN PARLIAMENT AND OF THE COUNCIL relating to arsenic, cadmium, mercury, nickel and polycyclic aromatic hydrocarbons in ambient air, Official Journal of the European Union, 2004.

European Union: DIRECTIVE 2008/50/EC OF THE EUROPEAN PARLIAMENT AND OF THE COUNCIL on ambient air quality and cleaner air for Europe, Official Journal of the European Union, 2008.

Fuzzi, S., Andreae, M. O., Huebert, B. J., Kulmala, M., Bond, T. C., Boy, M., Doherty, S. J., Guenther, A., Kanakidou, M., Kawamura, K., Kerminen, V. M., Lohmann, U., Russell, L. M., and Pöschl, U.: Critical assessment of the current state of scientific knowledge, terminology, and research needs concerning the role of organic aerosols in the atmosphere, climate, and global change, Atmospheric Chemistry and Physics, 6, 2017–2038, 2006.

Galton, F.: Regression towards mediocrity in hereditary stature., Journal of the Anthropological Institute, 15, 246–263, 1886.

Gelencser, A.: Carbonaceous Aerosol, Springer, Dordrecht, 2004.

Glasius, M., la Cour, A., and Lohse, C.: Fossil and nonfossil carbon in fine particulate matter: A study of five European cities, Journal of Geophysical Research, 116, D11 302, doi:10.1029/2011JD015 646, 2011.

Graber, E. R. and Rudich, Y.: Atmospheric HULIS: How humic-like are they? A comprehensive and critical review, Atmospheric Chemistry and Physics, 6, 729–753, 2006.

Griffin, A., Fraser, A., Kent, A., Loader, A., Martinez, C., Stedman, J., Stevenson, K., Vincent, K., Willis, P., Yardley, R., Bush, T., Connolly, E., and Bayley, C.: Air Pollution in the UK 2009 Edition B, Tech. rep., Department for Environment, Food and Rural Affairs, 2010.

Grubbs, F. E.: Procedures for detecting outlying observations in samples, Technometrics, 11, 1–21, 1969.

Harris, D. C.: Exploring Chemical Analysis, W.H.Freeman & Co Ltd, 1996.

Harrison, D., Maggs, R., and Booker, J.: UK equivalence programme for monitoring of particulate matter, Tech. rep., Bureau Veritas, 2006.

Harrison, R. M., Jones, A. M., and Lawrence, R. G.: A pragmatic mass closure model for airborne particulate matter at urban background and roadside sites, Atmospheric Environment, 37, 4927–4933, 2003.

Harrison, R. M., Jones, A. M., and Lawrence, R. G.: Major component composition of PM_{10} and $PM_{2.5}$ from roadside and urban background sites, Atmospheric Environment, 38, 4531–4538, 2004.

Havers, N., Burba, P., Lambert, J., and Klockow, D.: Spectroscopic characterization of humic-like substances in airborne particulate matter, Journal of Atmospheric Chemistry, 29, 45–54, 1998.

Heal, M. R., Hibbs, L. R., Agius, R. M., and Beverland, I. J.: Interpretation of variations in fine, coarse and black smoke particulate matter concentrations in a northern European city, Atmospheric Environment, 39, 3711–3718, 2005.

Heal, M. R., Naysmith, P., Cook, G. T., Xu, S., Raventós Duran, T., and Harrison, R. M.: Application of ^{14}C analyses to source apportionment of carbonaceous $PM_{2.5}$ in the UK, Atmospheric Environment, 45, 2341–2348, 2011.

Heintzenberg, J.: Fine particles in the global troposphere — A review, Tellus, 41B, 149–160, 1989.

Hibbs, L. R.: Metal content of airborne particulate matter in Edinburgh, Ph.D. thesis, The University of Edinburgh, 2002.

Hoek, G., Brunekreef, B., Goldbohm, S., Fischer, P., and van den Brandt, P. A.: Association between mortality and indicators of traffic-related air pollution in the Netherlands: a cohort study, Lancet, 360, 1203–9, 2002.

ISO 9835: Ambient air - Determination of a black smoke index, 1993.

Ivleva, N. P., Niessner, R., and Panne, U.: Characterization and discrimination of pollen by Raman microscopy, Analytical and Bioanalytical Chemistry, 381, 261–267, 2005.

Ivleva, N. P., McKeon, U., Niessner, R., and Pöschl, U.: Raman microspectroscopic analysis of size-resolved atmospheric aerosol particle samples collected with an ELPI: Soot, humic-like substances, and inorganic compounds, Aerosol Science and Technology, 41, 655–671, 2007a.

Ivleva, N. P., Messerer, A., Yang, X., Niessner, R., and Pöschl, U.: Raman microspectroscopic analysis of changes in the chemical structure and reactivity of soot in a diesel exhaust aftertreatment model system, Environmental Science and Technology, 41, 3702–3707, 2007b.

Joint Committee for Guides in Metrology: JCGM 100:2008. Evaluation of measurement data — Guide to the expression of uncertainty in measurement, 2008.

Kiss, G., Varga, B., Gelencsér, A., Krivácsy, Z., Ágnes Molnár, Alsberg, T., Persson, L., Hansson, H.-C., and Facchini, M. C.: Characterisation of polar organic compounds in fog water, Atmospheric Environment, 35, 2193–2200, 2001.

Kiss, G., Varga, B., Galambos, I., and Ganszky, I.: Characterization of water-soluble organic matter isolated from atmospheric fine aerosol, Journal of Geophysical Research, 107, D21 8339, doi:10.1029/2001JD000 603, 2002.

Kiss, G., Tombacz, E., Varga, B., Alsberg, T., and Persson, L.: Estimation of the average molecular weight of humic-like substances isolated from fine atmospheric aerosol, Atmospheric Environment, 37, 3783–3794, 2003.

Knauer, M., Carrara, M., Rothe, D., Niessner, R., and Ivleva, N. P.: Changes in structure and reactivity of soot during oxidation and gasification by oxygen, studied by micro-Raman spectroscopy and temperature programmed oxidation, Aerosol Science and Technology, 43, 1–8, 2009a.

Knauer, M., Schuster, M. E., Su, D., Schlögl, R., Niessner, R., , and Ivleva, N. P.: Soot structure and reactivity analysis by Raman microspectroscopy, temperature-programmed oxidation, and high-resolution transmission electron microscopy, Journal of Physical Chemistry A, 113, 13 871–13 880, 2009b.

Krivacsy, Z., Kiss, G., Varga, B., Galambos, I., Sarvari, Z., Gelencser, A., Molnar, A., Fuzzi, S., Facchini, M., Zappoli, S., Andracchio, A., Alsberg, T., Hansson, H., and Persson, L.: Study of humic-like substances in fog and interstitial aerosol by size-exclusion chromatography and capillary electrophoresis, Atmospheric Environment, 34, 4273–4281, 2000.

Krivacsy, Z., Gelencser, A., Kiss, G., Meszaros, E., Molnar, A., Hoffer, A., Meszaros, T., Sarvaris, Z., Temesi, D., Varga, B., Baltensperger, U., Nyeki, S., and Weingarter, E.: Study on the chemical character of water soluble organic compounds in fine atmospheric aerosol at the Jungfraujoch, Journal of Atmospheric Chemistry, 39, 235–259, 2001.

Krivacsy, Z., Kiss, G., Ceburnis, D., Jennings, G., Maenhaut, W., Salma, I., and Shooter, D.: Study of water-soluble atmospheric humic matter in urban and marine environments, Atmospheric Research, 87, 1–12, 2008.

Legendre, P. and Legendre, L.: Numerical ecology. Number 20 in Developments in Environmental Modelling. 2nd edition., Elsevier, Amsterdam, 1998.

Lenschow, P., Abraham, H.-J., Kutzner, K., Lutz, M., Preuß, J.-D., and Reichenbächer, W.: Some ideas about the sources of PM10, Atmospheric Environment, Volume 35, Supplement 1, S23S33, 2001.

Maggs, R., Harrison, D., Carslaw, D., and Stevenson, K.: Analysis of trends in gravimetric particulate mass measurements in the United Kingdom, Tech. rep., Bureau Veritas UK Ltd, 2009.

Mertes, S., Dippel, B., and Schwarzenböck, A.: Quantification of graphitic carbon in atmospheric aerosol particles by Raman spectroscopy and first application for the determination of mass absorption efficiencies, Journal of Aerosol Science, 35, 347–361, 2004.

O'Dowd, C., Facchini, M., Cavalli, F., Ceburnis, D., Mircea, M. Decesari, S., Fuzzi, S., Yoon, Y., and Putaud, J.-P.: Biogenically driven organic contribution to marine aerosols, Nature, 431, 676–680, 2004.

Ofner, J., Kruger, H.-U., Grothe, H., Schmitt-Kopplin, P., Whitmore, K., and Zetzsch, C.: Physico-chemical characterization of SOA derived from catechol and guaiacol — a model substance for the aromatic fraction of atmospheric HULIS, Atmospheric Chemistry and Physics, 11, 1–15, 2011.

Park, S. S., Hansen, A. D., and Cho, S. Y.: Measurement of real time black carbon for investigating spot loading effects of Aethalometer data, Atmospheric Environment, 44, 1449–1455, 2010.

Peuravuori, J. and Pihlaja, K.: Molecular size distribution and spectroscopic properties of aquatic humic substances, Analytica Chimica Acta, 337, 133–149, 1997.

Pope, C. A.: Review: Epidemiological basis for particulate air pollution health standards, Aerosol Science and Technology, 32, 4–14, 2000.

Pöschl, U.: Atmospheric aerosols: Composition, transformation, climate and health effects, Angewandte Chemie (International Edition), 44, 7520–7540, 2005.

Potgieter-Vermaak, S. S. and Van Grieken, R.: Preliminary evaluation of micro-Raman spectrometry for the characterization of individual aerosol particles, Applied Spectroscopy, 60, 39–47, 2006.

Prescott, G. J., Cohen, G. R., Elton, R. A., Fowkes, F. G. R., and Agius, R. M.: Urban air pollution and cardiopulmonary ill health: a 14.5 year time series study, Occupational & Environmental Medicine, 55, 697–704, 1998.

Puett, R. C., Schwartz, J., Hart, J. E., Yanosky, J. D., Speizer, F. E., Suh, H., Paciorek, C. J., Neas, L. M., and Laden, F.: Chronic particulate exposure, mortality, and coronary heart disease in the Nurses Health Study, American Journal of Epidemiology, 168, 1161–1168, 2008.

QUARG: Airborne Particulate Matter in the United Kingdom, Tech. rep., Quality of Urban Air Review Group, Department of Environment, 1996.

Quincey, P.: A relationship between Black Smoke Index and Black Carbon concentration, Atmospheric Environment, 41, 7964–7968, 2007.

R Development Core Team: R: A Language and Environment for Statistical Computing, R Foundation for Statistical Computing, Vienna, Austria, URL `http://www.R-project.org`, ISBN 3-900051-07-0, 2011.

Reich, S. and Thomsen, C.: Raman spectroscopy of graphite, Philosophical Transactions of the Royal Society A, 362, 2271–2288, 2004.

Rosen, N. and Novakov, T.: Raman scattering and characterisation of atmospheric aerosol particles, Nature, 266, 708–710, 1977.

Rupprecht & Patashnick Co., Inc.: Operating Manual, Partisol-Plus Model 2025 Sequential Air Sampler, 25 Corporate Circle, Albany, NY 12203 USA, revision b edn., 1998.

Sadezky, A., Muckenhuber, H., Grothe, H., Niessner, R., and Pöschl, U.: Raman microspectroscopy of soot and related carbonaceous materials: Spectral analysis and structural information, Carbon, 43, 1731–1742, 2005.

Salma, I., Ocskay, R., Chi, X., and Maenhaut, W.: Sampling artefacts, concentration and chemical composition of fine water-soluble organic carbon and humic-like substances in a continental urban atmospheric environment, Atmospheric Environment, 41, 4106–4118, 2007.

Samburova, V., Szidat, S., Hueglin, C., Fisseha, R., Baltensperger, U., Zenobi, R., and Kalberer, M.: Seasonal variation of high-molecular-weight compounds in the water-soluble fraction of organic urban aerosols, Journal of Geophysical Research, 110, D23 210, doi:10.1029/2005JD005 910, 2005a.

Samburova, V., Zenobi, R., and Kalberer, M.: Characterization of high molecular weight compounds in urban atmospheric particles, Atmospheric Chemistry and Physics, 5, 2163–2170, 2005b.

Samburova, V., Didenko, T., Kunenkov, E., Emmenegger, C., Zenobi, R., and Kalberer, M.: Functional group analysis of high-molecular weight compounds in the water-soluble fraction of organic aerosols, Atmospheric Environment, 41, 4703–4710, 2007.

Sannigrahi, P., Sullivan, A. P., Weber, R. J., and Ingall, E. D.: Characterization of water-soluble organic carbon in urban atmospheric aerosols using solid-state C-13 NMR spectroscopy, Environmental Science & Technology, 40, 666–672, 2006.

Schmid, J., Grob, B., Niessner, R., and Ivleva, N. P.: Multiwavelength Raman microspectroscopy for rapid prediction of soot oxidation reactivity, Analytical Chemistry, 83, 1173–1179, 2011.

Solomon, S., Qin, D., Manning, M., Chen, Z., Marquis, M., Averyt, K., M.Tignor, and Miller, H., eds.: IPCC, 2007: Summary for Policymakers. In: Climate Change 2007: The Physical Science Basis. Contribution of Working Group I to the Fourth Assessment Report of the Intergovernmental Panel on Climate Change, Cambridge University Press, Cambridge, United Kingdom and New York, NY, USA, 2007.

Sun, J. and Ariya, P. A.: Atmospheric organic and bio-aerosols as cloud condensation nuclei (CCN): A review, Atmospheric Environment, 40, 795–820, 2006.

Sun, Y., Zhang, Q., Zheng, M., Ding, X., Edgerton, E. S., and Wang, X.: Characterization and source apportionment of water-soluble organic matter in atmospheric fine particles ($PM_{2.5}$) with high-resolution aerosol mass spectrometry and GC-MS, Environmental Science and Technology, 45, 4854–4861, 2011.

Sze, S., Siddique, N., Sloan, J., and Escribano, R.: Raman spectroscopic characterization of carbonaceous aerosols, Atmospheric Environment, 35, 561–568, 2001.

Szidat, S., Jenk, T. M., Gaggeler, H. W., Synal, H. A., Fisseha, R., Baltensperger, U., Kalberer, M., Samburova, V., Reimann, S., Kasper-Giebl, A., and Hajdas, I.: Radiocarbon (C-14)-deduced biogenic and anthropogenic contributions to organic carbon (OC) of urban aerosols from Zurich, Switzerland, Atmospheric Environment, 38, 4035–4044, 2004.

Szidat, S., Jenk, T. M., Synal, H. A., Kalberer, M., Wacker, L., Hajdas, I., Kasper-Giebl, A., and Baltensperger, U.: Contributions of fossil fuel, biomass-burning, and biogenic emissions to carbonaceous aerosols in Zurich as traced by C-14, Journal of Geophysical Research, 111, D07 206, doi:10.1029/2005JD006 590, 2006.

Szidat, S., Ruff, M., Perron, N., Wacker, L., Synal, H.-A., Hallquist, M., Shannigrahi, A. S., Yttri, K. E., Dye, C., and Simpson, D.: Fossil and non-fossil sources of organic carbon (OC) and elemental carbon (EC) in Göteborg, Sweden, Atmospheric Chemistry and Physics, 9, 1521–1535, 2009.

Szymanski, H. A.: Raman spectroscopy, theory and practice, Plenum Press, New York, New York, 1967.

Tuinstra, F. and Koenig, J. L.: Raman spectrum of graphite, Journal of Chemical Physics, 53, 1126–1130, 1970.

Varga, B., Kiss, G., Ganszky, I., Gelencser, A., and Krivacsy, Z.: Isolation of water-soluble organic matter from atmospheric aerosol, Talanta, 55, 561–572, 2001.

Virkkula, A., Makela, T., Hillamo, R., Yli-Tuomi, T., Hirsikko, A., Hameri, K., and Koponen, I. K.: A simple procedure for correcting loading effects of aethalometer data, Journal of the Air & Waste Management Association, 57, 1214–1222, 2007.

Wang, Y., Alsmeyer, D. C., and McCreery, R. L.: Raman spectroscopy of carbon materials: structural basis of observed spectra, Chemistry of Materials, 2, 557–563, 1990.

Warton, D. I., Wright, I. J., Falster, D. S., and Westoby, M.: Bivariate line-fitting methods for allometry, Biological Reviews, 81, 259–291, 2006.

WHO: Particulate matter air pollution: how it harms health, Tech. rep., World Health Organisation, Berlin, Copenhagen, Rome, 2005.

Williams, D. and Fleming, I.: Spectroscopic Methods in Organic Chemistry, McGraw-Hill, London, UK, second edn., 1973.

Witham, C. and Manning, A.: Impacts of Russian biomass burning on UK air quality, Atmospheric Environment, 41, 8075–8090, 2007.

Yin, J. and Harrison, R. M.: Pragmatic mass closure study for $PM_{1.0}$, $PM_{2.5}$ and PM_{10} at roadside, urban background and rural sites, Atmospheric Environment, 42, 980–988, 2008.

Yin, J., Harrison, R. M., Chen, Q., Rutter, A., and Schauer, J. J.: Source apportionment of fine particles at urban background and rural sites in the UK atmosphere, Atmospheric Environment, 44, 841–851, 2010.

Zappoli, S., Andracchio, A., Fuzzi, S., Facchini, M. C., Gelencser, A., Kiss, G., Krivacsy, Z., Molnar, A., Meszaros, E., Hansson, H. C., Rosman, K., and Zebuhr, Y.: Inorganic, organic and macromolecular components of fine aerosol in different areas of Europe in relation to their water solubility, Atmospheric Environment, 33, 2733–2743, 1999.

Zhang, Q., Jimenez, J. L., Canagaratna, M. R., Allan, J. D., Coe, H., Ulbrich, I., Alfarra, M. R., Takami, A., Middlebrook, A. M., Sun, Y. L., Dzepina, K., Dunlea, E., Docherty, K., DeCarlo, P. F., Salcedo, D., Onasch, T., Jayne, J. T., Miyoshi, T., Shimono, A., Hatakeyama, S., Takegawa, N., Kondo, Y., Schneider, J., Drewnick, F., Borrmann, S., Weimer, S., Demerjian, K., Williams, P., Bower, K., Bahreini, R., Cottrell, L., Griffin, R. J., Rautiainen, J., Sun, J. Y., Zhang, Y. M., and Worsnop, D. R.: Ubiquity and dominance of oxygenated species in organic aerosols in anthropogenically-influenced Northern Hemisphere midlatitudes, Geophysical Research Letters, 34, L13 801, doi:10.1029/2007GL029 979, 2007.